UNSTEADY-STATE BEHAVIOUR OF AN IMMOBILIZED-CELL FLUIDIZED-BED BIOREACTOR FOR PHENOL BIODEGRADATION

by

Kira Alison Onysko

A thesis
presented to the University of Waterloo
in fulfillment of the
thesis requirement for the degree of
Doctor of Philosophy
in
Chemical Engineering

Waterloo, Ontario, Canada, 1999

THE UNIVERSITY OF WATERLOO requires the signatures of all persons using or photocopying this thesis. Please sign below, and give address and date

ABSTRACT

The phenol biodegradation and microbial growth kinetics of suspended cultures of the psychrotrophic microorganism *P. putida* Q5 were modeled as a function of temperature in the range of 10 to 25°C. The Haldane parameter, K_i, decreased with decreasing temperature, indicating the inhibition effect was stronger. The Luong model was found to better fit the kinetics of unacclimated cultures.

The response of an immobilized-cell fluidized-bed reactor (ICFBR) to step changes in phenol loading (ranging from 40 to 500% through step changes in either feed concentration or dilution rate) was investigated for a pure culture of *Pseudomonas putida* Q5. Two external-loop airlift ICFBRs containing biofilm-covered sand particles were operated at steady-state feed concentrations of 180 to 590 mg/L phenol and dilution rates from 0.025 to 0.069 h^{-1} at 10°C. Steady-state biofilm thicknesses ranged from 3 to 35 μm, depending upon the organic loading and the sand concentration (11-23 g/L). Two types of responses were noted. Low-level responses were characterized by a lack of response in the bulk phenol concentration. High-level responses were characterized by a rapid increase in the bulk phenol concentration and washout of the suspended biomass, the bioparticles were retained in the system.

A unique unsteady-state process model which simulated the response of all four process variables: the bulk phenol concentration, the suspended biomass concentration, the concentration profile of the substrate in the biofilm and the biofilm thickness, was implemented. Unique features included a balance on suspended cells, the consideration of an inactive fraction in the biofilm, and liquid-biofilm diffusional resistance and detachment. The model represented the wide range of conditions (described above) and the responses observed in four verification experiments. Accurate simulation of the experiments depended upon the use of kinetics determined using unacclimated suspended cells, as they were found to be more sensitive to phenol inhibition than the acclimated cultures. Also, growth rate hysteresis was included by adding a simple function that decreased the growth rate in proportion to the level of phenol present in the bulk fluid during a transient. The solution was simple enough to be used for future work with estimation and nonlinear control.

ACKNOWLEDGEMENTS

It has been said that it takes a village to raise a child; this is certainly true for a doctoral thesis Many people have offered their time, experience, encouragement and equipment to enable this to happen.

I wish to express my sincere gratitude to my supervisors, Dr C W Robinson and Dr H M Budman. I have appreciated their support and encouragement, particularly during difficult times. I have appreciated their experience and their integrity; they have been good mentors to me

I would like to thank those who helped me in the laboratory Ina Ohlemeyer and Xia Mann are thanked for their help with some of the batch kinetic experiments. Bernhard Kamp and Dr José-Luis Garcia Sanchez are thanked for their involvement with the dynamic suspended-cell culture experiments. David Stuivenberg is thanked for his involvement in one of the dynamic ICFBR experiments and extensive repairs to the reactors. My appreciation is also extended to Francis Muzio for tending my reactors on occasion and to Edmund Kwong for running GC-MS samples.

Dr. J Semple graciously set up a computer for me in his botany lab and taught me how to use his photomicroscope to capture digital images of the bioparticles. Thank-you! I am also grateful for loan of the spectrofluometer for an extended period of time from Dr. M. Moo-Young. Both pieces of equipment were crucial to my work.

I have also been supported by many outside the University – a community of friends and family I thank them for their support, encouragement and prayers. In particular, I would like to thank Devi Loy for her loving care of our children Karina and Elena, so that I could continue with my research.

Finally, I would like to thank my husband, Robert Black. He was there for our family when I couldn't be, and has been a tremendous support.

This work was made possible through grants from the Natural Sciences and Engineering Research Council (NSERC) and the Eco-Research Tri-council Secretariat.

CONTENTS

FIGURES

TABLES

1 Introduction

Historically, the focus in water pollution abatement has been the removal of suspended solids, nutrients and biochemical oxygen demand. However, the focus in wastewater treatment has recently shifted to the removal of toxic or persistent compounds. Despite the xenobiotic nature of these compounds, many are at least partially degradable by microorganisms, particularly if the microorganisms have been acclimated to a given wastewater.

The most common biological wastewater treatment method is the activated sludge process, which consists of a mixed culture of freely suspended microorganisms that use pollutants both as a carbon source and for energy. Some limitations of the activated sludge process include a restriction on the maximum permissible biomass concentration to allow for floc formation and settling under quiescent conditions, and a restriction on the dilution rate (flow rate per unit liquid volume) to avoid washout of the biomass. Activated sludge systems are sensitive to fluctuations in flow, concentration and temperature, arising from either periodic variations in the feed conditions or by shock loads due to spills, malfunctions or equipment backwashing upstream of the activated sludge bioreactor (Christiansen and Spraker, 1982).

Biofilm processes, in which the microorganisms are attached to a support material, offer a number of advantages over conventional suspension cell systems.

- Biofilm systems are more resistant to process fluctuations (Holladay et al., 1978).
- Biofilms are better protected against toxic or inhibitory compounds (eg. phenol) than free-suspension cultures (Heipieper et al., 1991) and may degrade these compounds at higher rates (Stevens, 1988). This may be a result of the protective effects of concentration gradients that occur within biofilms.
- Higher dilution rates can be tolerated in biofilm systems without washout of the bioparticles (Tang et al., 1987) (although at high substrate loadings and low temperatures a "lift-out" phenomenon is possible (Patoine, 1989)).
- Biomass concentrations can be 5-10 times higher than for conventional systems (Sutton and Mishra, 1990), thereby allowing for higher degradation rates (Holladay et al., 1978) and smaller reactors (Stathis, 1980).
- Biomass settling characteristics are less important than for conventional systems.

Biofilm systems occur in a number of configurations, including trickling filters, submerged filters, rotating disks and fluidized beds. An advantage of immobilized-cell fluidized bed reactors (ICFBRs) is a larger surface area for biofilm formation (e.g. 3300 m^2/m^3 compared to 160 m^2/m^3 for rotating disks and 80 m^2/m^3 for trickling filters (Stathis, 1980)). Another advantage is that ICFBRs can be well mixed with respect to the liquid phase which allows for better external mass transfer and allows for better control of biofilm thickness and the prevention of clogging.

1.1 Research Needs

Traditional design approaches for biofilm reactors include the empirical loading approach (which was adapted from conventional system design), and the use of empirical design formulae based on data-fitting (Arvin and Harremoes, 1990). Neither approach has been effective for designing complex biofilm reactors such as ICFBRs.

Research on biofilm processes has demonstrated the importance of the diffusional resistance to the movement of substrate within sufficiently-thick biofilmw prior to its degradation. Recently, models (Stevens, 1988, Elmaleh, 1990) that use lumped reaction rates within the biofilm (using concepts similar to those used for heterogeneous catalysis) have been proposed; however, these models cannot be used to predict steady-state biofilm thickness (and therefore biomass holdup), nor do they allow for biofilm growth.

Thus, phenomenologically-based design methodologies for fluidized bed bioreactors are needed. Such design methodologies should depend on system models which describe the system with reasonable accuracy, but which are simple enough to be applied in practice for simulation, optimization and scale-up purposes and possibly for enhanced process control. Also, most of the biofilm models have been developed for steady state conditions. Due to the variable nature of industrial effluents, an unsteady state model is needed so that the dynamic behaviour and limitations of the ICFBR can be evaluated prior to the design stage.

Several unsteady-state biofilm models have been applied to ICFBRs. These models, however, have several limitations, as described below.

Temperature

Existing ICFBR models have been developed for a constant temperature environment. Wastewater treatment systems normally do not have temperature control and are exposed to fluctuating temperatures (2-

25°C) arising from changes in process conditions or seasonal variations, particularly in cold climates. Although the effects of temperature change on suspended cell cultures with non-inhibitory substrates have been studied, there is little information on the effects of temperature changes on biofilm cultures or on cultures that are degrading inhibitory substrates. Temperature changes will affect both mass transfer rates and microbial kinetics and may even alter the extent of substrate inhibition.

Hydrodynamics

Most models consider idealized systems in which the hydrodynamics do not affect reactor performance. In practice, reactor hydrodynamics dictate important aspects of its performance, liquid-biofilm mass transfer resistance and biofilm adhesion and detachment rates. These should be taken into account in models.

Inactive Fraction in the Biofilm

To date, many biofilm models assume that all of the measured biofilm volume consists of active biomass (see Section 2.2.2). However, up to 90% (as TOC) of the biofilm may be composed of extracellular polymeric substances (EPS) (Bakke et al., 1984) and up to 50% of the microorganisms in the film may be metabolically inactive (Rittmann et al., 1992). Thus the presence of an inactive fraction should be investigated and if necessary should be taken into consideration in the model if kinetic relationships obtained for suspended cell cultures are to be applied to biofilm cultures of the same microorganisms.

Model Verification

There has been limited verification of existing dynamic ICFBR models. Results from shock loading experiments with suspended cell cultures indicate that the response of the system varies dramatically with the magnitude of the change imposed on the system. Thus, experimental verification of a model over a range of variable conditions is needed.

In addition to the limitations of existing models, there are other areas in which our understanding of ICFBRs is lacking. These include the behaviour and performance of psychrotrophic bacteria (see below) in ICFBRs, the release of intermediate metabolites into the medium under stressed conditions, and performance compared with conventional suspended cell systems.

Psychrotrophic Bacteria

In cold climates, wastewater temperatures often reach levels that are below those at which mesophilic organisms - with optimum temperatures in the range 20-40°C - function optimally (or even at all). Thus, the use of psychrotrophic organisms which are active from 5 to 25-30°C for biological treatment has significant potential advantages. Furthermore, it is likely that wastewater treatment systems in northern regions self-select organisms of this type to some extent. However, virtually all of the wastewater treatment research, including biofilm research, has focused on mesophilic organisms at conditions preferred by them. There is a need to understand the performance of psychrotrophic organisms in ICFBRs under both steady state and dynamic conditions. In particular, there is a need to investigate the behaviour of ICFBR systems outside the 20-30°C range.

1.2 Research Objectives

In order to address the limitations of existing ICFBR models and to address the gaps in the understanding of ICFBR systems, the research focussed on the unsteady-state response of an ICFBR organic loading.

The ICFBR utilized a psychrotrophic bacterium immobilized on sand particles, to treat a model inhibitory wastewater containing phenol. The bacterium, *Pseudomonas putida* Q5, is a naturally occurring biofilm-forming phenol degrader (Patoine, 1989; Kotturi et al., 1991)

The overall goals of this research were:

1. to gain a better understanding of the growth and phenol biodegradation kinetics of *P. putida* Q5, particularly at temperatures between 10-25°C,
2. to investigate the response of *P. putida* Q5 and that of an ICFBR under shock or variable loading conditions of phenol concentration, feed rate and/or temperature, and
3. to develop a practical process model that can be used for the design, optimization and scale-up of industrial-scale reactors of this type.

Specific objectives were

a) to characterize the phenol degradation kinetics of *P. putida* Q5 within the temperature range of 10-25°C (ie. to evaluate the three parameters in a substrate inhibition kinetic model as a function of temperature),

b) to develop an unsteady-state model which incorporated phenol biodegradation kinetics, biofilm detachment and hydrodynamic effects, and

c) to verify the model experimentally to step changes in organic loading, by changing the feed concentration or the feed rate.

1.3 Model System

The model system used, consisted of two external-loop airlift reactors with working volumes of 3.5 and 4 L, containing pure cultures of *P. putida* Q5 and sand as a support material for biofilm formation. The two airlift bioreactors were operated separately.

P. putida Q5, a psychrotrophic strain, was selected for several reasons. It had been used successfully in a previous ICFBR study in which phenol was the substrate being degraded in steady-state operation (Patoine, 1989). Other strains of *P. putida* have been associated with the degradation of aromatic compounds in biological wastewater treatment plants (Howell and Jones, 1981; Lewandowski et al., 1986). A psychrotroph was chosen because the low-temperature aspects of the performance of the ICFBR were of interest, and at low temperatures psychrotrophic strains are likely to be self-selected in biological treatment processes.

Sand was selected as the support material for biofilm development. The sand used in the experiments had a very irregular and rounded surface, and had been used successfully as a support material in previous ICFBR studies (Wagner and Hempel, 1988; Patoine, 1989).

The reactor feed consisted of a defined salts medium containing phenol as the sole carbon source. Phenol is a contaminant which is common in petroleum industry and other industrial wastewaters. Shock loads of phenol have been responsible for severe disruptions in conventional industrial biological treatment facilities (Galil et al., 1988). Phenol has also been used as a model inhibitory compound in other research (Hill and Robinson, 1975; Yang and Humphrey, 1975; Sokol and Howell, 1981; Rozich and Gaudy, 1983), and consequently, there is a large body of information on the biodegradation kinetics of phenol and the response of

suspended-cell cultures to shock loading of phenol. There is little literature on the response of biofilm cultures to shock-loading of phenol.

Loading changes to the system were limited to step changes in either the dilution rate or the feed concentration.

1.4 Limitations and Assumptions of the Research

The ICFBR is a very complex system due to the interactions between the microorganisms, mass transport phenomena and hydrodynamics. The complex nature of the system and current approaches to modelling the system are discussed in Chapter 2.

There are many areas in which information is lacking. In some cases, general correlations for these interactions have not yet been developed. For example, there are not yet correlations for detachment rates of biofilms for systems in which abrasion of particles plays an important role. In other cases, certain phenomena are not well understood (such as the effect of immobilization on microbial physiology and phenol degradation kinetics). This lack of knowledge is complicated further when transient conditions are considered.

Because of the complexity of the system and the level of current understanding of biofilm systems, a number of simplifications and assumptions have been made in order to produce a model that will be useful in an engineering context. The assumptions of the dynamic ICFBR model are described in detail in Section 4.1. Several simplifications are listed here.

1. The model was developed and verified using a pure culture (*Pseudomonas putida* Q5). In practice, a mixed culture would be used for wastewater treatment; however, the interactions of species and degradation kinetics of a mixed culture (within a biofilm) under dynamic conditions would introduce too many parameters.
2. The model was developed for a synthetic wastewater containing a single limiting substrate. In this case, phenol was chosen as a model inhibitory compound. Industrial wastewaters typically include a number of contaminants, including others that are toxic or inhibitory.
3. The specific rate of cell detachment was determined for specific conditions used in the verification experiments. This parameter will not necessarily apply to other ICFBR systems using different conditions.

4. The ICFBR was operated under conditions in which the degradative capacity of the biofilm was limited only by the availability of phenol, and not by the availability of oxygen or other nutrients.

2 Literature Review

2.1 Biodegradation of Phenol

2.1.1 Metabolic Pathways of Phenol Biodegradation

Phenol must diffuse into the cell to be metabolized. Bacterial degradation of phenol is accomplished through the transformation of a catechol intermediate via one of two pathways, as illustrated in Figures 2.1 and 2.2.

The *ortho* pathway (Figure 2.1) involves cleavage of catechol by catechol 1,2-oxygenase to form *cis,cis*-muconate. The *cis,cis*-muconate induces three enzymes which catalyze the conversion of catechol to ß-ketoadipate enol-lactone (Feist and Hegeman, 1969). The metabolic products of the *ortho* pathway are carbon dioxide as well as succinate and acetyl-CoA, both which can be further degraded in the TCA cycle.

The *meta* pathway (Figure 2.2) involves cleavage of catechol by catechol 2,3-oxygenase to form 2-hydroxymuconic semialdehyde, which is sequentially metabolized to form acetaldehyde and pyruvate. The *meta* pathway is induced by a primary substrate such as phenol (Feist and Hegeman, 1969). The *meta* pathway appears to allow for the metabolism of a variety of substituted phenolic compounds, whereas the *ortho* pathway is more specific and is used in the catabolism of catechol and precursors of catechol (Feist and Hegeman, 1969).

The *ortho* pathway is more common. Stainer et al. (1966) found that only 8 out of 41 strains of *Pseudomonas putida* were capable of the *meta* cleavage pathway. The psychrotrophic strain used in this study, *P. putida* Q5 possesses the *ortho* but not the *meta* pathway (Kolenc et al., 1988).

2.1.2 Mechanisms of Phenol Inhibition

Phenol has been used as a model inhibitory compound in the literature. Phenol is growth inhibitory to bacteria at concentrations above about 50 mg/L and is bactericidal at concentrations of about 2000 mg/L (Heipieper et al., 1991). Typical phenol concentrations in industrial wastewaters are presented in Table 2.1. Many wastewaters listed in Table 2.1 contain phenol at inhibitory concentrations.

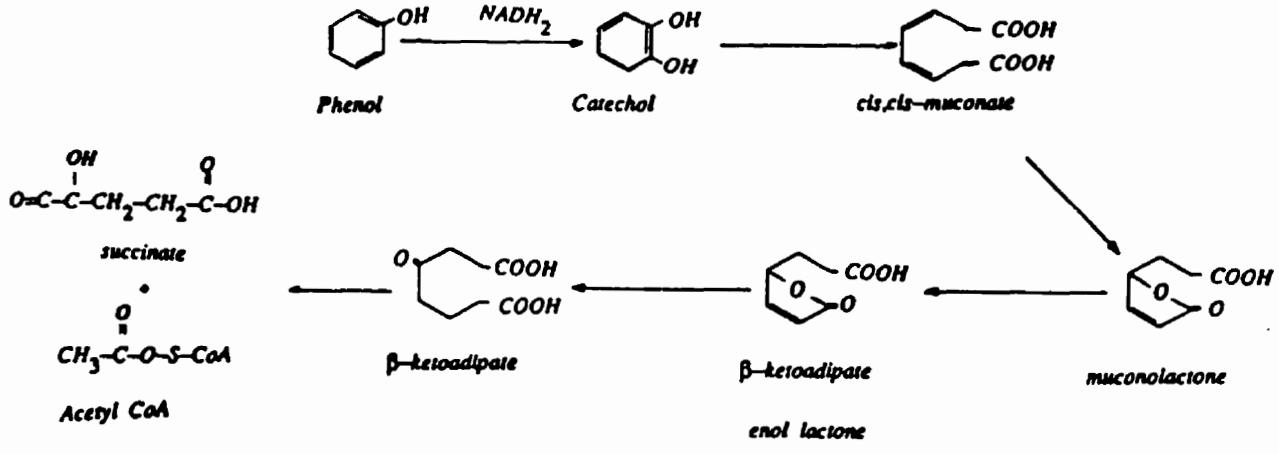

Figure 2.1. *Ortho*-cleavage pathway of phenol metabolism (from Yang and Humphrey, 1975)

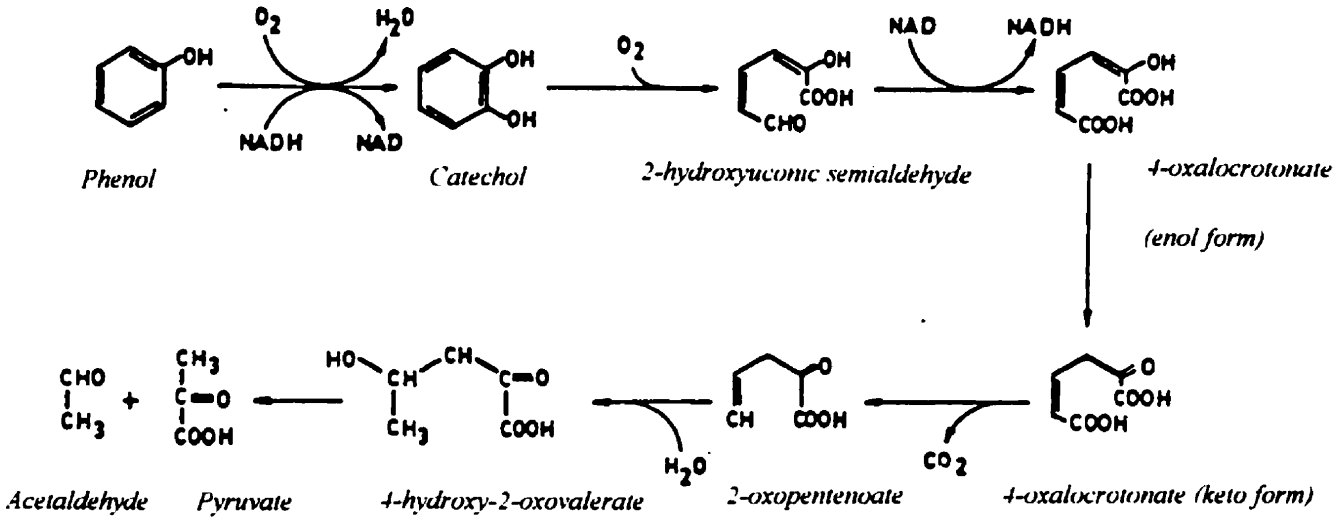

Figure 2.2. *Meta*-cleavage pathway of phenol metabolism (from Sala-Trepat et al., 1972)

Table 2.1 Levels of Phenol Reported in Industrial Wastewaters (after Sittig, 1975)

Industrial Source	Phenol Concentration (mg/L)
Coke Ovens	
Weak ammonia liquor without dephenolization	600-12,000
Weak ammonia liquor with dephenolization	4-330
Wash oil still wastes	30-150
Oil Refineries	
Low-temperature carbonization effluent	3395[1]
Sour water	80-185
General waste stream	10-100
Post-stripping	80
General (catalytic cracker)	40-50
Mineral oil wastewater	100
API separator effluent	1-7
Petrochemical	
General wastewater	50-600
Benzene refineries	210
Nitrogen works	250
Tar distilling plants	300
Aircraft maintenance	200-400
Herbicide manufacturing	210
Other	
Rubber reclamation	3-10
Orlon manufacturing	100-150
Plastics factory	600-2,000
Fiberboard factory	150
Phenolic resin production	15,000[2]
Dephenolization liquor	3,000[2]
Stocking production	6,000
Fiberglass manufacturing	40-400
Wood carbonizing	500

[1] Kumaran and Parachuri (1997)
[2] Weber et al. (1992)

Although the mechanisms of phenol inhibition are not known, it appears that effects on membrane functionality may play an important role. Exposure of *Escherichia coli* to phenol concentrations in the range of 0-2 g/L resulted in leakage of K^+ ions and ATP (Heipieper et al., 1990, 1991). The rate of K^+ efflux and the amount of ATP lost were proportional to the phenol concentration used (Heipieper et al., 1991). Leakage of nucleotides, particularly at bactericidal concentrations (2 g/L), has also been reported (Heipieper et al., 1991). Because growth inhibition by phenol was not affected by increasing the concentration of K^+ in the medium, Heipieper et al. (1991) suggested that the observed toxicity must be due to the loss of another ion or metabolite. Keweloh et al. (1990b) postulated that because phenol is highly lipid soluble, it can disturb the structural order of lipids in the membrane, resulting in leakage of cell metabolites and co-factors into the medium.

Keweloh et al. (1990b) reported changes in membrane structure by *E. coli* K-12 in response to exposure to phenol. Both the cytoplasmic and outer membranes showed higher protein to lipid ratios. The higher protein fraction in the membrane makes the fatty acid chains of the lipids more rigid and hence makes the lipoprotein membrane less permeable. The change in membrane structure could be a result of the inhibition of lipid synthesis or an adaptive effect to protect osmotic integrity. Heipieper et al. (1990) have also reported an increased ratio of saturated to unsaturated fatty acids in the cell membrane at bacteriostatic concentrations of phenol.

Bacterial cells appear to be able to restore gradients across the cell membrane, required for continuation of cell growth. Heipieper et al. (1990) reported that *P. putida* that was adapted to a sublethal concentration of phenol was able to reabsorb K^+ ions at phenol concentrations up to the concentration to which it was adapted. Unadapted cells showed irreversible losses of K^+ ions. Subsequently, Heipieper et al. (1991) showed that reuptake of cations occurred only when cells were supplied with an energy source such as glucose. The cells were able to reestablish K^+ membrane gradients within about one hour after having been exposed to high concentrations of phenol (at phenol concentrations which still allowed for growth).

2.1.3 Growth and Phenol Biodegradation Kinetics during Balanced Growth

Bacteria experience balanced growth in batch systems, where bacteria are in the logarithmic phase of growth, or in continuous systems at steady state. During balanced growth, extensive properties of the system such as total protein, DNA, and RNA, increase in direct proportion to the number of cells (Campbell, 1957).

In the following section, unstructured models developed for cell growth and phenol degradation during balanced growth in suspended-cell cultures are discussed. As kinetic models for phenol degradation in biofilms have not yet been developed, it will be assumed that kinetic models for suspended cell cultures apply equally well to biofilm cultures, when the internal diffusional resistances are accounted for separately from the inherent growth kinetics. Suspended-cell kinetic models have already been used in this context with some success (Tang and Fan, 1987; Tang et al., 1987; Worden and Donaldson, 1987; Livingston and Chase, 1989; Wisecarver and Fan, 1989). The basis for this assumption is discussed in Section 2.3.4.

2.1.3.1 General Kinetic Expressions

The rate of change of biomass concentration is dependent on the rates of cell growth, endogenous decay and death. The rate of change in substrate concentration is dependent on the substrate uptake rate for growth, as well as for maintenance requirements, possible energy spillage and product formation.

Growth

The rate of cell growth (r_X) is proportional to the concentration of active biomass present and is given as

$$r_X = \frac{dX}{dt} = \mu X \tag{2.1}$$

where μ is the specific growth rate and X is the concentration of viable cells. Equation (2.1), when integrated, describes logarithmic or exponential growth.

Maintenance and Endogenous Decay

Maintenance and endogenous decay are often used interchangeably because both result in a reduced yield of biomass and are not possible to distinguish from each other experimentally. The decay concept results in the rate of production of cell mass being lower than expected from a given substrate concentration and

theoretical yield coefficient. The maintenance concept results in the rate of substrate consumption being higher than would be predicted from a given cell concentration. The two concepts can be related mathematically using the true growth yield coefficient (Shuler and Kargi, 1992). The maintenance concept is used in the current work.

Energy is required to maintain and repair existing structures, to transfer some nutrients and products in and out of cells, to regulate the osmotic pressure inside the cells and in some cases for cell motility (Shuler and Kargi, 1992). This results in a diversion of substrate away from growth and a reduced yield of new biomass from the consumption of substrate. The expression for the maintenance rate (r_m) is given as:

$$r_m = -\left(\frac{1}{Y_m}\right)\left(\frac{dS}{dt}\right)_m = mX \tag{2.2}$$

where m is the maintenance coefficient. Maintenance requirements are included in the mass balance on substrate in a process.

Yield can also be reduced through the degradation of cells or cellular components with the result of decreasing biomass. Decay may be important in substrate-depleted regions in the innermost layers of the biofilm. The expression for the endogenous decay rate (r_d) is given as:

$$r_d = -\left(\frac{dX}{dt}\right)_d = k_d X \tag{2.3}$$

where k_d is the decay coefficient. The decay term is often considered to be negligible; however it should be included in the model if very thick biofilms, which can become substrate or oxygen-limited, are expected.

Death

Death is difficult to distinguish from decay and is not usually included in biofilm models unless cell death can be attributed to the presence of a biocide.

Product formation

Bacteria may produce a variety of products, including carbon dioxide, extracellular polymeric substances (EPS) and intermediate metabolites. The rate of product formation from energy associated metabolism (r_P) can be expressed by the generalized Leudeking-Piret equation (Leudeking and Piret, 1959), given as:

$$r_{P,total} = \sum_{i=1}^{n} r_{P,i} = \sum_{i=1}^{n} (k_{P,i}\mu X + k_{P',i} X) \tag{2.4}$$

where $k_{P,i}$ is the growth associated product formation coefficient and $k_{P,i}'$ is the non-growth associated product formation coefficient for the i^{th} product. The production of EPS by *Pseudomonas aeruginosa* obeys this rate law for the case where the non-growth associated coefficient is essentially zero (Robinson, J. A. et al., 1984). The specific rate of product formation is given as:

$$q_P = \frac{r_P}{X} \tag{2.5}$$

Robinson et al. (1984) reported that the cellular yield (Y_{XS}) (based on suspended solids concentration) for *P. aeruginosa* in biofilms would be overestimated by 100% if EPS production were to be neglected.

Substrate uptake

The rate of substrate uptake (r_S), is given as:

$$r_S = \frac{\mu X}{Y_{X/S}} \tag{2.6}$$

where Y_{XS} is the apparent growth yield. The apparent growth yield is not a true constant and will vary according to how the substrate is used (ie. for growth, energy, maintenance, energy spillage,and product formation) under various culture conditions. According to Pirt (1965), the true growth yield, Y_g, which is considered to be constant, and the apparent growth yield are related by,

$$\frac{1}{Y_{XS}} = \frac{m}{\mu} + \frac{1}{Y_g} \tag{2.7}$$

Thus, if maintenance requirements and product formation are also included, r_S is given as:

$$r_S = \left(\frac{\mu}{Y_g} + m + \sum_{i=1}^{n} \left(\frac{q_{P,i}}{Y_{P,i/S}}\right)\right)X \tag{2.8}$$

where $Y_{P,i/S}$ is the product yield based on substrate consumed.

2.1.3.2 Specific Growth Rate (μ)

The Monod Equation

Expressions for μ are based on the dependence of growth on the concentration of a limiting substrate and are usually semi-empirical because the mechanisms of bacterial reproduction are complex and not sufficiently well understood. A number of equations have been proposed for specific growth rate, based upon experimental observation and curve fitting, the most widely accepted being the Monod equation for non-inhibitory substrates (Monod, 1949):

$$\mu = \frac{\mu_m S}{K_S + S} \tag{2.9}$$

Here S is the concentration of the single limiting substrate (ie. phenol in this work), μ_m is the maximum specific growth rate and K_s is the Monod constant which corresponds to the substrate concentration at which the value of μ is half of μ_m. Although the Monod equation is strictly empirical, it has been found to fit quite well the data of a number of pure and mixed cultures growing on non-inhibitory substrates when only one of them is limiting (Grady and Lim, 1980).

The Haldane Equation

Phenol is an inhibitory substrate at moderate concentrations (50-100 mg/L) even to microorganisms which can use it as a substrate for growth, and can cause cell death at sufficiently high concentrations. Although phenol concentrations may not reach inhibitory levels at steady-state conditions in continuous culture (Livingston and Chase, 1989), inhibitory levels may be reached during transient conditions as a result of changes in feed concentration, dilution rate (feed rate per unit liquid volume in the bioreactor) or temperature. Thus an inhibitory model must be considered.

The Haldane model (Haldane, 1930), originally proposed to describe the effect of competitive substrate inhibition of a single enzymic reaction, has been adopted to describe inhibition of microbial growth, although the original enzyme mechanisms do not necessarily apply (Andrews, J. F., 1968):

$$\mu = \frac{\mu_{max} S}{S + K_S + \frac{S^2}{K_I}} \tag{2.10}$$

Here K_I is an inhibition constant, equivalent to the highest substrate concentration at which the specific growth rate (μ) is equal to half the maximum specific growth rate (μ_{max}) in the absence of inhibition. The Haldane model is illustrated in Figure 2.3.

The maximum specific growth rate attainable in the presence of an inhibitory substrate (μ^*) can be determined by taking the first derivative of Equation (2.10), setting it to zero and solving for μ. This results in,

$$\mu^* = \frac{\mu_{max}}{1 + 2\sqrt{\frac{K_S}{K_I}}} \tag{2.11}$$

The substrate concentration at which $\mu=\mu^*$ is,

$$S^* = \sqrt{K_S K_I} \tag{2.12}$$

In continuous cultures, the value of μ^* corresponds to the critical dilution rate, D^*, above which washout of the biomass would be expected under steady-state conditions for a completely-mixed suspended-cell system. The value of S^* is defined as the critical substrate concentration above which growth is limited by inhibition and beyond which the continous culture process is not stable. Although theoretically steady states are possible at values of S and D which are greater than S^* and D^*, in practice stable operation of a continuous reactor is not possible in that operating region without closed-loop control mechanisms.

The Haldane equation (Equation 2.10) has been used to model the relationship between μ and phenol concentration for both pure and mixed cultures, including both mesophilic (Pawlowsky and Howell, 1973a, b; Pawlowsky et al., 1973; Hill and Robinson, 1975; Yang and Humphrey, 1975; Sokol and Howell, 1981; Allsop, 1989; Livingston and Chase, 1989; Ong and Bowers, 1990; Livingston, 1993) and psychrotrophic (Kotturi, 1989; Patoine, 1989; Kotturi et al., 1991) bacteria. However, a number of problems have been reported in fitting experimental data to the Haldane model.

Allsop (1989) demonstrated that the Haldane model parameters are perfectly correlated and cannot be separated in several regions below a phenol concentration of 100 mg/L, by plotting the partial derivatives of μ with respect to each parameter. His analysis also showed that μ_{max} is the only parameter that can be obtained easily from kinetic data.

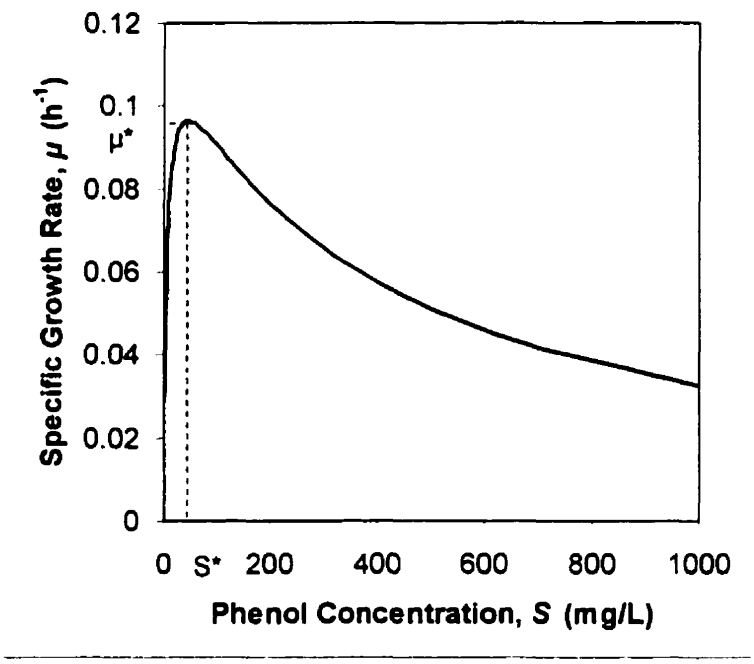

Figure 2.3. The Haldane model for freely-suspended cells of *P. putida* Q5 growing on phenol at 10°C (μ_{max}=0.119 h^{-1}, K_S=5.27 mg/L, K_I=377 mg/L; Kotturi et al., 1991)

Another difficulty with the determination of Haldane parameters is that K_S is best determined at low phenol concentrations where concentration measurements are least accurate. In addition, K_I is best evaluated under conditions of high substrate concentration ($S>>S^*$), which are not achievable in steady-state continous cultures without a controller (Schroder et al., 1997).

Linearization techniques often used in evaluating the parameters of the Monod equation are more difficult to apply to the Haldane equation (D'Adamo et al., 1984); thus, non-linear least-squares regression techniques have been used. Unfortunately, the least-squares technique is sensitive to the choice of initial values of the parameters, resulting in multiple values for the parameters (Sokol and Howell, 1981; D'Adamo et al., 1984). D'Adamo et al. (1984) proposed a set of limiting conditions to restrict the problem to realistic parameters.

The Haldane model overestimates values of μ in the higher phenol concentration range obtained in batch cultures (Yang and Humphrey, 1975; Kotturi et al., 1991). Yang and Humphrey (1975) found that the

model predictions deviated from experimental data for phenol concentrations above 300–400 mg/L. Kotturi et al. (1991) also reported overestimation of μ at phenol concentrations above 600 mg/L for *P. putida* Q5

Despite the problems reported for the Haldane model, its continued use has been recommended by several researchers (D'Adamo et al., 1984; Li and Humphrey, 1989).

Other Substrate Inhibition Models for μ

Because the Haldane equation originated as a description of enzyme kinetics, and the mechanism upon which it was based does not necessarily apply to microbial growth, other models have been proposed for phenol degradation. Some of these models are listed in Table 2.2.

Predictions based on the Haldane model (Equation 2.10) has been compared to the equations listed in Table 2.2 (Edwards, 1970; Pawlowsky and Howell, 1973a; Hill and Robinson, 1975; Yang and Humphrey, 1975; D'Adamo et al., 1984; Tan et al., 1996) with mixed results. The fit of the Haldane model was either statistically indistinguishable from the others (Edwards, 1970; Pawlowsky and Howell, 1973a; D'Adamo et al., 1984), better (Edwards, 1970) or significantly worse (Edwards, 1970) depending on the scatter in the kinetic data, the range of concentrations, the type of organism and the inhibitory substrate chosen. The models are not all that different in form. The use of the Haldane model has been recommended (Edwards, 1970; Pawlowsky and Howell, 1973a; D'Adamo et al., 1984) because it is relatively simple and easier to manipulate than Equations 2.12-2.19).

Han and Levenspiel (1988) proposed Equation 2.21 which unlike the other models in Table 2.2 (except for the model of Luong, 1987), predicts a critical inhibitor concentration above which reaction ceases. Unfortunately, Equation 2.21 has five parameters which makes it less practical to use than the Haldane model which has three parameters.

Sokol and Howell (1981) reported that although the Haldane equation fitted data for the growth of a mesophilic *P. putida* on phenol in batch culture (but taken from continuous cultures at various dilution rates), Equation 2.19, which was converted to a two-parameter model, namely:

$$\mu = \frac{k_1 S}{k_2 - S^2} \tag{2.22}$$

Table 2.2 Other Substrate-Inhibition Models

Source	Model	
Webb (1963)	$\mu = \frac{\mu_{max} S(1 + \frac{S}{K})}{S + K_S + \frac{S^2}{K_I}}$	(2.12)
Yano and Koga (1969)	$\mu = \frac{\mu_{max} S}{S + K_S + \frac{S^3}{K^2}}$	(2.13)
	$\mu = \frac{\mu_{max} S}{S + K_S + (\frac{S^2}{K_I})(1 + \frac{S}{K})}$	(2.14)
Aiba et al. (1968)	$\mu = \frac{\mu_{max} S e^{\frac{-S}{K_I}}}{S + K_S}$	(2.15)
Edwards (1970)	$\mu = \mu_{max}(e^{\frac{-S}{K_I}} - e^{\frac{-S}{K_S}})$	(2.16)
Yang and Humphrey (1975)	$\mu = \frac{\mu_{max} S (1 + \frac{S}{K})}{1 + \frac{K_S}{S} + \frac{S}{K_I}}$	(2.17)
Yang and Humphrey (1975)	$\mu = \frac{\mu_{max}}{1 + \frac{K_S}{S} + (\frac{S}{K_I})^2}$	(2.18)
Sokol and Howell (1981)	$\mu = \frac{\mu_{max} K_I S}{\sqrt{K_S K_I} + S^2}$	(2.19)
Luong (1987)	$\mu = \frac{\mu_{max} S (1 - \frac{S}{S_I})^n}{K_S + S}$	(2.20)
Han and Levenspiel (1988)	$\mu = \mu_{max}(1 - \frac{S}{S_I})^n \frac{S}{S + K_S(1 - \frac{S}{S_I})^m}$	(2.21)

fitted the data significantly better at a 95% confidence level for phenol concentrations up to 1000 mg/L. Because parameter estimation with the Haldane model (with three parameters) can be difficult, a two-parameter model would be easier to implement.

Beltrame et al. (1984) hypothesized that either an intermediate metabolite or a decay product competitively inhibited the growth rate in a continuous reactor. By assuming that the concentration of the inhibitor was proportional to the feed concentration (S_o), they proposed the following model based upon competitive inhibition.

$$\mu = \frac{k_1 S}{k_2 + S + \frac{S_o}{k_3}} \tag{2.23}$$

The model explained the apparent dependence of the effluent concentration, not only upon the dilution rate (flow per unit volume of the reactor), but the feed concentration as well.

2.1.3.3 True Growth Yield (Y_g)

Under conditions of balanced growth, Y_g is assumed to be constant at a given set of environmental conditions. If the medium composition, temperature or substrate concentration is changed, the yield may change. Kotturi et al. (1991) reported that the true growth yield for *P. putida* Q5 using phenol as a substrate at 10°C is 1.44 g/g, based upon theoretical considerations.

2.1.4 Effects of Temperature on Microbial Kinetics

Temperature can have a significant effect on microbial processes, influencing not only reaction rates but nutrient requirements, cell composition (Esener et al., 1981) and mass transfer of oxygen, substrate and reaction products through the biofilm. As a result, temperature affects important process parameters such as critical dilution rate in suspended cell cultures (Morgan and Edwards, 1971; Topiwala and Sinclair, 1971) and oxygen penetration depth in biofilm and floc-containing reactors (Eckenfelder and Englande, 1970). The effects of temperature on mass transfer is discussed in Section 2.2.3.3.

The effect of even a 10°C change in temperature on growth rate can be considerable. For example, the generation times of *P. putida* Q5 at 5°C and 15°C are 13.9 h and 3.2 h, respectively (Kolenc et al., 1988).

Much of the temperature-kinetics research has been conducted with batch suspended-cell cultures which are temperature-limited (not substrate-limited); thus, the observed growth rate for the culture is

equivalent to μ_m in the Monod equation (Equation (2.9)). In continuous systems where substrate concentrations are limiting and decay may not be negligible, temperature effects on microbial kinetics are not as straightforward.

The temperature-kinetic models described for μ_m in the following section were developed either for specific reactions or for temperature-limited growth in which the observed growth rate is maximal for a given temperature. All of the research has been conducted with suspended cell cultures. Very little work has been done with inhibitory substrates such as phenol considered in the current research.

2.1.4.1 Temperature Models for the Maximum Specific Growth Rate (μ_m)

It is generally accepted that as temperature increases from the minimum temperature for growth (T_{min}), the maximum growth rate (μ_m) (in the Monod equation) increases until some optimal temperature (T_{opt}) is reached, after which μ_m decreases to zero above the maximum temperature for growth (T_{max}). The curve representing this growth rate-temperature relationship, illustrated in Figure 2.4, can be divided into four temperature ranges: the sub-Arrhenius, Arrhenius, optimum and super-optimum ranges (Heitzer et al., 1991). Existing temperature-kinetic models attempt to describe this relationship over the full growth-permissible temperature range or a portion thereof.

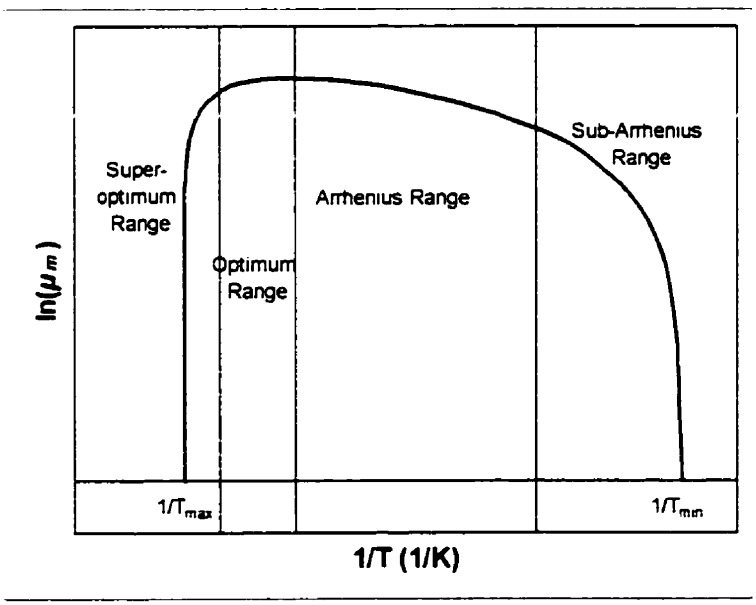

Figure 2.4. Relationship between temperature (T) and the maximum specific growth rate (μ_m) for microorganisms

There are essentially two types of temperature models currently in use in the literature. Arrhenius-type models are usually expressed with the dependent variable as ln(rate), whereas with square-root models the dependent variable is expressed as $(\text{rate})^{0.5}$

Arrhenius-type models

A list of Arrhenius-type models is presented in Table 2.3. An underlying assumption of all Arrhenius-type models is that μ_m is controlled by a single reaction, despite the vast number of complex enzymatic reactions taking place in the cell.

The Arrhenius and Eyring equations (Equations 2.24 and 2.25, respectively) have limited application to biological systems over wide temperature ranges because they predict ever-increasing rates with temperature. This is not consistent with observations of growth rates in biological systems, as illustrated in Figure 2.4. Also, in Equation 2.24 the temperature characteristic, ΔH^*, is assumed to be constant; however, ΔH^* can vary as much as threefold or fourfold, depending on the temperature range chosen (Ratkowsky et al., 1982). Despite these limitations, the Arrhenius equation has been used extensively in the biological and engineering literature, particularly when temperatures in the Arrhenius range are being considered.

Because the Arrhenius and Eyring models are not applicable to bacterial growth over the entire growth-permissible range, the theory was extended to include enzyme denaturation at temperature extremes. These extended models are called master reaction models. Two master reaction models are listed in Table 2.3 (Equations 2.26 and 2.27). These can be simplified to allow for only low- or high-temperature deactivation by neglecting the appropriate terms. Although the master reaction models have a basis in reaction theory, the parameters cannot be considered true thermodynamic constants and are essentially empirical. Both Equations 2.26 and 2.27 exhibit sensitivity to initial parameter guesses (Heitzer et al., 1991) and contain too many parameters to be practical.

Square-root models

Another approach was proposed by Ratkowsky et al. (1982) who developed a square-root relationship, Equation 2.30 in Table 2.4, to describe the relationship between growth rate and temperature below the optimal growth rate. Although the model is completely empirical, the square-root equation was found to well describe the growth rate/temperature data of over 70 data sets for a variety of suspended cell

Table 2.3. Arrhenius-type Temperature-kinetic Models

Source	Model	Parameters
Arrhenius (1908)	$\mu_m = Ae^{\frac{-\Delta H^*}{RT}}$ (2.24)	μ_m - max. specific growth rate A - frequency factor R - gas constant T - absolute temperature. ΔH^* - temperature characteristic
Eyring and Urry (1965)	$\mu_m = \frac{\kappa K_b T}{h} e^{\frac{\Delta S^\circ}{R} - \frac{\Delta H^\circ}{RT}}$ (2.25)	ΔS° - entropy of activation ΔH° - enthalpy of activation K_b - Boltzmann's constant h - Plank's constant κ - a transmission coefficient
Sharpe and DeMichele (1977)	$\mu_m = \frac{\frac{[E_T] K_b \kappa}{h} T e^{\frac{\Delta S}{R} - \frac{\Delta H^*}{RT}}}{1 + e^{\frac{\Delta S_L}{R} - \frac{\Delta H_L}{RT}} + e^{\frac{\Delta S_H}{R} - \frac{\Delta H_H}{RT}}}$ (2.26)	$[E_T]$ - concentration of enzyme present regardless of state. Subscripts L and H - low- and high-temperature enzyme inactivation, respectively.
Schoolfield et al. (1981)	$\mu_m = \frac{\rho_{25^\circ C} \frac{T}{298} e^{\frac{\Delta H^*}{R}\left(\frac{1}{298} - \frac{1}{T}\right)}}{1 + e^{\frac{\Delta H_L}{R}\left(\frac{1}{T_{0.5L}} - \frac{1}{T}\right)} + e^{\frac{\Delta H_H}{R}\left(\frac{1}{T_{0.5H}} - \frac{1}{T}\right)}}$ (2.27) $\rho_{25^\circ C} = 298 e^{\left(\phi - \frac{\Delta H^*}{298}\right)\frac{1}{R}}$ (2.28) $\phi = \Delta S^\circ - \ln\left(\frac{K_b [E_T]}{h}\right)$ (2.29)	$T_{0.5L}$, $T_{0.5H}$ - temperatures at which enzyme is half active due to low- or high-temperature inactivation. All other parameters as identified previously.

cultures including psychrophiles, psychrotrophes, mesophiles, and thermophiles at temperatures below T_{opt} (Ratkowsky et al., 1982).

Ratkowsky et al. (1983) subsequently extended the square-root equation to include the full growth-permissible temperature range in Equation 2.31. Although the regression coefficient, T_{min}, does not necessarily correspond to the actual minimum temperature for growth, (Ingraham et al., 1983), McMeekin et al. (1987) reported that the relationship remains valid while cells are growing. Heitzer et al. (1991) reported that the square-root model was able to well

Table 2.4. Square-root Temperature-kinetic Models

Source	Model	Parameters
Ratkowsky et al. (1982)	$\sqrt{\mu_m} = b(T_o - T_{min})$ **(2.30)**	b is a regression coefficient and T_o is a characteristic temperature
Ratkowsky et al. (1983)	$\sqrt{\mu_m} = b(T - T_{min})(1 - e^{c(T - T_{max})})$ **(2.31)**	Here b and c are regression coefficients and T_{min} (previously called T_o) and T_{max} represent the points at which regression lines intersect the axis
Zwietering et al. (1991)	$\mu_m = [b(T - T_{min})]^2 [1 - e^{c(T - T_{max})}]$ **(2.32)**	

describe the behaviour of four bacteria (*Klebsiella pneumoniae* NCIB 418, *E. coli* NC3, *Bacillus* sp. strain NCIB 12522 and *Coccobacillus* sp. strain NA17) in suspended cell cultures. The parameter values obtained were independent of initial estimates (Heitzer et al., 1991) due to the simplicity of the model structure.

Zwietering et al. (1991) modified the model by Ratkowsky et al. (1983) such that the decline of μ_m towards T_{max} is described by an exponential function rather than the square of an exponential function (i.e. Equation 2.31 squared). Equation 2.32 avoids the prediction of positive growth rates above the maximum growth temperature, T_{max}.

Comparison between models

Recently, there has been debate in the literature about the superiority of the model of Schoolfield et al. (1981) (Equation 2.27) versus the extended square root model (Equation (2.31)) (Adair et al., 1989; Ratkowsky et al., 1991). Zweitering et al. (1991) found that when using a minimum sum of squares criterion and weighting values to take into account the transformational changes inherent in each model, the modified version of the square-root model (Equation 2.30) was better than the model of Schoolfield et al. (1981), despite having fewer parameters. Heitzer et al. (1991) found that both models predicted growth data well when the model of Schoolfield et al. (1981) was solved in two steps. This was done by fitting a four parameter model, which considered only high temperature inactivation, to a partial data set and then by using the parameters obtained in the first step to fit the model, Equation 2.27, to the full data set

Both types of model have their advantages. The square-root models converge quickly, are not sensitive to initial parameter estimates and have the fewest parameters of the models described, but the resulting parameters are simply regression coefficients. The model of Schoolfield et al. (1981) requires very large data sets for accurate parameter estimation (Zwietering et al., 1991) and can be sensitive to initial parameter estimates; however, the parameters may have biological meaning, which allows for quantitative comparison of thermodynamic characteristics between bacterial species.

2.1.4.2 Temperature Effects on Other Kinetic Parameters

Monod constant (K_S)

The effect of temperature on the Monod constant, K_S, is not clear from previous work. A number of researchers have reported an increase in K_S with temperature in suspended cell cultures over narrow temperature ranges with Arrhenius temperature characteristic (ΔH^*) values ranging from 20.9 to 100 kJ/mol (Marr et al., 1963; Knowles et al., 1965; Sanders, 1973; Stevens et al., 1989; Zhang, W. et al., 1995). In contrast, Topiwala and Sinclair (1971) obtained a decreasing temperature relationship in the Arrhenius range with an activation energy of 46 kJ/mol when $1/K_S$ was expressed in the Arrhenius form. Muck and Grady (1974), who worked with activated sludge in a glucose-mineral salts medium, reported that K_S decreased slightly (from 130 to 112 mg/L) between 10 and 20°C, and rose (to 172 mg/L) as the temperature was increased to 30°C. Kim et al. (1981) reported that K_S was independent of temperature for methanol and phenol degradation in a mixed culture in the

range of 5-28°C. Esener et al. (1983) have suggested that if K_S can be considered to be a ratio of kinetic constants (analogous to the Michaelis-Menten constant K_M), then K_S may increase or decrease with increasing temperature depending on the specific reaction.

Inhibition Constant (K_I)

There is little information about the effects of temperature on the inhibition constant K_I. Almost all researchers have used non-inhibitory substrates and Kim et al. (1981) who used phenol as a substrate, employed a non-inhibitory kinetic model, while using inhibitory substrate concentrations.

Eismann et al. (1994) (unpublished work) reported that K_I decreased with decreasing temperature for a methanogenic culture degrading phenol; thus the degree of substrate inhibition was greater at lower temperatures. They also reported that the concentration limit at which there is no degradation was lower at lower temperatures, indicating an increased sensitivity to phenol toxicity at lower temperatures. Unfortunately, none of the data has been published. Reynolds et al. (1974) found that a linear competitive inhibition model (for which K_I would have different values than the K_I in the Haldane model) fitted their data best for the degradation of phenol by an alga, however, their analysis with an uncompetitive inhibition model (the Haldane equation) resulted in decreasing values of K_I with decreasing temperature.

Others have investigated the effect of temperature on substrate inhibition without looking explicitly at the kinetic models for growth. Near the upper range of inhibitory substrate concentration for growth, Huang and Chen (1988) found that substrate (ie. glucose) inhibition of cell growth for the yeast *Zymomonas mobilis* followed the general pattern of μ_m, increasing to a maximum at 37°C and decreasing above the optimum temperature. In the lower temperature range, Willocx et al. (1993) found that carbon dioxide inhibition of *Pseudomonas fluorescens* increased as temperature decreased. Buchanan and Klawitter (1992) reported an increase in T_{min} as conditions diverged from optimal (with respect to pH and salinity) for *E. coli*.

Although the effect of temperature upon K_I (or the degree of substrate inhibition) is not clearly indicated by previous research, it is likely that inhibition effects increase as conditions move away from optimal, resulting in a decrease in K_I at temperature extremes.

Specific rates of endogenous decay (k_d) and maintenance (m)

The specific rate of endogenous decay (k_d) or maintenance (m) described by Equations 2.2 and 2.3 may be significant in substrate-limited continuous cultures. In general, k_d (Muck and Grady, 1974, Kim, J. W et al., 1981) and m (Mainzer and Hempfling, 1976, Heijnen and Roels, 1981; Fieschko and Humphrey, 1983) have been found to increase with temperature, with some researchers reporting an Arrhenius relationship over limited temperature ranges, with values for ΔH^* ranging from 24.2 to 83.7 kJ/mol (Marr et al , 1963, Palumbo and Witter, 1969; Mennett and Nakayama, 1971; Topiwala and Sinclair, 1971; Farmer and Jones, 1976; Moletta et al., 1978; Esener et al., 1983; Stevens et al., 1989). It should be pointed out that these values for the temperature characteristic were determined over the Arrhenius range in most cases and with few data. Zhang et al. (1995) determined that the decay coefficient for naphthalene degradation was independent of temperature in the range of 10-22°C. Mainzer and Hempfling (1976) reported a non-linear temperature effect on m in the range of 17.5 to 42°C, with a minimum at the optimum temperature for growth at 37°C.

2.1.4.3 Temperature Effects on Biomass Yield and Maintenance

When analyzing yield data it is essential to distinguish between true yield (Y_g) and apparent yield (Y_{XS}). For various microbial systems (typically for substrates other than phenol), true yield does not appear to vary significantly within the Arrhenius range (Topiwala and Sinclair, 1971; Mainzer and Hempfling, 1976; Moletta et al., 1978; Kim, J. W. et al., 1981; Esener et al., 1983; Fieschko and Humphrey, 1983; Bajpai and Margaritis, 1987; Huang, S.-Y. and Chen, 1988; Zhang, W. et al., 1995); however, at temperatures above some optimum, significant drops in true yield have been reported (Brown and Rose, 1969; Muck and Grady, 1974; Mainzer and Hempfling, 1976; Esener et al., 1983; Bajpai and Margaritis, 1987; Huang, S.-Y. and Chen, 1988), possibly as a result of significant changes in the biosynthetic pathway or uncoupled growth (Mainzer and Hempfling, 1976; Huang, S.-Y. and Chen, 1988).

Observed yield tends to decrease with increasing temperature (Tempest and Hunter, 1965; Topiwala and Sinclair, 1971; Muck and Grady, 1974), likely as a result of increasing maintenance energy requirements or increased decay, observed as an increase in k_d. In a continuous system, at steady state, the following relationship results (Muck and Grady, 1974):

$$Y_{X\,S}(T) = \frac{Y_g(T)}{1 + HRT\ k_d(T)} \tag{2.33}$$

where HRT is the mean hydraulic retention time in the reactor. Muck and Grady (1974) pointed out that for small values of the HRT, Y_{XS} will tend to follow the same relationship with temperature as Y_g, at large values of the HRT, Y_{XS} will decrease because $k_d(T)$ is an increasing function. Note that here k_d is based upon a decreased yield of biomass due to decay rather than an additional consumption of substrate for maintenance purposes as expressed in Equation 2.7.

2.2 Biofilm Processes

2.2.1 Primary Biofilm Formation

Primary biofilm formation refers to the deposition of the initial layer of microorganisms on a support material. Once this layer is formed, the microorganisms reproduce and a biofilm is formed. In this section the mechanisms of primary biofilm formation and the influence of ICFBR operating conditions on the rate of primary biofilm formation will be discussed.

2.2.1.1 Mechanisms of Primary Biofilm Formation

Primary biofilm formation through surface adhesion is the net result of the following processes (Bryers and Characklis, 1982).

1. *Adsorption of organics.* After contacting the support material with the fermentation broth, a conditioning film, usually composed of polysaccharides and glycoproteins (Baier and Weiss, 1975; Baier, 1980), forms on the surfaces within minutes (Bryers and Characklis, 1982). The conditioning film alters the surface either by decreasing its hydrophobicity (Baier, 1975), by giving the surface a negative charge (Loeb and Neihof, 1975), or by affecting the zeta potential, contact potential and critical surface tension (Baier, 1975).

2. *Transport of cells to the surfaces.* Under turbulent flow conditions, cells are transported from the bulk fluid to the conditioned surfaces. Eddy diffusion, frictional drag forces and turbulent bursts of fluid appear to be important means by which particles are deposited (Characklis, 1990).

3 *Adhesion of cells* Adhesion of cells to the substratum is thought to occur in two stages (Marshall et al., 1971, Powell and Slater, 1983): (1) reversible adsorption, followed by (2) irreversible adsorption. Reversible adsorption refers to weak adhesion of the cells due to the presence of long range attractive forces including van der Waals forces, electrostatic interactions and possibly polymer bonding (where the cells are held to the substratum with extracellular polymers) and through one-way chemical reactions with the surface. The degree to which cells adsorb depends on surface properties of the bacteria (which are affected by cell age, growth rate, type of nutrients present and the strain used) as well as substratum surface chemistry and morphology and fluid characteristics. Shreve et al. (1991) reported that the best surfaces for adsorption of *P. putida* were those that were charged, followed by hydrophobic surfaces; hydrophilic surfaces supported little biofilm development. The conditioning film alters the substratum surface and may either inhibit (Meadows, 1971; Tosteson and Corpe, 1975; Fletcher, 1976) or enhance (Meadows, 1971; Fletcher, 1976; Fletcher and Loeb, 1979; Fletcher and Marshall, 1982) cellular adsorption, depending on the system.

Once the first layer of biofilm is in place attachment to the biofilm rather than adsorption to the substratum occurs. The mechanisms are similar to adsorption.

4. *Cell growth and production of extracellular polymeric substances.* Once attached to the substratum, bacteria colonize the surface by reproducing and by producing EPS. Primary biofilm formation is not restricted by substrate or oxygen limitations because the initial biofilm layers are thin; only once the biofilm matures and becomes thick are nutrient limitations likely.

5. *Cell detachment.* Detachment of primary biofilm occurs through erosion and abrasion. Erosion is a continuous process in which small portions of the biofilm are re-entrained into the bulk fluid as a result of hydrodynamic forces. It is likely that turbulent bursts from the bulk fluid penetrate the viscous sublayer and generate a lift force normal to the surface sufficient to detach adsorbed cells (Characklis, 1990). Rougher surfaces may offer protection to the attached cells, reducing the rate of detachment and allowing for growth (Gjaltema et al., 1994; van Loosdrecht et al., 1995a). Abrasion from carrier collisions in fluidized bed bioreactors also causes detachment of cells.

2.2.1.2 Effects of Operating Conditions on Primary Biofilm Formation

The rate of biofilm formation is a function of factors influencing both adhesion and detachment. Some of these factors are reactor variables that can be chosen to favour adhesion or to minimize detachment. The results of studies investigating the effects of operating conditions on primary biofilm formation are described below.

Biomass Concentration

The greater the concentration of cells in the bulk fluid, the greater the probability of contact between cells and the support surface. Duddridge et al. (1982) and Bryers and Characklis (1982) reported increases in deposition rates with increasing biomass concentrations in the bulk fluid in the ranges of $5x10^7$-$5x10^8$ cells/mL and 4.0-19.5 mg total suspended solids (TSS)/L, respectively.

Dilution Rate

Primary biofilm formation occurs more quickly at high dilution rates for a given volumetric COD loading rate (Heijnen et al., 1992). At lower dilution rates, the suspended biomass is washed out more slowly and consumes more substrate, leaving less for the biofilm biomass. It has also been suggested that the unattached biomass can hydrolyse the attachment polymers of the biofilm microbes and for this reason the dilution rate should be greater than the maximum specific growth rate of the microorganisms (Tijhuis et al., 1992a). Note that dilution rate has a much stronger impact once a primary biofilm layer has been established, as there is a trade-off between the benefit of a high dilution rate and the benefit of high biomass concentration for initial attachment.

Growth Phase

The effect of growth phase upon attachement is not consistent across species. Powell and Slater (1982) reported that *Bacillus cereus* cells from the late stationary stage adhered more strongly to a glass surface than other stages during the growth cycle, possibly due to the release of proteins by cell lysis or the excretion of EPS during this stage. Fletcher (1977) reported that log phase cultures of a marine pseudomonad (NCMB 2021) attached to polystyrene most easily, followed by stationary and death-phase cultures. Fletcher (1977) attributed these results to the greater proportion of motile cells in the log phase and also suggested that there may have been different levels of EPS secretions.

Shear Stress

Hydrodynamics strongly influence attachment and detachment. Increasing turbulence decreases the depth of the viscous sublayer next to the substratum, resulting in a steeper velocity gradient across the layer and leading to an increase in the deposition rate (Rutter and Vincent, 1988). Fowler and McKay (1980) have reported a minimum shear stress required for attachment of 2.62-5.38 N/m^2 for various substratum materials (Pyrex, siliconized and plate glass, and stainless steel).

Increasing shear stress, however, may also increase the rate of detachment or reduce sticking efficiency (Bryers and Characklis, 1982; Duddridge et al., 1982; Powell and Slater, 1982), which may counter-balance any increase in transport of cells to the surface. Bryers and Characklis (1982) reported that the number of bacteria (*P. fluorescens*) attached to type AISI 316 stainless steel decreased with increasing shear stress up to a critical range of 6-8 N/m^2, after which the rate of reduction levelled off. Powell and Slater (1982) have reported critical shear stresses of 1-53 N/m^2 required to remove various bacterial species from glass surfaces.

Abrasion

It is expected that abrasion will be a significant factor in determining detachment rates in an ICFBR. In mechanically-stirred tanks, the degree of abrasion is affected by the amount of turbulence (measured as the Reynolds number), the loading of cells on the support particles, the particle size and the volume fraction of particles (Klein and Eng, 1979). It appears that these factors will also influence abrasion in an ICFBR.

For the same glass airlift ICFBR that was used in this research, Patoine (1989) reported that immobilization of *P. putida* Q5 on sand particles was prevented by high levels of turbulence (as a result of riser superficial gas velocity ($u_{G,r}$) of 2.7 cm/s; maximum Reynolds number at the wall of the riser, $Re_w=d_c V \rho_L/\mu_L$, of 1080). At a lower level of turbulence ($u_{G,r}$=1.06 cm/s; Re_w=424), reduced abrasion allowed for biofilm formation.

The concentration of support particles also affects the degree of abrasion and hence the rate of initial biofilm formation. Patoine (1989) reported that the initial colonization time of *P. putida* Q5 at the lower level of turbulence was less at 8 g sand/L (3.7-5 days) than at 20 g sand/L (7 days). Tijhius et al. (1995) also found that startup times were shorter for lower carrier particle concentrations and after long periods of time (around 60 days) a larger portion of the biomass was present as biofilm in the reactor with a lower particle concentration (60% as biofilm at 69 g/L, but only 10% as biofilm at 150 g/L).

Support Particle Characteristics

Although surface chemistry may play a role in primary biofilm formation, the physical characteristics of the support particles may be more important due to the significance of abrasion in ICFBRs. Gjaltema et al. (1997a) found that although bacteria tend to adhere best to hydrophobic or positively charged surfaces (van Loosdrecht et al., 1989), the adhesion of *P. putida* cells in a small airlift reactor was not affected by the surface chemistry of the particles (glass beads); however, roughened glass beads retained more biomass than did the smooth glass beads. Surface roughness is important (Heijnen et al., 1992; van Loosdrecht et al., 1995a) because surface cavities protect the primary biofilm from shear effects and from abrasion arising from collisions between particles. Biofilm development on smooth particles is much slower (Heijnen et al., 1992) or may not occur (Tijhuis et al., 1995). Smaller particle diameters (ie. less than 0.3 mm) favour biofilm development as well, possibly because the impact of larger particle collisions may be more significant (Heijnen et al., 1992).

Temperature

Temperature influences the rate of primary biofilm formation. Fletcher (1977) reported that the attachment (in 2 hours) of a marine pseudomonad (NCMB 2021) to polystyrene decreased when the temperature was reduced from 20°C to 3°C, but that the minimum biomass concentration required for saturation of the attachment surface did not change. She suggested that the reduced attachment may have been due to an increase in the viscosity in the medium or bacterial surface polymers, reduced rates of chemisorption at the low temperature or a change in the physiology of the microorganisms.

In airlift reactors, where detachment due to abrasion plays an important role, van Loosedrecht et al. (1995a) reported that temperature in the range of 11-20°C strongly influenced the rate of primary biofilm formation on smooth quartz sand, possibly because the slow growth rates at lower temperatures are not able to compete with the rate of detachment. This effect was not as severe for a rough carrier (pumice particles), possibly because the rough surface offered shelter to attached cells.

Although the discussion has focussed upon primary biofilm formation, it is likely that many of the factors mentioned are also important once the biofilm has developed more fully. Biofilm development occurs over fairly long periods of time. Periods of 16-45 days (Heijnen et al., 1992; Tijhuis et al., 1993; van

Loosdrecht et al., 1995b) are typical prior to reaching steady state with respect to the biofilm at constant operating conditions.

2.2.2 Biofilm Characteristics

Biofilms are complex mixtures of cells and EPS, which enable the cells to stick to supporting surfaces. The make-up and properties of biofilms depend on the constituent microorganisms and environmental conditions such as the availability of nutrients and oxygen, and the degree of turbulence and abrasion to which the biofilm is exposed. Understanding of biofilm properties is important because they influence biofilm processes such as mass transport within the biofilm and detachment, which are of interest to the biochemical engineer. This section will discuss assumptions that have been made about biofilm characteristics and the modelling approaches taken.

2.2.2.1 Biofilm Structure

Until recently, biofilms have been conceptualized as cells embedded uniformly in a gel-like matrix of extracellular polysaccharides. Virtually all biofilm models have assumed a homogeneous distribution of components and properties (Howell and Atkinson, 1976; Rittmann and McCarty, 1980a; Park et al., 1984b; Suidan et al., 1987; Livingston and Chase, 1989) in order to simplify the model even when more than one microbial species are present. In these models, gradients were one dimensional and mass transport was assumed to be through diffusion only. These assumptions were assumed to be appropriate until researchers began to take a closer look at biofilm structure.

Recent advances in experimental techniques have revealed highly heterogeneous structures in some biofilms with clusters of cells separated by channels which extend deep into the biofilm (de Beer et al., 1994a, b; Bishop et al., 1995; de Beer and Stoodley, 1995; Massol-Deya et al., 1995; Okabe et al., 1997) and which extend beneath the cell clusters in thicker biofilms (180 μm. thick and thicker) (de Beer et al., 1994b). The void fraction is in the order of 50% (de Beer et al., 1994b) and the surface area for exchange is about twice that of a planar surface (de Beer et al., 1994b). Convective transport has been observed in the channels (de Beer et al., 1994a; Nagaoka and Sugio, 1994; de Beer and Stoodley, 1995; Okabe et al., 1997) which challenges the

classical modelling assumption of diffusive transport only. Most of the work on biofilm structure has been done using flow cells or concentric-tube reactors, which are low-shear systems.

Modelling of these structures has been hampered by a lack of information. Nagaoka and Sugio (1994) have developed a turbulent-diffusion model which allows for convective transport within the biofilm; however, because it was developed for an open-channel type reactor, it may not be easily transferable to other biofilm reactor types. It has been suggested that because of the diversity in biofilm structures, neural networks may eventually be used to model biofilm growth instead of mechanistic models (de Beer and Muyzer, 1995).

The significance of heterogeneous structures in ICFBRs in which there is high shear due to abrasion, has not been thoroughly investigated. Biofilms in both full-scale and bench-scale airlift ICFBRs vary from very smooth to very rough (van Loosdrecht et al., 1995a). Van Loosdrecht et al. (1995a) suggested that biofilms will preferably grow in highly heterogeneous structures with protuberances. The structure that results appears to depend upon a balance between the rates of growth and detachment, which depends upon the substrate loading rate and the level of abrasion in ICFBRs. They suggested that at high particle shear rates, the protuberances do not have a chance to grow to macroscopic proportions; similarly at low organic loading rates, the bacteria grow slowly and the protuberances are eroded as they form, resulting in a smooth biofilm. They hypothesized that at low shear rates and/or at high organic loading rates, the biofilms grow preferentially in the form of protuberances without a strong detachment mechanism to keep the biofilm in check. These hypotheses were confirmed by the work of Kwok et al. (1998). They found that in a fluidized-bed airlift reactor, the biofilm on the basalt carrier particles became thinner and smoother, as the particle concentration was increased (resulting in a higher detachment force). This effect was counterbalanced by increased substrate loading rates, which resulted in less dense biofilms. At a high substrate loading (20 kg COD/m^3.d), a filamentous biofilm structure was regularly observed.

The morphology or composition of the biofilm may also change in response to shock loading or dynamic conditions. For example, Worden and Donaldson (1987), who assumed the existence of an average species, noted changes in the physical appearance, density, growth rate and relative concentrations of the species of the biofilm over a period of dynamic experimentation. Physiological changes may also occur in pure cultures. For example, oxygen deprivation (Jensen and Woolfolk, 1985), high temperatures (Kolenc et al., 1988) and large shock loads of phenol (Tang et al., 1987) may trigger filamentous growth.

2.2.2.2 Biofilm Thickness

The biofilm is usually assumed to be uniformly distributed on each particle for modelling purposes. Some researchers have noted patchy (Livingston, 1991) or highly branched biofilms (Livingston and Chase, 1989; Patoine, 1989), depending on the substrate or hydrodynamic conditions. The biofilm thickness is also assumed to be of average thickness throughout the reactor. In practice, bioparticles are not the same size, which leads to stratification in conventional fluidized bed bioreactors (Andrews, G. F., 1982; Kwok et al., 1998). In airlift reactors, the shear stress and substrate are more uniformly distributed than in conventional fluidized bed reactors, so biofilm thickness are expected to be more uniform (Kwok et al., 1998). Typical biofilm thicknesses in ICFBRs are in the range of 12-500 μm (Tang et al., 1987; Worden and Donaldson, 1987; Wagner and Hempel, 1988; Hermanowicz and Cheng, 1990). Biofilm thickness is closely linked with biofilm density (Kwok et al., 1998) and will be discussed further in Section 2.2.2.3.

2.2.2.3 Biofilm Density

Most biofilm models include the assumption of constant biofilm density regardless of biofilm thickness or location within the biofilm (Howell and Atkinson, 1976; Rittmann and McCarty, 1978, 1980b, 1981; Benefield and Molz, 1983; Suidan, 1986; Suidan et al., 1987; Worden and Donaldson, 1987). However, a number of researchers have reported that biofilm dry density varies with biofilm thickness (Hoehn and Ray, 1973; Tang and Fan, 1987; Tang et al., 1987; Livingston and Chase, 1989; Cheng and Hermanowicz, 1990; Hermanowicz and Cheng, 1990; Coelhoso et al., 1992). Biofilm dry density is defined as the mass of dry biomass (as volatile solids or dry weight) per unit volume of wet biofilm. In general, biofilm dry density was observed to decrease with increasing thickness (Tang and Fan, 1987; Livingston and Chase, 1989; Cheng and Hermanowicz, 1990; Coelhoso et al., 1992; Zhang, T. C. and Bishop, 1994b) from 70-220 kg/m^3 for thin biofilms (less than 50 μm)(Tang and Fan, 1987; Livingston and Chase, 1989) to some limiting value (25-60 kg/m^3) (Hoehn and Ray, 1973; Cheng and Hermanowicz, 1990; Coelhoso et al., 1992; Bishop et al., 1995) as the biofilm thickness increases, possibly due to endogenous respiration and decay in the inner layers due to oxygen or substrate limitations (Hoehn and Ray, 1973). In another study, the active outer layer (dry density of 160 kg/m^3) was found to be more dense than the inner layer (density of 81 kg/m^3) which was inactive (Gjaltema et al., 1997c). Cheng and Hermanowicz (1990) did not find a relationship between biofilm dry

density and biofilm thickness, particularly below biofilm thicknesses of 35 μm; however, they did find a decreasing exponential relationship between the average dry density of the bioparticles and biofilm thickness. There was considerable scatter in the data for thin biofilms, possibly because they used only 15 particles per sample.

Biofilm density also depends upon shear, which influences biofilm thickness, and upon the type of microorganisms. Highly branched biofilms, typical of low-shear systems, consume much of the substrate before it reaches the base biofilm, resulting in little growth and lower densities in the inner portion of the biofilm (Kaballo et al., 1995). In high shear systems with smooth biofilms, deeper penetration of the substrate by diffusion results in higher densities because cells are growing throughout the biofilm (Horn and Hempel, 1997). Also, biofilms with slowly-growing bacteria tend to be more dense. (van Loosdrecht et al., 1995a).

Biofilm density for mixed populations has also been found to increase with increasing shear stress at low substrate loadings (Characklis and Christensen, 1990) and increased abrasion in ICFBRs (Mulcahy and Shieh, 1987; Wagner and Hempel, 1988). Biofilm density may also be related to substrate loading (Characklis and Christensen, 1990) and biofilm age (Hoehn and Ray, 1973). Kwok et al. (1998) have reported that in fluidized-bed airlift reactors, the biofilm density, thickness and structure are determined by the balancing effects of detachment forces and the biomass surface production rate, which are a result of the carrier concentration and the substrate loading. They have found that at high carrier concentrations, thin dense biofilms are produced. At high substrate loading rates, the biomass production rate at the surface of the bioparticles is high, and the tendency is towards thick, porous, heterogeneous biofilms, unless counterbalanced by a high detachment force.

A number of empirical models have been developed to describe the changes in biofilm density, although none include the balancing effects of substrate loading and detachment force. Benefield and Molz (1985) have incorporated a decay-related density-change term in their biofilm model. Using a different approach, Tang et al. (1987) constructed an empirical correlation which was used to calculate biofilm dry density as a point property at any radius within the film. Cheng and Hermanowicz (1990) proposed a relationship between the dry density of the bioparticle (including the carrier) and biofilm thickness. Wanner (1995) pointed out that the change in density with time is likely due to a change in porosity as the void spaces

between cell clusters are filled in with growing cells; they presented an empirical correlation for the liquid-phase fraction. It is not clear if any of these models can be transferred to other systems with different carriers, microorganisms or hydrodynamics.

2.2.2.4 Biofilm Activity

Most researchers have assumed in their biofilm models that all the biofilm is active (Young and Bungay, 1973; Sáez and Rittmann, 1988; Kim, B. R. and Suidan, 1989; Livingston and Chase, 1989). However, a portion of the biofilm (up to 90% of the biofilm organic carbon (Bakke et al., 1984) or as little as 3% (Ohashi and Harada, 1996)) may be composed of EPS. The rate of EPS production varies inversely with the rate of growth (Robinson, J. A. et al., 1984), so slowly growing biofilms or the inner layers of a biofilm may have higher EPS concentrations. Neglecting EPS in the biofilm may result in an overprediction of reaction rate (Worden and Donaldson, 1987) or may otherwise distort biofilm kinetics (Bakke et al., 1984). Also, up to 50% of the bacteria present in a biofilm may not be metabolically active (Rittmann et al., 1992). This will depend upon the extent of penetration of the substrate and other essential nutrients. Bishop et al. (1995) found that the fraction of viable cells decreased from 72-91% in the top layer of a biofilm to 31-39% near the substratum interface. Subsequently, Zhang and Bishop (1994b) found that for very thick biofilms (up to 1000 μm thick) in flow cells only one-quarter to one-seventh of the biofilm was active in the bottom layer (although biofilms of this thickness would not be expected in an ICFBR). Thus, the presence of an inactive fraction, either due to EPS, inactive bacteria, or both, should be considered when modelling biofilms.

Several researchers have included the concept of an inactive fraction in their models. Kissel et al. (1984) and Gadani et al. (1993) included inactive fractions in their multi-species biofilm models to allow for the production of decay products within the biofilm. The production of inert material through the formation of EPS was not included. In trial simulations, both models predicted little change in the inactive fraction with depth in the biofilm for thin biofilms (<100 μm). The model of Kissel et al. (1984) (which did not include detachment) predicted variations in the inactive fraction of up to 20% across the biofilm when biofilm thicknesses became large (up to 300 μm) and that the biofilms were substrate- and oxygen-depleted. The results of the simulations were not confirmed experimentally. The inactive fraction of a fully developed fluidized-bed biofilm which is subject to shearing and abrasion can likely be assumed to be constant across the biofilm profile and over long

time periods as long as the biofilm remains relatively thin (<100 μm) and does not become substrate or oxygen depleted in the inner layers.

2.2.3 Mass Transfer in Biofilms

Mass transfer limitations significantly affect the performance of biofilm reactors and their response to inhibitory or dynamic conditions. The effects of both external and internal mass transfer resistance on substrate concentration within the biofilm are shown in Figure 2.5, which illustrates the three characteristic substrate concentration profiles defined by Rittmann and McCarty (1981). When the biofilm is fully penetrated (ie. for thin biofilms or slow reactions relative to the diffusion rate), the substrate concentration within the biofilm (S_f) is equal to the substrate concentration at the biofilm surface (S_s). In deep biofilms the substrate is depleted at or before the particle surface. In shallow biofilms, the substrate concentration at the surface of the particle is between zero and S_s. Similar profiles could be constructed for oxygen and other nutrients.

2.2.3.1 External Mass Transfer

The mass transfer of dissolved oxygen to the biofilm is controlled by the resistances of the gas film, the gas-liquid interface, the liquid film at the gas bubble interface, the bulk liquid resistance and the liquid-biofilm interface. In a well-mixed system and for sparingly-soluble gases such as oxygen, usually only the liquid film and the liquid-biofilm resistances are considered to be of importance.

In a well mixed system, only the liquid-biofilm resistance is considered to be important to the mass transfer of the substrate to the biofilm.

Liquid Film Resistance

The main resistance to the transport of oxygen from the gas bubbles to the liquid phase is the liquid film resistance. The rate of oxygen transfer from the gas phase to the liquid phase can be described as:

$$\frac{dC_O}{dt} = K_L a V_L (C_O^* - C_{Ob}) \tag{2.34}$$

where K_La is the overall volumetric gas-liquid mass transfer coefficient, V_L is the volume of liquid in the reactor, C_o^* is the equilibrium dissolved oxygen concentration at the gas-liquid interface and C_{Ob} is the

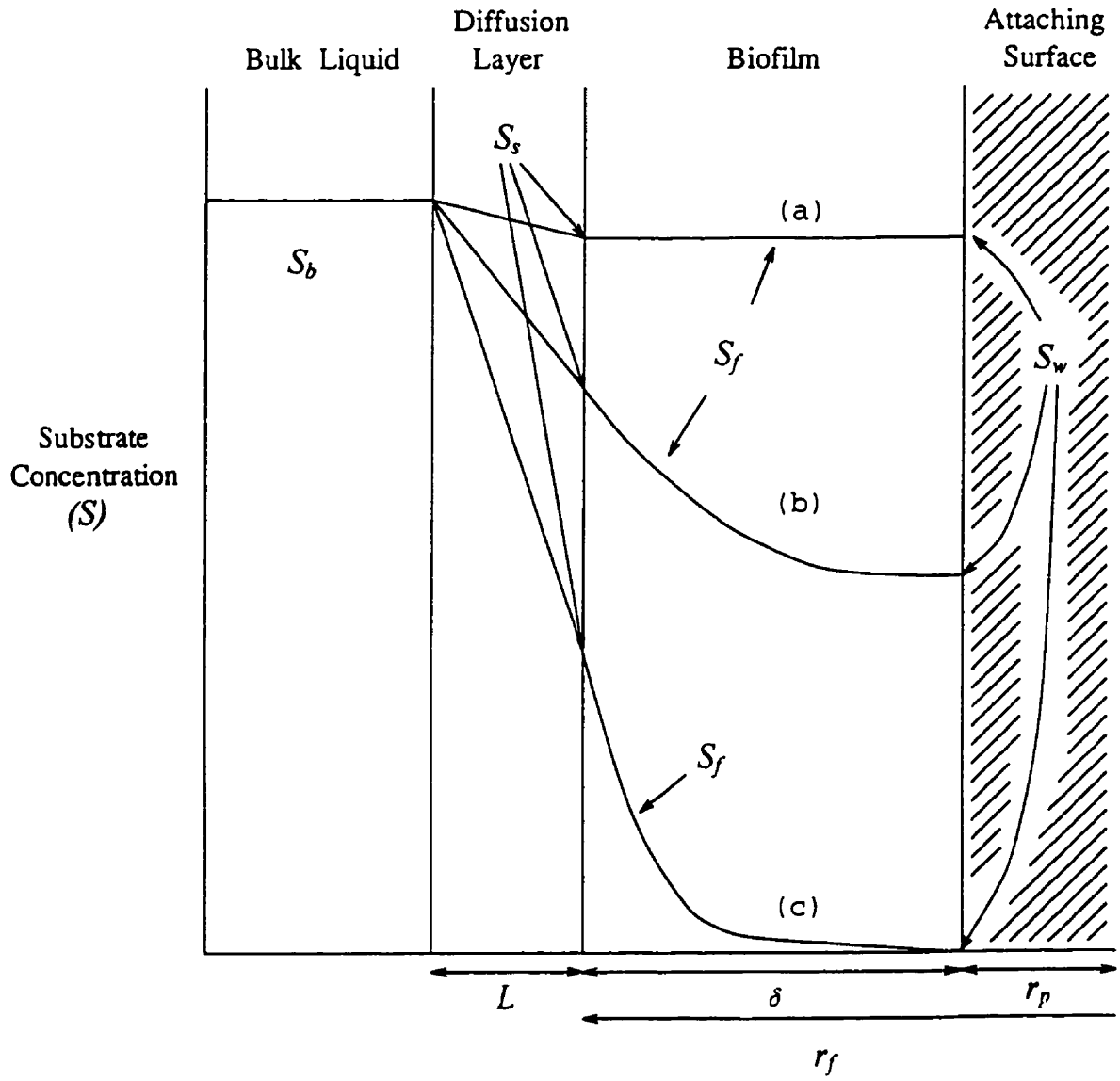

Figure 2.5. Substrate Profiles Within Idealized Biofilms

(a) a fully penetrated biofilm, (b) a shallow biofilm and (c) a deeply penetrated biofilm (after Gantzer, 1989 and Suidan et al., 1987)

dissolved oxygen concentration in the bulk fluid. Empirical correlations developed to predict $K_L a$ in airlift reactors are discussed in Section 2.4.2

Liquid-biofilm Mass Transfer Resistance

Depending upon system hydrodynamics, the resistance to mass transfer from the bulk fluid to the surface of the biofilm can be important in biofilm systems (Williamson and McCarty, 1976). The substrate transfer rate is expressed as

$$-\frac{dS}{dt} = k_s a_s (S_b - S_s) \tag{2.35}$$

where S_b is the bulk substrate concentration, k_s is the liquid-biofilm mass transfer coefficient for the substrate, S_s is the substrate concentration at the external surface of the biofilm and a_s is the interfacial area of the biofilm surface per unit liquid volume. The model for the rate of oxygen transfer is given as

$$-\frac{dC_O}{dt} = k_l a_s (C_{Ob} - C_{Os}) \tag{2.36}$$

where C_{Ob} and C_{Os} are the oxygen concentrations in the bulk fluid and at the biofilm surface, respectively, and k_l is the oxygen mass transfer coefficient across the liquid-solid boundary layer.

Liquid-biofilm mass transfer resistance has been neglected in many biological fluidized bed models (Shieh, 1980; Stathis, 1980; Mulcahy et al., 1981, Andrews, G. F., 1982; Park et al., 1984a, b; Worden and Donaldson, 1987; Hermanowicz and Cheng, 1990; Coelhoso et al., 1992) without establishing that the mass transfer resistance was negligible. The importance of liquid-biofilm mass transfer depends upon the rate of liquid-biofilm mass transfer relative to the rate of reaction (which depends on biofilm thickness, density and activity) (Tang and Fan, 1987). Thus, liquid-biofilm mass transfer should not be considered negligible without evaluation of the system.

Liquid-biofilm mass transfer has been found to be important in some airlift ICFBRs (Tijhuis et al., 1995). Livingston and Chase (1989) determined decreases of 16-54% in the substrate concentration across the liquid-biofilm boundary layer. Tang and Fan (1987) found that neglecting liquid-biofilm mass transfer would cause a 15% error in predicting the phenol degradation rate in their experiments. From steady-state modelling

studies, Suidan et al. (1987) predicted that the influence of the liquid-biofilm boundary layer depends upon the degree of penetration of a substrate in the biofilm, with less effect with full penetration. Thus the effect of liquid-biofilm mass transfer is likely to be more important when there is strong diffusional resistance to mass transfer within the biofilm (eg., dense biofilms). Using microelectrodes, Zhang and Bishop (1994a) found that the external mass transfer resistance was significantly reduced when the organic loading was increased only when the biofilm was in a diffusion-controlled regime; when the kinetics were reaction-controlled there was no significant effect of organic loading.

The presence of the diffusion boundary layer may also be important even with highly heterogeneous biofilms with channels (which are less dense). De Beer and Stoodley (1995) reported that the diffusion boundary layer in such biofilms was significant at low flow velocities (less than 0.04 m/s). The diffusion boundary layer decreased with increasing flow velocities and increasing surface roughness (Zhang, T. C. and Bishop, 1994a; Bishop et al., 1997). Because of the potential importance of liquid-biofilm mass transfer resistance, external mass transfer should not be neglected without careful consideration when developing dynamic ICFBR models.

2.2.3.2 Internal Mass Transfer

The structure of the biofilm has a profound impact upon how substrate, dissolved oxygen and other nutrients are transported through the biofilm. Until recently it was assumed that diffusion, as a result of concentration gradients, was the sole process by which dissolved components penetrated the biofilm. All the biofilm models to date employ diffusive transport exclusively.

Recent studies using microelectrodes and flow cells have revealed that liquid flow may occur in the void spaces found in heterogeneous biofilms, although liquid is stagnant in the cell clusters (de Beer et al., 1994a; de Beer and Stoodley, 1995). For such biofilms, a three-dimensional model for calculating mass transport is necessary, because diffusion occurs in directions normal to the cell clusters. The horizontal component of the dissolved oxygen gradient was as important as the vertical gradient in a microelectrode study of a heterogeneous biofilm grown in a flow cell (de Beer et al., 1994b). Convective transport must also be included. Unfortunately, convective transport within biofilms is poorly understood. The existence of cell clusters and channels in the structure does not always imply convective transport; at low liquid flow velocities

(<0 04 m/s), de Beer and Stoodley (1995) reported that there was no flow in the void spaces and that the biofilm behaved as if it were a homogeneous structure with diffusion as the principal mass transport mechanism. In the cell clusters, substrate is transported by diffusion only; de Beer and Stoodley (1995) were able to characterize the cell clusters as being similar to a gel network with pore diameters of 80 nm. Biofilms with fairly homogeneous structures are not uncommon in fluidized-bed airlift reactors, so diffusion alone will be applied to the transport of substrate through the biofilm.

Diffusion within a film formed on a spherical bioparticle follows Fick's second law (Bird et al., 1960) given as:

$$\frac{\partial C}{\partial t} = D_{c,f}\left(\frac{\partial^2 C}{\partial r^2} + \frac{2}{r}\left(\frac{\partial C}{\partial r}\right)\right) \tag{2.37}$$

where $D_{c,f}$ is the effective diffusion coefficient of component c in the film, C is the concentration of component c and r is the radial position within the film..

In his review of diffusion coefficients in biofilms, Stewart (1998) makes several important distinctions. Equation 2.37 applies to a uniform film. Biofilms consist of a number of compartments including the extracellular aqueous phase, cells, EPS, precipitates, silt or fibrous material and possibly gas bubbles (Stewart, 1998). The concentration C, in Equation 2.37 refers to the volume-averaged concentration of component c in the total biofilm at a given radial position, r. The effective diffusion coefficient described in Equation 2.37 is determined from transient data. Another parameter, the effective diffusive permeability, D_e, is defined as:

$$J = -D_e \nabla C_{aq} \tag{2.38}$$

which depends upon the concentration gradient of the component in the aqueous phase, ∇C_{aq}. The aqueous-phase concentration is the one applied to kinetic expressions or that is measured using a diaphragm cell (Stewart, 1998). There appears to be some confusion about this concept in the literature, as many of the 'effective diffusion coefficients' appear to have been determined in such a way to yield the effective diffusive permeabilities instead. The two parameters have different applications. For reaction-diffusion analysis, Stewart (1998) suggests the use of the effective diffusive permeability. The effective diffusion coefficient is to be used for the analysis of unsteady-state behaviour of non-reactive solutes. Thus, when

substrate with a concentration in the aqueous phase, S, is consumed as it diffuses through a biofilm, the appropriate expression is:

$$\frac{\partial S}{\partial t} = D_{S,w}\left[\frac{\partial^2 S}{\partial r^2} + \frac{2}{r}\left(\frac{\partial S}{\partial r}\right)\right] - R_S \qquad \textbf{(2.39)}$$

where R_S is a reaction term for the consumption of substrate.

The effective diffusive permeability is difficult to measure. Often it is expressed as a fraction of the diffusion coefficient of the component in water ($D_e D_w$); this ratio is called the relative diffusive permeability. $D_e D_w$ can vary widely, ranging from 0.05 to 1.1 in the literature (Stewart, 1998) for determinations made using intact biofilms. Stewart (1998) attributed the variation in relative effective diffusive permeability measurements to differences in biofilm composition and the chemical properties of the solute. He reported that the biofilm density had a significant effect upon the relative diffusive permeability of a wide range of solutes. The effect of biofilm density upon $D_e D_w$ for phenol is shown in Figure 2.6. The effective diffusion coefficient (and presumably effective diffusive permeability) has also been shown to vary with total biofilm thickness (Tang and Fan, 1987; Tang et al., 1987).

Fan et al. (1990) developed the following correlation between the ratio of diffusivities in the biofilm and the water and the total dry biofilm cell density (ρ_f) [kg/m^3], applied to the range of 12-400 kg/m^3:

$$\frac{D_e}{D_w} = 1 - \frac{0.43\,\rho_f^{0.92}}{11.19 - 0.27\,\rho_f^{0.99}} \qquad \textbf{(2.40)}$$

This empirical equation was based on their experimental work combined with literature results for different types of biofilms and flocs (from 11 other sources), substrates and temperatures (between 15-30°C). This was used to determine a point effective diffusivity within the biofilm using a correlation of dry density with biofilm thickness. It is likely that many of the biofilms used to develop this correlation, particularly those from flat surfaces, rotating cylinders and bioflocs, were highly heterogeneous in nature and may have been subject to convective transport as well as diffusive transport.

Beyenal et al. (1997) developed the following correlation for the effective diffusivity of phenol , D_{Sf} [m^2/s], in biofilms at 25°C in a differential fluidized bed reactor.

$$D_{S,f} = 8.154 \times 10^{-10} \times 10^{-0.0070053X_f} \quad (2.41)$$

where X_f was the biofilm dry density [kg dry microorganisms/m^3]. The effective diffusivities determined in their experiments ranged from 17–44% of the value in the medium. The models of Fan et al. (1990) and Beyenal et al. (1997) are compared in Figure 2.6. The model of Fan et al. (1990) appears to fit the data better.

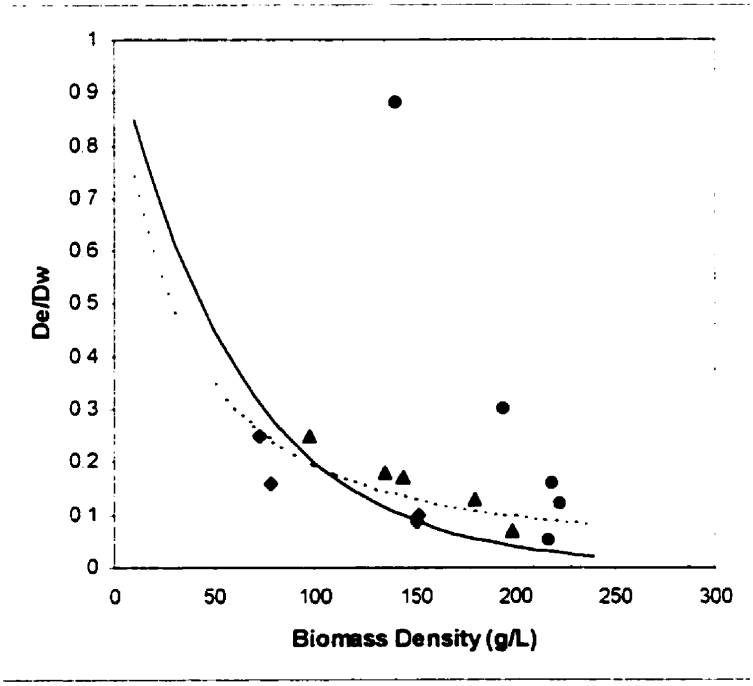

Figure 2.6. Relative effective diffusive permeabilities in ICFBR biofilms for phenol using the data of Tang and Fan (1987) [◆], Livingston and Chase (1989) [●] and Fujie et al. (1979) as cited in Fan et al. (1990)[▲] (adapted from Stewart, 1998). The curves were generated using the models of Fan et al. (1990) [- - - -] and Beyanal et al. (1997) [——].

Effective diffusivity likely varies within the biofilm profile (Cheng and Hermanowicz, 1990; Bishop et al., 1995; van Loosdrecht et al., 1995a) because biofilm density is not constant. Bishop et al. (1995) found that biofilm porosity of a heterogeneous biofilm decreased from 84-93% in the top layer to 58-67% in the bottom layer. There was a corresponding decrease of the effective diffusivity for glucose from 50-81% of the value in water at the surface to 20-50% of the value in water at the bottom layer. They found that a cylindrical model used to describe diffusion through catalysts worked well because it allowed for varying diffusivity with depth.

2.2.3.3 Effects of Temperature on Mass Transfer

Internal Mass Transfer

The effect of temperature on the diffusivity of a dissolved substance in water can be described by a modified version (Hayduk and Laudie, 1974) of the Wilke-Chang correlation (Wilke and Chang, 1955):

$$D_{S,w} = \frac{(7.4 \times 10^{-8})(2.26\, M_w)^{0.5} T}{\mu_w V_M^{0.6}} \tag{2.42}$$

where $D_{S,w}$ is the diffusivity of the substance in water, M_w and μ_w are the molar mass and viscosity [cP] of water, respectively, and V_M is the molar volume of the substance at the normal boiling point [cm^3/gmol].

The viscosity of water (in $N \cdot s/m^2$) is given by (Touloukian et al., 1975)

$$\mu_w = 2.414 \times 10^{-2}\, 10^{\frac{247.8}{T - 140}} \tag{2.43}$$

for T in degrees Kelvin.

External Mass Transfer

The effect of temperature on gas-liquid mass transfer depends upon the influence of temperature upon the driving force and the overall volumetric mass transfer coefficient, K_La. The driving force is controlled by the saturation concentration of oxygen in water, for which the temperature dependency is known, and the concentration of oxygen in the bulk liquid, which is in part dependent upon the oxygen uptake rate of the microorganisms, for which the temperature dependency will be known. There is very little information about the effect of temperature on K_La in airlift reactors in which there are solid particles. Many of the correlations for K_La are linked to the superficial gas velocity and the gas holdup. Saxena et al. (1992) investigated the effect of temperature in the range of 24-80°C on gas holdup in a bubble column containing glass beads and concluded that temperature effects could be neglected for particle diameters greater than 0.150 mm. The implication of this study on the effect of temperature on K_La in an airlift reactor containing bioparticles with particle diameters greater than 0.200 mm is not clear.

The effect of temperature on the liquid-solid mass transfer coefficient (k_S) in three-phase airlift reactors has not been investigated. Because the correlations for k_S, described in Section 2.4.2.2, depend on the

physical properties of the solvent and the diffusivity of the dissolving substance, adjusting k_S by correcting the values of $D_{S,w}$ and μ_w, according to Equations 2.42 and 2.43, respectively, is a reasonable approximation.

2.2.4 Detachment

Detachment refers to the removal of both cells and EPS from the attached biofilm to the medium and may result through erosion, sloughing and abrasion. Erosion (the loss of individual or small groups of cells) and sloughing (the loss of large portions of the biofilm) result from shear and normal forces exerted by the moving fluid, as well as internal biofilm processes such as decay and gas bubble formation. In an ICFBR, abrasion resulting from particle-particle collisions is the most important detachment mechanism (Tijhuis et al., 1995, Gjaltema et al., 1997c).

2.2.4.1 Erosion and Abrasion

Currently, there is not enough information on the interrelationships between hydrodynamics, abrasion effects and biofilm characteristics to predictively model biofilm detachment (Wilderer et al., 1995). Only recently has some work has been done to characterize detachment in three-phase ICFBRs.

Gjaltema et al. (1995, 1997b, c) studied detachment of non-growing bioparticles (0.5-1 mm in diameter) with basalt as the carrier. Although detachment is not necessarily the same for growing and non-growing biofilms (van Loosdrecht et al., 1995a), the results may be generally applicable to the system in this study. They determined that the specific detachment rate was approximately constant (3.2×10^{-3} h^{-1}) at various bioparticle concentrations as long as the bare carrier concentration was the same. Collisions with bare carrier particles appeared to be the dominant detachment mechanism (also reported by Tijhuis et al., 1995) and they obtained a linear detachment rate as a function of bare carrier concentration. This agrees with the findings of Tijhuis et al. (1992b), who determined that the detachment rate depended upon the particle concentration and that the substrate loading influenced the biofilm thickness, but not the detachment rate. Gjaltema et al. (1997b) also reported that the detachment rate was higher for larger particles, because the impact of collisions was greater; however, it is not simply a function of size and mass. Surface roughness was found to be very important as well (Gjaltema et al., 1997b). Sand grains, which had rounded edges, caused less damage than irregular and sharp-edged basalt particles of the same size and mass. Although

gas hold-up and bubble size were affected by the bioparticle concentration, gas hold-up did not appear to affect the detachment rate.

Several detachment models have been developed for idealized ICFBR systems in which particle-particle interactions are neglected (Tang et al., 1987; Gadani et al., 1993). Other ICFBR models assume that an equilibrium is reached between the growth rate of the biomass and detachment (Kissel et al., 1984; Livingston and Chase, 1989); thus the biofilm thickness is considered to be a constant known value at constant operating conditions. However, accurate prediction of the biofilm thickness (and thus detachment rates) under different or varying operating conditions is important because biomass loading is an important design parameter (Mulcahy and Shieh, 1987).

Chang et al. (1991) identified turbulence and attrition through abrasion as the most important factors controlling detachment in a biological fluidized bed reactor. The following empirical model was developed for the specific biofilm detachment rate coefficient, r_D [day^{-1}]:

$$r_D = -3.14 - 0.0335 C_p - 19.3 Re_p - 3.46\tau \qquad \textbf{(2.44)}$$

where C_p is the particle concentration [g/L], Re_p is the particle Reynolds number ($Re_p = \rho d_p \mu \mu_l$) and τ is the liquid shear stress [dyne/cm^2]. Use of this model is limited to reactor systems similar to the one used in their study (a two phase fluidized bed with glass beads as the support medium).

Tang et al. (1987) developed an empirical detachment model for an internal loop airlift ICFBR which depended solely on the biofilm volume on a single bioparticle (V_{bp}). Their model,

$$r_D = 3.4 \times 10^4 \rho_f V_{bp} \qquad \textbf{(2.45)}$$

is applicable to their system only under the conditions (ie C_p, Re_p, τ) for which it was developed.

Nicolella et al. (1996) reported that detachment was a strong function of the liquid velocity in a two-phase fluidized-bed reactor with sand as a carrier. Particle concentration and liquid shear stress also influenced detachment, but were less significant. Their correlation was based upon dimensionless numbers and may be transferrable to other systems; however, it was developed for a narrow range of values of shear stress (0.14-0.17 N/m^2).

2.2.4.2 Sloughing

Detachment through erosion and abrasion (occurring near the upper layer of the biofilm) is a continuous process, whereas sloughing is a sporadic process involving the removal of large portions of the biofilm, possibly to the level of the support particle. Sloughing is common in biofilms exposed to low-shear conditions (Ohashi and Harada, 1994) in which they form thick, low-density and heterogeneous structures. Sloughing has been observed when the biofilm is subjected to concentrated shock loadings of substrate (Bakke, 1983; Donaldson et al., 1987) and when internal layers of the biofilm become substrate or oxygen depleted (Wagner and Hempel, 1988; Applegate and Bryers, 1991). Sloughing has been induced by the addition of EGTA, a calcium-specific chelant (Turakhia et al., 1983), likely because of an important role of calcium in preserving the structural integrity of the biofilm. Sloughing has also been induced by transferring biofilms from a medium with a high concentration of calcium (100 mg/L) to a medium without calcium (Huang, J. and Pinder, 1995).

Sloughing has also been attributed to the presence of nitrogen bubbles produced by denitrifying bacteria within the biofilm (Harremoës et al., 1980). Using video monitoring to observe an open channel flow reactor, Ohashi and Harada (1994) determined that gas vacuole formation in a denitrifying biofilm was an important cause of sloughing. They observed that sloughing was also caused by cavity formation, possibly as a result of varying density at the biofilm-substratum interface at high growth rates. Although sloughing has not been attributed to the production of carbon dioxide from the oxidation of substrates within biofilms, the presence of carbon dioxide in a biofilm has been noted in an ICFBR degrading phenol where it may have caused "lift-out" of the bioparticles (Patoine, 1989). The possibility of "lift-out" or sloughing due to carbon dioxide production would place a limitation on the allowable organic loading to an ICFBR system (Krouwel and Kossen, 1981; Patoine, 1989).

Sloughing is not yet well understood (Nielsen and Harremoës, 1995) and predictive detachment models including sloughing have not yet been developed. However, existing biofilm models can be used to predict some conditions under which sloughing may occur, such as substrate or oxygen depletion in the inner layers of the biofilm.

2.2.5 The Effects of Immobilization on Microbial Kinetics

It is important to consider the effect of cell attachment on cell physiology and on cell response to an inhibitory substrate such as phenol. In all models developed to date, the kinetics of immobilized cultures have been assumed to be identical to those of suspended cell cultures under otherwise the same environmental conditions. Undoubtedly, the physiology of attached cells differs from suspended cells. What is relevant in this work is the significance of the impact of any physiological changes of immobilization upon phenol biodegradation kinetics and the extent to which this should (or could) be included in an ICFBR model.

Bakke et al. (1984) reported that when the presence of accumulated EPS in the biofilm was taken into account, there was no difference at a 5% level of significance between the rate of uptake of glucose in suspended cell and biofilm cultures of *P. aeruginosa* as long as the microenvironment of the cells (eg. pH and substrate concentration) was the same. They also reported that when total biomass (as suspended solids) without EPS accounted for was used as a measure of biomass concentration, the kinetics of suspended and biofilm cultures would have appeared to be different. Thus incorporation of the EPS content of the biofilm into a model may be important when applying yield and rate data from suspended cell cultures to biofilm systems.

Van Loosdrecht et al. (1990) have critically reviewed the recent literature on cell immobilization and have tried to replicate some of the experiments. They concluded that there is no clear evidence of changes in cell physiology upon attachment to a surface. Many of the observed effects of biofilms can be attributed to mass transfer effects or other changes in the cell environment arising from biofilm formation.

Karel et al. (1985) have also critically reviewed the immobilization literature and concluded that although under certain conditions the metabolic activities of free and immobilized cells may differ, it is not possible to predict how they will differ. Because the reaction behaviour of free and immobilized cells is essentially the same for so many cases, they suggested that it be assumed that activity does not change upon immobilization.

However, in other studies, immobilization has been reported to alter cell physiology in ways that may affect the response of cells to phenol. Keweloh et al. (1990b) reported that the protein to lipid ratio of immobilized *E. coli* K12 was higher than for a suspended cell culture, with and without phenol in the medium (Keweloh et al., 1990a). This difference in cell membrane structure may increase the rigidity of the cell membrane and improve the ability of the cell to prevent leakage of cell constituents (Keweloh et al., 1990b).

Immobilization of *S. cereviseae* has been found to lower the total unsaturated fatty acid level and raise the levels of shorter-chain residues in the cell membrane (Hilge-Rotmann and Rehm, 1990). Hilge-Rotmann and Rehm (1990) suggested that these changes may be responsible for the increased tolerance of the cells to ethanol (which seems to have a similar effect on cells as phenol).

Although increased tolerance of immobilized cells to phenol has been observed (Heipieper et al., 1990, 1991; Keweloh et al., 1990a), it is not clear that it is due to physiological changes resulting from immobilization or if it is due to changes in the cell environment caused by mass transfer limitations. Heipieper et al. (1991) found that for cells immobilized in calcium alginate, similar protective effects were observed with 1.5 and 3.2 mm diameter beads; thus, the different times of diffusion of substrate (4-chlorophenol in this case) into the gel matrix and efflux of K^+ ions had little effect. The protective effect increased however with the age of the immobilized culture (and hence the size of microcolonies within the gel matrix) so the effects due to diffusional resistances cannot be ruled out.

The previous studies of the effects of immobilization on phenol tolerance did not include measurements of kinetic parameters, which would quantitatively demonstrate improved resistance to phenol inhibition. Shreve and Vogel (1993) investigated the effects of immobilizing *Pseudomonas fluorescens* degrading toluene and *Pseudomonas cepecia* degrading 2,4-D in a packed-bed immobilized-cell differential reactor which allowed for control over substrate mass transfer rates as well as fluid shear stresses. They reported that the growth and degradation kinetics of 2,4-D were unaffected by immobilization. The degradation kinetics of toluene were within 1.2 standard deviations of those for suspended cells. However, the growth kinetics for *P. fluorescens* degrading toluene did change, with intrinsic values for μ_m and K_S being 3 times lower and 30 times higher, respectively, for immobilized cells as compared to suspended cells. Mirpuri et al. (1997) reported that the specific activity ($\mu\, Y_{XS}$) of a free-cell culture of *P. putida* 54G degrading toluene was the same as the specific activity of a biofilm in a vapour-phase bioreactor at the same concentration (3 mg/L); however, as the biofilm continued to be exposed to toluene over a three-week period, the activity of the biofilm decreased significantly due to the accumulation of inactive cells as a result of injury or toxicity due to toluene.

The possibility that phenol degradation or microbial growth kinetics is affected by immobilization through changes in cell physiology cannot be ruled out. Because carefully controlled studies of immobilized-

cell phenol degradation kinetics have not been done it is not yet possible to determine how important this effect could be. The assumption that immobilization has no significant effect on phenol degradation kinetics has been successfully applied to models of biofilm systems in the past (Tang and Fan, 1987; Tang et al., 1987; Worden and Donaldson, 1987; Livingston and Chase, 1989; Wisecarver and Fan, 1989); thus, this simplifying assumption is likely to be reasonable.

2.3 Dynamic Conditions in Biological Wastewater Treatment

Industrial wastewaters often vary widely in their characteristics and most wastewater treatment systems are not operated at steady state (Daigger and Grady, 1982b; Galil et al., 1988).

Under rapidly changing conditions, microbial kinetics do not necessarily follow balanced-growth kinetics. When the microbial environment is changed (ie. substrate concentration or temperature) not only do reaction rates change, but microbial composition, the quantity of enzymes available and depending on the change, the synchronization of catabolic and anabolic pathways. Thus, dynamic microbial kinetics are difficult to model.

The following sections describe the effects of changing organic loading and temperature upon microbial physiology and upon the stability of biological wastewater treatment plants The dynamics of suspended cell cultures have been most actively investigated because of the importance of the activated sludge treatment process. Relatively little research on the response of biofilm cultures to shock loading has been done. The results from investigations of the response of suspended cell cultures to shock loading are reviewed here briefly because they may apply to biofilm cultures to some extent.

2.3.1 The Effects of Changes in Substrate Loading

2.3.1.1 Microbial Response to Changes in Substrate Loading

As cells respond to a changing reactor environment during shock loading, they may experience unbalanced growth. During unbalanced growth, extensive properties of the system such as total protein, DNA, and RNA, increase out of direct proportion to the number of cells (Campbell, 1957). Physiological changes which are more subtle than the percentage of lipids or proteins may also occur, such as changes in the type of proteins synthesized.

During unbalanced growth, the kinetics developed for balanced growth cultures may not apply. The following section describes how cells respond to changing conditions.

Physiological Response

Bacteria adapt their physiology when exposed to changes in the nutrient composition of their growth medium by adjusting a number of biochemical components. In suspended cell cultures under steady state conditions, higher growth rates are accompanied by significant increases in RNA content (Schaechter et al., 1958; Tempest et al., 1965; Tempest, 1967; Daigger and Grady, 1982a; Yun et al., 1996). RNA is responsible for protein synthesis and the majority of the cell mass is protein; thus, the increased RNA content at higher specific growth rates indicates a higher capacity for protein synthesis. DNA levels have been observed to remain the same (Tempest et al., 1965; Tempest, 1967), increase (Schaechter et al., 1958) or decrease slightly (Daigger and Grady, 1982a) with increasing specific growth rate. Cells also tend to be larger (Schaechter et al., 1958). The carbohydrate level may remain constant (Tempest et al., 1965; Tempest, 1967) or decrease slightly (Daigger and Grady, 1982a). Depending on the environment, carbohydrate or lipid content may increase significantly as microorganisms store glycogen and poly-β-hydroxybutyrate for carbon and energy.

Under transient conditions, bacteria adjust to new conditions through growth and storage responses. Growth involves the oxidation of substrate for energy and for biomass synthesis, whereas storage involves the oxidation of a smaller portion of the substrate and synthesis of carbohydrate and lipid polymers for storage.

Growth Response to Transient Conditions

Microorganisms may respond to increases or decreases in substrate loading in a manner called growth rate hysteresis (GRH) (Perret, 1960). GRH is the tendency of the specific growth rate to differ from the predicted steady-state value at an equivalent substrate concentration during dynamic conditions. In cultures with non-inhibitory substrates, when substrate concentrations increase, μ is less than predicted; when substrate concentrations decrease, μ is greater. Delayed response in μ to changing substrate loadings in suspended cell cultures have been reported for pure and mixed cultures with glucose as a substrate (Aiba et al., 1967; Gilley and Bungay, 1968; Nagai et al., 1969; Young et al., 1970; Blackwell, 1971; Young and Bungay, 1973; Sundstrom et al., 1976) and with phenol as a substrate (Yang and Humphrey, 1975; Yongaçoglu et al., 1981; Sokol, 1988b).

A number of researchers have linked the lags in growth response to delays in adjusting the RNA content to that required by the new state (Aiba et al., 1967; Nagai et al., 1969; Young and Bungay, 1973; Chi and Howell, 1976; Cooney and Wang, 1976; Perez and Jeffries, 1992; Yun et al., 1996). For example, Yun et al. (1996) reported that in response to a three-fold increase in the dilution rate, the cell concentration (of *E. coli* K-12) decreased quickly to a transient minimum until the cells produced a sufficient amount of ribosomes to support a new higher growth rate. This new level of ribosome content (0.35 g/g cell) was developed in approximately 5 hours. Daigger and Grady (1982a) reported that with continuous cultures of *P. putida* (ATCC 12633), under a variety of steady state and transient conditions, the relationship between RNA content and growth rate was not adequate to explain the observed response; they suggested that delays in adjusting the levels of other unidentified molecules in the cell may also play a role in the observed lags. The lags could also be related to metabolic changes in which particular pathways are induced or shut down.

There are conflicting reports about the influence of the initial growth rate upon the response of a culture to step increases in concentration. Daigger and Grady (1982a) reported that the responses of the culture depended upon the initial growth rate of the culture prior to the disturbance. However, Kjeldgaard et al. (1958) reported that the time lag was independent of specific growth rate at a given temperature for very dilute suspended-cell cultures of *Salmonella typhimurium* and *E. coli* (strains K12 and ML37) in a variety of media.

In cultures where phenol is the substrate, the lag time may be due to the time required by the bacteria to alter membrane structure in response to changes in phenol concentration. Increases in protein/lipid ratios (Keweloh et al., 1990b) and saturated to unsaturated fatty acid ratios (Heipieper et al., 1990; Keweloh et al., 1990a) have been observed in cell membranes exposed to phenol and may help bacteria prevent leakage of cell constituents into the media, resulting in dramatic shifts in gradients across the membrane. Restoration of gradients is required for cell growth. The time required to restore K^+ membrane gradients was approximately 1 hour (Heipieper et al., 1991), which is in the order of magnitude of the delays described in the literature.

Another type of growth response is called the available reaction potential (ARP) which is defined as the ability of a culture to rapidly change its growth and substrate removal rate in response to a change in substrate loading (McLellan and Busch, 1969; Chase, 1977) rather than continuing at the previous rate for a period of time. ARP has been observed in continuous suspended cell cultures that have been subjected to a quantitative or hydraulic shock load without any increase in substrate level in the effluent stream, indicating

that the specific substrate utilization rate was able to adjust immediately (Tempest, 1967; McLellan and Busch, 1969; Krishnan and Gaudy, 1976; Saleh and Gaudy, 1978). Tempest et al. (1967) increased the dilution rate from 0.004 to 0.24 h^{-1} and observed no rise in substrate concentration for one hour. McLellan and Busch (1969) observed that a step increase did not result in an increase in glucose concentration in the reactor.

Suspended cell cultures may also show both GRH and ARP responses when subjected to shock loadings. There are a number of examples in the literature where the value of μ immediately after an increase in substrate loading is higher than the preshift value but less than the new steady state value, which is reached after a lag period (Harvey, 1970; Schaezler et al., 1971; Chi and Howell, 1976; Chase, 1977).

Storage Response to Transient Conditions

Storage is likely to occur under conditions where the growth rate is limited by a nutrient in the presence of excess carbon and energy supplies or when a system is operated periodically, such as fill-and-draw activated sludge processes (Daigger and Grady, 1982b). During transient conditions, transformation and storage of intracellular intermediates may occur to prevent the accumulation of these compounds which may reach otherwise toxic levels. Alternatively, microorganisms may release the intermediate metabolites into the medium to prevent internal accumulation (Daigger and Grady, 1982b).

Metabolic overflow, the enhanced uptake of substrate and secretion of intermediates, has been observed in a number of systems grown with excess substrate (Liu, 1998; Xiu et al., 1998). These cultures are normally characterized by substrate or product inhibition of growth (Xiu et al., 1998). Under dynamic conditions, the time to reach steady state may be prolonged, or the transitions between steady states may be oscillatory in nature (Xiu et al., 1998). Beltrame et al. (1984) reported that in the case of phenol degradation in continuous culture, the effluent concentration of phenol depended not only upon the dilution rate, but also upon the influent concentration. They hypothesized that an inhibitory intermediate or decay product is secreted into the medium and that its concentration is proportional to the concentration difference between that in the influent and that in the reactor. Although an intermediate compound was not identified, others have reported transient intermediates present in the medium during phenol degradation (Storer and Gaudy, 1969; Rozich and Gaudy, 1983; Li and Humphrey, 1989; Allsop et al., 1993; Garcia Sanchez et al., 1998).

2.3.1.2 Response of Continuous Suspended Cell Cultures to Changes in Phenol Loading

General Results

Quantitative shock loading (rapid changes in substrate concentration) and hydrodynamic shock loading (rapid changes in dilution rate) each have the result of increasing organic loading, however, the effect may not be the same. Manickan and Gaudy (1983) reported that although the mass leakage of COD was similar for both types of shock loading, higher concentrations of effluent COD were observed for quantitative shock loading and higher effluent suspended solids were observed for hydraulic shock loadings. These effects cannot necessarily be applied to biofilm systems.

Three types of response to increases in phenol loading are evident in the literature for freely-suspended cell cultures. The first is a low level response typically caused by a small step change in the inlet phenol concentration or dilution rate (eg. D_1=0.15 h^{-1} to D_2=0.20 h^{-1} (Li and Humphrey, 1989) or S_1=200 mg/L phenol to S_2=500 mg/L (Allsop et al., 1993)). In such cases, the phenol concentration in the effluent did not change and no intermediates were detected in the culture (Yang and Humphrey, 1975; Li and Humphrey, 1989; Allsop et al., 1993; Garcia Sanchez et al., 1998). Depending on the experiment, cell concentrations either increased to the new steady state (Allsop et al., 1993) or did not change (Yang and Humphrey, 1975; Li and Humphrey, 1989).

The second type of response is an intermediate one, to moderate step increases in organic loading (eg. D_1=0.15 h^{-1} to D_2=0.25 h^{-1} (Li and Humphrey, 1989) or S_1=300 mg/L phenol to S_2=1500 mg/L using activated sludge (Allsop et al., 1993)). Under these conditions Chi and Howell (1976), Yang and Humphrey (1975) and Li and Humphrey, (1989) reported transient peaks in phenol concentrations and transient dips in cell concentration before a new steady state was reached. In contrast, other researchers did not observe increases in the effluent phenol concentration (Lu and Ganczarcyk, 1984; Allsop et al., 1993); however, transient increases in the levels of excreted intermediate compounds were reported. These included a compound, which absorbed light at 375 nm (Li and Humphrey, 1989), COD (Storer and Gaudy, 1969; Rozich and Gaudy, 1983) or non-phenol non-glucose dissolved organic carbon (Allsop et al., 1993). Allsop et al. (1993) suggested that the intermediate observed in their system was coenzyme A because of a similar UV spectra. Coenzyme A is an intermediate in the degradation of phenol via the *ortho* and *meta* pathways. Li and Humphrey (1989)

considered the intermediate accumulating in their system to be 2-hydroxymuconic semialdehyde, also an intermediate in the *meta* pathway.

The third type of response occurred when the cultures were exposed to large step increases in phenol loading (eg. D_1=0.15 h^{-1} to D_2=0.33 h^{-1} or S_1=500 mg/L phenol to S_2=3500 mg/L phenol (Allsop et al., 1993)). In such cases, the phenol concentrations rose rapidly and washout of biomass occurred (Yang and Humphrey, 1975; Rozich and Gaudy, 1983; Li and Humphrey, 1989; Allsop et al., 1993). In two cases the predicted steady-state values for μ were less than μ^* (the maximum specific growth rate) and the systems should have been stable (Rozich and Gaudy, 1983; Li and Humphrey, 1989). Rozich and Gaudy (1983) noted that under dynamic conditions the specific growth rate of the culture may overshoot and will be forced past μ^* (on the downward side of the Haldane model in Figure 2.3) and the system will not be able to recover as the substrate concentration increases beyond S^*. With the large step increase in phenol concentration, Allsop et al. (1993) did not observe the presence of an excreted intermediate, however, other researchers reported the presence of intermediates during large shock loads (Rozich and Gaudy, 1983; Li and Humphrey, 1989).

It is clear that the responses of suspended-cell cultures to shock loads is not a simple matter. The Haldane model, although perhaps appropriate for balanced growth kinetics, cannot describe the phenomena that occur during transient states such as GRH, ARP, metabolic overflow or lags in the synthesis of RNA. It is not surprising that many researchers have found that the Haldane model or other balanced growth models do not predict the response of cultures to shock loads (Howell and Jones, 1980; Chiam and Harris, 1983; Rittmann et al., 1992; Garcia Sanchez et al., 1998).

Time Delay and Time Lag Models

The Monod and Haldane equations imply that μ changes instantaneously with a change in S. In cases where the increase in substrate loading exceeded the capacity of the organism to utilize the substrate, time lags in growth and substrate utilization have been reported (Yang and Humphrey, 1975; Chi and Howell, 1976; Yongaçoglu et al., 1981; Rozich and Gaudy, 1983; Sokol, 1988b; Li and Humphrey, 1989). The phenomenon has not been well documented for biofilm cultures.

When steady-state kinetics are used to describe suspended cell cultures under shock-loading conditions, predicted and experimental transient values for biomass and particularly substrate concentration do not agree well (Storer and Gaudy, 1969). A number of delay and lag functions have been incorporated into

unsteady-state models for suspended cell cultures with varying degrees of success. Some of these are listed in Table 2.5

Table 2.5 Time Delay and Lag Functions used in Unsteady-state Models for Suspended-Cell Cultures

Source	Delay Function	Variables	Comments
Young et al. (1970)	$\bar{S} = S - S_S$ (2.46) $\bar{\mu} = \mu - \mu_S$ (2.47) $\frac{\bar{\mu}(s)}{\bar{S}(s)} = \frac{K e^{-Ts}}{\tau s + 1}$ (2.48)	$\bar{S}$ $\bar{\mu}$ deviation variables; S_S, μ_S - steady- state values; K, T - constants; s denotes Laplace domain	time delay gave improved fit of model to data, for small perturbations only
Yang and Humphrey (1975)	$\mu = \mu(0) + \alpha t$ (2.49)	$\mu(0)$ - value of μ immediately after disturbance; α - time response constant	time delay gave improved prediction of trends in transient data
Li and Humphrey (1989)	$\varepsilon(t) = \frac{1}{2 - e^{-t D_2 / D_1}}$ (2.50)	D_1 - initial steady-state dilution rate; D_2 - dilution rate after disturbance	key to fitting data to model
Yongaçoglu et al. (1981)	$\frac{dA_E}{dt} = \frac{A_{EM} - A_E}{\tau_1}$ (2.51)	A_E - enzyme activity; A_{EM} - maximum enzyme activity; τ_1 - time constant	time delay gave improved fit but too many parameters to be useful; assumes enzymes switched on and off depending on S
Chiam and Harris (1983)	$\mu(t) = \mu(1 - \hat{t}\, e^{-\hat{t}})$ (2.52) $\hat{t} = \frac{t}{\tau}$ (2.53)	τ - time constant	time delay gave improved prediction of trends in transient data

All of the time delay and lag functions in Table 2.5 were reported to improve the fits of unsteady-state models for chemostats to experimental data; however, most models did not predict the behaviour accurately. In this regard, most of the delay functions did not incorporate substrate concentration or dilution rate. Sokol (1988b) pointed out that a problem with the function suggested by Yang and Humphrey (1975), Equation 2.50, is that μ is assumed to be independent of substrate concentration during unsteady state. Chiam and Harris (1983) have also pointed out that the idea of a single term representing growth rate immediately after a step change is untested. Also, a time delay function may not sufficiently describe the dynamics of the culture. Chiam and Harris (1983) reported that in addition to a time delay model, they needed to partially decouple the uptake and biosynthesis steps in order to fit their models to their dynamic data.

Historical Approach

Another approach to unsteady-state kinetics has been the use of the history concept. Sokol and Howell (1981) demonstrated that the relationship between μ and S depended on the dilution rate (or mass loading of phenol) in the reactor from which the cells were taken for phenol concentrations ranging from 0.1 to 1000 mg/L. The largest effects on μ were for substrate concentrations less than 50 mg/L. In a subsequent study performed at substrate concentrations between 1-50 mg/L, Sokol (1987) developed empirical equations for the Haldane kinetic parameters (which became variables) based upon the steady state phenol concentration in the chemostat in which the cells were originally cultured. An adaptation parameter and a lag time parameter were also included. The resulting equation fit the kinetic data significantly better than the Haldane equation with constant-value parameters.

The history approach was compared to the time-delay model proposed by Yang and Humphrey (1975) in predicting the response of *P. putida* to step increases in phenol concentration and dilution rate in a CSTR (Sokol, 1988a). Use of the history model fitted the experimental data for biomass concentration and substrate concentration better than the time delay model. The maximum dilution rate without washout and the corresponding feed substrate concentration predicted by the model were about 20% lower than found experimentally.

One disadvantage of this approach is the large number of experiments that must be conducted to determine the relationships between the Haldane parameters and culture pre-history. Another disadvantage is the relatively high number of parameters that are involved.

Other Models

Howell and Jones (1980) based their dynamic response model upon an operon type of induction mechanism assuming that the maximum uptake rate is related to a critical enzyme level within the cells. Thus, rather than delays in protein synthesis, the inducer-repressor relationship controls the rate of reaction. The two-compartment model (which includes an equation for enzyme density) was able to predict a lag phase and oscillatory growth.

Garcia Sanchez et al. (1998) postulated a dual-inhibition model based upon the hypothesis that during concentration shock loads of phenol, an inhibitory metabolic intermediate is excreted to and accumulates in the medium. Their model was able to successfully predict the time delays observed experimentally as well as the three types of dynamic response discussed previously. The time delays were predicted without the use of a time-delay equation. A low-level stable response was predicted for step changes in which the intermediate accumulated below inhibitory levels. A medium-level response was predicted for step changes in which the intermediate reached inhibitory levels, but the phenol did not inhibit growth (single inhibition). A high level response resulting in washout was predicted when the phenol concentration reached inhibitory levels, which added to the inhibition resulting from inhibitory concentrations of the intermediate (double inhibition). Although the intermediate responsible for the dynamic response of the system was not specifically identified, the presence of intermediate compounds in the medium was confirmed through HPLC analysis and is additionally supported in the literature, as discussed previously.

2.3.1.3 Response of Biofilm Cultures to Changes in Phenol Loading

Physiological Response

There is very little information on the response of biofilms to sudden changes in substrate loading. Bakke (1983) reported that when a *P. aeruginosa* biofilm in a Roto Torque® fermenter was subjected to large step increases in inlet substrate concentration, massive sloughing resulted. He determined that, despite the loss of biofilm material, the biofilm cell numbers remained constant, suggesting that only EPS was shed by the biofilm. The effect was more pronounced when lactate or lactose were used as substrates as compared to glucose. He suggested that the effect may be due in part to rapid changes in electric field because both lactate and lactose require H^+ for transmembrane transport, whereas glucose does not. Biofilm shedding has also been

observed in a biological fluidized bed reactor treating coal gasification wastewater, in response to prolonged pulses of organics (Donaldson et al., 1987).

General Results

There is limited information about the effects of changes in phenol loading (or any other substrate) on biofilm reactors. Several researchers have used a "black box" approach (Pisano et al., 1990; de Mendonca et al., 1992) in which the effluent characteristics of biofilm systems in response to shock loading were evaluated. The results of these studies are difficult to apply to other systems because the responses were highly system-specific. Also, the effects of shock loads on the biomass (ie. morphology, thickness, loading) were not investigated. Thus, the results are difficult to interpret.

Other researchers have developed dynamic models of biofilm systems and have performed a limited number of dynamic experiments (Tang et al., 1987; Worden and Donaldson, 1987; Stevens et al., 1989). Details of these models are presented in Section 2.4.4. It appears that some of the trends observed with suspended cell cultures may apply to biofilm cultures.

A low level response, similar to those observed in suspended cell cultures, was reported by Tang et al. (1987) for a draft tube fluidized bed bioreactor with *P. putida* as a predominant species. When the inlet phenol concentration was increased by 40% (initial concentration not reported), no significant transient response was observed and the biofilm thickness did not change. This response may have been due to phenol adsorption to the activated carbon used as the carrier. Note that the dilution rate used in this experiment, 2 h^{-1}, was approximately ten times higher than for the dynamic work done with suspended cell cultures, implying high robustness of the biofilm system as compared to the suspended cell one.

Intermediate responses, similar to those observed in suspended cell cultures, have also been reported for ICFBR cultures, although at much higher dilution rates. When inlet phenol concentrations were doubled (from 49 mg/L and 38 mg/L), relatively small transient peaks in substrate concentration were observed by Tang et al. (1987). In both cases, the biofilm thicknesses increased significantly (from 18 and 13 μm to 40 and 48 μm, respectively) over a period of 7.5 hours.

Worden and Donaldson (1987) also reported an intermediate-type response when a pulse, increasing the reactor phenol concentration from 10 mg/L to 65 mg/L, was added to a CSTR operating at a dilution rate of 3 h^{-1} containing bioparticles from a fluidized bed reactor that was operated under the same conditions. The

phenol uptake rate rapidly increased and then returned to the original level once the reactor phenol concentration returned to pre-shock levels. Worden and Donaldson (1987) did not report the effects of the shock loading, if any, on the biofilm. Tang et al. (1987) and Worden and Donaldson (1987) measured neither COD nor possible excreted intermediates; hence the presence of excreted intermediate metabolites in the reactor, if any, were not detected.

Unlike the case for suspended cell cultures, system failures resulting from large step or pulse changes have not been reported for biofilm cultures. Thus, limiting criteria (such as critical dilution rate) have not been established for biofilm systems.

Tang et al. (1987) increased the inlet phenol concentration to their draft-tube fluidized bed reactor from 33 mg/L to 96 mg/L at a dilution rate of 2 h^{-1}. Although the transient phenol concentration in the reactor rose sharply from approximately 2 mg/L to over 20 mg/L, the system recovered within 30 hours. The biofilm thickness increased markedly from 30 μm to 159 μm during this period, in part due to the development of loosely-packed filamentous bacteria in the biofilm. The development of heterogeneous biofilms with large protuberances in ICFBRs as a result of increasing the organic loading has also been reported by Kwok et al (1998) and Tijhuis et al. (1996). The protuberances slowly eroded to form thinner and smoother biofilms (Kwok et al., 1998).

Worden and Donaldson (1987) subjected a CSTR containing bioparticles from a fluidized bed reactor (with a dilution rate of 3 h^{-1}) to a pulse which increased the phenol concentration in the reactor from 15 mg/L to 170 mg/L. The substrate uptake rate dropped significantly, possibly due to phenol inhibition, and then increased as the phenol concentration in the reactor decreased by reaction and convection until it peaked slightly above the steady state value and then stabilized. The bulk phenol concentration in the reactor reached the original steady-state value within 1.5 hours.

If the "large" perturbations used by Tang et al. (1987) and Worden and Donaldson (1987) had been larger, perhaps the fluidized bed bioreactors would have failed. However, it is not clear under what circumstances the reactors would fail nor what size of the perturbation is required for system failure. Unlike suspended cell culture systems, the limitations of biofilm reactors have not been well explored.

Donaldson et al. (1987) noted that when treating coal gasification wastewater in an ICFBR pilot plant, prolonged pulses of organics (possibly 80-100% strength wastewater instead of 50%) caused shedding of the

biofilm and caused inhibition of the bioactivity of the system, which returned to normal within 1-2 days. The nature and duration of the perturbations and the system response were not reported in detail. More information is needed to understand when the performance of an ICFBR becomes compromised, and how the microorganisms deal with perturbations.

Time Lag Models

Tang et al. (1987) used the time lag model proposed Yang and Humphrey (1975) (Equation 2.49) to modify the predicted response of the model to match experimental results. The parameters were estimated from shock-loading experiments conducted on a suspended cell CSTR under similar conditions. Use of the time delay model allowed for a better prediction of trends in the substrate concentration in the reactor for a range of step increases in substrate concentration. Inclusion of a term to account for adsorption of the phenol to the activated carbon carrier was also needed to fit the model to the phenol concentration data. No attempt was made to model the biofilm or any suspended biomass that may have been in the reactor.

Worden and Donaldson (1987) did not use time delay models as part of their dynamic fluidized bed model and they were able to predict the response of the system (for the bulk phenol concentration only) to pulse loadings of phenol quite well; however, they reported the results of only two experiments. Stevens et al. (1989) did not use a time delay model either.

2.3.2 The Effects of Temperature Changes

There is little control of temperature in conventional industrial-scale wastewater treatment reactors (Friedman and van Doesburg, 1980). The reactor temperature is determined by the temperature of the raw wastewater and the heat exchange with the environment, which may vary depending upon meteorological conditions and the design of the system (Friedman and van Doesburg, 1980). Although sudden temperature changes in industrial-scale bioreactors are not likely, significant variations in temperature can occur from day to day (Friedman and van Doesburg, 1980) which may result in unbalanced growth (Chohji et al., 1983). Thus, the dynamic behaviour of an ICFBR under conditions of changing temperature may be important. This section summarizes the effects of temperature shifts on microorganisms and the results reported for both continuous suspended-cell cultures and biofilm cultures.

2.3.2.1 Physiological Effects of Temperature Changes

Changes in temperature can have significant effects on cell physiology. When exponentially growing batch cultures are subjected to shifts in temperatures within the normal range for growth, cells respond immediately to the new growth temperature without a lag period (Ng et al., 1962; Chohji et al., 1976). However, when temperatures are shifted between the normal range for growth and the super-optimal or sub-Arrhenius ranges there is a delay in attaining the predicted growth rate (Ng et al., 1962). For example, a shift from 37°C to 12°C caused *E. coli* to stop growing for four hours before growth began again at a new rate (Ng et al., 1962). Delays in response have also been observed in nutrient-limited continuous cultures within the normal temperature range for growth (Chohji et al., 1983; Yun et al., 1996). For example, Yun et al. (1996) reported a decrease in the functioning ribosome content of *E. coli* K-12 cells with a lag period of 2 hours, accompanied by a decrease of cell mass in a continuous-flow reactor when temperature was shifted from 33 to 37°C.

Herendeen et al. (1979) reported that the concentrations of a large fraction of cellular proteins do not vary significantly within the normal temperature range for growth; however, outside this range, the concentrations of some cellular proteins can be much different. When bacteria are subjected to sudden increases in temperature, they synthesize heat shock proteins (Gounot, 1991) which may result in a greater degree of thermotolerance (McCallum et al., 1986; Julseth and Inniss, 1990). Some bacteria change to a filamentous phenotype when exposed to heat shock (McCallum et al., 1986). When bacteria are subjected to a sudden decrease in temperature they synthesize cold shock proteins (Gounot, 1991) and cold acclimation proteins (Whyte and Inniss, 1992), which prepare the cells for growth at lower temperatures (Jones et al., 1987). Psychrotrophic bacteria synthesize unique proteins which may help them function at low temperatures (Potier et al., 1990).

Bacteria also may increase the proportion of unsaturated fatty acids in their cell membranes to maintain membrane fluidity when temperatures are decreased, although not all bacteria have been shown to do so (Herbert, 1986). Lag periods accompany changes in membrane composition. For example, *A. globiformis*, which has only saturated fatty acids in its membrane at 32°C, experienced a lag in growth when shifted from 32°C to 2°C until the proportion of unsaturated fatty acyl residues increased to 20% (Canillac et al., 1982).

2.3.2.2 Effects of Temperature Changes in Suspended Cell Cultures

The response of continuous, substrate-limited cultures to temperature shocks is complex and difficult to model. System response appears to depend upon the size of temperature change (Ryu and Mateles, 1968), the direction of change (Topiwala and Sinclair, 1971), the preshift specific growth rate (George and Gaudy, 1973; Gaudy, 1975; Visser et al., 1993), the ecology of the system (Visser et al., 1993) and the postshift temperature relative to the optimum temperature or normal range for growth (George and Gaudy, 1973, Carter and Barry, 1975; Gaudy, 1975).

Small changes in temperature (±10°C) appear to have little effect on some continuous cultures. Ryu and Mateles (1968) reported that the specific growth rate increased and decreased in response to small step increases and decreases in temperature, respectively, before returning to the initial steady-state value corresponding to the dilution rate. Transient maxima and minima in μ were observed within 1.5 hours of the step changes. Substrate (ammonia) concentrations in the reactor reached new steady-state values within 8 hours (at dilution rates of 0.635, 0.347 and 0.504 h^{-1}). Carter and Berry (1975) reported no inhibition of COD degradation for activated sludge units with milk as the substrate for small changes within the mesophilic or thermophilic range (depending on the culture), although lags in response in the order of two hours were reported. When a mixed culture with glucose as a substrate was subjected to a temperature increase from 25°C to 36°C, George and Gaudy (1973) observed only a slight fluctuation in effluent COD and biomass concentration before new steady-state values were reached.

The magnitude of the temperature change does not always indicate the type of response. George and Gaudy (1973) reported that with a shift from 25°C to 17°C (only 8°C) for a culture at a dilution rate of 0.25 h^{-1}, there was severe disruption of cell metabolism even 40 hours after the shift, with leakage of intermediate metabolites. Effluent COD concentrations did not recover by 200 hours after the shift. The same temperature shift with a slower growing culture (D=0.125 h^{-1}) resulted in only a small transient increase in COD. George and Gaudy (1973) also reported similar results for a shift from 25°C to 47°C. The culture with the higher dilution rate (D=0.25 h^{-1}) displayed larger transients than the culture with the lower dilution rate (D=0.125 h^{-1}). Thus they concluded that slower growing cultures are able to adapt more easily to temperature shock. The implications of these findings on the response of ICFBRs (which operate at higher dilution rates, but possibly low growth rates within the biofilm) are not clear.

Large temperature shocks can cause severe upsets, particularly if the postshift temperature is outside the usual range for growth. Both George and Gaudy (1973) and Carter and Barry (1975) reported significant inhibition of COD removal when mixed cultures were shifted from the mesophilic to the thermophilic range. Carter and Barry (1975) reported complete inhibition of COD removal when the temperature was shifted down from the thermophilic range to the mesophilic range. Gaudy (1975) also reported washout without recovery after 200 hours when a mixed mesophilic culture was subjected to a temperature shift from 25°C to 8°C.

Time Lag Models

Topiwala and Sinclair (1971) used a first-order time lag model to account for the lag in response observed in their temperature shift experiments. They determined relationships between their kinetic parameters and temperature for steady state conditions, and substituted an effective temperature (T') to model unsteady state conditions. They used the following expression for T':

$$T' = T_i - \Delta T(1 - e^{\frac{-t}{\tau}}) \tag{2.54}$$

where T_i is the initial temperature, ΔT is the change in temperature (in either direction), t is time and τ is a time constant. They obtained values for τ of 0.83 and 1.43 h for 10 C° shifts down and up, respectively. Because there is no basis for the choice of τ, except as a curve fitting parameter after the fact, the time lag model used by Topiwala and Sinclair (1971) is not useful for *a priori* predictions.

2.3.2.3 Effects of Temperature Changes on Continuous Biofilm Cultures

There is little information on the effects of temperature changes on the performance of ICFBRs or other biofilm reactors. Results with flocs in activated sludge plants suggests that there are likely masking effects on microbial kinetics due to temperature effects on the diffusion of oxygen and substrates. Eckenfelder and Englande (1970) observed that at high temperatures, only a small portion of the floc was active due to oxygen depletion as a result of high respiration rates, whereas, at low temperatures, substrates and oxygen diffused deeper into the floc due to the lower uptake rates. Thus it is possible that the overall performance of the plant may be comparable under both warm and cool conditions, even if the intrinsic kinetics are different.

In fluidized-bed reactors treating chlorophenolic-contaminated groundwater, Melin et al. (1998) reported that although the substrate uptake rates were highly influenced by temperature in batch tests, the

removal efficiencies were not influenced by temperature during continuous operation down to temperatures of 4°C. The systems were operated at steady state for the most part, with small transitions (2-4°C) between steady states; thus, the dynamic response to temperature changes could not be assessed. Also, the dilution rates used in the experiments were not specified, but they may have been very low. Larger shifts between steady states or shifts at higher dilution rates may have resulted in more sensitivity to temperature.

2.4 Immobilized-Cell Fluidized-Bed Reactors (ICFBRs)

2.4.1 General Characteristics

ICFBRs are biofilm reactors in which small particles, some which are covered or partly covered by microorganisms, are fluidized by the movement of process medium and gas bubbles. ICFBRs are characterized by high biomass holdups - up to 30000 to 40000 mg VS/L (Mulcahy et al., 1980) (compared to 1500-2500 mg VS/L for activated sludge systems); this is due to the high surface areas available for biofilm formation (above 3000 m^2/m^3) (Mulcahy et al., 1980). The high biomass holdup coupled with retention of the biomass on support particles results in cost savings due to higher dilution rates without the danger of washout, smaller reactors, and shorter treatment times. For example, the volumetric phenol degradation rate in an ICFBR is 5-10 times higher than in an activated sludge system (Donaldson et al., 1987). Donaldson et al. (1987) have estimated that the fluidized bed process may require half the capital investment and half the operating costs of an activated sludge process for the treatment of coal conversion wastewater.

Advantages of an ICFBR system over other biofilm systems include

- higher external mass transfer rates (Stephenson and Murphy, 1980)
- uniform solids distribution (Stephenson and Murphy, 1980)
- lower pressure drop through the system
- higher surface area for biofilm formation
- no need for frequent backwashing to control biomass thickness.

Although ICFBRs have been operated at full scale in secondary treatment (Mulcahy et al., 1980; Stathis, 1980; Burton and Ravishankar, 1989) and industrial wastewater treatment (Burton and Ravishankar, 1989; Heijnen et al., 1990; Sutton and Mishra, 1990) applications for over fifteen years, much work remains to

characterize and establish a sound basis for design, optimization, and control of ICFBRs. Most of the research on aerobic wastewater treatment has focused on denitrification applications (Harremoës et al., 1980; Mulcahy et al., 1980; Stephenson and Murphy, 1980; Denac et al., 1983; Mulcahy and Shieh, 1987; Lazarova et al., 1992), but has also included the removal of toxic (Arvin et al., 1991; Suidan et al., 1991, Iwami et al., 1992; Voice et al., 1992; Clarkson et al., 1993) and inhibitory (Tang and Fan, 1987; Wagner and Hempel, 1988; Etzensperger et al., 1989; Livingston and Chase, 1989) contaminants. General characteristics of ICFBRs are described in Table 2.6.

Table 2.6. Characteristics of Selected ICFBR Systems

Source	Substrate	Support Material	Biofilm Thickness [μm]	Biofilm Density [mg DW/ cm^3]	Solids Holdup [%v/v]	Biomass Loading [gDW/L]
Tang and Fan (1987)	phenol	activated carbon	12-48	72-151	4.8-8.0	1.5-3.2
Worden and Donaldson (1987)	phenol	coal	180-210	-	6-7	-
Livingston and Chase (1989)	phenol	celite	23-26	141-222	9.75	13.6-21.6
Etzensperger et al. (1989)	phenol	sand	-	-	-	3-6
Mulcahy and Shieh (1987)	municipal wastewater, methanol, sodium nitrate	glass beads	40-1200	21-58	-	5-16
Stevens et al. (1989)	secondary effluent	sand	50-68	-	-	13
Koch et al. (1991)	synthetic coke plant wastewater	sand	-	-	35-45 g/L	3.5-6.0
		activated carbon	-	-	27-33 g/L	6.0-8.7
Coelhoso et al. (1992)	molasses	activated carbon	800	60	-	10-14
Ryhiner et al. (1988)	glucose-yeast hydrolysate	sand	-	-	7-14	2.4-3.5
Wagner and Hempel (1988)	napthalene-2 sulfonate	sand	65-85	-	-	2-7
Patoine (1989)	phenol	sand	20-39	-	20	0.8
Heijnen et al. (1990)	Industrial wastewater (ammonia, sulphide, COD)	sand	50-100		200 g/L	15-25

Overall Mass Balances

A general schematic representing the ICFBR as a completely mixed system is shown in Figure 2.7. The assumption of complete mixing of the liquid phase has been shown to be appropriate for 3-phase airlift reactors (Tang et al., 1987).

For a continuous well-mixed bioreactor containing both immobilized and suspended biomass, the following general material balances apply.

Balance on substrate (S):

$$\frac{dS_b}{dt} = D(S_0 - S_b) - \frac{(X_S \mu_b + X_f \mu_f)}{Y_{X/S}} \tag{2.55}$$

Balance on suspended biomass (X_S):

$$\frac{dX_S}{dt} = D(X_{S_0} - X_S) + X_S \mu_b + R_{det} - R_{ad} \tag{2.56}$$

Balance on immobilized biomass (X_f):

$$\frac{dX_f}{dt} = X_f \mu_f + R_{det} + R_{ad} \tag{2.57}$$

where D is the dilution rate ($D=Q/V_L$), R_{det} is the rate of detachment of cells from the biofilm and R_{ad} is the rate of adhesion of cells to the biofilm. Whereas μ_b refers to the specific growth rate of cells based on the bulk substrate concentration according to the Haldane kinetic model, μ_f in this contex refers to the same parameter averaged over the depth of the biofilm. The parameters μ_b and μ_f are different in this context due to the substrate concentration gradient that exists within the biofilm (i.e. the substrate concentration in the bulk fluid and biofilm are different). The biofilm model is developed in more detail in Section 4.2.

2.4.3 Airlift Reactors

Airlift reactors are pneumatic reactors in which the fluid is circulated in a loop caused by the difference in hydrostatic pressure between the bottom of the riser and the bottom of the downcomer (see Figure 2.8); this pressure results from the difference in fractional gas holdup between the riser ($\varepsilon_{G,r}$) and downcomer

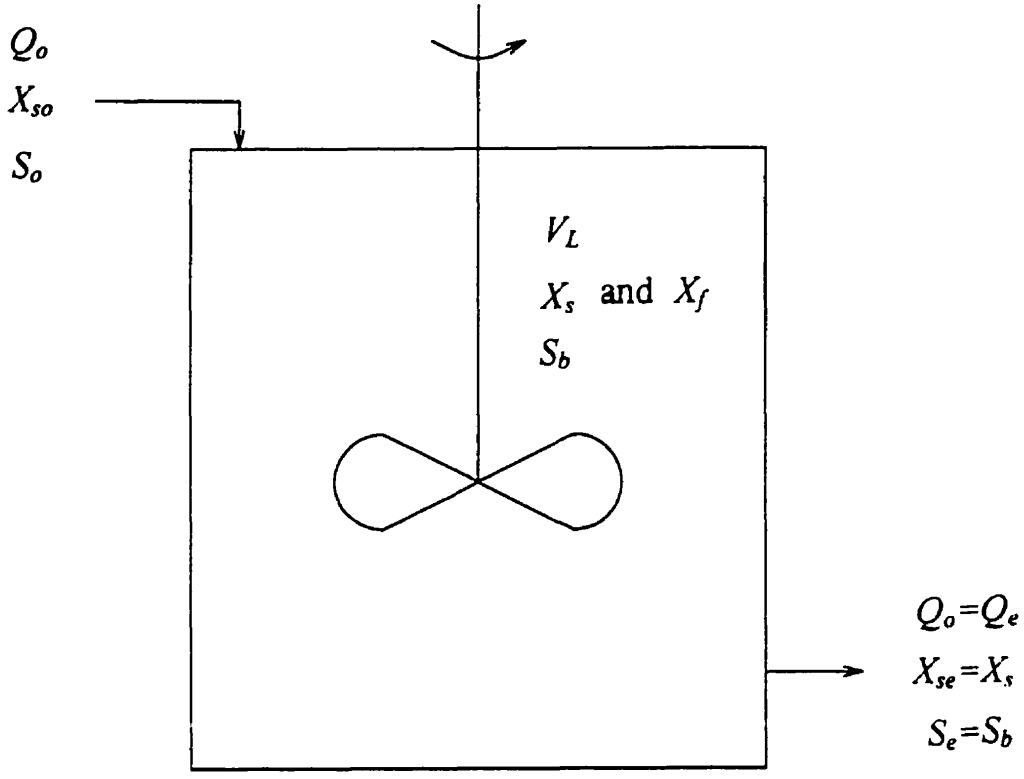

Figure 2.7. Schematic of an ICFBR as a well-mixed reactor where Q, X, and S refer to the flow rate, biomass concentration and substrate concentration, respectively, and the subscripts o, s, f, b, and e refer to the feed, suspension, biofilm, bulk reactor and effluent, respectively. V_L is the liquid volume of the reactor.

($\varepsilon_{G,d}$). Airlift reactors offer several advantages compared to traditional biological fluidized bed reactors. High reactor volumes can be accommodated at high aspect ratios without sacrificing mixing (Joshi et al., 1990). Airlift reactors also provide relatively consistent shear stress exerted on bioparticles throughout the system (Siegel and Robinson, 1992), which should allow for better control of biofilm thickness and should avoid the problems with wide variations in biofilm thickness and stratification found in traditional biological fluidized beds (Shieh, 1981; Kaballo et al., 1995).

Successful use of an immobilized culture for the biodegradation of a contaminant depends on the following reactor characteristics (Patoine, 1989):

- sufficient gas-liquid mass transfer for oxygen,
- sufficient mass transfer of nutrients to the inner layers of the biofilm and transport of dissolved carbon dioxide to the bulk fluid,
- a balance between substrate surface loading and detachment (Kwok et al., 1998), and
- retention of bioparticles in the reactor.

Thus knowledge of the mass transfer and hydrodynamic characteristics of airlift reactors is important so that design and operation variables such as biofilm thickness, bulk substrate concentration, and substrate concentration profiles within the biofilm can be predicted.

Currently there are many design correlations for airlift reactors in the literature for key hydrodynamic variables (liquid circulation velocity and gas holdup) and mass transfer characteristics; however, many of these are limited to specific types of airlift reactors or specific systems (Siegel and Robinson, 1992). The following sections summarize the effects of various parameters on the phase holdups and mass transfer that will be appropriate for this study.

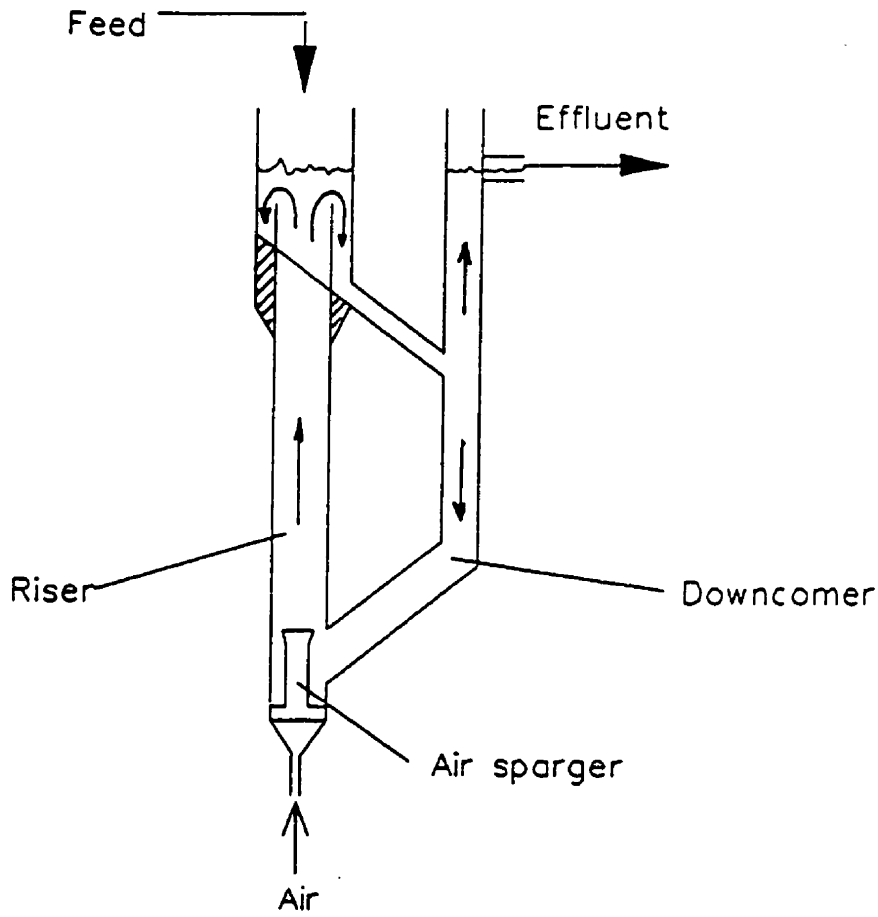

Figure 2.8. External-loop Airlift Reactor

2.4.3.1 Phase Holdups

The solid (ε_S), liquid (ε_L) and gas (ε_G) phase holdups in a three phase system are related by the expression,

$$\varepsilon_S + \varepsilon_L + \varepsilon_G = 1 \tag{2.58}$$

Solid Holdup, ε_S

Generally, the amount of solid particles added to the system is known and the solid phase holdup (for bare support particles only) can be defined as

$$\varepsilon_S = \frac{M_p}{\rho_p V_R} \tag{2.59}$$

where M_p is the mass of particles added to the system, ρ_p is the particle density, and V_R is the working volume of the reactor (expressed in cm^3 in this case). If the solid particles of radius r_p are covered with a biofilm resulting in a bioparticle radius of r_f, ε_S can be defined as

$$\varepsilon_S = \frac{M_p}{V_R}\left[\frac{1}{\rho_p} - \frac{4\pi(r_f^3 - r_p^3)}{3m_p}\right] \tag{2.60}$$

where m_p is the mass of one solid particle and ρ_{bf} is the wet density of the biofilm. The typical range for ε_S in ICFBR systems is 5-15%.

Gas Holdup, ε_G

Most data and correlations for ε_G in airlift reactors and bubble columns have been developed for two-phase systems in which there are no bioparticles. Average gas holdup is dependent upon sparger design, liquid phase physical properties, trace impurities, column geometry and superficial phase velocities (Joshi et al., 1990).

There is conflicting information in the literature about the effect of solids on gas holdup in bubble columns and airlift reactors. Several researchers have reported that the presence of particles had little or no effect on gas holdup (Sun et al., 1988; Jian-an and Nieuwstad, 1992; Kochbeck et al., 1992; Saxena et al., 1992; Potthoff and Bohnet, 1993). Many others have reported that the addition of solids resulted in a reduction of gas

holdup (Godbole et al., 1983; Fan et al., 1984; Koide et al., 1984; Herskowitz and Merchuck, 1986; O'Dowd et al., 1987; Schumpe et al., 1987; Ryhiner et al., 1988; Tang and Fan, 1989, 1990; Saxena et al., 1992).

The effect of particles on gas holdup is complex and not well understood. Sauer and Hempel (1987) reported that three results - no effect, enhancement and reduction - were possible in a bubble column, depending upon the particle characteristics, solids fraction and superficial gas velocities chosen. They found that with particles with low densities (ρ_p<1300 kg/m^3), at low superficial gas velocities (1<u_{Gi}<4 cm/s) and at solids fractions less than 10% v/v, the average gas holdup was higher than for the two-phase case. At higher particle densities, solids fractions and gas velocities, a reduction was observed. These results are reasonably consistent with the literature reports. Most of the reductions in gas holdup were in systems in which dense particles such as sand, glass beads or aluminum oxide were used. Gjaltema et al. (1997c) reported that in a three-phase internal loop airlift reactor containing bioparticles the gas hold-up decreased linearly with the concentration of the bioparticles (40-125 g/L bare carriers) to approximately half of its value without bioparticles present. They also noted changes in bubble size, gas recirculation and observable turbulence particularly at high biofilm thicknesses. Despite the changes in gas-hold-up and flow characteristics, the specific detachment rate was not affected. In contrast, Heijnen et al. (1990) did not observe any systematic effect of sand concentration in the range of 50-250 g/L on gas hold-up in a pilot-scale internal-loop airlift reactor. Clearly, the effects of bioparticle characteristics and concentrations upon gas-holdup, bubble size and hydrodynamics are not well understood in ICFBRs.

Bioparticles are characterized by relatively low densities due to the presence of the biofilm, which has a wet density close to that of water. Correlations which have been developed for two-phase systems or for those developed specifically for high-density particles do not necessarily apply to systems with bioparticles. Currently there are few correlations which can be used for systems with low-density particles. Several correlations for gas holdup in three-phase bubble columns containing solid particles have been developed which include fluid properties and reactor geometry (Koide et al., 1984; Sauer and Hempel, 1987; Sun et al., 1988).

Patoine (1989) investigated gas holdup in the glass airlift reactor that was used in this study with sand as the carrier. She reported that the gas holdup was unaffected by sand concentrations in the range of 0.4 to 8 g/L and superficial gas velocities in the riser of up to 6 cm/s. Patoine (1989) also reported that the salts and the

phenol (which was used as the substrate) did not significantly affect the gas holdup compared to results obtained for water. A correlation was provided between the gas holdup (ε_G) and the superficial gas velocity in the riser ($u_{G,r}$) [cm/s]

$$\varepsilon_G = 0.018\, u_{G,r}^{0.9} \qquad \textbf{(2.61)}$$

The experimental results upon which the Equation 2.61 was based, agreed reasonably well with the predictions of other empirical correlations (Begovich and Watson, 1978; Chisti and Moo-Young, 1987).

Liquid Holdup, ε_L

The liquid-phase holdup can be easily determined once ε_S and ε_i are known using the relationship in Equation (2.58).

2.4.3.2 External Mass Transfer Correlations

The successful operation of an airlift ICFBR to degrade phenol with *P. putida* Q5 depends upon efficiently transferring oxygen from the air bubbles to the bulk fluid, and transferring oxygen, phenol and nutrients through the liquid-biofilm boundary layer to the biofilm surface and into the biofilm by diffusion. These processes were discussed in detail in Section 2.2.3. The external mass transfer coefficients K_La and k_s, described in Section 2.2.3.1 depend upon the reactor type, fluid characteristics and operating conditions. External mass transfer correlations for systems similar to the ICFBR used in the current research will be discussed here.

Overall Gas-liquid Volumetric Mass Transfer Coefficient, K_La

The overall gas-liquid volumetric mass transfer coefficient, K_La, depends upon the properties of the liquid and bioparticles as well as reactor geometry and operating conditions. Much of the work on K_La in bubble columns and airlift reactors has been done on systems without particles.

Jian-an and Nieuwstad (1992) reported that the presence of basalt particles (d_p=0.245 mm) did not affect K_La values in an internal-loop airlift reactor; however, their particle concentrations were small ($0.009<\varepsilon_S<0.03$ v/v). Other researchers have reported reductions in K_La values due to the presence of particles (Koide et al., 1984; Nguyen-Tien et al., 1985; Schumpe et al., 1987; Ryhiner et al., 1988; Sun and Furusaki, 1988; Sun et al., 1988; Tang and Fan, 1990), particularly for small particles ($0.05<d_p<1$ mm) (Nguyen-Tien et

al., 1985). K_La was reported to decrease with increasing solids concentration (Koide et al., 1984; Nguyen-Tien et al., 1985; Herskowitz and Merchuck, 1986; Ryhiner et al., 1988; Sun and Furusaki, 1988, Sun et al., 1988)

Ryhiner et al. (1988) reported that the presence of sand particles ($0.2<d_p<0.3$ mm) reduced K_La by up to 60-70% over a range of gas flow and solids holdup ($0.07<\varepsilon_S<0.14$) in a fluidized bed reactor. The presence of a biofilm on the sand particles increased values of K_La (over those with only sand present) by 10-15%; however, the K_La values were much less than those without sand present. They found that the correlation developed by Nguyen-Tien et al. (1985) for small glass beads in a bubble column (Equation 2.62), fit the data for biofilm-covered particles quite well.

$$K_L a_D = 0.39\left(1 - \frac{\phi_S}{0.58}\right) u_G^{0.67} \tag{2.62}$$

where,

$$\phi_S = \frac{\varepsilon_S}{1 - \varepsilon_G} \tag{2.63}$$

Note that K_La_D is based on the dispersion volume as opposed to the liquid volume in the reactor.

Other correlations have been developed as well. The following are companion correlations to those developed by the same researchers for gas holdup; thus the correlations were developed using the same experimental systems and the variable and parameter definitions are the same. Sauer and Hempel (1987) proposed the following based on a variety of particle densities:

$$K_L a\left(\frac{\nu_{sus}}{g\, u_G}\right)^{1/2} = K\left[\frac{u_G}{(\nu_{sus}\, g\, u_G)^{1/4}}\right]^{B1}\left[\frac{\nu_{sus}}{\bar{\nu}_{eff,rad}}\right]^{B2}\left[\frac{C_p}{C_{po}}\right]^{B3} \tag{2.64}$$

where K, B_1, B_2, and B_3 are dimensionless constants dependent on the sparger type, ν_{sus} is the kinematic viscosity of the slurry [m^2/s], $\bar{\nu}_{eff,rad}$ is the radial momentum transfer coefficient [m^2/s], C_p is the particle concentration in the reactor [kg/m^3], and C_{po} is the particle concentration over the sparger [kg/m^3]. Equation 2.65 did not fit the data of Koide et al. (1984) well in the lower range (for K_La values below 0.05 s^{-1}) but fit the data better for higher K_La values. Sun et al. (1988) proposed,

$$K_L a\left(\frac{d_c}{D_{O,w}}\right) = 2.5x10^{-3} Sc^{1/2} Fr^{0.63} Bo^{1/1} Ga^{0.45} \left(\frac{d_p}{d_c}\right)^{0.16} e^{-1.7\varepsilon_G} \quad (2.65)$$

where $D_{O,w}$ is the diffusivity of oxygen in the liquid. Equation (2.65) applies for systems with Froude numbers in the range of 0.01-0.08 and agrees reasonably well with the results of Koide et al. (1984). Koide et al. (1984) proposed the following correlation for their system.

$$K_L a\left(\frac{\sigma}{\rho_L g D_{O,w}}\right) = \frac{2.11\left(\frac{\mu_L}{\rho_L D_{O,w}}\right)^{0.500}\left(\frac{g\mu_L^4}{\rho_L \sigma^3}\right)^{-0.159}\varepsilon_G^{1.18}}{1 + 1.47x10^4\left(\frac{C_p}{\rho_p}\right)^{0.612}\left(\frac{u_t}{\sqrt{d_c g}}\right)^{0.486}\left(\frac{d_c^2 g \rho_L}{\sigma}\right)^{-0.477}\left(\frac{d_c u_G \rho_L}{\mu_L}\right)^{-0.345}} \quad (2.66)$$

Liquid-Solid Mass Transfer Coefficient, k_S

Transfer of substrate and nutrients from the bulk fluid to the exterior surface of the biofilm has been shown to be an important consideration in several ICFBR systems (Tang et al., 1987; Wagner and Hempel, 1988; Livingston and Chase, 1989). The mass transfer characteristics of fluidized three-phase systems have been investigated by a number of researchers using a variety of system configurations and conditions, which are described in Table 2.7. General correlations for the Sherwood number ($Sh = k_S d_p D_L$), which includes the liquid-solid mass transfer coefficient (k_S) for these systems, are listed in Table 2.8. The correlations relate the Sherwood number to the Schmidt number ($Sc = \nu / D_L$) and some form of the Reynolds number depending upon the theory used to develop the correlation.

Kolmogoroff's theory of isotropic turbulence (described by Hinze, 1975), has been used to explain the mechanism of liquid-solid mass transfer in a number of three-phase fluidized bed systems (Sänger and Deckwer, 1981; Arters and Fan, 1986; Goto et al., 1989; Livingston and Chase, 1990; Gaspillo and Goto, 1991; Mao et al., 1992). It is assumed that the conditions of isotropic turbulence, in which the energy dissipation per unit mass (ε) is independent of the nature of the bulk liquid flow, applies to the systems. Several researchers have pointed out that this assumption is likely to be invalid under typical operating conditions (Sänger and Deckwer, 1981; Arters and Fan, 1986; Livingston and Chase, 1990) and that Kolmogoroff's theory may not

include all factors which influence k_S (Jadhav and Pangarkar, 1988). However, this theory has been applied successfully in liquid-solid mass transfer correlations for a variety of systems.

Another approach has been to use the particle Reynolds number ($Re_p = ud_p\rho_L/\mu_L$) (Jadhav and Pangarkar, 1988, 1991; Kushalkar and Pangarkar, 1994). Jadhav and Pangarkar (1988) used the hindered setting velocity, u_p, to represent the particle velocity under turbulent conditions; however, in subsequent work with larger columns, they used the average turbulence intensity, u', because they discovered a dependence of u_p on column diameter (Jadhav and Pangarkar, 1991).

Table 2.7. Fluidized Three-phase Systems for which Solid-Liquid Mass Transfer Correlations have been Developed

Reference	System configuration	System components	Operating conditions
Sano et al. (1974)	agitated vessels and bubble columns	benzoic acid, βnapthol, $KMnO_4$ in water; IER in HCl solution	$0.005 \le u_G \le 0.17$ m/s $0.060 \le d_p \le 1.10$ mm $200 < Sc < 400$
Sänger and Deckwer (1981)	bubble column	IER in water, glucose and glycol	$0 < u_G < 0.26$ m/s $1.6 < d_p < 4.5$ mm
Arters and Fan (1986)	3-phase fluidized bed	benzoic acid and water	$0 < u_G < 0.13$ m/s $1960 < Sc < 3500$ $2.0 < d_p < 4.0$ mm
Livingston and Chase (1990)	internal loop airlift reactor	IER in HCl solution	$0.655 < d_p < 1.120$ mm $Sc = 143$ $5 < \varepsilon_S < 10\%$ $0.005 < u_G < 0.05$ m/s
Jadhav and Pangarkar (1988)	3-phase fluidized bed (d_c=0.1 m)	benzoic acid in water, glucose, CMC	
Goto et al. (1989)	internal loop airlift reactor	IER + water + NaOH	
Jadhav and Pangarkar (1991)	3-phase fluidized bed (d_c=0.1-0.4 m)	benzoic acid in water, glucose, CMC	$0.55 < d_p < 0.92$ mm
Mao et al. (1992)	external loop airlift reactor	benzoic acid coated nylon-6 particles in water	$0 < u_G < 0.08$ m/s $0.3 < \varepsilon_S < 3.5\%$ $d_p = 3.8$ mm
Kushalkar and Pangarkar (1994)	internal loop airlift reactor	benzoic acid in water	$0.550 < d_p < 2.234$ mm $0.08 < u_G < 0.35$ m/s $\varepsilon_S = 0.5\%$

CMC - carboxymethylcellulose
IER - ion exchange resin

Table 2.8. Correlations for the Sherwood Number in Fluidized 3-Phase Systems

Reference	Correlation	
Sano et al. (1974)	$Sh = \Phi_c(2 + 0.4(\frac{\varepsilon d_{ps}^4}{\nu^3})^{\frac{1}{4}} Sc^{\frac{1}{3}})$	(2.67)
Sanger and Deckwer (1981)	$Sh = 2 + 0.545(\frac{\varepsilon d_p^4}{\nu^3})^{0.264} Sc^{\frac{1}{3}}$	(2.68)
Arters and Fan (1986)	$Sh = \Phi(2 + 0.695(\frac{\varepsilon d_p^{*4}}{\nu^3})^{0.200} Sc^{\frac{1}{3}})$	(2.69)
Livingston and Chase (1990)	$Sh = 2 + 0.275(\frac{\varepsilon d_p^4}{\nu^3})^{0.274} Sc^{\frac{1}{3}}$	(2.70)
Jadhav and Pangarkar (1988)	$Sh = \begin{cases} 2 + 0.42(\frac{u_p \rho_L d_p^*}{\mu_L})^{0.278} Sc^{0.454} & \text{for } d_p \le 1100\ \mu m \\ 2 + 0.408(\frac{u_p \rho_L d_p^*}{\mu_L})^{0.44} Sc^{0.45} & 1540 \le d_p < 3680\ \mu m \end{cases}$	(2.71)
Goto et al. (1989)	$Sh = 2 + 1.01(\frac{\varepsilon d_p^4}{\mu_L^3})^{0.173} Sc^{\frac{1}{3}}$	(2.72)
Jadhav and Pangarkar (1991)	$Sh = \begin{cases} 0.0915(\frac{u^* \rho_L d_p}{\mu_L})^{0.625} Sc^{0.45} & \text{for } d_p \le 1100\ \mu m \\ 0.102(\frac{u^* \rho_L d_p}{\mu_L})^{0.75} Sc^{0.45} & 1540 \le d_p \le 3680\ \mu m \end{cases}$	(2.73)
Mao et al. (1992)	$Sh = 2 + 0.48(\frac{\varepsilon d_p^4}{\nu^3})^{0.24} Sc^{\frac{1}{3}}$	(2.74)
Kushalkar and Pangarkar (1994)	$Sh = 2 + 0.156(\frac{u^* \rho_L d_p}{\mu_L})^{0.48} Sc^{0.45}$	(2.75)

In general, the k_S values determined for airlift reactors (both internal and external loop configurations) are higher than those determined for bubble columns (Goto et al., 1989; Mao et al., 1992; Kushalkar and Pangarkar, 1994), fluidized bed reactors (Mao et al., 1992) and stirred tank systems (Mao et al., 1992)

2.4.4 Unsteady-state ICFBR Models

The dynamic behaviour of ICFBRs has been examined by several research groups using unsteady-state models as a basis for discussion (Park et al., 1984b; Tang et al., 1987; Worden and Donaldson, 1987; Stevens et al., 1989; Gadani et al., 1993). A summary of the important features of these unsteady-state models is presented in Table 2.9.

The complexity of the models varied greatly - from the relatively simple model of Worden and Donaldson (1987) with 18 parameters, to the complex model of Stevens et al. (1989) which included the kinetics of two microbial species, with multiple substrates incorporating both pH and temperature effects, a mixing model which approximated the observed residence-time distribution of the system and a fluidization model with predicted bed height (33 parameters not including those for temperature effects and the fluidization model). The unsteady-state models will not be examined in detail; however, important results and features will be discussed.

Experimental Verification Results

The number of experiments used to verify the models is very limited. Park et al. (1984b) and Gadani et al. (1993) provided simulations but did not confirm the model predictions. However, with the available data, some observations can be made.

Tang et al. (1987) reported significant increases in biofilm thickness due to step increases in substrate concentration (eg. 18 to 40 μm within 30 hours after a 100% step increase in phenol concentration). This demonstrates the importance of allowing for biofilm growth in an unsteady-state model. Other researchers (Worden and Donaldson, 1987; Stevens et al., 1989) did not report biofilm thickness increases; however, it is possible that biofilm thickness was not measured during their experiments. Note that models which include biofilm growth but do not include detachment (eg. Park et al., 1984b; Worden and Donaldson, 1987; Stevens et al., 1989) result in unbounded biofilm growth, which is not reasonable.

Table 2.9. Comparison of Unsteady-state ICFBR Models

Assumption / Condition	Worden and Donaldson (1987)	Tang et al. (1987)	Park et al. (1984b)
System:			
Reactor type	tapered fluidized bed with CSTR	draft tube fluidized bed bioreactor	fluidized bed bioreactor
Number of phases	2	3	not stated
Support material	coal particles	activated carbon	inert spheres
Culture	mixed	mixed	pure
Substrate	phenol	phenol	glucose
Number of parameters	18	24	24 for back-mixed model
Hydrodynamics:			
Mixing model	CSTR	CSTR	CSTR or plug flow
Shearing / detachment of biofilm	not considered	evaluated from steady-state model	considered negligible
Kinetics:			
Number of species	1	1	1
Microbial kinetics	dual (substrate and oxygen)	dual (substrate and oxygen)	dual (substrate and oxygen) and product formation
Cell maintenance / decay	no	included with detachment	considered negligible (product decay included)
Time lag	no	yes	no
Mass transfer:			
Gas-liquid mass transfer	no	yes	yes
Liquid-biofilm mass transfer	liquid-biofilm mass transfer resistance considered negligible	yes	no
Biofilm properties:			
Uniform biofilm density	yes	function of biofilm thickness	yes
Uniform biofilm diffusivity	yes - D_e/D_f=0.24	yes - related to biofilm thickness	yes
Experimental verification	2 pulse experiments	4 step change experiments	no
Microorganisms	activated sludge	mixed culture with *P. putida*	-

continued

Table 2.9 continued

Assumption / Condition	Stevens et al. (1989)	Gadani et al. (1993)
System:		
Reactor type	fluidized bed bioreactor	fluidized bed bioreactor
Number of phases	3	3
Support material	sand particles	inert bead
Culture	mixed	mixed
Substrate	ammonia	ammonia
Number of parameters	33 for 2 species (without fluidization model or temperature effects)	15 for pure culture; 21 for 2 species
Hydrodynamics:		
Mixing model	CSTRs in series	CSTR
Shearing / detachment of biofilm	not considered	evaluated from steady-state experiments
Kinetics:		
Number of species	2	flexible (2 in simulations)
Microbial kinetics	dual (substrate and oxygen) for multiple substrates	substrate only
Cell maintenance / decay	decay	decay
Time lag	no	no
Mass transfer:		
Gas-liquid mass transfer	no	no
Liquid-biofilm mass transfer	predicted mass transfer resistance to be negligible	yes
Biofilm properties:	no biofilm growth	
Uniform biofilm density	yes	yes
Uniform biofilm diffusivity	yes – D_e/D_w=1	yes – D_e/D_w=0.8
Other	included pH and temperature effects; predicted fluidized bed height	no allowance for phase holdups; allowed for variable active fractions for each species and inert biomass
Experimental verification	1 pulse	no

Tang et al. (1987) reported dramatic changes in a mixed-culture biofilm morphology with a large (200%) step increase in substrate concentration. Worden and Donaldson (1987) also reported changes in the appearance, density, growth rate and distribution of microbial species within the biofilm over long periods of time. Thus caution must be used when species-averaged kinetic parameters and biofilm properties are applied to mixed-culture biofilm systems.

The responses of the experimental systems agreed reasonably well with model predictions (although the results of very few experiments were presented), indicating that the approaches used in modelling were not unreasonable. Note that Worden and Donaldson (1987) found that their model over-predicted the response of the system and attributed this to the presence of inactive biomass in the biofilm. Thus the presence of EPS or inactive cells, which was not accounted for in any of the models, may be important. Also, Stevens et al. (1989) attributed the over-prediction of substrate concentration in the reactor to neglecting the contribution of suspended biomass in the system (concentration not specified). Thus in a system where the dilution rate is not significantly greater than the growth rate, the presence of suspended cells should be included in the model. Both Worden and Donaldson (1987) and Stevens et al. (1989) adjusted kinetic parameters to allow for a better fit of their models.

Worden and Donaldson (1987) and Stevens et al. (1989) were able to predict trends in the response of their experimental systems without the need for time-delay models. Tang et al. (1987) reported that a time-delay model was necessary to predict the trends in their experimental data; however it is not clear if there were factors other than a delay in microbial response to the step changes (such as changes in biofilm thickness, activity, density, EPS content, and population distribution) that could be used to explain the response of the system. Thus, it is not clear that a time-delay model is needed in a dynamic ICFBR model.

Similarly, Worden and Donaldson (1987) and Stevens et al. (1989) were able to predict experimental trends with models which included the assumption of constant biofilm properties (i.e. biofilm density and substrate diffusivities). It is not clear that the added complexity introduced by Tang et al. (1987) to vary these properties is needed.

Limitations of Previous Unsteady-State ICFBR Studies

Although the proposed models appear to predict experimental trends reasonably well, experimental verification of all the proposed models has been inadequate (at least according to published results)

- Too few verification experiments have been performed and reported (see Table 2.9).
- The predictions of changes in biofilm thickness in the models have not been compared to experimental results.
- The release of metabolites into the medium by biofilm cells in response to perturbations has not been investigated.

The models also have some shortcomings:

- They do not include an inactive fraction to allow for EPS or inactive cells, which may be a significant component of biofilms.
- Several models do not include detachment (Park et al., 1984b; Worden and Donaldson, 1987; Stevens et al., 1989), which would result in unbounded biofilm growth (if growth is included). This is unrealistic.
- Temperature effects have not been included (Park et al., 1984b; Tang et al., 1987; Worden and Donaldson, 1987; Gadani et al., 1993). Because an important application of ICFBRs is wastewater treatment where temperature changes are common, description of the effect of temperature on ICFBRs would be useful. Stevens et al. (1989) included temperature effects in their dynamic model, but reported experimental results at a constant temperature only.
- Some of the models (Park et al., 1984b; Tang et al., 1987; Stevens et al., 1989) have large numbers of parameters, many of which cannot be determined independently. Simpler but realistic models are needed if they are to be useful for design and optimization.

3 Materials and Methods

3.1 Materials

3.1.1 Bacterium

The bacterium, *Pseudomonas putida* Q5, used in this research, is a naturally occurring psychrotroph which was isolated from the sediments of the Bay of Quinte in Lake Ontario (Inniss and Mayfield, 1978). It was obtained from the culture collection of Professor W. E. Inniss, Department of Biology, University of Waterloo. *P. putida* Q5 is a motile Gram-negative rod, approximately 0.8 μm wide and 3 μm long, which may possess up to three flagella (Kolenc et al., 1988). At high temperatures (ie. 30°C) it adopts a filamentous form (Kolenc et al., 1988).

P. putida Q5 is capable of growth at 0°C, but has its maximum growth rate (with salicylate as the carbon source) at temperatures between 25 and 30°C (Kolenc et al., 1988). Its maximum temperature for growth is between 30 and 37°C (Kolenc et al., 1988).

P. putida Q5 can degrade a wide variety of organic substrates including phenol, as it possesses the *ortho*-cleavage pathway (Kolenc et al., 1988). Its phenol degradation kinetics have been determined at 10°C (Kotturi et al., 1991) and it has been used successfully to degrade phenol in an ICFBR under steady-state conditions (Patoine, 1989).

3.1.2 Medium

A dilute basal salts medium (DBSM) was used for all experimental work, including the kinetics experiments and the ICFBR studies. The composition of the dilute basal salts medium is given in Table 3.1. The medium composition is the same as that described by Patoine (1989), except that calcium concentration has been increased to 50 mg/L as Ca to improve biofilm cohesiveness as described by Turakhia and Characklis (1989). The composition of the medium was designed such that the substrate – phenol - would be growth-limiting. The medium was prepared and autoclaved in two parts to prevent precipitation of the medium components. Solution A consisted of the K_2HPO_4, KH_2PO_4 and $(NH_4)_2SO_4$ with sufficient solid sodium hydroxide to maintain the reactor pH at 6.9-7.3 (eg. 25 pellets in a 20 L batch with 300 mg/L phenol) dissolved in 80% of the deionized water listed in Table 3.1. Solution B consisted of the remaining

Table 3.1. Compositions of the Dilute Basal Salts Medium (DBSM)

Component	Concentration (g/L)
K_2HPO_4	0.17
KH_2PO_4	0.13
$(NH_4)_2SO_4$	0.71
$MgCl_2.6H_2O$	0.34
+ 1 mL of each of the following solutions per litre of medium:	
$MnCl_2.4H_2O$	0.1 g/100 mL H_2O
$FeSO_4.7H_2O$	0.06 g/100 mL H_2O
$CaCl_2.2H_2O$	2.6 g/100 mL H_2O
$Na_2MoO_4.2H_2O$	0.2 g/100 mL H_2O

Note: Deionized water added to volume.

components, dissolved in the remaining deionized water. The two solutions were combined asceptically by pumping Solution B through sterile tubing into Solution A immediately prior to use.

3.1.3 Support Particles

Sand particles, used in previous ICFBR studies (Wagner and Hempel, 1988; Patoine, 1989), were used as the support material. Sand is inexpensive and widely available and has been shown to be an acceptable substratum for biofilm formation by *P. putida* Q5 (Patoine, 1989). The sand used in this study was obtained from the Universitat Gesamthochschule Paderborn and is characterized by an approximate diameter of 212 μm and a density of 2580 kg/m^3 (Patoine, 1989).

3.2 Experimental Apparatus

3.2.1 Growth Kinetics Experiments

Batch growth experiments with initial phenol concentrations in a range of 20-600 mg/L were performed in 250 mL Erlenmeyer flasks with a working volume of 70 mL. The flasks were stirred constantly at 170 rpm on a New Brunswick Scientific Gyratory Water Bath Shaker, Model G76 (New Brunswick Scientific, New Brunswick, NJ). Temperatures were maintained at 10, 15, 20 and 25°C +/- 0.2 °C with a refrigerated circulator (RTE-111 Refrigerated Bath/Circulator, Neslab Instruments Inc., Newington, NH). The flasks were sparged continuously with filter-sterilized air (Whatman Polycap 75 TF,

0.1 μm pore size, Whatman International Ltd., Maidstone, England) using an aeration manifold and sparging apparatus as described by Donovan et al. (1995), in order to avoid oxygen limitation of the cultures. The inoculum was grown in batch culture (S_o=20-600 mg/L phenol) and was acclimated to the initial phenol concentration used in each experiment.

Growth experiments at phenol concentrations less than 20 mg/L were performed in a 1-litre continuous flow stirred tank reactor (CFSTR) (Bioflo, New Brunswick Scientific, New Brunswick, NJ) with a working volume of 0.450 L. The system was sterilized by autoclaving at 121°C for 30 minutes. The reactor was sparged with filter-sterilized air (Whatman Polycap 75 TF, 0.1 μm pore size, Whatman International Ltd., Ann Arbor, MI) and was equipped with a galvanic oxygen probe (New Brunswick Scientific, New Brunswick, NJ) to ensure that the culture was not oxygen limited. Temperature was maintained constant at preset levels (10, 15, 20 and 25°C) by simultaneously chilling the reactor by means of a cooling coil operating at a coolant temperature several degrees below the desired reactor temperature (using a RTE-111 Refrigerated Bath/Circulator, Neslab Instruments Inc., Newington, NH), and by simultaneously heating the reactor with an immersion heater (C30 Immersion Heater, New Brunswick Scientific, New Brunswick, NJ) activated by an on-off closed-loop controller (which was part of the Bioflo system). Feed was delivered by a peristaltic pump (30 rpm model, Hurst, Princeton, IN). The effluent was withdrawn with another pump (6 rpm Masterflex pump drive fitted with an Easy Load pump head, Cole Parmer, Niles, IL) at a preset liquid level and at a higher volumetric flow rate, so that there would not be any build-up of broth in the system.

3.2.2 Immobilized-Cell Fluidized Bed Reactors (ICFBRs)

Two external-loop airlift reactors containing biofilm-coated sand were used for shock-loading experiments. One reactor was constructed of glass; the other was constructed of Plexiglass. Both reactors had similar dimensions and geometry. Characteristics of each system are listed in Table 3.2. A schematic of the reactors is shown in Figure 3.1. For both reactors, the bottom of the top section of the riser consisted of a flat surface inclined at an angle of 45 degrees. This prevented settling of the bioparticles in the gas disengagement section prior to their recirculation (as a slurry) to the downcomer and hence to the bottom of the riser.

Filtered air was passed through a rotameter and a sterilizing filter (Whatman Polycap 75 TF, 0.1 μm pore size, Whatman International Ltd.,Ann Arbor, MI) and was sparged at the bottom of the riser sections.

The spargers consisted of a 1-cm diameter stainless steel tube with 6 holes of 1 mm diameter, in a 1 cm thick stainless steel plate. Dissolved oxygen was monitored in the riser section with a galvanic dissolved oxygen probe (New Brunswick Scientific, New Brunswick, NJ) connected to a chart recorder (Model 285, Linear Instruments Corporation, Reno, NV). Exhaust air was filtered (Whatman Polycap 75 TF, 0.2 μm pore size, Whatman International Ltd., Ann Arbor, MI).

The temperature of the reactor was controlled by circulating a polyglycol (commercial antifreeze) solution from a RTE-111A Non-CFC Analog Refrigerated Bath Circulator (Neslab, Mississauga, ON) through a cooling jacket on the riser. Temperature was measured with a thermometer inserted through the top of the downcomer. The Plexiglass reactor also was equipped with a thermometer in the downcomer at the junction of the circulating external loop and the settling zone.

The pH of the circulating suspension in the glass reactor was measured with a glass electrode in the downcomer. The pH of the Plexiglass reactor was periodically measured off-line from samples taken from the riser. In both cases the pH was maintained in a range of 6.9-7.3.

Feed was stored in autoclaved 20-litre carboys, equipped with filters (Polydisk, 0.1 μm, Whatman International Ltd., Ann Arbor, MI) to sterilize air that was drawn into the tanks as the medium was pumped into the reactor. Feed was delivered with a peristaltic pump (Model XX 80000000, 6-600 rpm, Millipore, Bedford, MA) at various flow settings to achieve the desired dilution rates. The liquid level was kept constant by pumping broth from effluent ports at the top of the downcomer section above the solids settling zone, using a 6 rpm Masterflex pump drive fitted with an Easy Load pump head, (Cole Parmer, Niles, IL) at a preset liquid level and at a higher volumetric flow rate, so that there would not be any build-up of broth in the system.

Table 3.2 Characteristics of the Glass and Plexiglass Airlift Reactors

Characteristic	Glass Reactor	Plexiglass Reactor
Working Volume (L)	3.46	4.22
Internal Diameter of the Riser (cm)	7	7.6
Internal Diameter of the Downcomer (cm)	4	3.2
Diameter at the top of the Riser (cm)	10	8.7
Height of the settling zone (cm)	32	48

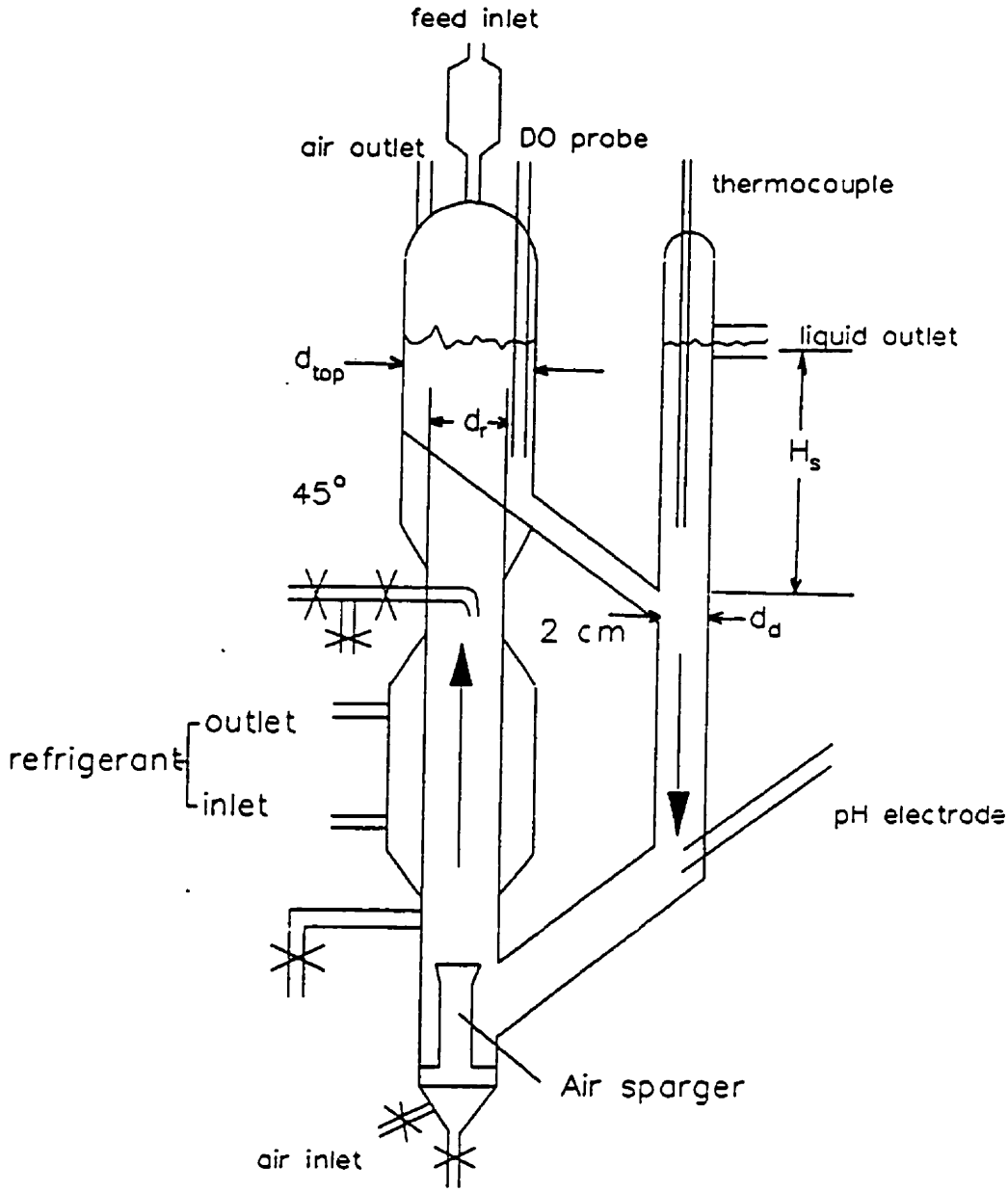

Figure 3.1. Schematic of the ICFBR reactors.

3.3 Analytical Methods

3.3.1 Phenol

Phenol concentrations were measured by UV spectrofluorometry (UV spectrofluorometer, Turner Model 430, Palo Alto, CA) at the UV emission and excitation wavelengths of 314 and 273 nm, respectively. Samples containing bacteria were centrifuged at 8,000 rpm for 3 minutes (Eppendorf Centrifuge 5415C, Brinkmann Instruments (Canada) Ltd., Rexdale, ON) and the supernatant was withdrawn for analysis. Samples were stored in a freezer when analysis could not be performed immediately. Samples were diluted with deionized water such that the phenol concentrations were within the range of 0-15 mg/L in order to obtain a linear response with the spectroflurometer. The detection limit was 0.02 mg/L phenol (Kotturi et al., 1991). A calibration curve is shown in Figure 3.2.

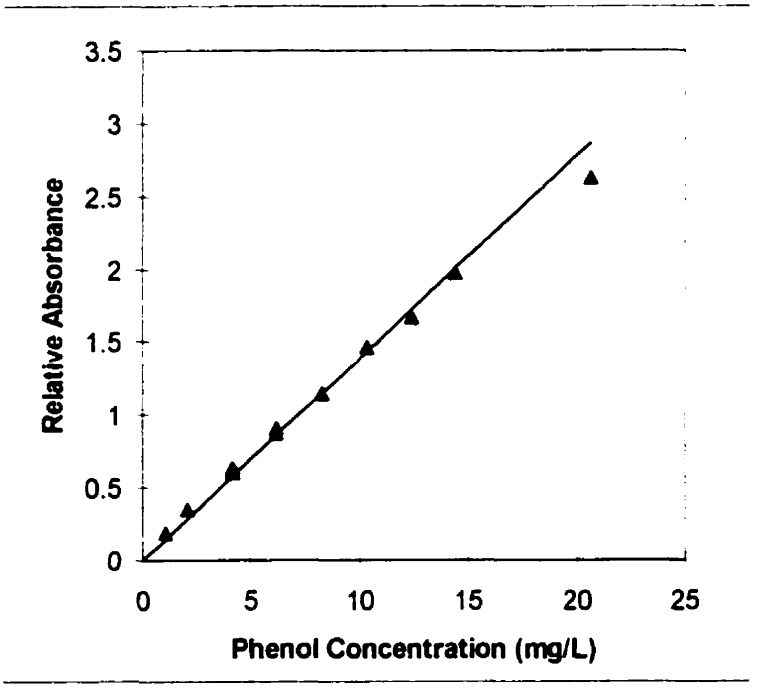

Figure 3.2. Phenol calibration curve for the Turner spectrofluorometer

3.3.2 Intermediate Metabolites

The absorbance spectra of filtered samples from the broth were measured to indicate the presence of intermediate metabolites. Samples in quartz glass cuvettes (Hellma 104-QS, Fisher Scientific, Toronto, ON) were scanned in the range of 230–450 nm using a spectrophotometer (Spectronic Genesys 5, Milton Roy, Rochester, NY).

3.3.3 Suspended Biomass Concentration, X_s

Cell growth was monitored by optical density (OD) measurement using a spectrophotometer (Novaspec II Model 4040011, LKB Biochrome Ltd., Cambridge, England) at a wavelength of 650 nm. Biomass concentrations on a dry weight basis were determined by filtering the cell suspension through a 0.2 μm filter (cellulose nitrate filter, Sartorius, Göttingen, Germany) and drying the filter and cells to a constant weight for 24 hours at 80°C. A linear relationship (shown in Figure 3.3) between OD below 0.40 and dry weight was observed at each temperature. The biomass concentration (X_S), expressed as dry weight (mg DW/L) was calculated from optical density measurements using the relationship $OD650=kX_S$, where k was 0.435, 0.423, 0.464 and 0.500 for cells grown at 10, 15, 20 and 25°C, respectively. The 95% confidence intervals for the slopes at 10, 20 and 25°C intersected, indicating that the curves were statistically indistinguishable, given the degree of scatter in the data. The 95% confidence interval at 15°C fell outside those at 20 and 25°C.

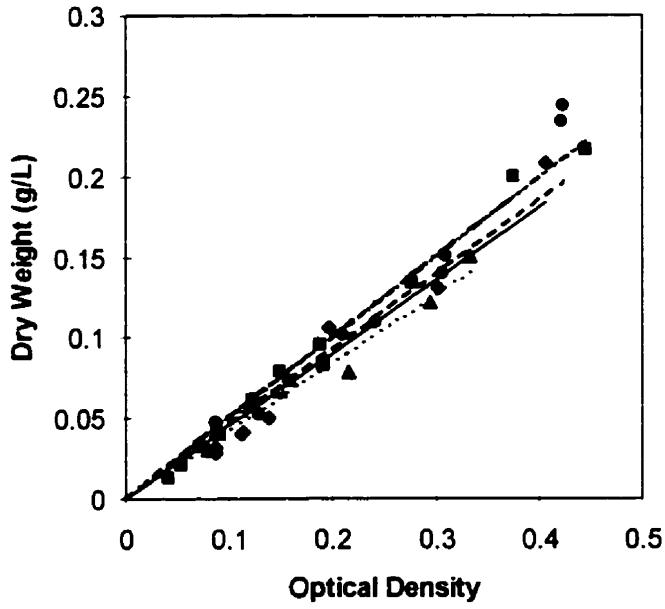

Figure 3.3 Dry weight data at 10°C (♦), 15°C (▲), 20°C(●) and 25°C (■) plotted with calibration curves at 10°C (———), 15°C (- - - - -), 20°C (– – – –), and 25°C (– - - –)

3.3.4 Bioparticle Diameters and Biofilm Thickness

Bioparticle diameters were measured through image analysis of digital photographs taken of 200-400 particles per sample using a photomicroscope. A video camera (Sony Hyper HAD CCD-IRIS/RGB Color Video Camera, Model DXC-15A, coupled with a Sony Camera Adaptor CMA-22, Sony Corporation, Japan) was mounted on a Nikon microscope (Nikon Optphot Phase Contrast Microscope, Nippon Kogku KK, Tokyo, Japan) and was connected to a 80486 computer equipped with a Snappy Video Snapshot Hardware Module and Snappy Software Version 1.0 (Play Incorporated, Rancho Cordova, CA). The digital images were analysed using UTHSCSA Image Tool Version 2.0. The image analysis software was calibrated spatially using an image of a stage micrometer, which had been photographed at the same magnification (X40) and resolution (640x640) as the bioparticles.

All of the digital images were captured using the bright field setting. Identification of objects in the images was based upon differences in gray levels. Thresholding was performed manually. Bioparticles that were touching slightly were separated using a pixel editor. Bioparticles that were cut off at the edge of the image field, or were partially covered with other bioparticles were not included. Particles, which were

essentially free of biofilm growth, appeared white (on a white background) or slightly gray. It was not possible to obtain information about the size of the bare particles because of difficulties separating portions of the particles from the background. The number of bare particles for each sample was determined subjectively, and was recorded for comparison with the total number of particles. Particles which were covered with biofilm appeared to be gray, dark gray or black, depending upon the amount of biofilm coverage and the degree to which the biofilm blocked the light. Note that during Runs 2 and 3, the digital camera was not available and photographs were taken using the dark field setting. The pictures appear to be reverse images of the others described above, with covered particles appearing bright white on a dark background.

The ferret diameter, defined as the diameter of a circle having the same area (A) as the object, was computed as:

$$d_{bp} = \sqrt{4A/\pi} \tag{3.1}$$

The biofilm thickness (δ) was calculated as half the difference between the average bioparticle diameter (d_{bp}) and the average bare sand particle diameter (d_p), which was calculated for bare sand particles using the same procedure.

The 80% confidence interval ($CI_{80\%}$) of the biofilm thickness was calculated as follows (Box et al., 1978):

$$CI_{80\%} = \frac{1}{2} t_{0.1} s \sqrt{\frac{1}{n_{bp}} + \frac{1}{n_p}} \tag{3.2}$$

where

$$s^2 = \frac{(n_{bp}-1)s_{bp}^2 + (n_p-1)s_p^2}{(n_{bp}-1)+(n_p-1)} \tag{3.3}$$

Here n_{bp} and n_p are the numbers of particles in the bioparticle and bare carrier samples, respectively, with sample standard deviations of s_{bp} and s_p, respectively.

3.3.5 Extracellular Polysaccharides (EPS) in the Biofilm

An adaptation of the method of Pacepavicius et al. (1997) was used to measure the polysaccharide content of the biofilm. The method is based on the conversion of hexoses to 5-(hydroxymethyl)-2-furaldehyde (HMF) in the presence of strong acid and the subsequent development of a colour chromogen between phenol and HMF.

Samples, approximately 5 mL in volume, were taken from the riser section of the ICFBR and were placed in pre-weighed 25 mL test tubes. The sand in each sample was washed with DBSM to remove suspended biomass and the liquid was removed with a Pasteur pipette. 1 mL of deionized water and 1 mL of a 10% phenol solution were added to each test tube and the contents were agitated gently. Next, 5 mL of concentrated sulphuric acid were added rapidly. The samples stood for 20 minutes, during which time the contents were swirled periodically to ensure that the samples were well mixed. The absorbance of the supernatant in a quartz glass cuvette (Hellma 104-QS, Fisher Scientific, Toronto, ON) was measured at a wavelength of 484 nm (corresponding to the peak in the absorbance maximum shown in Figure 3.4) against a reagent blank in a spectrophotometer (Spectronic Genesys 5, Milton Roy, Rochester, NY). The amount of EPS

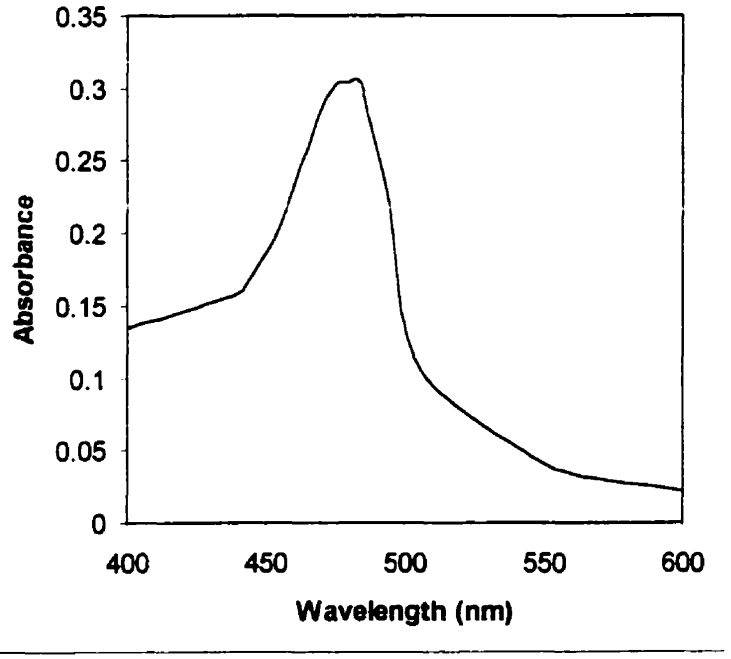

Figure 3.4 Scan of a biofilm sample treated with concentrated phenol and sulphuric acid as described in Section 3.3.5.

present was determined from a standard curve for glucose, shown in Figure 3.5, and was expressed as grams glucose equivalents per gram sand.

3.3.6 Biofilm Biomass Concentration and Sand Concentration

Samples for biofilm and sand concentration were taken from the middle of the riser by withdrawing fluid quickly from a sampling port with a sterile 20-mL syringe. The sample volume (V_s) was measured and recorded (±0.1 mL). The bioparticles were allowed to settle in a preweighed test tube (of mass M_1) and then the supernatant containing suspended cells was removed with a Pasteur pipette. The sample was dried at 105°C until a constant mass (M_2) was reached (24 h). The dry sample was burned in a muffle furnace at 500°C for 1 hour and then was reweighed (M_3) after cooling in a dessicator.

The particle concentration in the sample was calculated as

$$C_p = \frac{M_3 - M_1}{V_S} \tag{3.4}$$

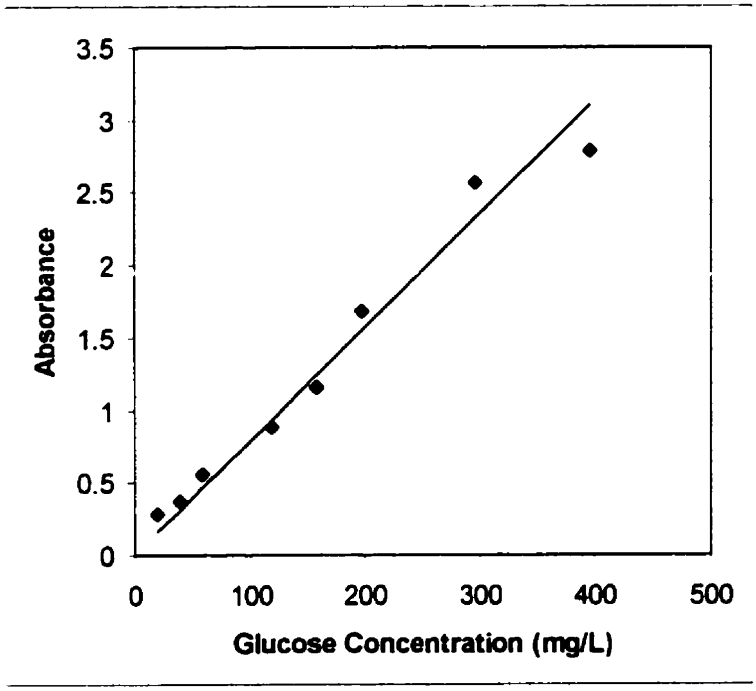

Figure 3.5 Effect of glucose concentration on absorbance development at 484 nm.

The biofilm concentration (X_f) [g DW/L] was calculated as:

$$X_f = \frac{(M_3 - M_2)}{V_s} \tag{3.5}$$

On a sand basis, the biofilm concentration (X_{DW}) [g DW/g sand] was calculated as:

$$X_{DW} = \frac{X_f}{C_p} \tag{3.6}$$

3.3.7 Number of Particles, N_p

The mass of a single sand particle (m_p) was calculated as:

$$m_p = \frac{\pi d_p^3}{6\rho_p} \tag{3.7}$$

The average ferret diameter of the bare sand (d_p) was determined according to Section 3.3.4 and the particle density (ρ_p) was given as 2.58 g/cm^3 (Patoine, 1989).

The mass of sand added to the reactor (P_i) was determined prior to sterilization. Thus, the initial number of particles (N_{pi}) is given as:

$$N_{pi} = \frac{P_i}{m_p} \tag{3.8}$$

The volume of samples withdrawn from the reactor was recorded. The average mass of sand withdrawn per mL sample was calculated using Equation 3.4 , and the value of N_p was adjusted over the course of the experiments.

3.3.8 Biofilm Dry Density

The biofilm density, dry basis (ρ_f) [g DW/cm^3 wet biofilm] was calculated as follows, where N_{ps} is the number of particles in a sample and d_{bp} is the ferret diameter of the bioparticles in a corresponding sample taken at approximately the same time.

$$\rho_f = \frac{M_3 - M_2}{N_{ps}(\frac{\pi}{6})(d_{bp}^3 - d_p^3)} \tag{3.9}$$

3.4 Experimental Procedures

3.4.1 Sterilization

To maintain a pure culture of *P. putida* Q5, and to avoid contamination of the laboratory, all equipment and media were sterilized.

Small fermenters, shake flasks and any other glassware as well as the basal salts medium in carboys were autoclaved at 121°C. Time for sterilization ranged from 20 minutes for shake flasks to 3 hours for a 20-L carboy filled with medium or 4 hours for two 20-L carboys.

The glass external-loop airlift reactor was autoclaved in sections prior to assembly. Both airlift reactors were sterilized by filling them with bleach solution (15% v/v Javex) for 6-12 hours, followed by thorough rinsing with sterile deionized water, with one rinse cycle lasting at least 12 hours.

The sand was autoclaved wet for 1 hour and then was autoclaved again for 1 hour immediately before adding it to the airlift reactors. This technique was found to be necessary to destroy flagellate cysts that were contained in the sand.

3.4.2 Phenol Biodegradation Kinetics Experiments

Phenol biodegradation kinetics experiments were carried out in both batch and continuous cultures.

Batch growth experiments with initial phenol concentrations in a range of 20-600 mg/L were performed in 250 mL Erlenmeyer flasks at 10,15, 20 and 25°C. The working volume of the batch cultures was 70 mL. The apparatus used during the experiments is described in Section 3.2.1. The inoculum was grown in batch culture (S_o=20-600 mg/L phenol) and was acclimated to the initial phenol concentration used in each experiment. A number of batch growth experiments were also performed at phenol concentrations ranging from 20-180 mg/L with suspended cells which were obtained from the effluent

stream of the ICFBR. These were acclimated to the very low phenol concentrations occurring in the ICFBR, but had not adapted to growth at the concentrations used in the batch experiments.

Growth experiments at phenol concentrations less than 20 mg/L were performed in a small CSTR described in Section 3.2.1. The reactor was started up in batch mode with an initial concentration of 200 mg/L phenol and 5 mL inoculum, which had been grown in a shake flask with an initial phenol concentration of 200 mg/L. Once the phenol was exhausted, as indicated by a sharp increase in dissolved oxygen, the feed pump was started up and the system was operated continuously. Runs were terminated within 4 days of start-up to minimize any possible effect of biofilm growth on the walls of the reactor.

3.4.3 Shock-loading Experiments in the ICFBRs

The ICFBR reactors were started up by injecting approximately 20 mL of inoculum from a batch culture into the reactor containing sterile medium with a phenol concentration of 200 mg/L. Once the cell density was high, feed containing 200 mg/L phenol was delivered to the system and sterile sand was added with a 60 mL syringe through a port at the top of the downcomer section. The reactor was operated continuously for 20-30 days until a stable biofilm had developed, indicated by a relatively constant EPS concentration on the sand particles.

Once steady-state was established the system was perturbed, either by increasing the feed flow rate (for a dilution shock-load) or by changing the feed tank to another with a different phenol concentration (for a concentration shock-load). The response of the system was followed over a period of 50 to 250 hours, depending upon the experiment.

3.5 Numerical Methods

3.5.1 Estimation of Kinetic Parameters

The Haldane kinetic parameters μ_{max}, K_S and K_I and the parameters of true growth yield, Y_g, and the maintenance coefficient, m, were determined from batch- and continuous-culture kinetic data at each temperature.

$\underline{Y_g \text{ and } m}$

In a batch culture the observed yield is defined by

$$\frac{1}{Y_{XS}} = \frac{m}{\mu} + \frac{1}{Y_g} \tag{2.7}$$

Y_{XS} for each substrate concentration was estimated by determining the slope of a plot of $X_v(t)$ versus $S(t)$ for the exponential growth phase of the culture at each temperature. The specific growth rate, μ, at specific phenol concentrations was similarly determined as the slope of a plot of $\ln X_v$ versus time. Y_g and m were estimated from a plot of $1/Y_{XS}$ versus $1/\mu$, which had a slope m with an ordinate intercept of $1/Y_g$.

In a continuous culture at steady state the specific rate of substrate utilization (q_S) is given as

$$q_S = \frac{D(S_o - S)}{X_v} = \frac{D}{Y_g} + m \tag{3.10}$$

Thus using experimentally determined values of S and X_v a plot of q_S versus D will have the slope $1/Y_g$ and an ordinate intercept of m.

Haldane Kinetic Parameters (μ_{max}, K_S and K_I)

Estimation of the Haldane kinetic parameters is inherently difficult due to the nature of the Haldane model (Equation (2.10)). As discussed in Section 2.1.3.2, the model is nonlinear, the parameters are highly correlated (Allsop, 1989) and the data required to estimate K_S (which must be attained at low substrate concentrations) is difficult to obtain accurately with batch cultures.

Two approaches have been used to estimate the Haldane kinetic parameters: linearization followed by linear regression and nonlinear regression. The approach used by Hill and Robinson (1975) was used to divide the Haldane curve (see Figure 2.3) into two sections. At high substrate concentrations ($S >> K_S$),

$$\mu = \frac{\mu_{max}}{1 + \frac{S}{K_I}} \tag{3.11}$$

which can be linearized as follows:

$$\frac{1}{\mu} = \frac{1}{\mu_{max}} + \frac{S}{K_I \mu_{max}} \tag{3.12}$$

A plot of $1/\mu$ versus S_o with slope $1/K_I\mu_{max}$ and ordinate intercept $1/\mu_{max}$ was used to estimate K_I and μ_{max}

The problems usually encountered when obtaining batch-culture data at low substrate concentrations (with small changes in biomass concentration over time) needed to determine K_S, were to be avoided by using a steady-state continuous culture to obtain kinetic data. At low substrate concentration ($S<<K_I$), the Haldane equation (Equation 2.10) can be simplified as follows:

$$\mu = \frac{\mu_{max} S}{K_S + S} \tag{3.13}$$

Then at steady state (where $\mu=D$), the following relationship may be obtained:

$$K_S = \frac{S(\mu_{max} - D)}{D} \tag{3.14}$$

Equation 3.14 can be used to estimate K_S from S and D data when the value for μ_{max} is known from the batch suspended-cell-culture experiments.

Thus, estimates of μ_{max} and K_I were determined using the technique described for batch cultures. An estimate of K_S was obtained from continuous data. Next, non-linear regression of the μ and S_o (or steady-state S) data from the full data set (combining batch and continuous data) with the previously estimated values of μ_{max}, K_S and K_I as initial guesses was performed using Systat®.

3.5.2 Solution of the Unsteady-state ICFBR Model

The unsteady-state ICFBR model described in Chapter 4 consists of a set of ordinary and partial differential equations (ODEs and PDEs) along with the required boundary and initial conditions. There are four interdependent variables which were determined by the model:

- the bulk substrate concentration, S_b,
- the biofilm substrate concentration as a function of radial distance within the biofilm, $S_f(r)$,
- the freely-suspended biomass concentration X_S, and
- the biofilm thickness, δ, which can also be expressed in terms of the radial distance to the biofilm surface, r_f.

Four key equations define the system:

- a balance on the bulk substrate concentration, ODE, Equation 4.1,
- a balance on the substrate concentration within the biofilm, PDE, Equation 4.5,
- a balance on freely suspended biomass, ODE, Equation 4.10, and
- a balance on biomass in the biofilm, ODE, Equation 4.16.

The resulting system was difficult to solve numerically due to the stiffness of the equations and the existence of a moving boundary-value problem. The stiffness arises from the wide differences in the characteristic times of the various processes in the ICFBR.

Several techniques were used to render the system of equations into something more manageable. First, the shape of the substrate concentration profile within the biofilm was approximated as a parabola to simplify the defining equation for S_f (Equation 4.5). This resulted in a curvature-related parameter a', which replaced S_f as a variable. Second, Leibniz's Rule was applied to an expansion of Equation 4.5 (see Appendix B) to address the issue of the moving boundary (in the variable r_f) arising from biofilm growth. The resulting integral equation was ungainly and difficult to approach using the available numerical solver. The variable θ was then introduced, to consolidate an untidy group within a differential term and the variable a', was redefined as a function of θ. Another term resisted analysis and was integrated numerically. The result was a set of four ODEs in the variables S_b, θ, X_S, and r_f, which was amenable to numerical methods. The transformation of the model is given in Appendix B.

The system was solved with MATLAB's ODE23s solver which is based on Gear's method and is appropriate for sets of stiff equations.

3.5.3 Model Calibration Procedure

The steady-state form of the model was coded in MATLAB (listed in Appendix C) and was used to determine the initial steady-state values of the four variables (S_b, X_S, a', and r_f). The variable θ was calculated using these values in a separate program (listed in Appendix C). The parameter values used in these determinations are described in Section 5.1 and listed in Appendix B. When possible, experimental values

or those obtained using relevent correlations were used. Two exceptions were the values of r_D and m which were adjusted to better fit the model simulations to the experimental data as described in Section 5.3.2.1.

The unsteady-state model (described in Appendix A-2 and with code listed in Appendix C) was solved using the input variables (S_h, X_S, θ, and r_f) generated with the steady-state model. The two high-response experiments (Runs 1 and 8) were investigated first as a means of exploring the influence of alternate kinetics and the concept of growth rate hysteresis through trial and error. Once agreement was obtained between the model and the first two experiments, the model was verified by simulating the responses in the two low-response experiments (Runs 2 and 3) and comparing the simulations with the experimental data. The same parameters used in the expressions for the kinetics and growth rate hysteresis were used in each simulation. Also, the parameters used in the unsteady-state simulations were the same as those used in the steady-state simulations within each run.

3.6 Safety Considerations

The general safety guidelines described by Robinson (1992) and the specific procedures outlined by Onysko (1993) were followed for handling chemicals and biologicals and for disposing of wastes.

4 Dynamic Model

4.1 Model Assumptions

It should be clear from the review of the literature in Chapter 2, that the ICFBR is a very complex system. The relationships between the microorganisms and the reactor environment (and *vice versa*) are difficult to model accurately. Even if all the relationships determining system behaviour were known, the parameters could not be determined independently of each other and the large number of parameters would make the model difficult to implement in an engineering context. Thus, simplifying assumptions are necessary for the development of an appropriate model.

Processes occurring within the ICFBR and the variables which have been reported to influence them are listed in Table 4.1. Those variables which were considered in the proposed ICFBR model are presented in bold type. Table 4.2 lists the variables that were controlled at constant or non-critical values for all experiments.

Table 4.1. Processes Occurring within the ICFBR and Potential Variables[1]

Microbial Reaction Kinetics		
substrate concentration and rate of change	death	pH
biomass activity	oxygen limitation	temperature
maintenance	nutrient limitations	microorganism type
decay	unbalanced growth	acclimation/history
immobilization effects	growth phase	product type and yield
Liquid-bioparticle mass transfer		
fluid properties	superficial gas velocity	particle size and density
solids holdup	reactor geometry	temperature
Gas-liquid Mass Transfer		
fluid properties	superficial gas velocity	media composition
solids fraction	reactor geometry / type	temperature
Mass Transfer within the Biofilm		
biofilm thickness	component concentration	dispersion
biofilm properties	ionic effects	temperature
Detachment/Attachment		
nutrient limitations within biofilm	**abrasion (particle concentration)**	**biofilm thickness/volume**
shear stress	media characteristics	microorganism type
growth rate / substrate concentration	support particle surface properties	biofilm surface properties
suspended biomass concentration	temperature	

[1] Variables printed in bold font are incorporated into the proposed model.

Table 4.2. Potential Variables that Were Held Constant or at Non-critical Values

Variables that were monitored and controlled		
superficial gas velocity	dissolved oxygen	temperature
	pH	
Potential variables that were set		
initial media composition (except for phenol concentration)	support particle characteristics (type, size, density)	microorganism type
reactor geometry	media fluid properties at specified temperature	

For a process or variable to be incorporated into a model the following conditions must be met.

1. A method of accurate measurement or a reliable correlation to predict the variable must be available.

2. The effect of the variable must be independently distinguishable from those of other processes or variables (ie. not evaluated solely as a result of multi-variable data fitting).

3. The effect must be important to the overall performance of the system.

These criteria were used to select potentially important variables and to develop a dynamic ICFBR model.

System Description

The system was an external loop airlift reactor in which sand particles covered with a pure culture biofilm were fluidized due to air sparging in the riser section. The reactor contained both immobilized and freely-suspended biomass; the latter was produced through detachment of microorganisms from the biofilm and growth of freely-suspended cells. The excess suspended cells left the system along with the effluent stream; the bioparticles were retained. The feed was a synthetic wastewater with phenol as the sole carbon source.

Model Assumptions

The following assumptions define the scope of the model.

Reactor and components

- *The bulk fluid in the reactor is completely mixed.* This assumption has been justified for airlift reactors in general (Merchuk et al., 1992) depending on operating conditions and for an internal loop airlift reactor containing bioparticles (Tang et al., 1987). Thus, bulk fluid-phase concentrations can be assumed to be uniform throughout the reactor for the sand concentrations used in this work, namely 6-25 g/L bare carrier..

- *The sand particles can be represented as being spherical in shape and uniform in size (average diameter)* The method for determining the average particle diameter used in the model was described in Section 3.3.5.

Growth Kinetics

- *Only a portion of the measured immobilized biofilm is active.* This has been shown to be the case due to the presence of extracellular polymeric substances (EPS) (Bakke et al., 1984) and inactive bacteria (Rittmann et al., 1992) in the biofilm.
- *The fraction of active biomass in a mature biofilm remains constant over the expected range of operating conditions and during system disturbances.* The inactive fraction of the biofilm (due to the presence of EPS and inactive cells) was expected to not change significantly, even during disturbances. In the literature, there is not enough information about the effects of system variables on EPS content or inactive cells in biofilms to provide the basis for a model which describes the change in the active biomass fraction. Models which do so (Benefield and Molz, 1985; Gadani et al., 1993), incorporate the concept of decay only, and neglect the existence of EPS. This assumption was likely reasonable for nutrient-sufficient biofilms (ie. substrate concentration profiles of the types (a) and (b) in Figure 2.5) which would correspond to biofilms of thicknesses less than 40 μm in this case.
- *Balanced growth occurs within the biofilm under the expected operating conditions.* This means that the extensive properties of the cells change in proportion to the change in cell number. While this is a reasonable assumption under steady state conditions, under dynamic conditions, particularly if the step changes are large, this may not be the case. However, to include unbalanced growth, structured kinetic models would have to be developed. This may unnecessarily complicate the model for engineering use. This assumption is discussed in detail in Section 5.3.2.2.
- *Immobilization does not affect the stoichiometry or the kinetics of biological transformations.* This assumption was discussed in detail in Section 2.2.5. Studies in which the microenvironment was carefully controlled have shown this to be a reasonable assumption (Bakke et al., 1984; van Loosdrecht et al., 1990; Shreve and Vogel, 1993), and it has been used with reasonable success to model other biofilm systems with phenol as a substrate (Tang and Fan, 1987; Tang et al., 1987; Worden and Donaldson, 1987). Conflicting studies described in Section 2.2.5 have not provided the

kind of information that could be included in a mathematical model (eg. Keweloh et al., 1989; Hilge-Rotmann and Rehm, 1990; Heipieper et al., 1991).

- *The active biomass in the biofilm is phenol limited only.* Other nutrients and oxygen were provided in excess of cellular requirements
- *Growth kinetics follow a substrate inhibition model.* The Haldane model, a substrate inhibition model, has been used previously to describe the phenol degradation kinetics of *P. putida* Q5 (Patoine, 1989; Kotturi et al., 1991), as well as other phenol-degraders. During the dynamic experiments phenol concentration in the reactor reached inhibitory levels; hence a substrate-inhibition model was required. A simplified version of the Luong model (Luong, 1987), another substrate inhibition model, was also investigated.

Liquid-solid mass transfer

- *Liquid-solid mass transfer cannot be neglected.* This has been shown to be the case for other ICFBRs (Tang and Fan, 1987; Livingston and Chase, 1989).

Gas-liquid mass transfer

- *Gas-liquid mass transfer is not included in the model.* The quantity of oxygen supplied to the ICFBR was considered to be in excess of biofilm requirements; hence there was no need to describe the transfer of oxygen to the bulk fluid in the model (see Appendix F).

Mass transfer within the biofilm

- *On each bioparticle, the biofilm is uniform in thickness, density and the distribution of cells, EPS and interstitial fluid and can be treated as a continuum.* Although it is possible that biofilm properties may change with radial distance, only the measurement of average properties over the biofilm for many particles was possible.
- *Transport of dissolved components into and out of the biofilm is by molecular diffusion and can be described by Fick's second law of diffusion.* The biofilm was thick enough (up to 40 μm) in some experiments that diffusional effects cannot be neglected.
- *Concentration gradients are significant only in the direction perpendicular to the support surface; thus, a one-dimensional model is adequate.* The assumption was based upon the assumed symmetry of the bioparticles.

- *The ratio of the diffusion coefficient in the biofilm to that in pure water of all soluble components is independent of radial direction and component concentration and can be treated as a constant value at any particular temperature.*

Detachment

- *The specific rate of detachment of microorganisms from the biofilm is constant under the expected operating conditions.* In this context, the net specific rate of detachment, r_D, also includes the specific rate of attachment, which is not possible to separately determine experimentally. Detachment in an airlift reactor is a function of many variables and correlations have not yet been developed. Because the development of a comprehensive detachment model was beyond the scope of this project, the rate of detachment was calculated according to Section 5.1.4.4, and was assumed to be constant as a first approximation

Adsorption

- *Adsorption of phenol to the biofilm and sand particles is considered to be negligible.*

Temperature

- *The temperature of the biofilm is the same as the bulk fluid temperature.* It was assumed that there was no significant effect of metabolic heat generation. The transfer of heat through the biofilm and then to the bulk fluid was considered to be sufficiently rapid. This is discussed further in Appendix G. The assumptions of the model are compared to those made in other dynamic ICFBR models in Table 4.3.

Table 4.3 Comparison of the Assumptions of the Proposed Model to Other Unsteady-state ICFBR Models

Assumptions	Proposed Model	Other Unsteady-state Models				
		1	2	3	4	5
Complete mixing of liquid	■	■	■	■	□	■
Uniform particles	■	■	■	■	■	■
Biofilm growth	■	■	■	■	□	■
Single microbial species	■	■	■	■	□	□
Suspended cells	■	□	□	□	□	□
EPS present	■	□	□	□	□	◊
Balanced growth	■	♦	■	■	■	■
No immobilization effect on kinetics	■	■	■	■	■	■
Single substrate limitation	■	□	□	□	□	■
Dual/multiple substrate limitation	□	■	■	■	■	□
Liquid-solid mass transfer	■	■	□	□	□	■
Gas-liquid mass transfer	□	■	□	■	□	□
Uniform biofilm	■	□	■	■	■	■
Fickian diffusion in biofilm	■	■	■	■	■	■
Detachment	■	■	□	□	□	■
Adsorption to biomass	□	□	□	□	□	□

■ - assumption made / condition included
□ - assumption not made / condition not included
◊ - inert fraction due to decay only, not EPS
♦ - balanced growth in kinetics but time delay added to model as a correction term

Unsteady-state models
1. Tang et al. (1987)
2. Worden and Donaldson (1987)
3. Park et al. (1984b)
4. Stevens et al. (1989)
5. Gadani et al. (1993)

4.2 Model Development

Phenol biodegradation in the external-loop airlift reactor involves the following processes, which have been included in the model:

1. transport of phenol from the bulk fluid across a boundary layer to the external surface of the biofilm,
2. simultaneous diffusion and consumption of phenol and oxygen in the biofilm,
3. biodegradation of phenol by the suspended cells in the reactor,
4. biofilm growth and detachment.

The following is the unsteady-state model developed for the external-loop airlift ICFBR. The key variables are the phenol concentration in the bulk fluid (S_b), the concentration of the freely-suspended biomass (X_S) and the biofilm thickness (δ) as indicated by the bioparticle radius (r_f).

Substrate balances

The bulk fluid concentration of phenol (S_b) in the reactor can be expressed as follows by performing an overall mass balance on the bioreactor:

$$\frac{dS_b}{dt} = D[S_o - S_b(t)] - (\frac{\mu_b}{Y_g} + m) X_S - \frac{A_{bp} J}{\varepsilon_L V_R} \tag{4.1}$$

Here, phenol is consumed by the suspended biomass and is also transported into the biofilm. The total biofilm surface area (A_{bp}) is expressed as,

$$A_{bp} = 4\pi r_f^2 N_p \tag{4.2}$$

where r_f is the bioparticle radius at the external biofilm surface and N_p is the number of bioparticles in the system. The flux (J) of phenol from the bulk fluid to the biofilm surface at r_f is expressed as,

$$J = k_s(S_b - S_{f\,r_f}) \tag{4.3}$$

and the specific growth rate of suspended cells in the bulk fluid (μ_b) is,

$$\mu_b = \frac{\mu_{max} S_b}{K_s + S_b + \frac{S_b^2}{K_I}} \tag{4.4}$$

To solve Equation 4.3, the phenol concentration profile in the biofilm is required. A balance on phenol concentration in the biofilm (S_f) is given by

$$\frac{\partial S_f}{\partial t} = D_{S,f}\left(\frac{\partial^2 S_f}{\partial r^2}\right) - \left(\frac{\mu_f}{Y_g} + m\right) f \rho_f \tag{4.5}$$

Here, f is the active fraction of biomass and ρ_f is the biofilm density [g DW cells/cm^3 wet biofilm]. The local specific growth rate in the biofilm (μ_f) is given by

$$\mu_f = \frac{\mu_{max} S_f}{K_S + S_f + \frac{S_f^2}{K_I}} \tag{4.6}$$

and the diffusivity of phenol in the biofilm is given by

$$D_{S,f} = \frac{D_e}{D_w} \times D_{S,w} \tag{4.7}$$

Here $D_{S,w}$ is the diffusivity of phenol in pure water and D_e/D_w is a correction factor as described in Section 2.2.3.2. The above system of equations is subject to the following boundary conditions:

$$D_{S,f}\frac{\partial S_f}{\partial r} = 0 \quad at \quad r = r_p \tag{4.8}$$

which accounts for the fact that the substrate cannot diffuse into the solid, non-porous support particle at the particle-biofilm interface and

$$D_{S,f}\frac{\partial S_f}{\partial r} = k_s\left(S_b - S_{f\,r_f}\right) \quad at \quad r = r_f \tag{4.9}$$

which expresses the continuity of the phenol flux at the bulk fluid-biofilm interface.

Balance on suspended biomass

Suspended biomass is produced through detachment of the biofilm and through growth of the existing freely-suspended biomass. A balance on the suspended biomass is given as

$$\frac{dX_S}{dt} = \mu_b X_S - DX_S - R_{det} \tag{4.10}$$

where R_{det} is an overall rate of detachment [g DW/L.h]). R_{det} is given as,

$$R_{det} = \frac{4\pi(r_f^3 - r_p^3) N_p \rho_f r_D}{3\varepsilon_L V_R}. \tag{4.11}$$

where r_D is the specific detachment rate [h^{-1}] and is considered to be constant under conditions of constant solids fraction in the suspension, gas velocity and temperature.

Balance on biofilm biomass

For a single bioparticle the rate of increase of biofilm mass (m_{bf}) is given as,

$$\frac{dm_{bf}}{dt} = r_{growth} - r_{detachment} \tag{4.12}$$

Because the inactive fraction in the biofilm is assumed to be constant, EPS and inactive cells must be produced in the biofilm at some rate that results in a constant fraction of inactive biomass (f_I). The rate of biofilm growth cannot be based solely on the rate of growth of active biomass. Instead, the rate of biofilm growth must be based on the increase in active and inactive biomass. This introduces a problem, in that the kinetics will be determined in suspended cell cultures in which EPS is not produced and essentially all the bacteria are active. However, at this point in the model, the production of EPS and inactive bacteria must be assumed to allow for a constant inactive fraction in the biofilm when it is growing. This inconsistency is not expected to pose a problem. Because $f+f_I=1$, the rate of biofilm growth for a single bioparticle is given as,

$$r_{growth} = 4\pi \rho_f \int_{r_p}^{r_f} \mu_f r^2 dr \tag{4.13}$$

Similarly, because the rate of detachment is assumed to be the same for the active and the inactive fractions, the rate of detachment for a single bioparticle is given as,

$$r_{detachment} = 4\frac{\pi}{3}(r_f^3 - r_p^3)\rho_f r_D \tag{4.14}$$

Because the biofilm is assumed to be of constant density, the rates of change in biomass and volume are equal; hence,

$$\frac{dr_f}{dt} = \frac{1}{4\pi r_f^2 \rho_f}\frac{dm_{bf}}{dt} \tag{4.15}$$

Thus the rate of biofilm growth in the radial direction is given as,

$$\frac{dr_f}{dt} = \frac{1}{r_f^2}\left(\int_{r_p}^{r_f} \mu_f r^2 dr - \frac{1}{3}(r_f^3 - r_p^3)r_D\right) \tag{4.16}$$

Because the biofilm thickness may change with time, the above system of equations represent a moving boundary problem. This was dealt with by using the Leibniz rule (see Appendix A).

Influence of Reactor Hydrodynamics

Because complete mixing of the bulk fluid is assumed in the model, differences between conditions in the various sections of the airlift reactor are neglected. Reactor hydrodynamics are not explicitly considered in the model; however, the hydrodynamics of the system are implicitly considered in the choice of the correlation for the external mass transfer coefficient. The correlation of Mao et al. (1992), Equation 2.74, for k_S was chosen because it is the only correlation which was developed for an external-loop airlift reactor.

4.3 Summary of Model Parameters

The following is a summary of model parameters and the methods that were used to estimate them

Table 4 4. Summary of Model Parameters

Parameters	Description	Method of parameter estimation
μ_{max}	kinetic parameters	batch- and continuous-culture kinetic experiments (see Section 3.4.2)
K_S		
K_I		
Y_g	true growth yield	continuous culture experiments (see Section 3.4.2)
m	maintenance coefficient	
$D_{S,w}$	diffusivity of phenol in water	calculated using Equation 2.42
$D_e D_w$	ratio of diffusivities in the biofilm and water	average literature value (see Section 5 1.3)
ρ_f	biofilm density	calculated (see Section 3.3.8)
f	biomass active fraction	estimated (see Section 5.1.2.2)
r_D	specific detachement rate	calculated using Equation 5.9
k_s	liquid-solid mass transfer coefficient	calculated using Equation 2.74
ε_l	liquid hold-up	calculated using Equation 2.61
r_p	particle radius	measured (see Section 3.3.4)
V_R	volume of the reactor	measured
N_p	Number of particles	calculated (see Section 3.3.7)

5 Results and Discussion

This chapter includes:

- the results of batch- and continuous- culture studies performed to assess the phenol biodegradation kinetics of *P. putida* Q5, including temperature effects,
- parameter estimates obtained from a compilation of steady-state and dynamic conditions in the ICFBRs,
- a discussion of the response of the ICFBRs to shock-loads in both phenol concentration in the influent and dilution rate, and
- an assessment of the ability of the model to describe the dynamics of the response of the ICFBRs to shock-loading..

5.1 Parameter Estimation

5.1.1 Phenol Biodegradation Kinetics

A conventional method for estimating kinetic parameters is to conduct continuous or shake flask experiments with cultures acclimated to the substrate at concentrations at which the experiments are performed. In the case of phenol, which can be inhibitory at concentrations above 30 mg/L, acclimation is helpful because shake flask experiments at concentrations above 300 mg/L are useful in providing information for the determination of K_I, the inhibition term in the Haldane model. Without acclimation, the delay before the culture begins to grow can be very long. For example, a delay of approximately 10 days was noted in a culture with an initial phenol concentration of 600 mg/L, which had been exposed to low levels of phenol at 10°C. Some cultures under similar conditions showed no signs of growth after a month. Working with acclimated cultures is convenient; however, whether the data can be applied to reactors, which at steady state operate at a very low phenol concentrations, is an open question.

The application of degradation kinetics determined from acclimated cultures to the cultures in the ICFBR conditioned to low-level phenol concentrations was examined in a series of batch experiments at 10°C. The results of these experiments are discussed in Section 5.1.1.2, and are compared to the kinetics determined using acclimated cultures which are discussed in Section 5.1.1.1.

5.1.1.1 Phenol Biodegradation Kinetics with Acclimated Cultures

The kinetics of phenol degradation of *P. putida* Q5 were determined by combining data from both batch and continuous suspended cultures operating at temperatures in the range of 10-25°C (similar to the approach taken by Hill and Robinson (1975)). Batch cultures were used to degrade phenol at inhibitory concentrations, at which stable operation of a continuous suspended cell reactor would not be possible. Continuous cultures were used to evaluate kinetics at dilution rates below the critical dilution rate (the point at which washout would occur).

Batch cultures were grown at phenol concentrations in the range of 20 to 600 mg/L. Lag times of up to 3 hours were observed at higher concentrations. However, these were shorter than some reported in the literature (Kotturi et al., 1991; Hill and Robinson, 1975); the reductions in lag times presumably were due to the use of acclimated inocula which were in the log phase of growth when transferred to the batch cultures. Also, relatively large inoculum sizes were used (approximately 20% v/v), which have been shown to minimize the lag time (Andrews, J. F., 1968). A typical batch-growth history is shown in Figure 5.1.

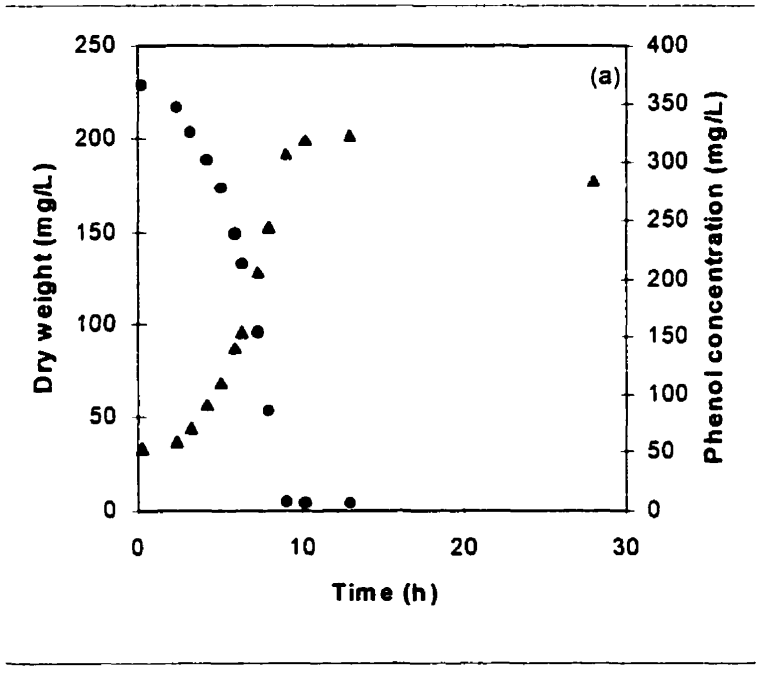

Figure 5.1. Typical cell growth (▲) and phenol degradation (•) during abatch experiment using *P. putida* Q5 at 25°C and S_o=366 mg/L phenol.

In batch cultures, the growth rate was determined as the slope of the straight line portion of a plot of $\ln X$ (where X is the cell dry weight concentration) versus time after the lag phase. In cultures with fairly high initial phenol concentrations (300-600 mg/L), the specific growth rate increased during the latter portion of the run, reflecting decreased inhibition as the phenol was consumed; thus, only the initial straight line portion of the curve was used in the analysis. The initial phenol concentration (S_o) was used to represent the phenol concentration at each growth rate. Initial guesses for the Haldane parameters, μ_{max} and K_I were obtained using a linearized form of the Haldane model at high phenol concentrations ($S>>K_S$). These were used as initial values when using nonlinear regression (using Systat®) to estimate the Haldane parameters for the full data set which also included the results from continuous experiments.

Continuous cultures without cell recycle were grown at phenol concentrations in the feed in the range of 200-300 mg/L and at dilution rates less than the expected critical dilution rate at a given temperature. The culture was assumed to have reached steady state when the optical density (indicating cell concentration) and phenol concentration were relatively constant over a 24-hour period. Experiments were run for more than 3 hydraulic retention times from the moment the shock was applied. The specific growth rate was taken as the dilution rate at which the system was operated. Five steady-state phenol concentrations were measured at each dilution rate and were averaged. Phenol concentrations were typically low (1-4 mg/L), but reached up to 38.5 mg/L when a high dilution rate was used (0.213 h^{-1} at 20°C).

A linearized form of the Haldane model at low phenol concentrations ($S<<K_I$) was used to estimate K_S from the continuous data, which was used as an initial guess in the nonlinear regression of the full data set.

Estimation of Kinetic Parameters

The Haldane parameters (μ_{max}, K_S, K_I) were determined using non-linear regression using a quasi-Newton technique using the statistical software package, Systat®. The parameter estimates for *P. putida* Q5 at four different temperatures are presented in Table 5.1 together with the results from other studies using various strains of *P. putida*, most of which are mesophiles. The parameter estimates at 25°C are similar to those estimated for mesophiles at 30°C, although it is surprising that the μ_{max} for two strains of mesophilic *P. putida* (Chi and Howell, 1976; Hutchinson and Robinson, 1988) at 30°C was lower than the value obtained

for psychrotrophic *P. putida* Q5 at 25°C. The parameter estimates at 10°C for μ_{max}, K_S, and K_I [0.112 ± 0.012 h^{-1}, 2.50 ± 0.75 mg/L, 175 ± 56 mg/L, respectively] are different from those of Kotturi et al. (1991)[0.119 h^{-1}, 5.27 mg/L, 377 mg/L] using the same strain of *P. putida* at the same temperature. Specific growth rates calculated from Kotturi's data (determined as the slope of the initial straight-line portion of the ln$X$ versus time curve for each experiment) are plotted in Figure 5.2, along with the data obtained in the present work; the two data sets are consistent within the variability obtained with this type of biological experiment. The data from the present work are also consistent with the results obtained by Kolenc et al. (1988) for *P. putida* Q5 with salicylate as the carbon source. Generation times calculated from experimental values of μ^* (*P. putida* Q5 growing on phenol), using Equation 2.11 agree well with Kolenc's values (*P. putida* Q5 on salicylate); for example, at 10 and 25°C the respective generation times of *P. putida* Q5 were 7.1 and 2.0 h with phenol as a substrate, and 6.3 and 2.1 h with salicylate as a substrate (Kolenc et al., 1988).

Table 5.1. Haldane Parameters Reported for Various Strains of *P. putida* Grown on Phenol

Reference	Culture	Experiment	Temperature [°C]	μ_{max} [h^{-1}]	K_S [mg/L]	K_I [mg/L]
Yang and Humphrey (1975)	*P. putida* ATCC 17514	continuous	30	0.567	2.39	106
Hill and Robinson (1975)	*P. putida* ATCC 17484	continuous	30	0.534	<1	470
Chi and Howell (1976)	*Pseudomonas* sp.	transient	30	0.369	5.94	227
Sokol and Howell (1981)	*P. putida* NCIB10015	batch (washed)		0.443-1.61*	0.16-5.22	7.5-19.4
Hutchinson and Robinson (1988)	*P. putida* ATCC 17484	batch	30	0.388	1.06	903
Kotturi et al. (1991)	*P. putida* Q5	batch	10	0.119	5.27	377
Present work	*P. putida* Q5	batch and continuous	10 15 20 25	0.112 0.193 0.297 0.419	2.50 3.59 4.71 7.09	175 172 213 221

* Specific uptake rate is reported: $U=\mu Y$

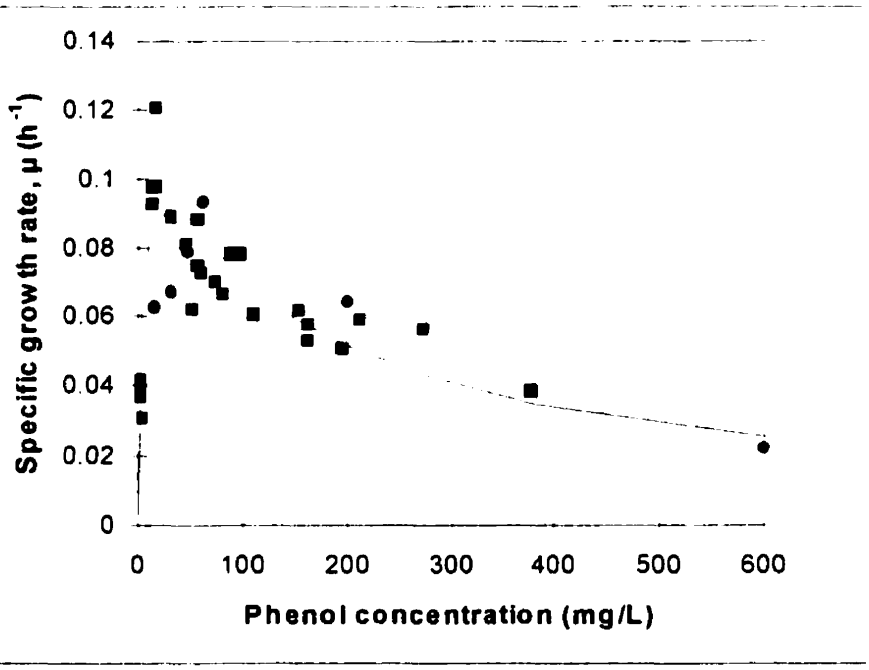

Figure 5.2. Data (■) from batch and continuous phenol degradation experiments using *P. putida* Q5 at 10°C compared to data (•) from batch experiments by Kotturi (1989). The fitted curve [——] was plotted using the Haldane parameters: μ_{max}=0.112 h^{-1}, K_S=2.50 mg/L, K_I=175 mg/L.

Several problems were encountered when fitting the data to the Haldane model. Non-linear regression techniques are sensitive to the choice of initial values of the parameters, resulting in multiple parameter sets (Sokol and Howell, 1981; D'Adamo et al., 1984). Multiple parameter sets were obtained at several of the temperatures by varying the initial estimates. The parameters presented in Table 5.1 (present work) are those with the higher r^2 values. They also more closely match the data close to the critical value, μ^*, which is where the growth rate peaks. The Haldane model was found to underestimate the observed μ^* values at all temperatures by 3-15%, depending upon the temperature (see Figure 5.3). The μ^* value is key in predicting washout in steady-state conditions for continuous reactors, so using the Haldane model would result in lower predicted critical dilution rates than the observed kinetic data would suggest.

In Figure 5.3, the fit of the Haldane model for μ versus S is compared to that of the other models shown in Table 2.2 using the parameter values given in Table 5.2. It is clear from the plots in Figure 5.3 and the r^2-values in Table 5.3, that there is little difference among the predictions of the various models at phenol concentrations below 250-300 mg/L, depending on the temperature. The model predictions diverge from each other at phenol concentrations above 350 mg/L; however, stable operation of a continuous

reactor, even with a biofilm present, is not expected at these higher concentrations. A slight improvement (2-3%) in the prediction of μ^* was obtained with the model of Webb (1963) at 10 and 25°C; however, in practice the improvement was not large enough to justify the use of a four parameter model instead of the Haldane model which has three. The model of Edwards (1970) also fit the data slightly better at 15 and 20°C; however, none of the models consistently described the data best at all temperatures.

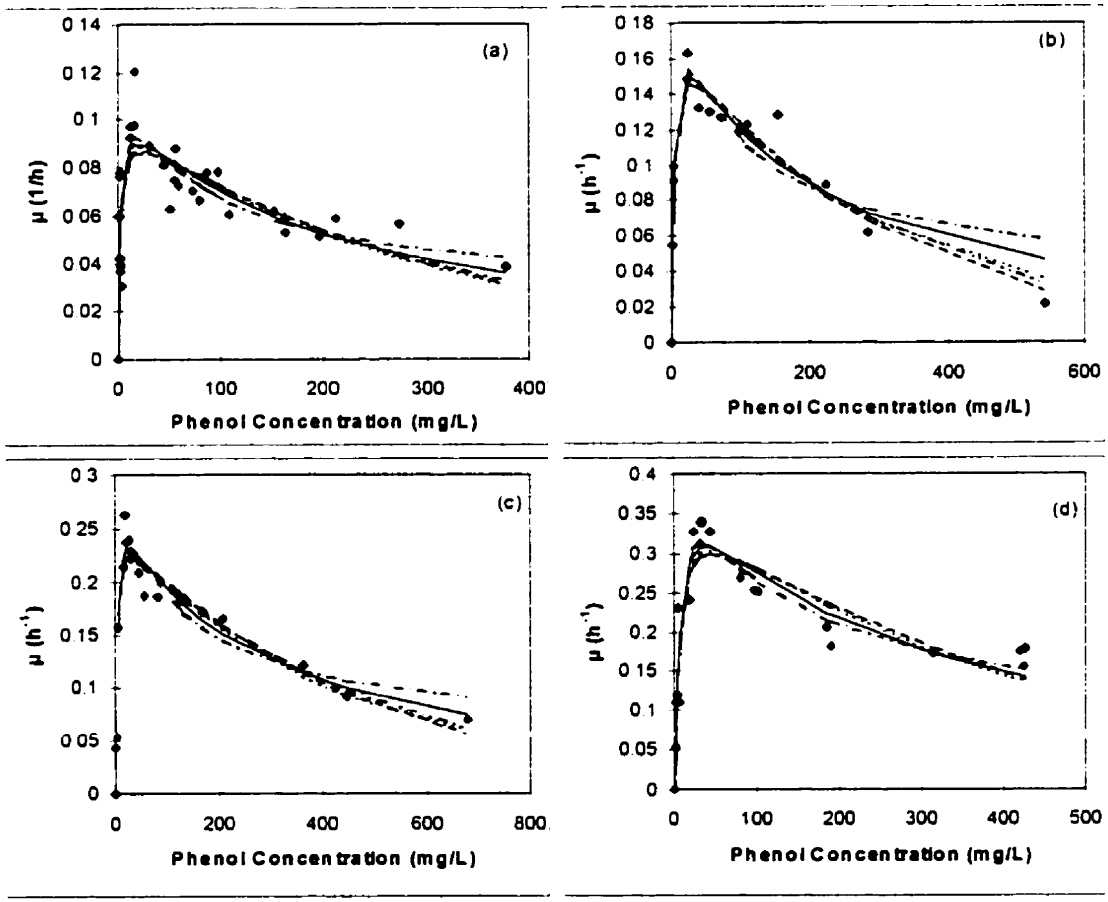

Figure 5.3. Comparison of the fit of substrate-inhibition models with the data [•] at: a) 10°C b) 15°C c) 20°C and d) 25°C for *P. putida* Q5 using the models of Haldane (1930)[——], Webb (1963)[- - - -], Yano et al. (1966)[------], Aiba et al. (1968)[- - -], and Edwards (1970)[- -- -]. The inhibition models are given in Table 2.2 and model parameters are given in Table 5.3.

Table 5.2. Parameter Estimates and Regression Statistics for Various Substrate-inhibition Models

Temperature (°C)	Model	Estimates				r^2 Values
		μ_{max} [h^{-1}]	K_S [mg/L]	K_I [mg/L]	K' [mg/L]	
10	Haldane (1930)	0.112	2.50	175		0.956
	Webb (1963)	0.127	3.24	73.4	357	0.958
	Yano et al. (1966)	0.108	2.35	137	356	0.955
	Aiba et al. (1968)	0.101	1.94	326		0.954
	Edwards (1970)	0.095	2.93	357		0.954
15	Haldane (1930)	0.196	3.87	167		0.989
	Webb (1963)	0.221	4.94	81.5	536	0.983
	Yano et al. (1966)	0.178	3.13	287	512	0.991
	Aiba et al. (1968)	0.178	3.10	300		0.992
	Edwards (1970)	0.163	4.14	340		0.993
20	Haldane (1930)	0.277	2.89	251		0.994
	Webb (1963)	0.306	3.98	119	669	0.993
	Yano et al. (1966)	0.255	2.12	438	638	0.993
	Aiba et al. (1968)	0.253	1.96	459		0.993
	Edwards (1970)	0.239	4.08	502		0.995
25	Haldane (1930)	0.419	7.09	221		0.976
	Webb (1963)	0.470	8.75	105.6	662	0.979
	Yano et al. (1966)	0.379	5.83	404	643	0.972
	Aiba et al. (1968)	0.371	5.49	446		0.971
	Edwards (1970)[1]	-	-	-	-	-

[1] No convergence obtained in curve fitting.

Effect of Temperature on Kinetic Parameters

The effect of temperature on the Haldane parameters is shown in Figure 5.4. All three Haldane parameters, μ_{max}, K_S, and K_I, increased with increasing temperature.

Haldane Maximum Specific Growth Rate, (μ_{max})

The Arrhenius (Equation 2.24) and square-root (Equation 2.30) models (both usually applied to the Monod model constant μ_m) were applied to the estimates of μ_{max} obtained from the batch and continuous experiments. The Arrhenius model was chosen over others in Table 2.3, because it is widely applied in the literature and it has the fewest number of parameters. Of the square-root models presented in Table 2.4, Equation 2.30 was chosen because it applies specifically to growth at temperatures below the optimum temperature for growth (between 25 and 30°C for *P. putida* Q5 (Kolenc et al., 1988). Parameter estimates for each of the models were obtained through linear regression of the Arrhenius and square-root plots.

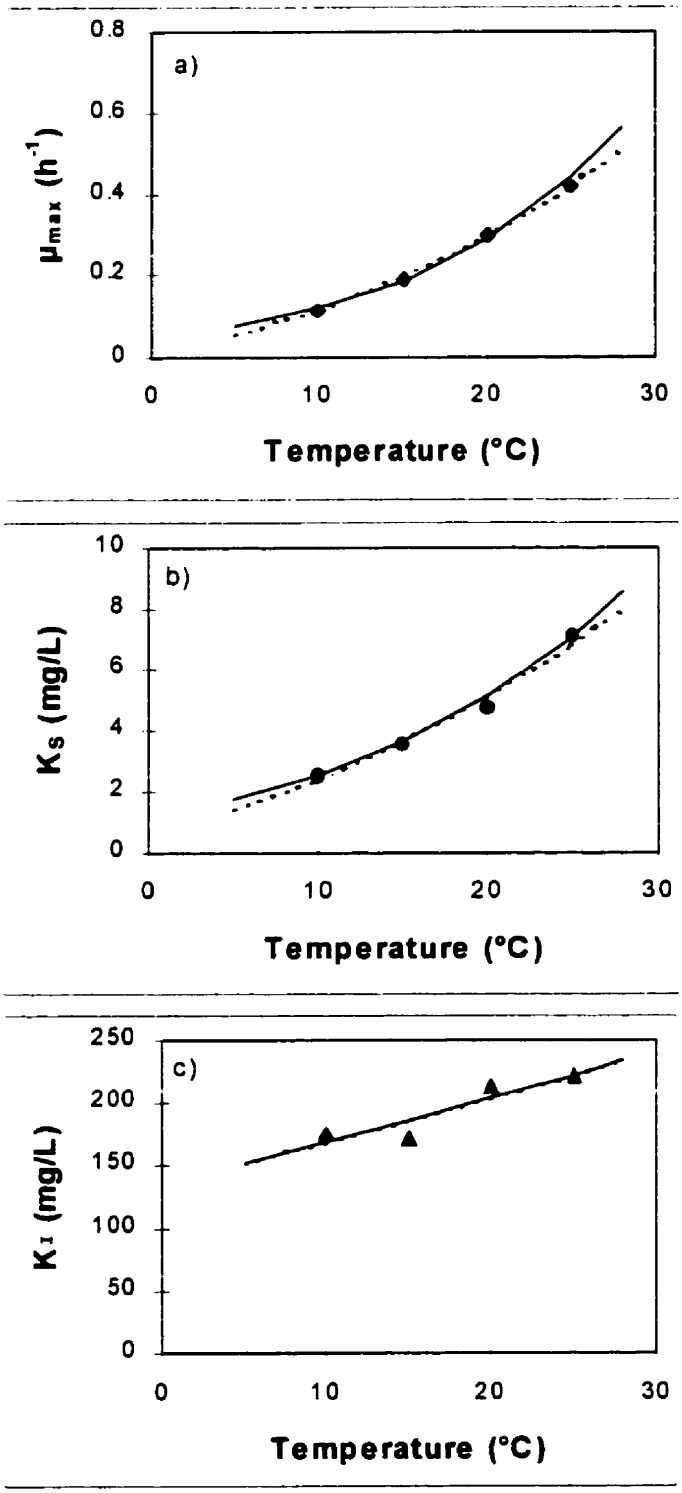

Figure 5.4. Temperature effect on the Haldane model parameters a) μ_{max} b) K_S and c) K_I using the Arrhenius model (Equations 2.24,5.1 and 5.3, respectively) [——] and the square-root model (Equations 2.30, 5.2 and 5.4, respectively)[------].

The estimate of the temperature characteristic for μ_{max} in the Arrhenius model (ΔH^*=61.6 kJ/mol; A=2.78x10^{10} h^{-1}) was well within the range of values reported in the literature for different organisms and substrates, but for similar temperature ranges (see Table 5.3). Note that the temperature characteristic is 'constant' only over narrow temperature ranges and tends to increase as temperature decreases. Activated sludge (presumed to be composed primarily of mesophiles) had a lower temperature characteristic [39.0 kJ/mol](Benedek and Farkas, 1970) in a similar range of temperatures (10-20°C), although the reason for this is not known.

Table 5.3. Comparison of the Arrhenius Temperature Characteristic for μ_{max} with Literature Values

Reference	Culture	Temperature Range (°C)	Medium	ΔH^* (kJ/mol)
Palumbo and Witter (1969)	*P. fluorescens*	8-30	glucose	35.3
Benedek and Farkas (1970)	Activated sludge	10-20	phenol	39.0
Reynolds et al. (1974)	*Selanastrum capricornutum*	20-28	phenol	28.4
Langeveld and Cuperus (1980)	*Pseudomonas* strain 423a	10-30	lactose	63.0
Brocklehurst and Lund (1981)	*Pseudomonas fluorescens* BL 78/34	0.2-20.8	synthetic	83.0
	Pseudomonas strain BL 78/50	0.2-20.8	synthetic	79.5
Melin et al. (1998)	mixed culture	4-16.5	2,4,6-trichlorophenol, 2,3,4,6-tetrachlorophenol, and pentachlorophenol	126-196 for TCP and TeCP; 59-130 for PCP
Willocx et al. (1993)	*P. fluorescens*	1.1-11.5	tryptone soy broth	120
Present work	*P. putida* Q5	10-25	phenol	61.6

In the case of the square-root model, the characteristic temperature (T_o) for μ_{max} was estimated as -6.4°C. This is comparable to the value reported for psychrotrophic *P. fluorescens* [T_o= -1.4°C] (Willocx et al., 1993). T_o corresponds approximately to the minimum temperature for growth, which in this case is not known for *P. putida* Q5. Kolenc et al. (1988) reported significant growth on salicylate at 0°C for *P. putida* Q5; thus, a predicted minimum temperature for growth on phenol of -6.4°C also seems reasonable.

Arrhenius and square root plots (Figure 5.5) for μ_{max} showed that either relationship could be applied to model μ_{max}. The r^2 value of 0.9999 for the square-root model (Equation 2.30) was higher than

the r-squared value of 0.992 for the Arrhenius model (Equation 2.24). While it would be preferable to have more data over a wider temperature range before one relationship is considered better than the other, nonetheless the square-root model was applied to the current work.

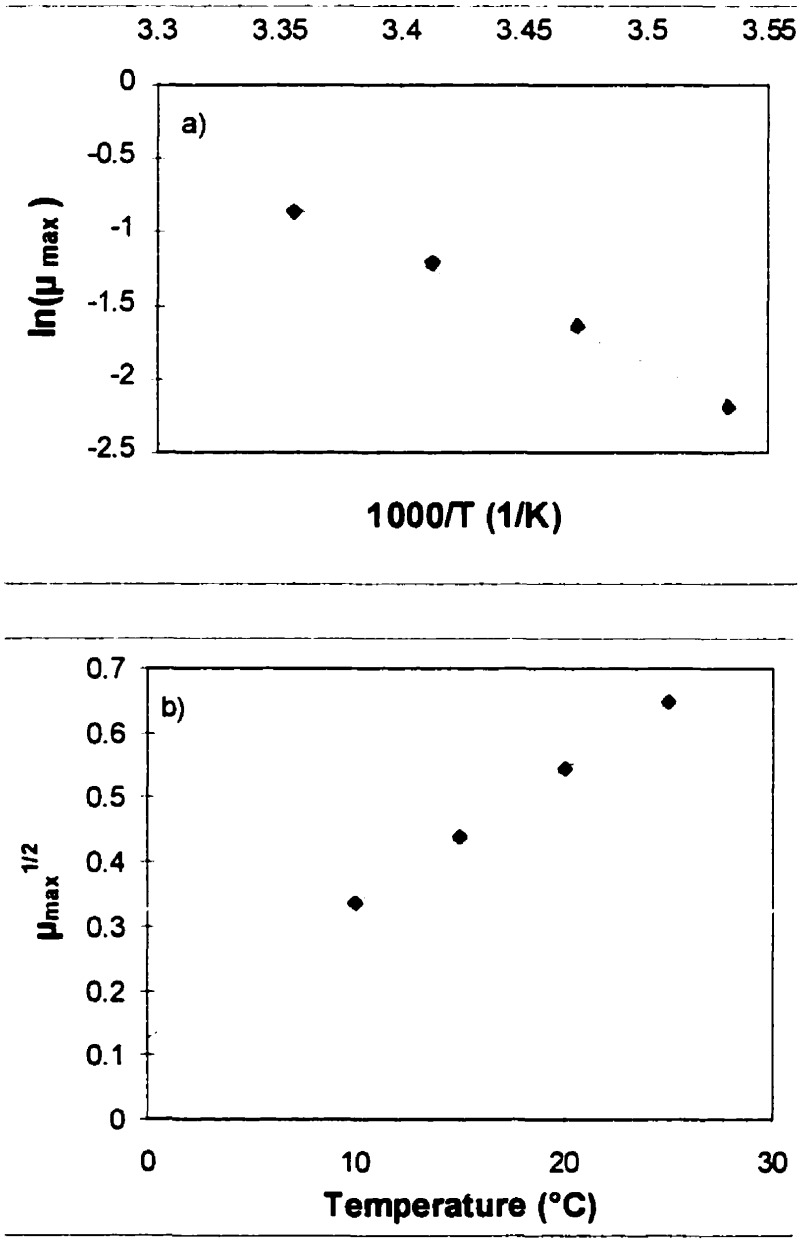

Figure 5.5. a) Arrhenius plot and b)square root plot for μ_{max}.

It should be noted that the Haldane and Arrhenius models are empirical models when applied to biological systems, as the original enzyme and thermodynamic bases for the models do not apply to

complex living systems in which potentially hundreds of reactions are occurring simultaneously Thus, one must be careful when inferring physical significance about parameters such as μ_{max} or ΔH^* The square-root models were developed as empirical models without any biological basis (Zwietering et al., 1991) T_o roughly corresponds to the minimum temperature for growth when applied to the maximum specific growth rate μ_m (and may also do so for the Haldane parameter μ_{max}), however, there is no reason to believe that it has any physical meaning when applied to other parameters such as K_S and K_I.

Saturation Constant, (K_S)

The Arrhenius and square-root models were also applied to the estimates of K_S using the equations:

$$K_S = A_S e^{\left(\frac{-\Delta H_S^*}{RT}\right)} \quad \textbf{(5.1)}$$

$$\sqrt{K_S} = b_S(T - T_{o,S}) \quad \textbf{(5.2)}$$

Both models are plotted with the data for K_S in Figure 5.4b. The Arrhenius model fit the estimates of K_S very well. Linear regression of the ln-transformation of the Arrhenius equation yielded a r^2-value of 0.993. The estimate of ΔH_S^* was 47.6 kJ/mol (A=1.53x10^7 mg/L), which is within the range of 20.9 to 100 kJ/mol reported in the literature (Marr et al., 1963; Knowles et al., 1965; Stevens et al., 1989). The fit of the square-root model to the estimates of K_S was not as good, with r^2-value of 0.982. The parameter values for b_S and $T_{o,S}$ were 0.0704 (mg/L·°C)$^{1/2}$ and −12.0°C, respectively. The Arrhenius model will be used to model the effect of temperature on K_S because the r^2-value was higher.

Haldane Inhibition Constant, (K_I)

K_I was less sensitive to temperature than the other parameters (see Figure 5.4c). K_I decreased as temperature decreased, suggesting that the inhibition effect of phenol increased as the temperature decreased. This effect was also reported by Eismann et al. (1994) for phenol-degrading methanogenic cultures. The Arrhenius and square-root models were applied to the estimates of K_I using the following equations:

$$\sqrt{K_I} = b_I(T - T_{o,I}) \quad \textbf{(5.3)}$$

$$K_I = A_I e^{\left(\frac{-\Delta H_I^*}{RT}\right)} \quad \textbf{(5.4)}$$

The square-root model (b_I=0.128 (mg/L·°C)$^{1/2}$ and $T_{o,I}$=-91.7°C), with an r^2-value of 0.826 fit the data slightly better than the Arrhenius model (ΔH_I^*=12.78 kJ/mol and A=3.86x10^4 mg/L) with an r^2-value of 0.818;

however, the two curves are almost indistinguishable, as shown in Figure 5.4c. The square-root model was chosen to model the effect of temperature on K_I in this work.

Yield and Maintenance Coefficients

The true growth yield (Y_g) and maintenance (m) coefficients were related to the apparent growth yield (Y_{XS}) using the relationship given by Pirt (1965).

$$\frac{1}{Y_{XS}} = \frac{1}{Y_g} + \frac{m}{\mu} \qquad (2.7)$$

Values of Y_g and m at the four temperatures tested in both batch and continuous cultures are given in Table 5.4.

The apparent yield (Y_{XS}= -dX/dS) was calculated for each batch experiment by determining, using linear regression, the slope of a plot of $X(t)$ versus $S(t)$ for the initial portion of the exponential growth phase (defined as the straight line portion of the ln$X$ versus time plot just after the end of the lag phase). Generally, Y_{XS} decreased with increasing phenol concentration (see Figure 5.6), as would be expected from the definition in Equation 2.7 (μ decreases with increasing S beyond S^*), approaching a value of approximately 0.4 g/g at higher phenol concentrations. This means that an average value for Y_{XS}, should not be applied over a wide range of substrate concentrations. Considerable variability in the values of Y_{XS} was observed, especially at low phenol concentrations (S<100 mg/L). The observed variability in the case of batch cultures was in excess of that expected from measurement error and may be due to some unknown factors impacting the growth or metabolic state of the bacteria during the experiments. On the other hand, there was much less variability in Y_{XS} in continuous cultures, possibly because the range of steady-state substrate concentrations was very narrow. As shown in Figure 5.6, the ranges of values for Y_{XS} determined from batch and average values for continuous cultures are consistent with those reported in the literature for various strains of *P. putida* [0.52-0.78 g dry weight/g phenol] (Chi and Howell, 1976; Hill and Robinson, 1975; Hutchinson and Robinson, 1988).

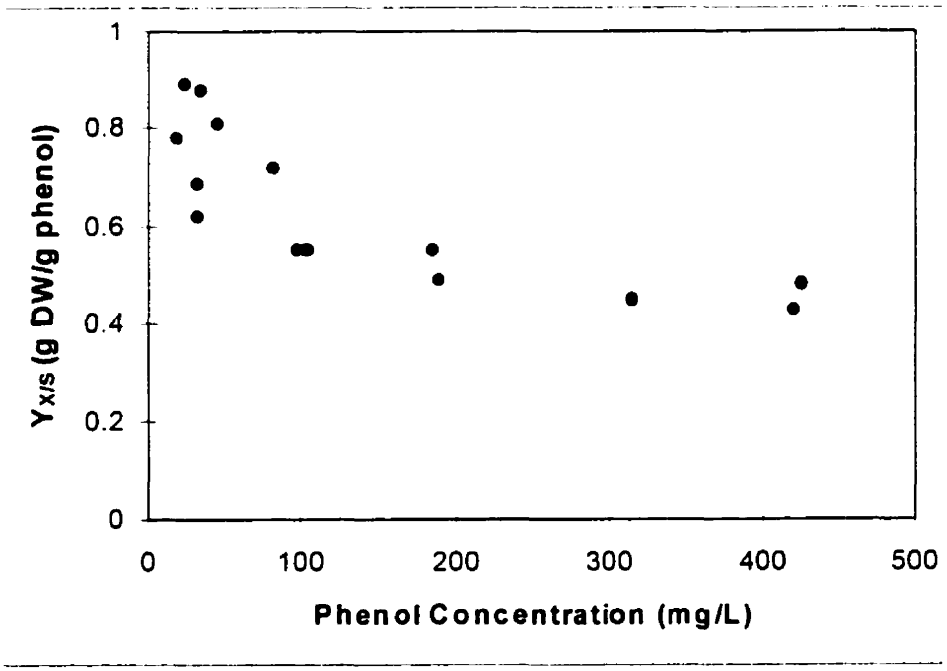

Figure 5.6. Observed yield values for *P. putida* Q5 in batch cultures at 25°C.

Y_g and m were estimated separately from batch and continuous data at each temperature using plots of $1/Y_{X/S}$ versus $1/\mu$ (which should have a slope, m, and an ordinate intercept, $1/Y_g$). Examples of these plots are shown in Figure 5.7 for temperatures of 10 and 25°C. (Note that the two outliers in Figure 5.7a were not included in the regression plot shown or the calculated values for Y_g or m in Table 5.5.) Variability in the yield data in batch cultures, particularly at 10°C, made it difficult to obtain meaningful parameter estimates. The cell-yield data from batch and continuous experiments (Table 5.5) were significantly different, indicating that yield data from batch experiments are likely to be poor predictors of yield parameters in continuous systems, and vice-versa.

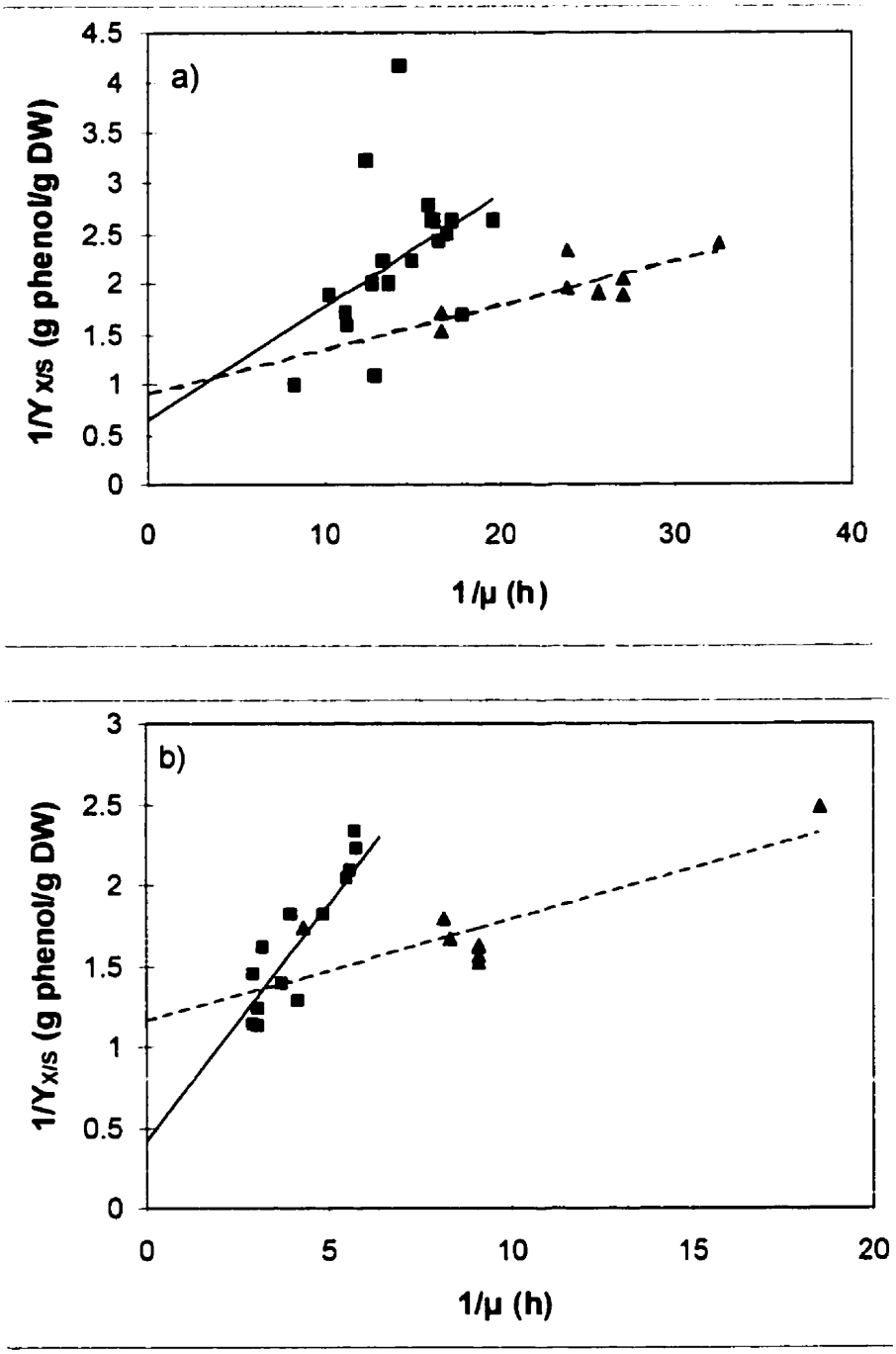

Figure 5.7. . Plots of $1/Y_{X/S}$ versus $1/\mu$ for the determination of Y_g and m for *P. putida* Q5 at a)10°C and b) 25°C for batch [——] and continuous [- - - -] data.

Table 5.4. Yield Parameters for *P. putida* Q5 from Batch and Continuous Experiments

Temperature (°C)	Batch Experiments			Continuous Experiments*		
	Y_g (g cells/ g phenol)	m (g phenol/ g cells·h)	R^2 value	Y_g (g cells/ g phenol)	m (g phenol/ g cells·h)	R^2 value
10	1.56	0.11	0.20	1.09	0.044	0.63
15	1.04	0.21	0.58	-	-	
20	1.43	0.23	0.76	-	-	
25	2.38	0.29	0.79	0.86	0.063	0.66

* Data at 15 and 20°C was insufficient to accurately evaluate Y_g and m.

As shown in Table 5.4, the maintenance coefficient was 3-5 times higher in batch cultures than in continuous ones at the same temperature. Intuitively, this makes sense because at high concentrations of phenol, as in batch cultures, at least initially, inhibition effects are stronger and the energy expended to maintain cell membrane integrity would be expected to be higher. Although the mechanisms of inhibition of phenol are not known, there is some evidence that effects on membrane functionality may play an important role. Exposure of *E. coli* to phenol has been shown to result in leakage of K^+ ions and ATP (Heipieper et al., 1990, 1991) and nucleotides (Heipieper et al., 1991). *E. coli* bacteria respond by changing their membrane structures by increasing the protein to lipid ratios in both the cytoplasmic and outer membranes to make the membranes less permeable (Keweloh et al., 1990a).

The nature of the Haldane curve, due to the inhibitory effect of phenol, results in two possible values of substrate concentration for each specific growth rate (e.g. 5 and 400 mg/L phenol at $\mu = 0.18\ h^{-1}$ at 25°C). However, the Pirt (1965) definition of the maintenance concept (Equation 2.7) would indicate that for a given growth rate, one would expect the same observed yield, assuming that the maintenance coefficient is constant. From Figure 5.6, it is clear that the observed yield values are not independent of substrate concentration. Thus, the maintenance coefficient cannot be assumed to be constant over wide ranges of substrate concentration. Equation 2.7 should be used with caution when applying it to inhibitory substrates; it should probably be used only for cases where the substrate concentration is less than S^*.

The average value for Y_g in Table 5.4 is 1.39 g DW/g phenol, which is very close to the theoretical value of 1.44 g DW/g phenol, calculated by Kotturi et al. (1989) based on an average biomass composition ($C_5H_7NO_2$). Because Y_g is defined as the theoretical yield assuming complete conversion of the substrate to cell material, its value should not change with the type of experiment performed or range of substrate concentration used.

The Effect of Temperature on True Yield and the Maintenance Coefficients

As mentioned previously, the yield data varied considerably between experiments. It is not possible to define quantitative relationships between Y_g and m and temperature. However, several general statements about the trends observed in the parameter estimates can be made.

For several types of microorganisms, Y_g has been reported to remain constant within limited temperature ranges (Bajpai and Margaritis, 1987; Esener et al., 1983; Fieschko and Humphrey, 1983; Huang and Chen, S.-Y., 1988; Kim et al., 1981a; Mainzer and Hempfling, 1976; Moletta et al., 1978; Topiwala and Sinclair, 1971; Zhang, W.E. et al., 1995). The values of Y_g observed in the current work in the range of 10-20°C (Table 5.4) are consistent with those previous observations, which are within the usual variability expected in the yield values. The maintenance coefficient increased with temperature in both batch and continuous cultures (Table 5.4), which is also consistent with prior results (Fieschko and Humphrey, 1983; Heijnen and Roels, 1981; Mainzer and Hempfling, 1976).

5.1.1.2 Phenol Biodegradation Kinetics of *P. putida* Q5 Acclimated to Low Levels of Phenol

Microbial cultures which occur in continuously operated systems at pseudo-steady-state conditions are not acclimated to the high transient phenol concentrations that might occur during a shock-load (or the high phenol concentrations used in batch kinetics testing). Many researchers have used acclimated cultures to determine phenol biodegradation kinetics (Pawlowsky and Howell, 1973a; Hill and Robinson, 1975; Sokol and Howell, 1981; Sokol, 1987; Hutchinson and Robinson, 1988; Folsom et al., 1990; Kotturi et al., 1991; Schröder et al., 1997).

To investigate the kinetics of cultures of *P. putida* Q5 which were not acclimated to high concentrations of phenol, batch kinetic experiments were conducted at 10°C using cells taken from the effluent stream of the ICFBR. Initial concentrations of phenol ranged from 25 to 315 mg/L phenol.

There were two types of response to the addition of phenol. In some cases, the result was balanced growth (eg. see Figure 5.8) after a brief lag period. In other cases, the result was unbalanced growth (see Figure 5.9) during which the phenol was consumed, likely converted to an intermediate but not to biomass, and after a delay, cell growth occurred. During unbalanced growth, traditional definitions of growth rate and yield were of no use. It is not clear why the two different types of growth were observed,

as the conditions and inoculum were the same. In the case of the two examples in Figures 5.8 and 5.9, the initial phenol concentrations were also the same.

Most experiments appeared to follow balanced growth kinetics (eg. range in S_o was 25 to 260 mg/L phenol). The few experiments in which the growth and phenol uptake appeared to be uncoupled were at initial phenol concentrations of 52, 83 and 148 mg/L. If the phenomenon had been due to a delay in the synthesis of RNA, a larger effect would have been expected at the higher phenol concentrations; instead, the opposite was true. As most of the experiments appeared to result in reasonably balanced growth (the cells grew at the same time as the phenol was consumed), the kinetics were calculated using the same approach for simplicity as for the acclimated cultures.

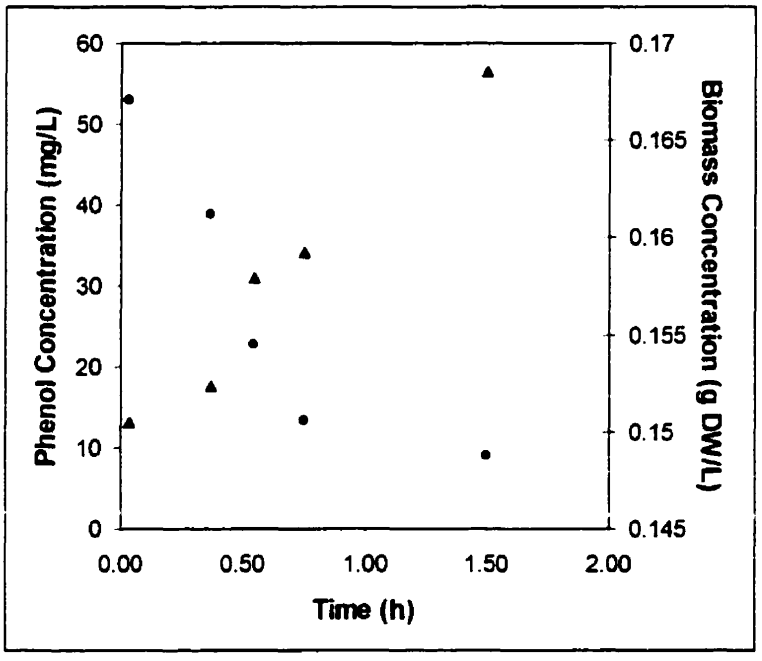

Figure 5.8 Balanced growth with cells acclimated to low levels of phenol at 10°C with S_o=53 mg/L phenol showing phenol concentration (•) and biomass concentration (▲).

Two other models were tested. The model of Yano and Koga (1969) was simplified to the form used by Schröder et al (1997) given as:

$$\mu = \frac{\mu_{max} S}{K_S + S + \frac{S^3}{K_I^2}} \qquad (5.5)$$

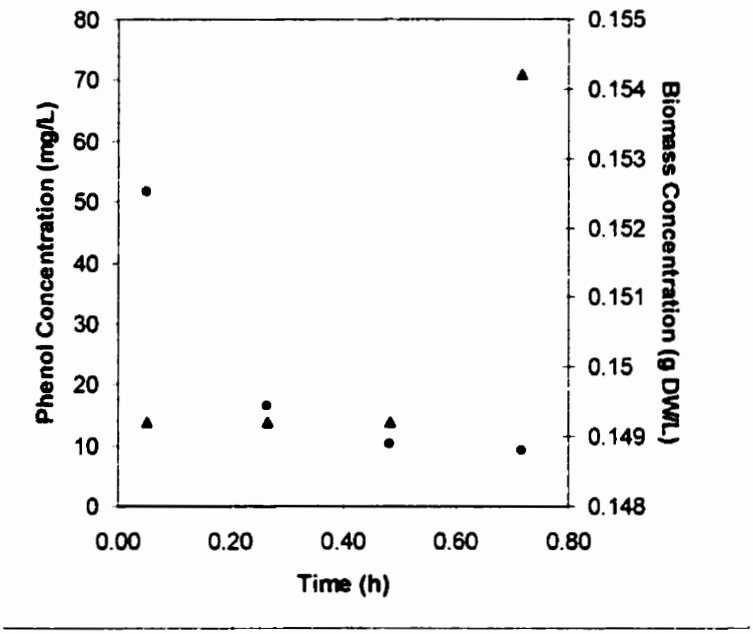

Figure 5.9. An example of unbalanced growth with cells acclimated to low levels of phenol at 10°C with S_o=52 mg/L phenol showing phenol concentration (•) and biomass concentration (▲).

The specific growth rates of the unacclimated batch cultures at each initial phenol concentration are shown in Figure 5.10, with the addition of the results from acclimated continuous cultures at low phenol concentrations. It was not possible to perform batch experiments at concentrations less than 20 mg/L phenol because the biodegradation occurred quickly, and the small changes in cell concentration were difficult to separate from measurement error. It was assumed that because the continuous experiments were performed at low phenol concentrations (below 20 mg/L) the response of acclimated and unacclimated cultures would be similar.

The Haldane parameters (μ_{max}, K_S, K_I) were determined using non-linear regression of the combined batch- and continuous-culture data set with the statistical software package, SPSS®. A least-squares non-linear regression of the data yielded a parameter set that did not represent the form of the curve very well. In particular, the Haldane model predicts a more gradual decrease in the specific growth rate (see Figure 5.10). Although the general shape of the model seems to apply to acclimated cultures (see Figure 5.11), the decrease in specific growth rate for unacclimated cultures was much steeper than the Haldane model predicted above initial substrate concentrations of 200 mg/L, even when the inhibition constant, K_I was decreased to 85 mg/L (not shown).

A simplified version of the model of Luong (1987) was used with n=1, given as:

$$\mu = \frac{\mu_{max} S(1 - \frac{S}{S_I})}{K_S + S} \qquad (5.6)$$

where S_I is the substrate concentration above which growth ceases. Both models fit the data better than the Haldane model (see the r^2 values listed in Table 5.6). The model of Luong (1987) predicted the decreasing specific growth rate at higher concentrations of phenol (200-300 mg/L) better than the others shown in Figure 5.10. The model of Han and Levenspiel (1988) was also tested, but did not provide any improvement to the model of Luong (1987) despite being more complex, but similar in form.

The model of Luong (1987) predicts that at approximately 401mg/L phenol, the unacclimated cells will stop growing. This cannot be confirmed by the data, as no experiments were performed at this concentration. Bacteriostatic concentrations as high as 2 g/L have been reported (to *Escherichia coli* cells) (Heipieper et al., 1991); however, other data have shown that 350 mg/L phenol can cause lysis of bacterial cells (*E. coli, Staphlococci and Streptococci*) (Howell and Jones, 1981). Heipieper et al. (1991) reported that irreversible leakage of K^+ occurred with unacclimated *P. putida*; however, acclimated cultures were able to reabsorb the K^+. It is likely that unacclimated cells will be damaged by phenol at concentrations that are well tolerated by acclimated cultures. Thus, a bacteriostatic concentration of 401 mg/L is possible for the unacclimated culture.

The kinetic data from acclimated cultures at 10°C are compared to the data from unacclimated cultures in Figure 5.11, plotted with the Haldane model for the acclimated kinetics and the simplified Luong model (Equation 2.21) for the unacclimated kinetics. The unacclimated cultures were more strongly inhibited by phenol than the acclimated cultures. The values for μ^* listed in Table 5.5, as calculated from the fitted curves, were lower for the unacclimated culture; however, the values for S^* appear to be higher for all three models tested. This is unexpected, given the higher inhibition that is apparent from the data. The lowest concentration tested in the unacclimated batch cultures was 25 mg/L, compared to the lowest concentration of 12 mg/L for the acclimated batch cultures. It is possible that the critical point for the unacclimated cultures was outside the range of initial substrate concentrations tested.

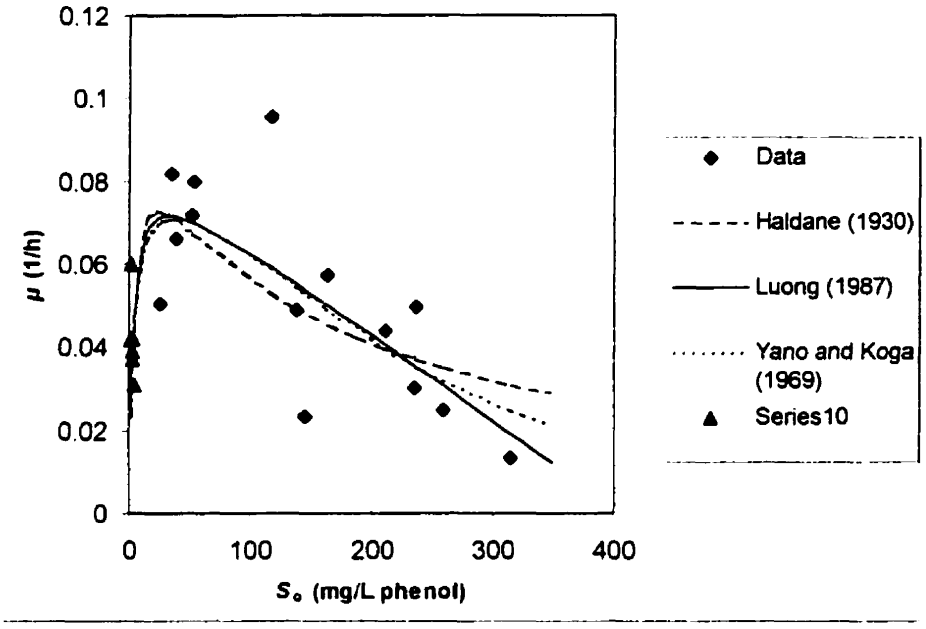

Figure 5.10. Specific growth rates of acclimated continuous cultures (▲) and batch cultures previously acclimated to low levels of phenol at 10°C (♦). Fitted curves are from the models of Haldane (1930), Luong (1987) and Yano and Koga (1969) using the parameters in Table 5.6.

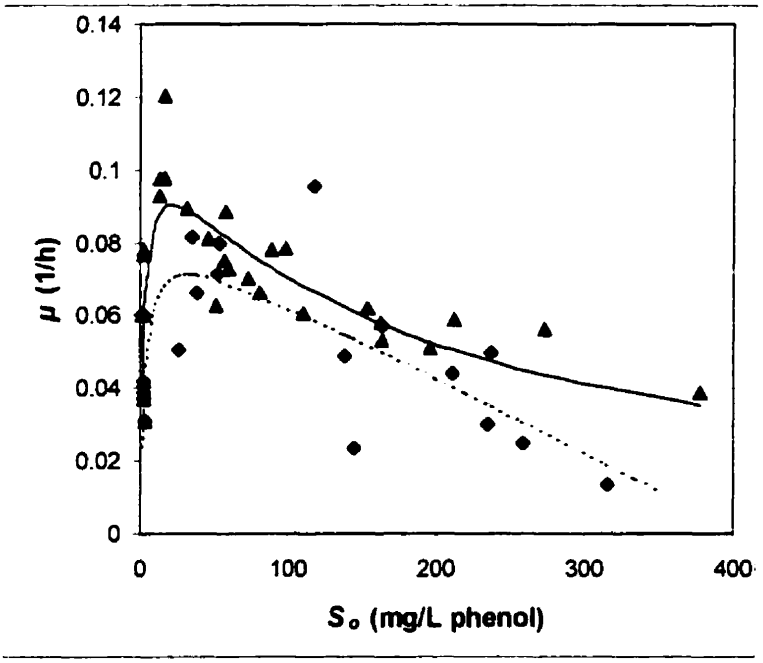

Figure 5.11. Plot of data from acclimated continuous and batch kinetics experiments (▲) and unacclimated batch experiments (♦) at 10°C with *P. putida* Q5. Fitted curves are for the Haldane model using parameters from Table 5.6 for acclimated (——) and unacclimated (- - - -) kinetics.

Table 5.5 Comparison Between the Phenol Degradation Kinetics of Acclimated and Unacclimated Cultures of *P. putida* Q5 at 10°C

Model		Acclimated Cultures	Unacclimated Cultures		
		Haldane (1930)	Haldane (1930)	Yano and Koga (1967)	Luong (1987)
R^2 value			0.694	0.770	0.784
Parameters	μ_{max} [h^{-1}]	0.112	0.0996	0.0798	0.0876
	K_S [mg/L]	2.50	5.43	3.68	4.38
	K_I [mg/L]	175	143	212	-
	S_I [mg/L]	-	-	-	401
Critical Points	μ^* [h^{-1}]	0.0898	0.0725	0.0708	0.0715
	S^* [mg/L]	16	24	37	34

5.1.1.3 Summary

The Haldane model was found to describe the phenol biodegradation kinetics of acclimated cultures of *P. putida* Q5 quite well at 10, 15, 20, and 25°C. The temperature dependence of μ_{max} was found to be better described by the square-root model (Equation 2.30) than the Arrhenius model (Equation 2.24). The saturation constant increased with increasing temperature and was best described by the Arrhenius model (given as Equation 5.1). The inhibition constant was found to increase with increasing temperature, indicating that the inhibition effect is stronger at lower temperatures. The overall temperature-dependent kinetic equation for acclimated cultures is expressed as:

$$\mu = \frac{[0.209(T+6.4)]^2 \times S}{S + 1.53\times 10^7 e^{\left(\frac{-5.72\times 10^3}{T+273}\right)} + \frac{S^2}{[0.128(T+91.7)]^2}} \qquad (5.7)$$

for T in °C.

The values for the maintenance coefficient, m, at 10 and 25°C were 0.044 and 0.063 g phenol/g cells·h, respectively, in the continuous cultures. The values for m in batch cultures were 3-5 times higher. The maintenance coefficient was found to increase with increasing temperature.

The average true growth yield (Y_g) value was 1.39 g cells/g phenol, which is very close to the theoretical value of 1.44 g cells/g phenol (Kotturi, 1989).

The phenol biodegradation kinetics of unacclimated cultures were better represented by a simplified form of the model of Luong (1987) (Equation 2.20) than the model of Haldane (1930) (Equation 2.10) because the inhibition effect seemed to be stronger at higher phenol concentrations than it was for

acclimated cultures. The critical specific growth rate, μ^*, was also lower (0.0715 compared with 0.089) than it had been for acclimated cultures. The resulting expression for the phenol biodegradation kinetics at 10°C was:

$$\mu = \frac{0.0876 \times S(1 - \frac{S}{401})}{4.38 + S} \qquad (5.8)$$

5.1.2 Biofilm Characteristics

5.1.2.1 Biofilm Dry Density (ρ_f)

The average biofilm dry density (ρ_f) was calculated according to Equation 3.7 using the biofilm dry weight and average bioparticle diameter for each sample. The values were corrected for the presence of uncovered particles; that is, the number of particles in the sample was corrected by the percentage of particles that had traces of biofilm according to image analysis software results. The resulting average biofilm densities are listed for each experiment in Table 5.6. All experiments were performed at 10°C. The biofilms appeared to be homogeneous in nature (in the experiments listed in Table 5.7 – see Section 5.2.2) and did not include protuberances. The data was collected for fairly thin biofilm thicknesses in which substrate and oxygen depletion was not expected. There seemed to be no relationship between biofilm thickness and the biofilm dry density. The values obtained for each experiment were used in the simulation of that experiment. The average value in Table 5.6 is a dry density of 0.23 g DW/cm^3, which was the value used in the simulations for Runs 1-4, for which there was no biofilm density data.

Table 5.6. Average Biofilm Densities Measured Experimentally at 10°C

Experiment	Biofilm Density[1] (ρ_f), [g DW/cm^3]		Biofilm Thickness[1] during Run (δ), [μm]
	Average	Standard Deviation	
5	0.24	0.10	7 - 28
6	0.16	0.04	13 – 40
7	0.23	0.19	1 – 8
8	0.29	0.23	4

[1] includes both steady-state and dynamic data

5.1.2.2 Inactive Fraction (f)

Biofilms consist of cells, extracellular polysaccharides (EPS), precipitates, silt or fibrous material and gas bubbles (Stewart, 1998). Calcium also accumulates within the biofilm because of its role as cross-

linking agent for the EPS (Applegate and Bryers, 1991). Also, a portion of the bacteria may be metabolically inactive, particularly in the inner layers of thick biofilms (Zhang, T. C. and Bishop, 1994b; Bishop et al., 1995) Thus, the conventional dry weight technique for evaluating the biomass concentration of suspended cells will likely include other components in addition to cells, when applied to biofilms. If growth and degradation kinetics (which are based upon dry weight measures of biomass) are applied to biofilms, the growth and substrate uptake rates of the biofilms will be overestimated unless an allowance is made for inactive cells and non-cell dry matter. The parameter, f, was defined as the portion of the biofilm (expressed as dry weight) that corresponded to metabolically active bacteria.

The data for extracellular polysaccharides were examined to determine if EPS was a major component of the biofilm dry weight. The EPS content of the biofilm (expressed as g glucose equivalents/g sand) appeared to comprise only 3-5% of the dry weight on a mass basis, as shown in Table 5.7, and did not appear to be related to biofilm thickness (listed in Table 5.6). This result appears to be low (compared to the range of 3% (Ohashi and Harada, 1996) to up to 90% (Bakke et al., 1984)) and may be a consequence of the technique used to evaluate biofilm thickness, possibly due to losses during agitation.

The biofilm was not expected to contain debris or particulate matter, because the feed was a synthetic one, composed of dissolved components (as described in Section 3.1.2). It is likely that a portion of the calcium in the medium was incorporated into the EPS matrix in the biofilm (Turakhia and Characklis, 1989). Although the metabolic activity of the bacteria in the biofilm was not measured, it is likely that most of the bacteria were metabolically active (Zhang, T. C. and Bishop, 1994b) because the biofilms were very thin and were not expected to be substrate or oxygen depleted. In other studies using much thicker biofilms (where less than 500 μm was considered thin) the ratio of viable cells to total biomass in the top layers was found to be 72-91% (Bishop et al., 1995, using lipid phosphate analysis) and 83-86% (Zhang, T. C. and Bishop, 1994b, using INT analysis, a dehydrogenase activity test). Thus, given the presence of EPS and the possibility of non-viable cells and calcium in the biofilm, a value of 0.85 was chosen for the parameter f.

Table 5.7 Average Fraction of the Biofilm Corresponding to EPS at 10°C

Experiment	% EPS (by mass)	
	Average	Standard Deviation
5	3.2	1.0
6	3.6	0.9
7	4.9	1.3

5.1.3 Mass Transfer Coefficients

Diffusion Coefficients ($D_{s,w}$, D_e/D_w)

The diffusion coefficient of phenol in water ($D_{s,w}$) was calculated according to Equation 2.40. The diffusion coefficients of phenol in water at temperatures between 10 and 25°C are listed in Table 5.8.

The relative effective permeability ($D_e D_w$) (see Section 2.2.3.2) was estimated by averaging literature data (Tang and Fan, 1987; Livingston and Chase, 1989; Fan et al., 1990) which had been obtained for phenol diffusing in biofilms which were of a similar density to the biofilms which formed in this study. The value used for $D_e D_w$ in the simulations was 0.1. This was similar to the value of 0.06 calculated using the model of Beyenal et al. (1997) (Equation 2.42) which was adjusted to yield the $D_e D_w$ parameter.

External Mass Transfer Coefficient (k_s)

The external mass transfer coefficient (k_s) was calculated according to Equation 2.74. The correlation was developed for a system which was similar to the one used in this study (Mao et al., 1992) (see Table 2.9), except that the particle diameter was much larger (3.8 mm as opposed to 0.2 mm). External mass transfer has been shown to be independent of particle size in the range of 1-4 mm (Arters and Fan, 1986). The values of k_s listed in Table 5.8 are 3 to 4 times higher than others listed in the literature for similar systems. Tang et al. (1987) obtained a value of 0.005 cm/s using the benzoic acid dissolution method in a draft tube fluidized-bed reactor. Livingston and Chase (1989) obtained a value of 0.0066 cm/s using an ion-exchange resin in a draft tube fluidized-bed reactor. Either k_s is higher in external-loop airlift reactors than in draft-tube reactors or the correlation does not apply well to the system that was used in this study. A value of 0.011 cm/s was used for simulations at 10°C. The importance of the external mass transfer coefficient in the ICFBR is discussed in Section 5.3.3.

Table 5.8. Diffusion and Mass Transfer Coefficients Calculated at 10, 15, 20, and 25°C

Temperature (°C)	Diffusion Coefficient of Phenol in Water ($D_{S,w}$), [cm^2/s]	External Mass Transfer Coefficient[1] (k_t), [cm/s]
10	1.582×10^{-5}	0.011
15	1.847×10^{-5}	0.013
20	2.137×10^{-5}	0.015
25	2.445×10^{-5}	0.018

[1] Gas flow rates in the riser sections were 0.91m/s and 0.93 m/s for the Plexiglass and glass reactors, respectively.

5.1.4 System-related Parameters (d_p, N_p, V_R, ε_L and r_D)

5.1.4.1 Bare Particle Diameter (d_p)

Bare sand particles were photographed and measured according to the image analysis technique described in Section 3.3.4. Sand particles were also retained from the EPS analysis and were photographed and measured in the same way. It was assumed that the concentrated sulphuric acid used in EPS analysis effectively dissolved the biofilm from the sand particles. The results are listed in Table 5.9.

The average ferret diameter (sphere-equivalent diameter as defined in Section 3.3.5) of the bare unused sand was lower than the average diameters of sand in the two reactors. This may have been due to attrition of smaller diameter particles from the reactors over time during the running of experiments. The distribution of particles shown in Figure 5.12 for the bare unused sand included a significant fraction of particles with diameters equal to or less than 0.16 mm.

The sand from the two reactors had a very similar size distribution (see Figures 5.13 and 5.14). It is interesting that despite the very different histories of the two reactors and the biofilm thicknesses achieved in each, the average bioparticle diameter and size distribution in the two reactors were almost identical. The values used for the average bare particle diameters in the simulations were those listed in Table 5.9 for each of the reactors.

Table 5.9. Average Particle Diameters of Bare Unused Sand and Bare Sand from Both Reactors

Description of Sand	Average Ferret Diameter (d_p), [mm]	Standard Deviation [mm]	Number of Particles in the Sample
Bare unused sand	0.1637	0.0461	289
Bare used sand from the Plexiglass reactor	0.1951	0.0404	325
Bare used sand from the glass reactor	0.1958	0.0407	323

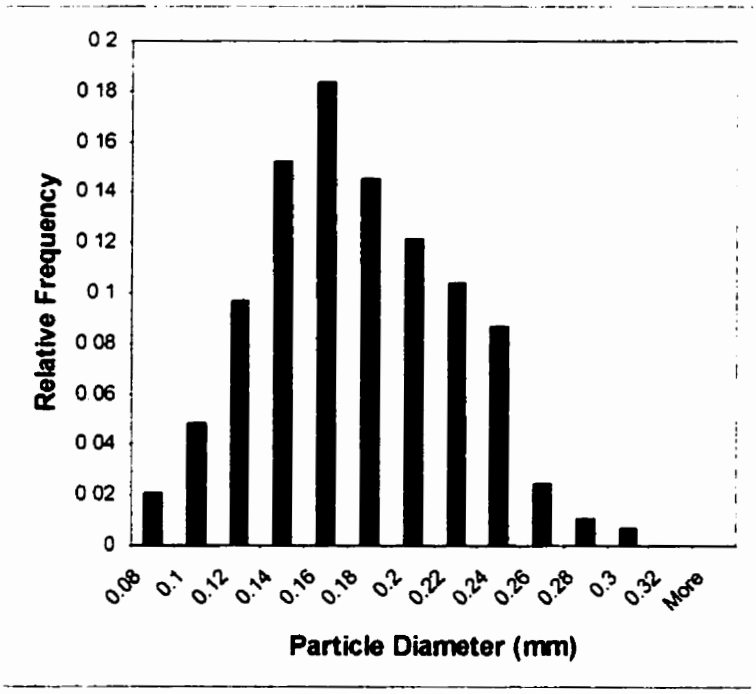

Figure 5.12. Histogram of unused bare sand particles

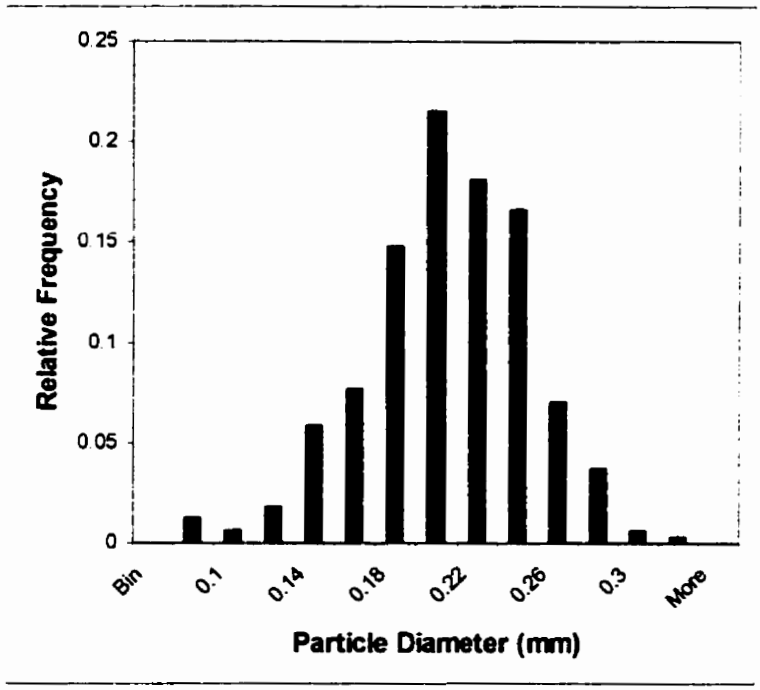

Figure 5.13. Histogram of used bare sand particles from the Plexiglass reactor

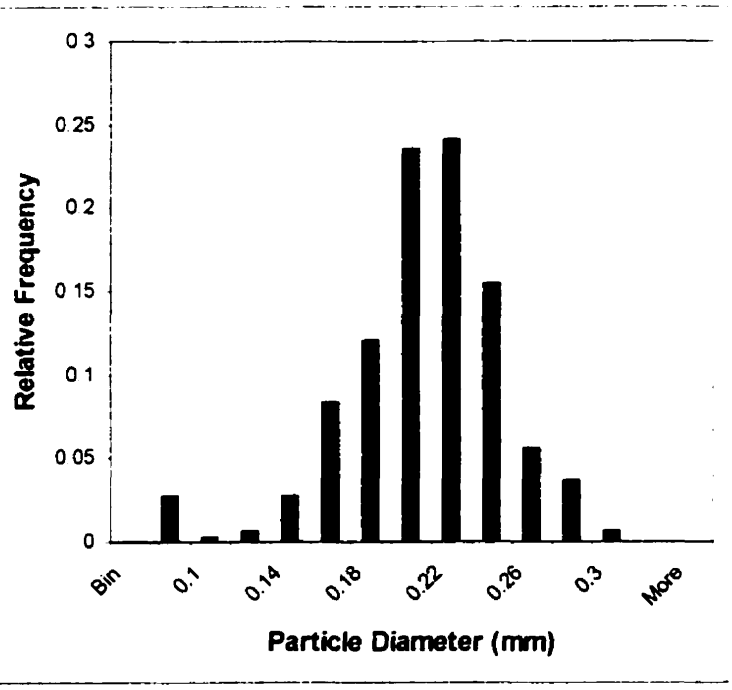

Figure 5.14. Histogram of used bare sand particles from the glass reactor

5.1.4.2 Number of Particles (N_p)

The number of particles (N_p) in the reactor during each experiment was determined according to Section 3.3.7. A known mass of sand was added to each reactor. Some of the sand settled out and deposited in similar locations in both reactors where there was not enough turbulence to dislodge it. Both reactors had deposits of sand in the bottom of the riser immediately below the sparger and next to the junction with the downcomer, at drainage and sampling ports and on the incline leading to the downcomer in the gas disengagement zone. Doubling the gas flow rate did not solve the problem. Unfortunately the sand dislodged when emptying the reactor, so it was not possible to empty the reactor of circulating sand and then wash out the settled sand to measure the mass of sand that had deposited. The mass of sand deposited in the reactors was estimated by visually comparing the volumes of sand that were deposited to an equivalent volume of sand outside the reactor. Approximately 24 grams of sand was deposited in each reactor. This amount was subtracted from the total amount added to each reactor.

Sand was lost from the reactors when fixing plugged spargers. Both spargers became plugged on several occasions due to rust particles blocking the holes. This problem particularly affected the Plexiglass

reactor because the sparger had been made of low-grade stainless steel. The spargers were exposed to severe conditions (15% bleach solution during sterilization and constant moisture) and began to rust inside after about a year of operation. A vacuum pressure was applied to the air chamber below the sparger until liquid from the reactor started to flow through. Then the air supply was turned on and the chamber was drained of fluid. During this process up to 3 g sand was lost each time. Due to an oversight, these losses were not measured during all of the experiments. It is possible that sand was also lost in the effluent stream of the reactor. Apart from a few reactor upsets that did not affect any of the experiments, sand was not detected in the effluent containers as they were emptied after autoclaving; however, it is possible that small quantities of sand were lost in the effluent over the long periods that the reactors were in operation (over 100 days for each reactor).

Sand was also lost during sampling. The volume of fluid withdrawn from each reactor was recorded and the volume of sand lost through sampling was estimated using the average mass of sand per millilitre sample (which was calculated as part of the EPS analysis). The average mass of sand per millilitre sample was relatively consistent during a run. Although the concentration of sand in each sample was not representative of the whole reactor due to the varied distribution of sand in the reactor volume, it was considered to be proportional to the mass of sand circulating in the reactor. Unfortunately, the cumulative mass of sand lost through sampling did not correspond proportionally to the decrease in the average sand concentration in samples. The average sand concentration in samples indicated a lower concentration than would be expected from measured losses. Thus, to get reasonable estimates of the number of particles and the concentration of sand circulating in the reactor, the total mass of sand initially added to the reactor was adjusted for settling and then was correlated with the average sand concentration in samples for the first run. The amount of sand circulating in the reactor for subsequent runs in the same reactor was adjusted according to the average concentration of sand in the samples relative to the initial one. The sand concentrations and number of particles for each run are listed in Table 5.10.

Table 5.10. Mass of Sand Circulating in the Reactor for each Run Expressed as Sand Concentration and Number of Particles

Run	Sand Concentration[1] (g/L)	Number of Particles (N_p)
1	20.8	8 740 000
2	22.6	7 610 000
3	11.4	4 790 000
4	10.5	3 560 000
5	20.6	8 690 000
6	6.5	2 190 000
7	18.5	6 230 000
8	16.7	5 630 000

[1] In circulation

5.1.4.3 Reactor Volume and Liquid Hold-up (V_R and ε_L)

The working volumes of the reactors were 3.46 and 4.22 L for the glass and Plexiglass reactors, respectively. The hold-up fractions for the gas, bioparticles and liquid are listed in Table 5.11. The gas hold-up fractions were calculated using the correlation of Patoine (1989) (Equation 2.61), which was developed for the current experimental system (glass reactor). The solids holdup fraction was calculated based upon values in Table 5.10, with an allowance for settled particles. The resulting liquid hold-up fraction (calculated using Equation 2.58), agreed well with experimental observations.

Table 5.11. Hold-up Volumes in the ICFBRs

Run	ε_G (%)	ε_S (%)	ε_L (%)
1	1.65	1.03	97.32
2	1.68	1.09	97.23
3	1.65	0.66	97.69
4	1.68	0.33	97.99
5	1.65	1.14	97.21
6	1.68	0.82	97.55
7	1.68	0.99	97.33
8	1.68	0.92	97.40

5.1.4.4 Detachment Rate (r_D)

The specific detachment rate, r_D, was calculated by solving Equations 4.10 and 4.11 at steady state conditions using the data obtained from the experiments. Thus r_D was calculated as:

$$r_D = \frac{3\varepsilon_L V_R X_S (D - \mu_b)}{4\pi N_p \rho_f (r_f^3 - r_p^3)} \qquad (5.9)$$

A difficulty with Equation 5.9 was that the values of D (measured) and μ_h (calculated using the Haldane model based upon measured values of S_h) each contained measurement error and were very close to each other. The result was that in Runs 5, 6 and 7, for which the measured values of phenol were higher than expected, the values calculated for r_D were less than zero. For Run 7, the value for r_D was 0.023 h^{-1}. The steady-state phenol concentration prior to Run 8 (4.1 mg/L) was probably inflated due to the presence of a coloured compound, likely a pigment secreted by the bacteria. A detachment coefficient based upon the same phenol concentration as for Run 7 (2.2 mg/L) would be 0.055 h^{-1}. Added complications were that wall growth was present during Runs 7 and 8, and solids build-up occurred during Run 6 due to settling problems of the suspended biomass (as discussed in Section 5.2.2). Thus, there were problems applying the measured values of Y_S in Equation 5.8 as well.

Due to difficulties obtaining reasonable estimates of r_D experimentally, values ranging from 0.016 to 0.025 h^{-1} were used in the simulations and were adjusted to better fit the steady-state model to the data.

5.1.5 Sensitivity Analysis

The sensitivities of the steady-state and unsteady-state models to changes in parameter values were investigated by independently increasing each parameter by 50% and examining the effect of the change upon each of the four variables. Both models are non-linear; thus, the sensitivities of the models to each of the parameters vary with the location in the solution space of each model. The conditions of Run 2 were chosen for the analysis, because the initial dilution rate was moderate (at 0.0451 h^{-1}) and the initial feed concentration was typical (180 mg/L). Thus, the steady-state values for the variables were considered to be representative of the initial conditions under which the ICFBRs were run. The step change, from a phenol loading of 0.195 to 0.268 g/L·day resulted in a low-level response.

5.1.5.1 Sensitivity of the steady-state model

The effect of increasing each parameter individually by 50% upon the steady-state model is shown in Table 5.12. Most of the changes had little effect upon the results of the model predictions. The kinetic parameters, μ_{max} and K_S, appeared to have a significant influence only upon the bulk phenol concentration. Presumably, the parameter, K_I would play a more significant role at higher phenol concentrations that are

not possible at steady state but would occur during transients after a step change or during a washout experiment. The maintenance coefficient, m, had a significant effect upon the suspended cell concentration in the reactor (decreased 24% with an increase in m of 50%). The detachment rate, r_D, also significantly affected both the bulk phenol concentration and the suspended biomass concentration. The detachment rate is the parameter for which there is the least information in the literature and was the most difficult to estimate in this research. The importance of this parameter on the predictions of the model underlines the need for further research in this area.

A number of parameters influenced the variable, a', which is a variable that describes the curvature of the phenol profile (S_f) within the biofilm. For example, the sensitivity analysis indicates that if the biofilm density, ρ_f, is increased by 50%, the biofilm thickness would decrease by 33% and the concentration gradient would be steeper. The variable a is described in detail in Section 5.3.1.1. and is developed in Appendix A-1.

A number of parameters also had a significant influence upon the biofilm thickness, δ. The models actually predict the variable r_f, the radial distance to the surface of the film; however, sensitivity analysis on this variable is not particularly useful because the parameter, r_p is included in r_f. The particle radius, r_p, comprises a large portion of r_f; thus, very small changes in r_f can have a significant effect upon the biofilm thickness, particularly because the biofilm thicknesses in this work were very small. Table 5.12 shows that, as expected, the detachment rate significantly affects the biofilm thickness, with a 64% decrease in biofilm thickness with an increase of 50% in the specific detachment rate. The average particle radius and the number of particles were other important parameters.

The sensitivity analysis in Table 5.12 also shows how the operating conditions affect each of the variables. One of the difficulties in this work was developing a thick biofilm. The results in Table 5.12 suggests that increasing the dilution rate would have the largest impact on biofilm thickness.

Table 5.12. Response of Process Variables to a 50% Change in Model Parameters and Process Conditions at Steady State

Parameter		Initial Value	S_b [mg/L]	X_S [mg/L]	a [mg/cm^3]	$\delta^{(2)}$ [μm]
			1.7	97.5	799	1.3
			% Change with an Increase in the Parameter Value of 50%			
Operating Conditions	D [1/h]	0.0451	1.0	3.0	-1.4	**109.2**
	S_o [mg/L]	180	1.8	**51.0**	-0.6	**47.5**
Kinetics	μ_{max} [1/h]	0.0876	**-40.0**	0.8	0.0	-1.0
	K_S [mg/L]	4.38	**49.4**	-0.6	0.0	0.0
	K_I [mg/L]	401	0.0	0.0	0.0	-0.1
	Y_g [g/g]	1.39	0.0	13.9	-12.3	**13.7**
	m [g/g·h]	0.03	0.0	**-24.0**	**32.2**	**-23.8**
Mass Transfer	D_{SW} [cm/s^2]	1.582×10^{-5}	0.0	0.0	**-33.3**	0.0
	D_e/D_w	0.1	0.0	0.0	**-33.3**	0.0
	k_s [cm/s]	0.011	-0.6	-0.1	0.0	0.4
Bioparticle Properties	ρ_f [mg/cm^3]	230	0.0	-2.6	**50.7**	**-33.0**
	f	0.85[1]	0.0	-7.0	**17.8**	-6.8
	r_p [μm]	97.5	-1.2	-0.2	1.0	**-54.8**
Reactor Characteristics	r_D [h^{-1}]	0.024	**82.4**	**20.4**	**19.3**	**-64.6**
	N_p	7.61×10^6	-0.6	-0.1	0.4	**-32.8**
	V_R [L]	3.46	1.8	0.3	-0.6	**47.3**
	ε_L	0.97[1]	0.0	0.0	0.0	3.1

[1] Parameter increased to a value of 1 for the sensitivity analysis.
[2] Of interest is the biofilm thickness, δ, which is the difference between the value of the variable, r_f, predicted by the model and r_p.

5.1.5.2 Sensitivity of the unsteady-state model

The effects of increasing selected parameters by 50% upon the dynamic response predicted by the unsteady-state model are shown in Figures 5.15 – 5.17. The effects are very similar to those described for the steady-state model. The transient in the bulk phenol concentration in Figure 5.15 was similar in form in all the simulations, but varied in magnitude. The parameters with the greatest impact were μ_{max}, K_S and r_D. The same was true for the suspended biomass concentration and the biofilm thickness in Figures 5.16 and 15.17. The forms of the predicted responses were similar to the baseline prediction; however, the magnitude of the predicted responses changed in ways that are consistent with the results described in Table 5.12 for the steady-state model. The parameters with the most impact were m and r_D. The increase in r_D in Figure 5.17 led to a condition where the detachment rate exceeded the growth rate of the biofilm, and the biofilm thickness decreased to a level less than the initial steady-state value. increased in response to the increased loading of phenol, and the biofilm became thicker. Runs 1, 4, 5 and 8 exhibited high-level responses during which the phenol concentration rose above the critical phenol concentration (21 mg/L phenol according to Equation 2.12), and the suspended cells washed out. The moderate type of response

described by Allsop et al. (1993) for continuous suspended-cell cultures was not observed in this work; in such cases there is a transient increase in the phenol concentration but the system recovers.

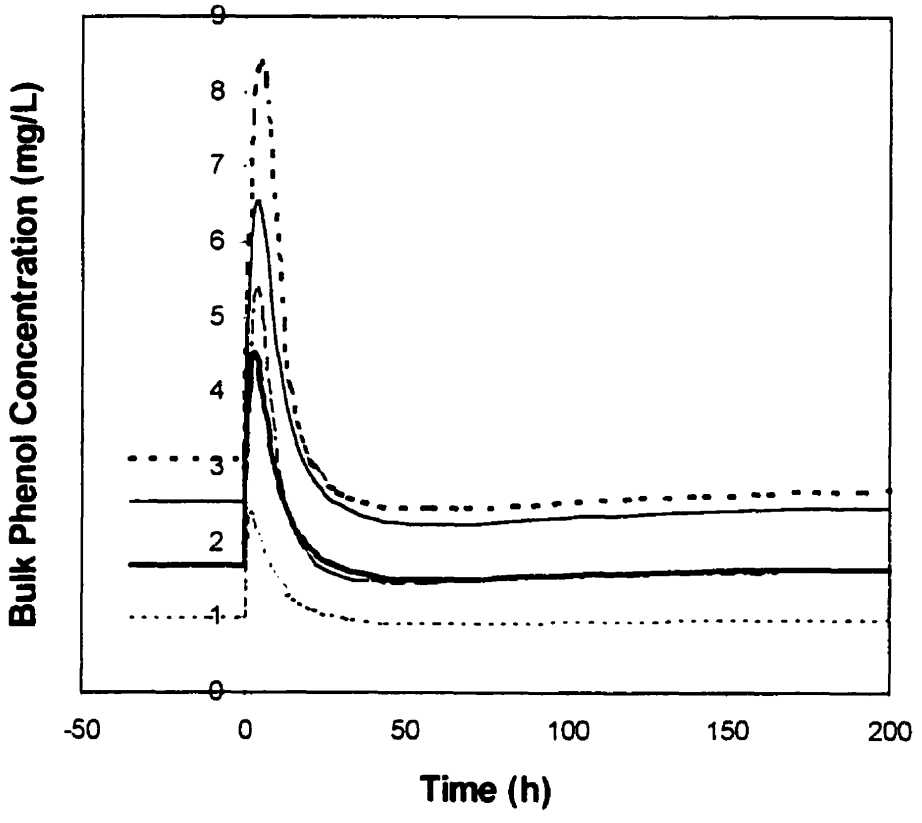

Figure 5.15. Effect of a 50% increase in selected parameters on the dynamic simulation of the bulk phenol concentration in response to a step increase in the feed concentration from 180 to 303 mg/L phenol and a change in dilution rate from 0.0451 to 0.0368 h^{-1} (Run 2). The plots refer to the baseline case [——], and simulations that resulted when the following parameters were changed: μ_{max}×1.5 [- - - -], K_S×1.5 [— —], K_I×1.5 [— - — -], m×1.5 [— - - —] and r_D×1.5[– – – –].

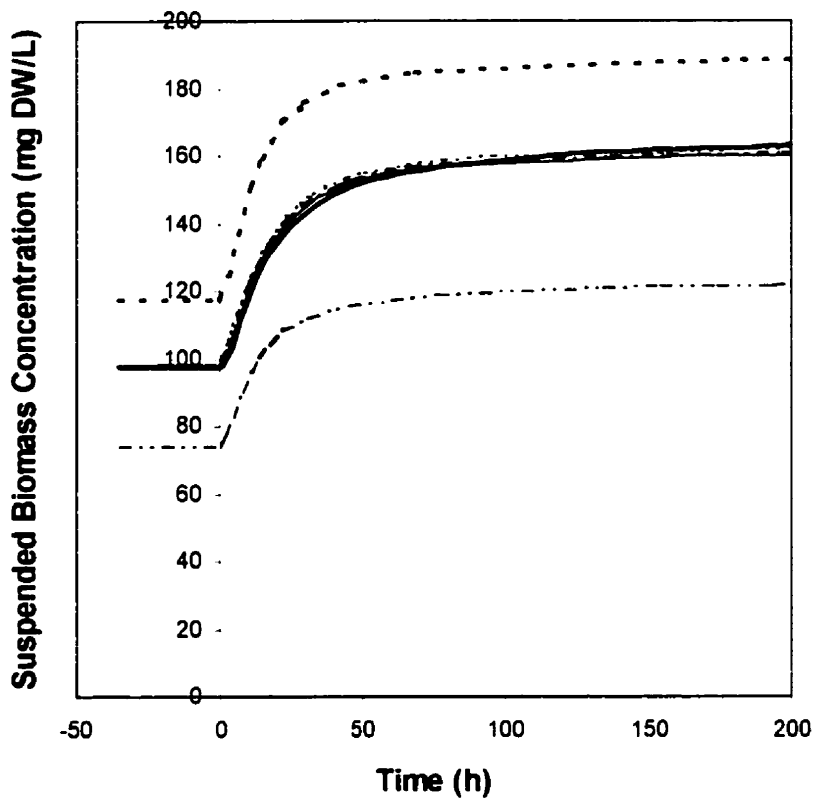

Figure 5.16 Effect of a 50% increase in selected parameters on the dynamic simulation of the suspended biomass concentration in response to a step increase in the feed concentration from 180 to 303 mg/L phenol and a change in dilution rate from 0.0451 to 0.0368 h^{-1} (Run 2). The plots refer to the baseline case [———], and simulations that resulted when the following parameters were changed: $\mu_{max} \times 1.5$ [- - - - -], $K_S \times 1.5$ [———], $K_I \times 1.5$ [— - — -], $m \times 1.5$ [— - - —] and $r_D \times 1.5$[– – – –].

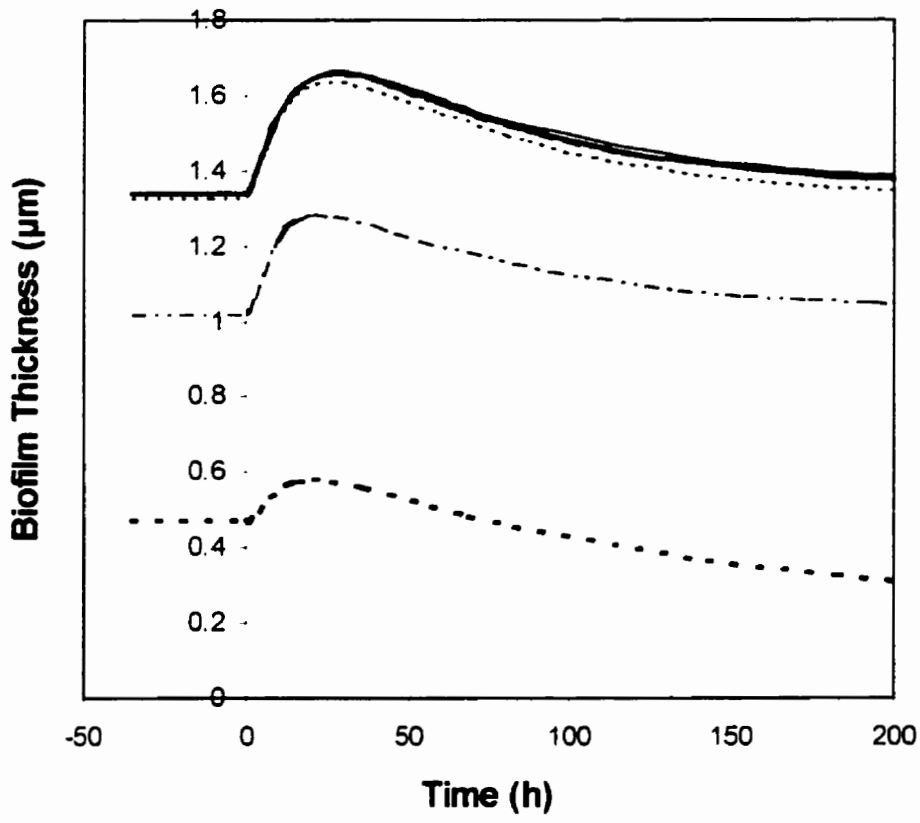

Figure 5.17. Effect of a 50% increase in selected parameters on the dynamic simulation of the biofilm thickness in response to a step increase in the feed concentration from 180 to 303 mg/L phenol and a change in dilution rate from 0.0451 to 0.0368 h^{-1} (Run 2). The plots refer to the baseline case [——], and simulations that resulted when the following parameters were changed: $\mu_{max} \times 1.5$ [- - - -], $K_S \times 1.5$ [— ——], $K_I \times 1.5$ [— - — -], $m \times 1.5$ [— - - —] and $r_D \times 1.5$[– – – –].

5.2 Shock-loading Experiments in the ICFBR

5.2.1 Overview

A total of eight step change experiments were performed in the ICFBR reactors. All experiments were performed at 10°C. The initial operating conditions and step changes are listed in Table 5.13. All initial dilution rates were below the calculated critical dilution rate of 0.071 h^{-1}, which was based upon model parameters and was calculated using Equation 2.11. Thus at the dilution rates listed in Table 5.13, suspended cells were present in the broth. The initial biofilm thicknesses were typically thin (approximately 5-10 μm).

Two types of response to the step increases were observed. Runs 2, 3, 6, and 7 exhibited low-level responses in which there was little or no change in the phenol concentration, the suspended biomass

Table 5.13 Summary of Step Change Experiments in the ICFBRs

Experiment	Initial Conditions			Type of Step Increase	% Change in Loading	Level of Response
	Feed Conc., S_o [mg/L]	Dilution Rate, D [h^{-1}]	Loading [g/L·d]			
1	251	0.0344	0.207	D and S_o	100	high
2	180	0.0451	0.195	D and S_o	40	low
3	248	0.0250	0.149	D	140	low
4	198	0.0425	0.202	S_o	130	high
5	158	0.0416	0.160	D	125	high
6	184	0.0693	0.306	S_o	80	low
7	192	0.0376	0.173	S_o	210	low
8	592	0.0374	0.497	D	500	high

The experimental conditions used in the current research contrast with those used in other work reported in the literature for ICFBRs subjected to shock loads (see Table 5.14). There are five major differences: the temperature, the type of microorganisms, the dilution rates, the feed concentrations and the initial biofilm thicknesses.

Previous work (listed in Table 5.14) was performed at 22°C with mesophilic mixed cultures. The current research was performed at 10°C with a psychrotrophic bacterium. Because the growth rates at 10°C are approximately three times slower than at 22°C and phenol inhibition is stronger (see Section 5.1.1), the system is probably more sensitive to shock-loading at the lower temperature.

The dilution rates were much higher in other studies than in the current research, and far exceeded the critical dilution rate for equivalent suspended-cell systems (approximately 0.23 h^{-1}); however the concentrations of phenol in the feed were very low. Tang et al. (1987) used initial concentrations in the feed that were similar to the critical substrate concentration of approximately 35 mg/L phenol. The feed concentrations used in the current work better represent the phenol concentrations found in industrial wastewater streams (see Table 2.1). The loadings of phenol delivered to the systems listed in Table 5.14 were much higher than those used in the current research; however, with an inhibitory substrate such as phenol, concentration is an important issue. If an inhibitory intermediate metabolite is secreted into the medium in proportion to the feed concentration as postulated by Beltrame et al. (1984), then the response of the system to step changes may be more strongly influenced by the feed concentration than what would

otherwise be expected. Also, if phenol transients occur during a shock load, the potential for the transient to enter an inhibitory regime is much more likely with the higher concentration of phenol in the feed. Thus, the potential to destabilize the system is also much greater at higher feed concentrations

The final major difference between the current work and the research listed in Table 5.14, is the biofilm thicknesses achieved in the ICFBRs. The initial biofilm thicknesses in this work tended to be very thin (1-14 μm – up to approximately 14 layers of cells thick). Tang et al. (1987) reported initial biofilm thicknesses in the range of 12-40 μm in a draft tube reactor. Worden and Donaldson (1987) reported thicknesses of around 180-210 μm in a fluidized bed reactor. The higher biomass holdup in the form of biofilm also affects the response of the system. Note that in addition to biodegradation capacity, the system of Tang et al. (1987) also was able to adsorb phenol during a step change because the carrier used was activated carbon.

Table 5.14. Summary of Other Shock-loading Experiments Reported in the Literature for ICFBRs with Phenol as a Substrate

Reference	Culture/ Substrate	T [°C]	Initial Conditions			Type of Step Increase	% Change in Loading	Level of Response
			S_o [mg/L]	D [h^{-1}]	Loading [g/L-d]			
Tang et al (1987)	mixed with *P. putida*/ phenol	22-23	49	2.3	2.70	S_o	100	moderate
			38	2.01	1.84	S_o	90	moderate
			-	2.01	-	S_o	40	low
			34	2.01	1.62	S_o	190	moderate
Worden and Donaldson (1987)	mixed/ phenol	30	50	3	1.08	S_o (pulse)	650[1]	low
			50	3	1.08	S_o (pulse)	1130[1]	High

[1] % change in reactor concentration during pulse (eg. from 10 mg/L to 65 mg/L)

The analyses which were performed for each experiment in the current work are listed in Table 5.15. Run 1 was intended to be an exploratory run, and biofilm data were not obtained except for the EPS content of the biofilm. During Runs 2 and 3, that were conducted concurrently, the sample size for the dry weight analysis (5 mL) was found to be too small for the results to be meaningful; 20-mL samples were taken for subsequent experiments. Also, during Runs 2 and 3, photomicroscopy was attempted for the first time. Unfortunately the first photographs were out of focus, and the initial parts of the runs were not captured. Digital imaging was used for subsequent experiments.

Table 5.15. Summary of Analysis Performed During the Step Change Experiments

Experiment	Suspended Biomass, X_S	Bulk Phenol, S_b	EPS	Biofilm Dry Weight	Biofilm Thickness, δ	Intermediate Compounds
1	✓	✓	✓	-	-	-
2	✓	✓	✓	-	-	-
3	✓	✓	✓	-	-	-
4	✓	✓	✓	-	✓	✓
5	✓	✓	✓	✓	✓	✓
6	✓	✓	✓	✓	✓	✓
7	✓	✓	✓	✓	✓	✓
8	✓	✓	✓	✓	✓	✓

5.2.2 Responses of the ICFBRs to Shock-loading

The step-change experiments in the ICFBRs have been grouped according to the type of response exhibited during the run, and are described separately. Runs 2, 3, 6, and 7 exhibited low-level responses in which there was little or no change in the phenol concentration. Runs 1, 4, 5 and 8 exhibited high-level responses during which the suspended cells reached or approached washout and the phenol concentration approached the feed concentration.

5.2.2.1 Low-level Responses

Run 2

The second run was begun after the glass reactor had been operating for 80 days. Many particles were covered with a thin biofilm, and a small portion of these included protuberances.

A small concentration step change was planned. The dilution rate was inadvertently changed as well. The resulting step change was from a feed concentration of 180 to 303 mg phenol/L and a phenol loading change from 0.195 to 0.268 g/L·d. The operating conditions before and after the step change are presented in Table 5.16.

Table 5.16. Operating and Reactor Conditions During Run 2

Operating Conditions and System Characteristics	Initial Conditions	Conditions after Step Change
Dilution Rate (h^{-1})	0.0451	0.0368
Phenol Concentration in Feed (mg/L)	180	303
Loading (g/L·d)	0.195	0.268
Suspended Biomass Concentration (mg DW/L)	112	168
Phenol Concentration in the Reactor (mg/L)	1.8	1.4
EPS (g glucose equiv. /g sand)	0.00066	0.00081
Sand Concentration (g/L)	22.6	

The response of the system to the step change is shown in Figure 5.18. The shock was applied at time=0 hours. There was no response in the phenol concentration, as it did not change significantly from the initial steady-state phenol concentration prior to the step change. The suspended biomass concentration quickly rose from 112 mg DW/L to 168 mg DW/L within 50 hours of the step change, after which a new steady state (with respect to the suspended biomass and phenol concentrations) was reached.

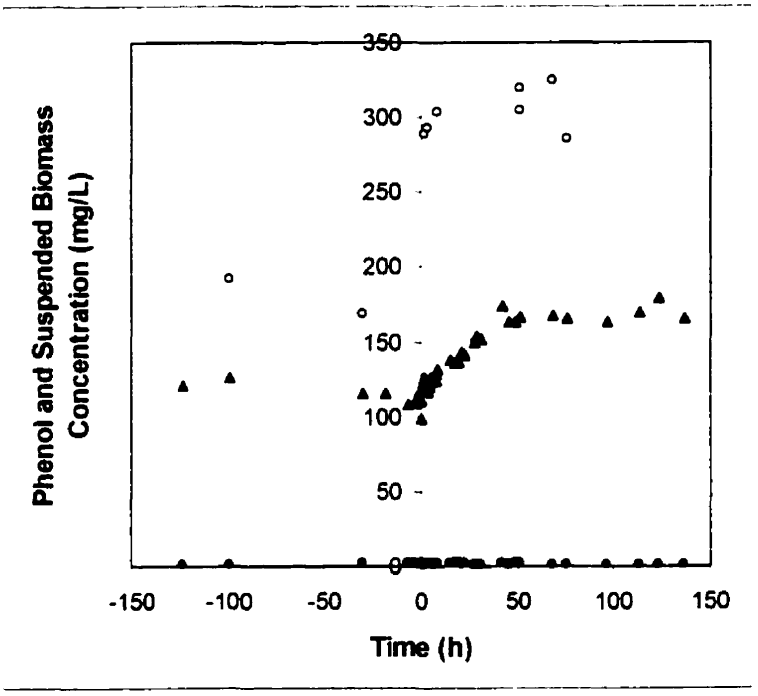

Figure 5.18. Response of the bulk phenol concentration (•) and the suspended biomass concentration (▲) to an increase in the feed concentration (○) from 180 to 303 mg/L and a decrease in dilution rate from 0.0451 to 0.0368 h^{-1} in the ICFBR during Run 2.

The biofilm grew visibly over the course of the experiment. A photomicroscope was used to photograph the biofilm on a dark field setting. The initial photographs taken immediately prior to the step change were out of focus. The appearances of the bioparticles 45 hours before and 118 hours after the step change are shown in Figures 5.19 and 5.20, respectively. The photographs show an increase in the presence of protuberances on the bioparticles. The increase in the amount of biofilm present was reflected in the EPS measurements in Figure 5.21 (samples taken at 51 and 116 hours corresponding to the photographs in Figures 5.19 and 5.20, respectively). The EPS concentration rose from an average of 0.00066 g glucose equiv./g sand immediately before the step change to an average of 0.00081 g glucose equiv./g sand at the end of the run.

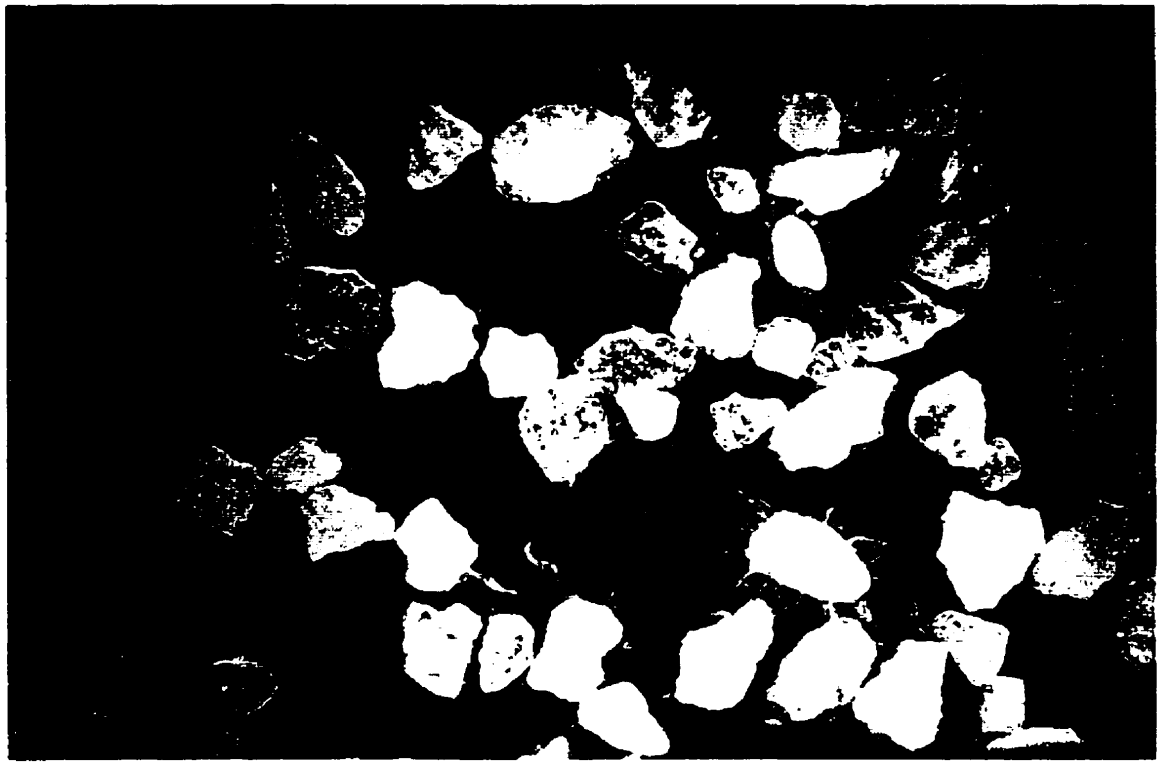

Figure 5.19. Appearance of the bioparticles at t=45 hours (40× magnification) during Run 2.

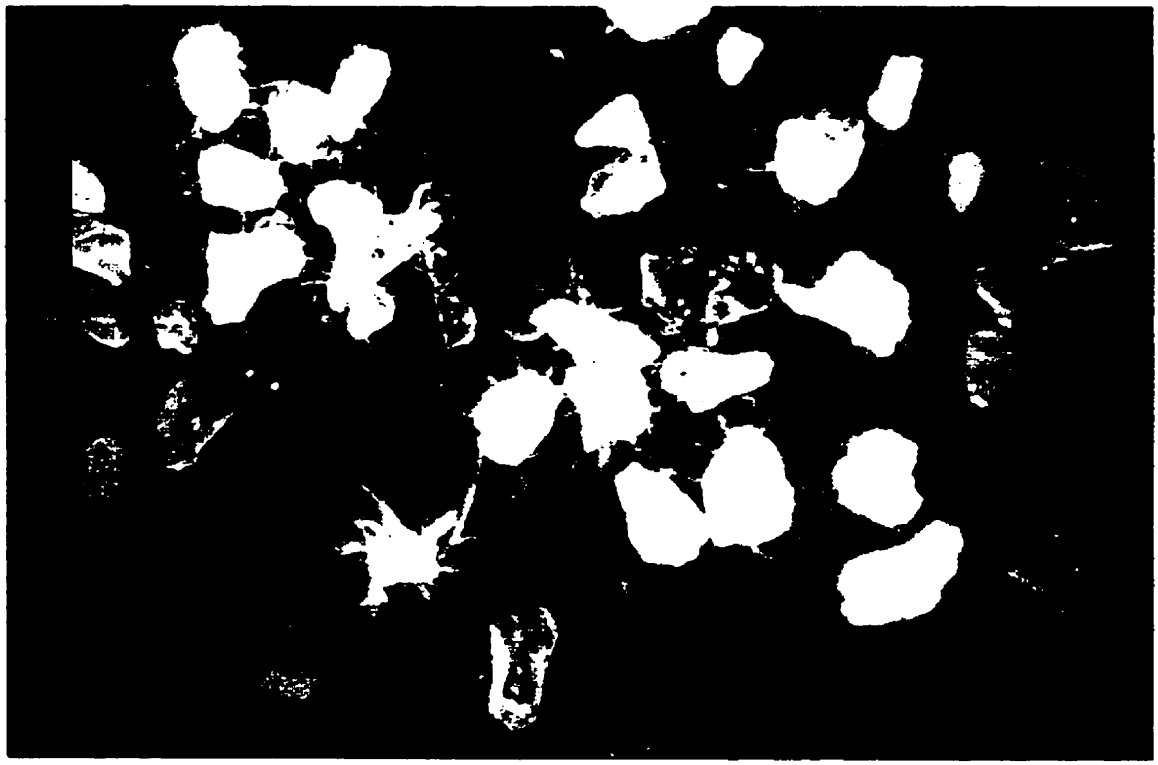

Figure 5.20. Appearance of the bioparticles at t=118 hours (40× magnification) during Run 2.

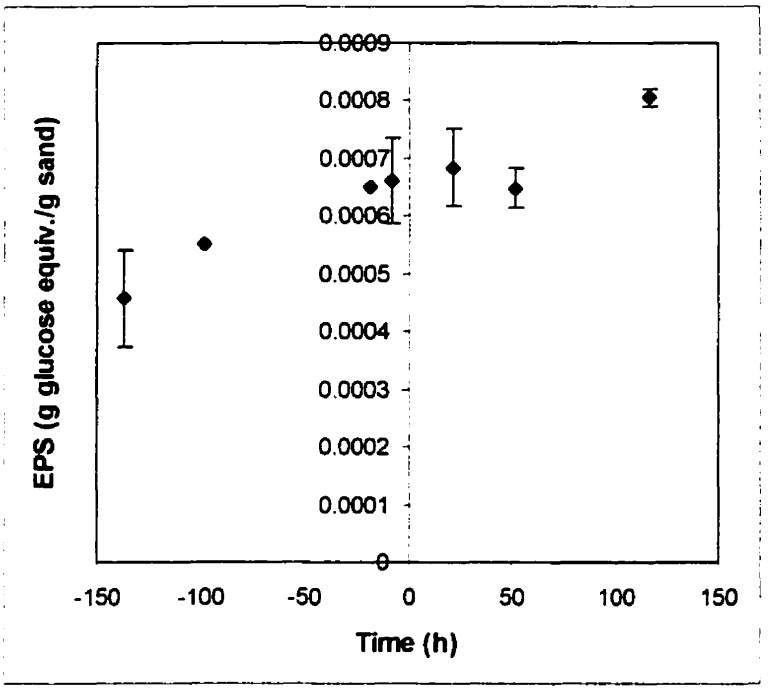

Figure 5.21. Response of the EPS content of the biofilm during Run 2.

Run 3

The glass reactor was allowed to reach a steady state for 47 days after a reactor upset following Run 1. Despite the long operating period (including the startup period prior to the first run), the bioparticles were covered with a thin biofilm, a portion of which included protuberances. The biofilm thickness was difficult to evaluate microscopically.

The dilution rate was shifted from 0.0250 h^{-1} to 0.0593 h^{-1}, while maintaining the phenol concentration in the feed at approximately 248 mg/L. The change in operating conditions are presented in Table 5.17.

Table 5.17. Operating and Reactor Conditions During Run 3

Operating Conditons and System Characteristics	Initial Conditions	Conditions after Step Change
Dilution Rate (h^{-1})	0.0250	0.0593
Phenol Concentration in Feed (mg/L)	248	238
Loading (g/L/d)	0.145	0.339
Suspended Biomass Concentration (mg DW/L)	111	143
Phenol Concentration in the Reactor (mg/L)	0.59	0.36
EPS (g glucose equiv. /g sand)	0.00048	0.00082
Sand Concentration (g/L)	11.4	

The response of the system is shown in Figure 5.22. There was no reponse in the phenol concentration. The suspended biomass concentration however, increased from 111 to 143 mg DW/L within the first 70 hours. The apparent dip in the suspended biomass concentration immediately after the step change in Figure 5.22 is likely artificial and due to experimental scatter in the optical density measurement and not a result of metabolic changes in the bacteria.

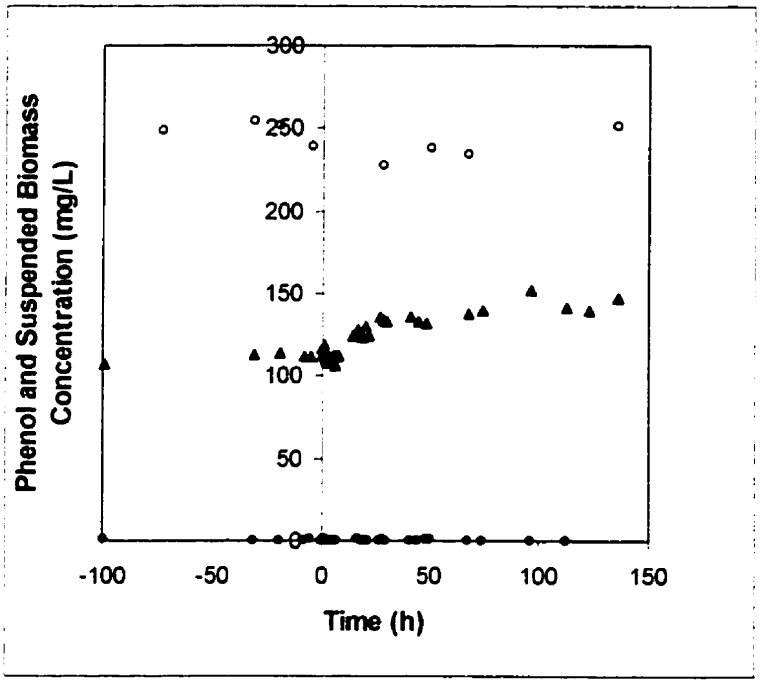

Figure 5.22. Response of the bulk phenol concentration (•) and the suspended biomass concentration (▲) at a feed concentration (○) of 248 mg/L phenol to an increase in the dilution rate from 0.0250 to 0.0593 h^{-1} in the ICFBR during Run 3

As with the photo-samples in Run 2, the photographs of the bioparticles immediately prior to the step change were out of focus and not useful. The biofilm grew somewhat over the course of the run, as shown in the photographs in Figure 5.23 and 5.24, taken at 45 and 118 hours after the step change. The biofilm growth was reflected in the EPS measurements shown in Figure 5.25. The samples taken at 51 and 116 hours correspond to the photographs in Figures 5.23 and 5.24, respectively.

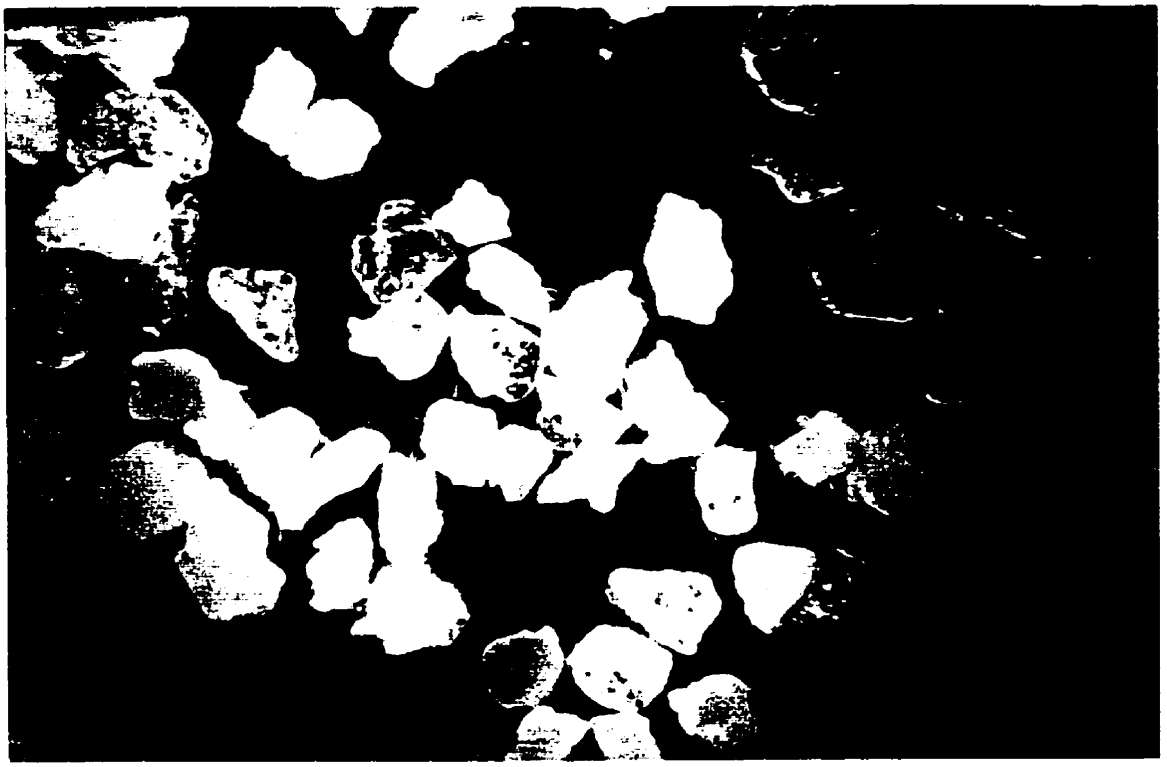

Figure 5.23. Appearance of the bioparticles at t=45 hours (40× magnification) during Run 3.

Figure 5.24. Appearance of the bioparticles at t=118 hours (40× magnification) during Run 3.

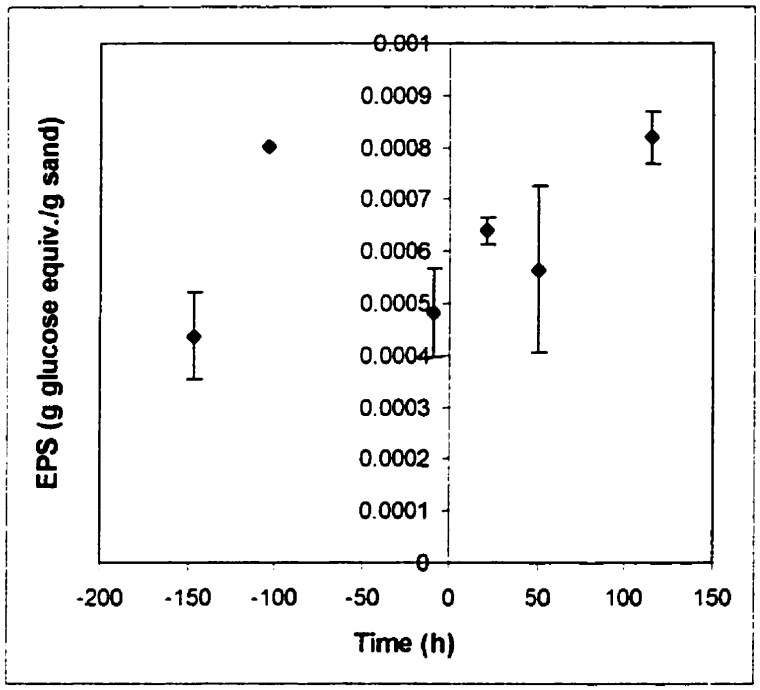

Figure 5.25. Response of the EPS content of the biofilm during Run 3.

Run 6

Run 6 was begun 40 days after Run 4 in the glass reactor. In the period between the two experiments, the suspended biomass changed in appearance from dispersed growth to flocs. The flocs were settleable and may have settled to some extent in the downcomer section, resulting in higher suspended biomass concentrations in the bulk fluid than would be expected. Portions of the walls in the reactor became coated with a heterogeneous biofilm. The sand particles were coated with a fairly thick biofilm with an average thickness of around 35 μm (see Figure 5.26). The biofilm appeared to be fairly smooth with some protuberances. A steady state was established at a dilution rate of 0.0693 h^{-1} and a feed concentration of 184 mg/L phenol. The conditions in the reactor are shown in Table 5.18.

Table 5.18. Operating and Reactor Conditions During Run 6

Operating Conditions and System Characteristics	Initial Conditions	Conditions after Step Change
Dilution Rate (h^{-1})	0.0693	0.0693
Phenol Concentration in Feed (mg/L)	184	336
Loading (g/L·d)	0.306	0.559
Suspended Biomass Concentration (mg DW/L)	290	Increased to 1270
Phenol Concentration in the Reactor (mg/L)	7.8	7.3
EPS (g glucose equiv. / g sand)	0.0039	0.0090
Biofilm DW (g /g sand)	0.15	0.18
Average Biofilm Thickness (μm)	35	13
Sand Concentration (g/L)	6.5	

Figure 5.26. Appearance of bioparticles prior to Run 6 using a bright field setting.

The feed concentration was increased to 336 mg/L. The response of the system is shown in Figure 5.27. There was little effect of the step change on the phenol concentration which averaged 7.8 mg/L before the step change and 7.3 mg/L after. There also appeared to be little immediate effect upon the suspended biomass concentration which averaged 290 mg DW/L before the step change and 310 mg DW/L after. As the run progressed, the effluent port became clogged with biomass, and the flocs could not leave

the system. The suspended biomass concentration increased to 1270 mg DW/L before the experiment ended.

There was considerable variability in the optical density measurements used to calculate the dry weight concentrations of the biomass. The flocs were settleable and settled out in the cuvette during the optical density measurement. Attempts were made to ensure that the sample was well mixed and that a representative reading was taken.

There was also more variability than usual in the phenol data. The flocs tended to come away from the clump of biomass at the bottom of the centrifuge tubes, when the supernatant was poured out of tubes and stored for phenol analysis after centrifuging. Using a syringe to remove the supernatant helped, but did not solve the problem. The phenol samples were frozen, and then were thawed and filtered through a 0.1 μm pore size filter before analyzing with the spectrofluorometer. It is possible that the cells that were present in the samples during the freezing and thawing processes degraded some of the phenol in the samples prior to analysis.

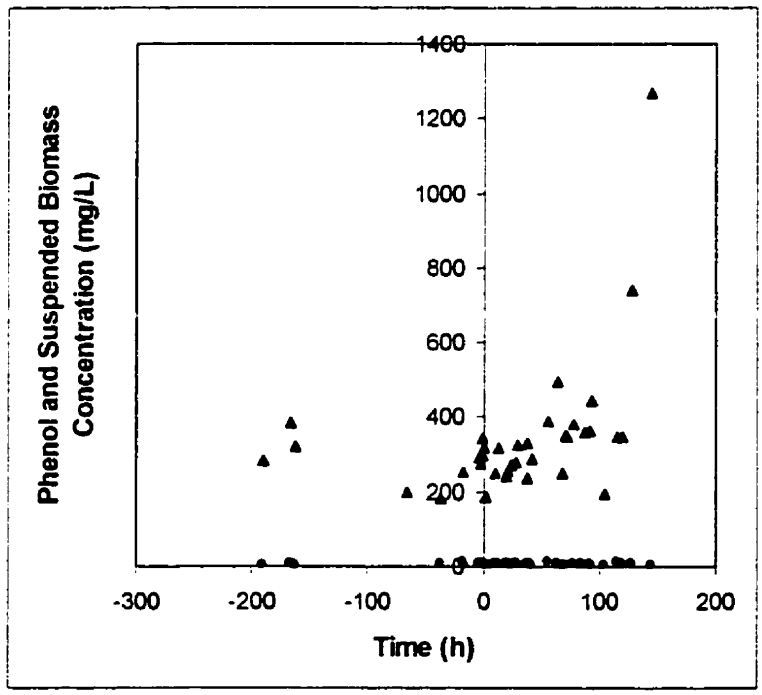

Figure 5.27. Response of the bulk phenol concentration (•) and the suspended biomass concentration (▲) to an increase in the feed concentration from 184 to 336 mg/L phenol at a dilution rate of 0.0693 h^{-1} in the ICFBR during Run 6.

The appearance of the bioparticles after the step change remained roughly spherical and smooth with fairly thick biofilms, without the protuberances which had formed in other experiments (see Figure 5.28). The image analysis indicated that as the run progressed, the average biofilm thickness decreased from up to 40 μm to 13 μm, as shown in Figure 5.29. It is not clear if the biofilm thickness truly decreased. Some of the flocs grew quite large, and formed granules which were smooth and rounded and were typically smaller than the average bioparticle. Under the microscope, the differences between the two types of particles were obvious; however, when the images were analyzed, it was more difficult to distinguish between the two. The large rounded particles in Figure 5.28 were bioparticles; however many of the smaller dark round objects were granules. It is possible that the bioparticle measurements were distorted by including some of the agglomerations that looked like biofilm-coated sand particles, in the calculation of biofilm thickness.

The EPS measurements indicate an increase after the shock load in Figure 5.30. The dry weight measurements, in Figure 5.31 are less clear. Both analyses were difficult to perform for this experiment because the flocs and bioparticles settled at a similar rate in the samples and were difficult to separate.

This experiment was not used for parameter estimation or modeling because of the difficulties that were experienced during the analysis and because of the solids buildup in the reactor. Such a system would also require a different model in which diffusion into the flocs and the wall growth were included as processes.

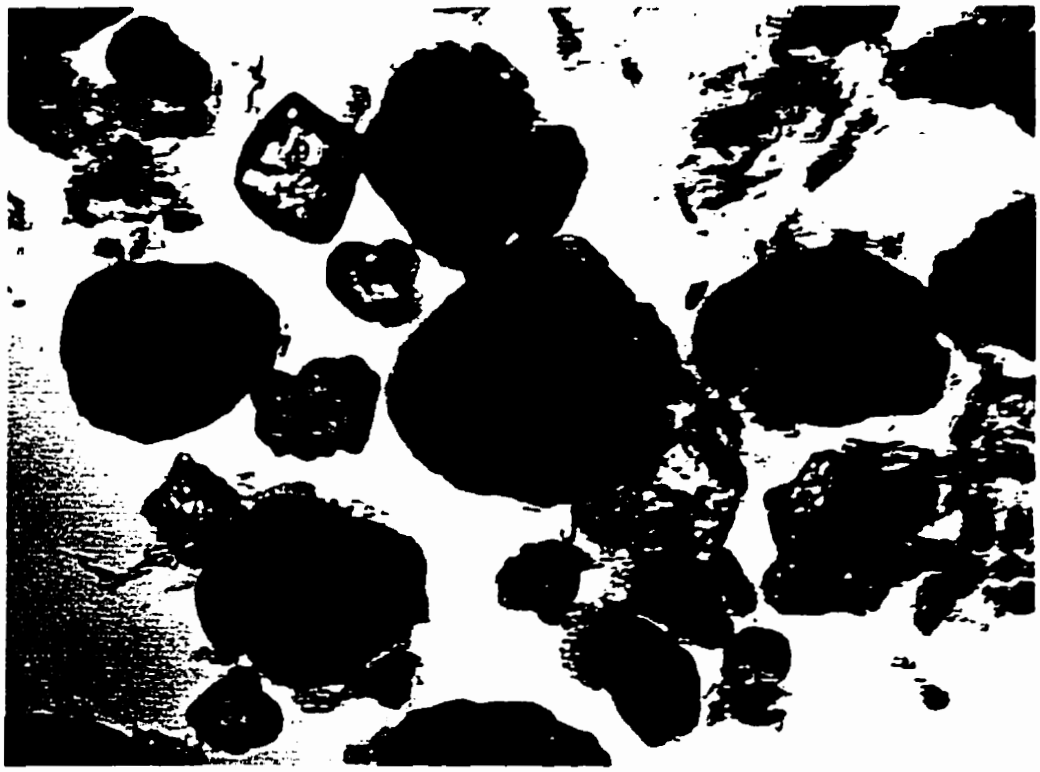

Figure 5.28. Appearance of the bioparticles 150 h after the step change during Run 6.

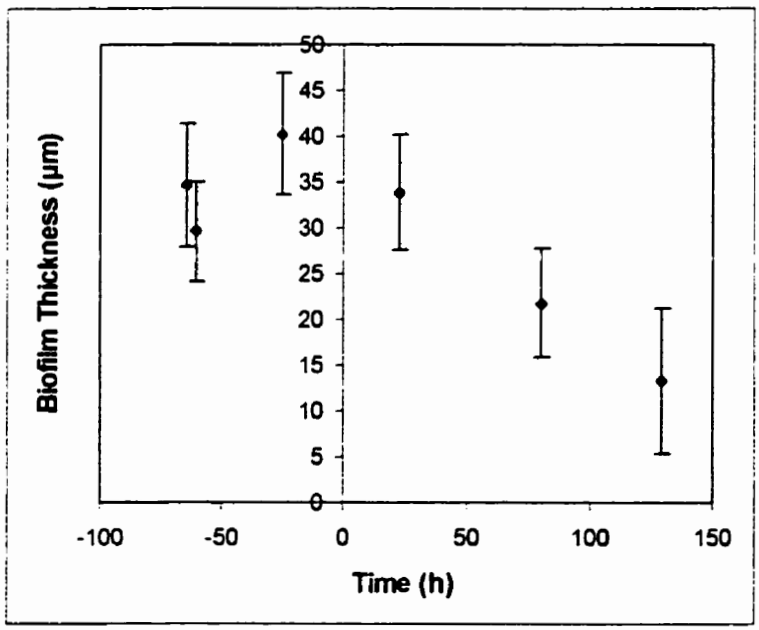

Figure 5.29. Average biofilm thickness during Run 6. Error bars refer to a 80% confidence interval.

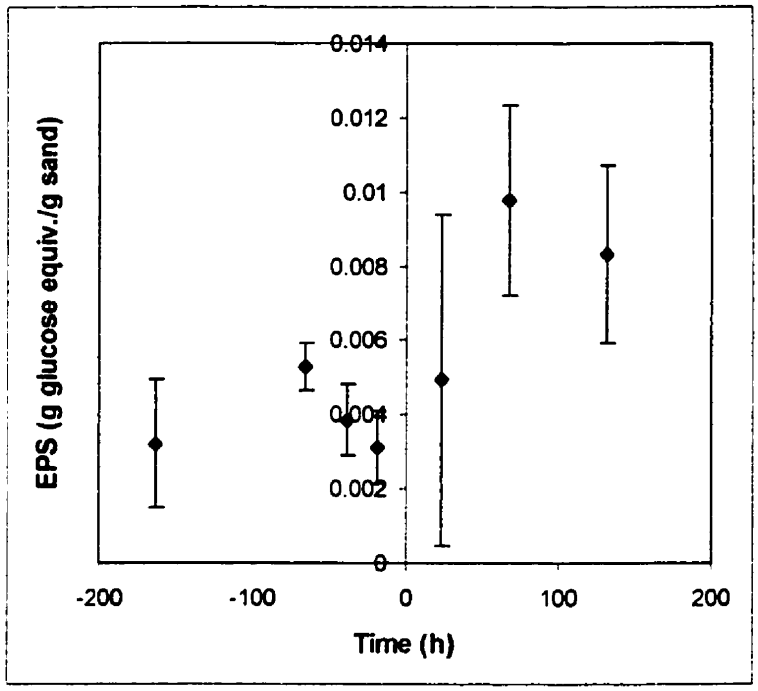

Figure 5.30. Average EPS content of the biofilm during Run 6. Error bars indicate the standard deviation.

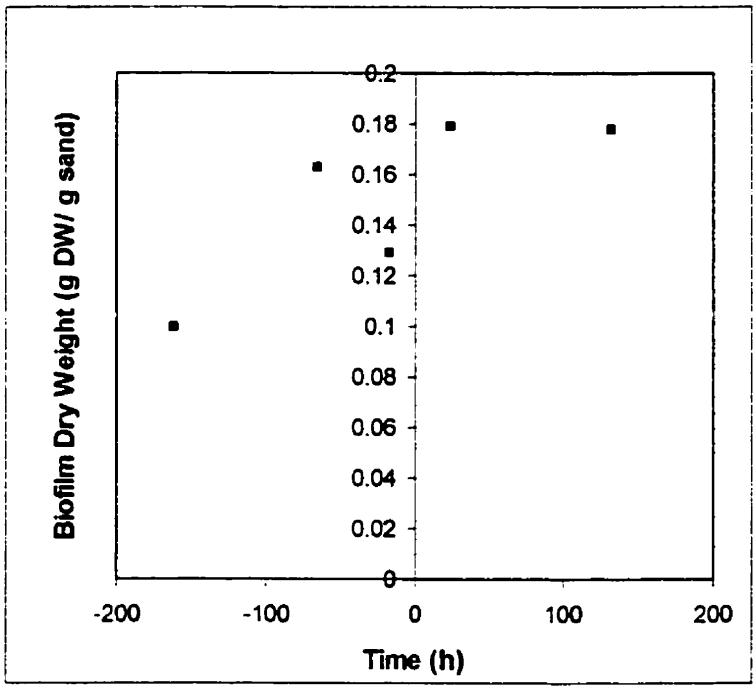

Figure 5.31. Biofilm dry weight during Run 6.

Run 7

Run 7 was begun after the glass reactor had been operating for 34 days. The dilution rate was increased from approximately 0.03 to approximately 0.09 h^{-1} for 24 hours twice during the start-up period in an effort to build up a thicker initial biofilm. Also, four days before the step change, an accidental release of feed solution to the reactor resulted in a perturbation to the system, so it was possible that the biofilm may not have been at a steady-state thickness immediately prior to the run. Despite the higher phenol loadings during the unsteady-state periods and also during the accidental release, the biofilm remained fairly thin (≈ 3 μm). The thin biofilm thickness may have been due to interparticle abrasion.

An image of the bioparticles is shown in Figure 5.32. The dark objects in Figure 5.32 were biofilm-coated particles. Most of the bare particles were transparent or very light gray in the images; thus, the degree to which the particle was covered in biofilm is partly reflected by the degree to which the particle blocked light under the microscope.

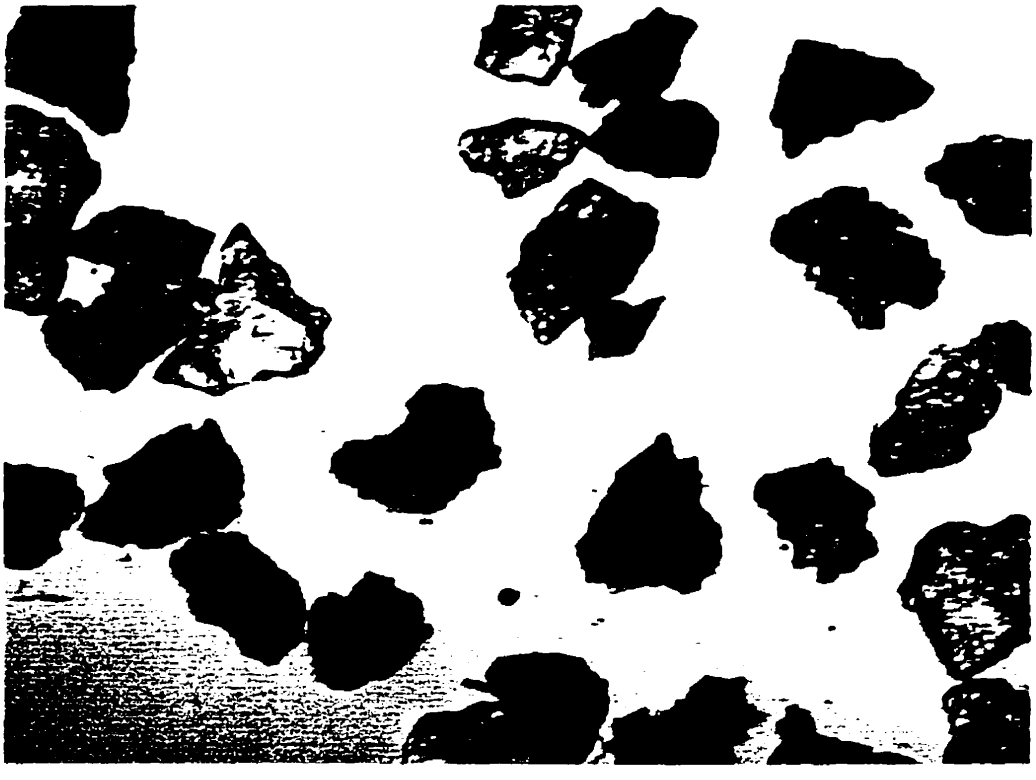

Figure 5.32. Appearance of the bioparticles prior to Run 7

Thirty days after startup a heterogeneous biofilm layer with streamers was noted on the upper portion of the riser section of the reactor. The characteristics of the biofilm and steady-state reactor conditions prior to the step change are shown in Table 5.19.

Table 5.19. Operating Conditions and System Characteristics During Run 7

Operating Conditions and System Characteristics	Initial Conditions	Conditions after Step Change
Dilution Rate (h^{-1})	0.0376	0.0314
Phenol Concentration in Feed (mg/L)	192	712
Loading (g/L·d)	0.173	0.477
Suspended Biomass Concentration (mg DW/L)	154	589
Phenol Concentration in the Reactor (mg/L)	2.2	3.6
Biofilm Dry Weight (g/g sand)	0.0069	0.016
EPS (g glucose equiv. /g sand)	0.00032	0.0011
Average Biofilm Thickness (μm)	2.9	5.4
% Bare Particles	30	20
Sand Concentration (g/L)	18.5	

The feed concentration was shifted from 192 up to 712 mg/L phenol. The initial dilution rate was 0.0376 h^{-1}. Due to several problems with the feed flow, the average dilution rate after the step change was 0.0314 h^{-1}.

In response, the suspended biomass concentration increased quickly, and peaked at 714 mg DW/L within 70 hours. The suspended biomass concentration eventually reached a pseudo-steady-state concentration of 590 mg DW/L. The peak and dip in the suspended biomass data, in Figure 5.33, was likely as a result of the variation in the feed concentration. The feed concentration may have varied due to volatilization of the phenol during autoclaving or differences in the amount of water added to each feed tank. Alternatively, the measured phenol concentrations may have underrepresented the phenol concentration in the tank due to poor mixing of the contents when the sample was taken; the feed was made in two parts and was combined immediately before switching feed tanks. This was done to minimize precipitation of salts during autoclaving.

The phenol concentration did not appear to change significantly despite the large change in the inlet phenol concentration. It appears that there was no lag in the ability of the bacteria to utilize phenol, from the phenol data. However, it is likely that there was formation of an intermediate metabolite that was excreted into the medium. The measured phenol concentrations increased slightly over the course of the experiment (up to 7 mg/L); the higher measured values (using the spectrofluorometer) were likely due to

interference of a compound which was excreted into the broth by the bacteria and which was a yellow-pigmented compound.

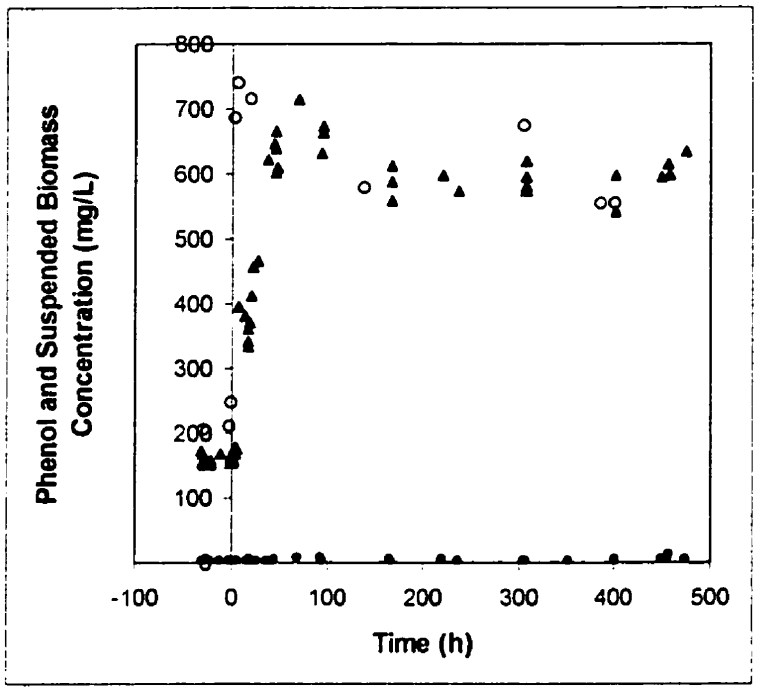

Figure 5.33. Response of the bulk phenol concentration (•) and the suspended biomass concentration (▲) to an increase in the feed concentration from 192 to 712 mg/L in the ICFBR during Run 7. The dilution rate shifted slightly from 0.0376 to 0.0314 h^{-1}.

The biofilm thickness increased slightly over the course of the run, from an average thickness of approximately 3 to 5 μm, as shown in Figure 5.34. Despite the small increase in average biofilm thickness, the EPS content (shown in Figure 5.35) and the dry weight of the biofilm (shown in Figure 5.36) both increased out of proportion to the measured change in biofilm thickness. The EPS increased by approximately 230% and the dry weight of the biofilm increased by approximately 130%. Perhaps these discrepancies can be explained, in part, by the presence of protuberances on some of the bioparticles, as shown in Figure 5.37. The protuberances were not included in the biofilm thickness measurement because they tended to be included with the background during image analysis.

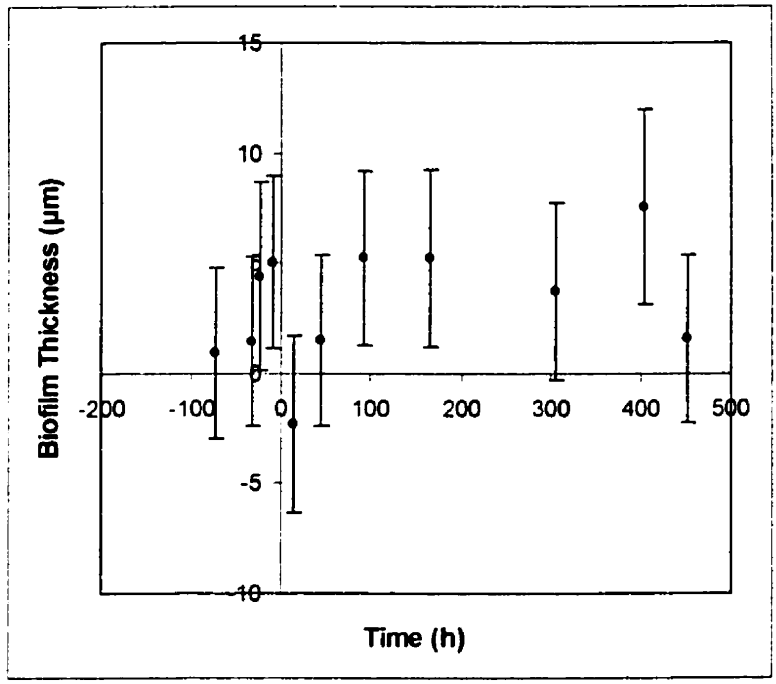

Figure 5.34. Average biofilm thickness during Run 7. Error bars indicate a 80% confidence interval.

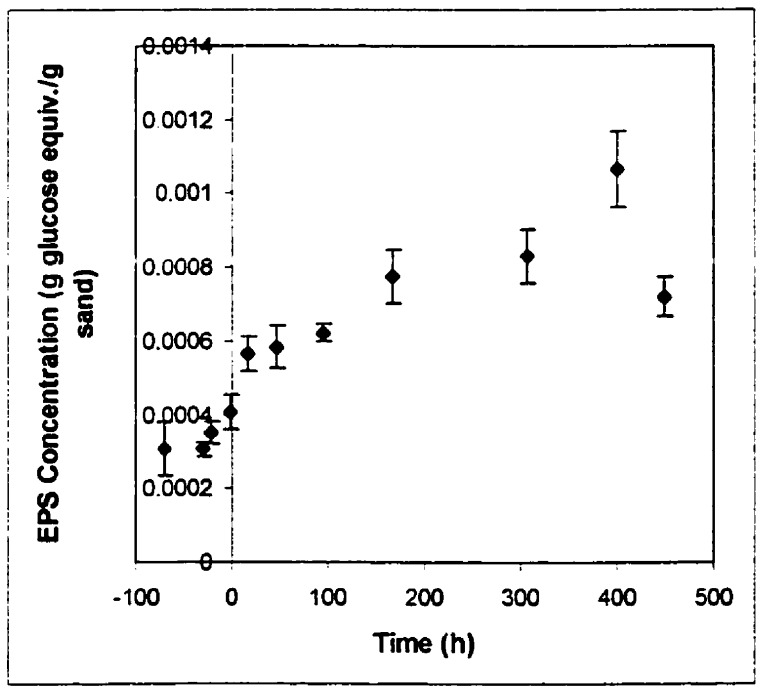

Figure 5.35. Average EPS content of the biofilm during Run 7. Error bars indicate the standard deviation.

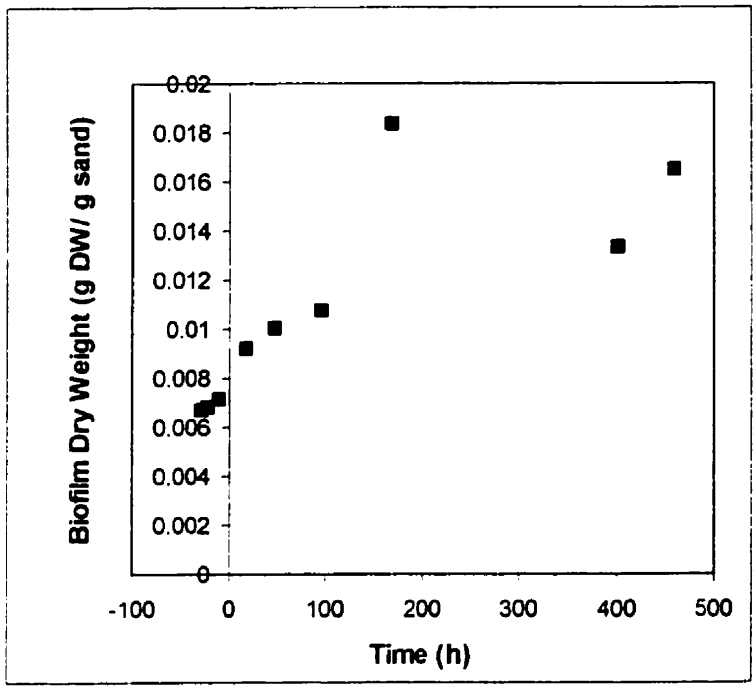

Figure 5.36. Biofilm dry weight during Run 7.

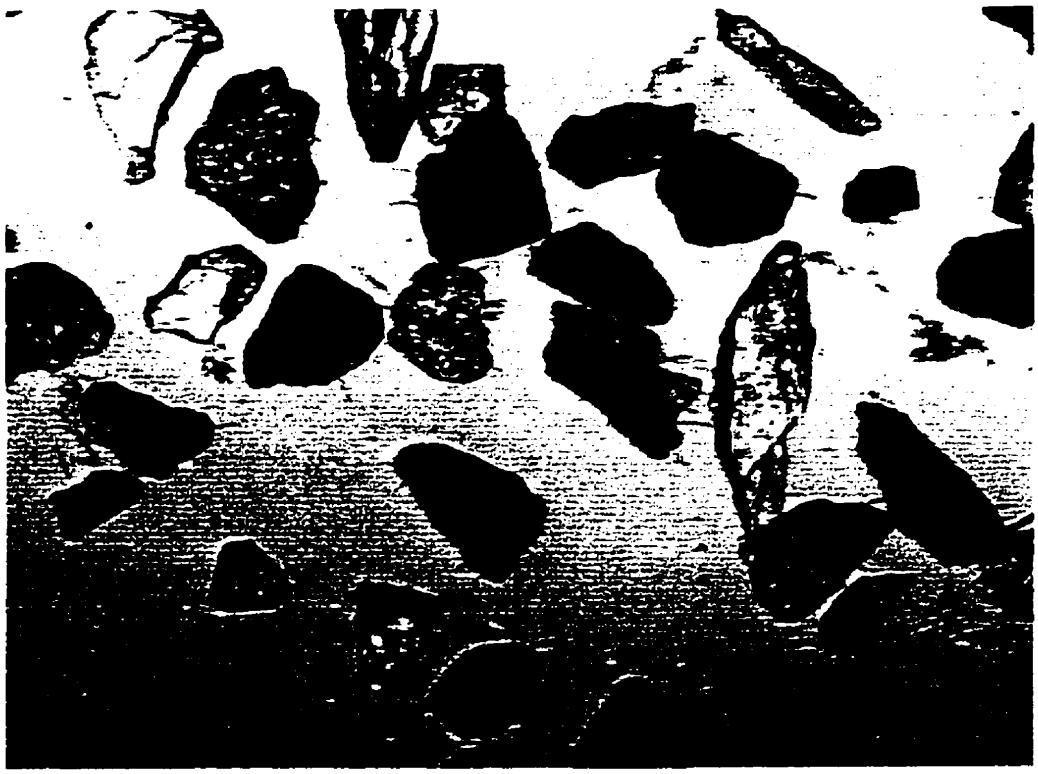

Figure 5.37. Appearance of the bioparticles 451 hours after the step change in Run 7.

5.2.2.2 High-level Responses

Run 1

The first run was begun after the reactor had been operating for 31 days. Although many particles appeared to be covered with biofilm, the biofilm was so thin that the thickness could not be easily discerned even under high magnification (1000X).

The run was originally intended to be a low-level feed concentration step change. Immediately before the step change, there were problems drawing feed due to an equipment problem. While solving the problem, the feed flow rate was temporarily increased to draw feed into the tubing. The feed flow rate was returned back to what appeared to be the original level; however, because the pump speed was highly sensitive to very small changes on the dial, the actual flow rate was somewhat higher. Thus, the resulting step change was a combination of changes in feed concentration and dilution rate. The changes in operating conditions are summarized in Table 5.20.

Table 5.20. Operating and Reactor Conditions During Run 1

Operating Conditions and System Characteristics	Initial Conditions	Conditions after Step Change
Dilution Rate (h^{-1})	0.0344	0.0592
Phenol Concentration in Feed (mg/L)	251	296
Loading (g/L/d)	0.207	0.421
Suspended Biomass Concentration (mg DW/L)	143	Reached 112
Phenol Concentration in the Reactor (mg/L)	1.1	Reached 100
EPS (g glucose equiv. /g sand)	0.00028	Reached 0.00039
Sand Concentration (g/L)	20.8	

The response of the reactor to the step change is shown in Figure 5.38. Within 2 hours of the step change, the phenol concentration in the reactor increased beyond 2 mg/L. The initial change in suspended biomass concentration is less dramatic than Figure 5.38 appears to indicate. For some unknown reason, the suspended biomass concentration increased from approximately 130 mg DW/ L, where it had been for several days, to 143 mg DW/L immediately before the step change (within 1 hour). Within 2-3 hours of the step change, the suspended biomass concentration increased to approximately 153 mg DW/L, then decreased gradually over a period of 36 hours to a concentration of 112 mg DW/L. During this period, the phenol concentration increased from 6.4 mg/L (at t=3 h) to 100 mg/L (at t=48 h) after which the experiment was terminated. The suspended biomass concentration appeared to recover slightly at the end of the run,

but in view of the increasing phenol concentrations and the scatter in the suspended biomass data, it is likely that the 'recovery' was simply a result of scatter in the data.

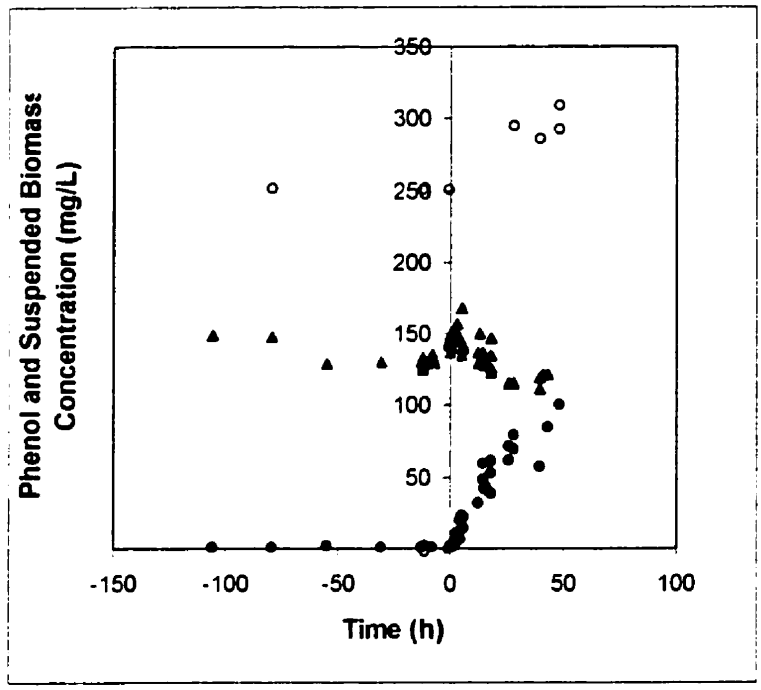

Figure 5.38. Response of the bulk phenol concentration (•) and the suspended biomass concentration (▲) to an increase in the feed concentration (○) from 251 to 296 mg/L and an increase in dilution rate from 0.034 to 0.059 h^{-1} in the ICFBR during Run 1.

The effect of the step change on the biofilm was more difficult to discern. There was no visible change in the biofilm within the 48 hours of the step change. After the system had recovered (a month later), small protuberances were visible on the particles. It was discovered that the sample volume used for the dry weight procedure had been too small (about 5 mL) and the weight differences were too small to evaluate the dry weight of the biofilm. The only information about the response of the biofilm to the step change comes from the EPS analysis. The results of this measurement are shown in Figure 5.39. An average increase of 0.0001 g glucose equiv./g sand was measured as a result of the step change, which is an increase of 36%.

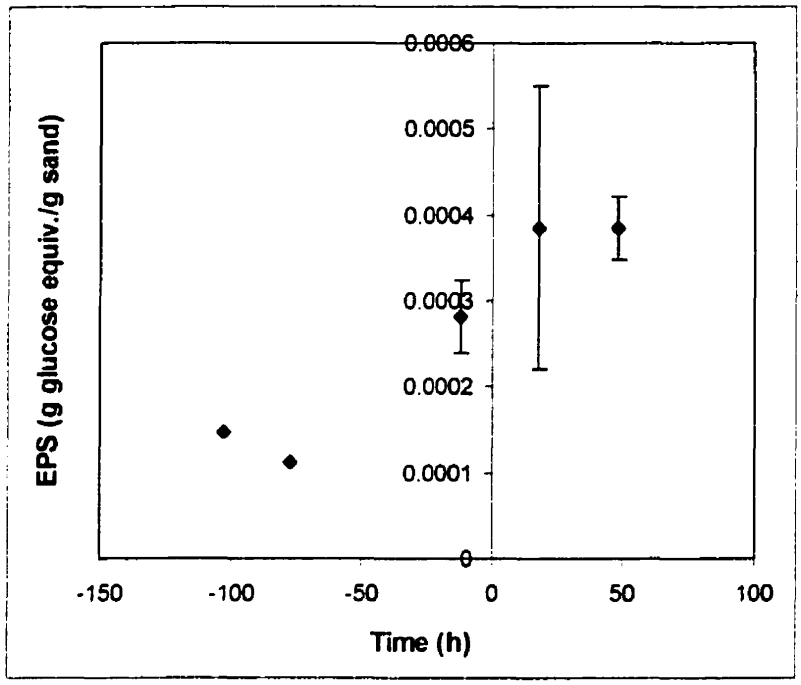

Figure 5.39. Average EPS content of the biofilm during Run 1. Error bars indicate the standard deviation.

Run 5

Run 5 was begun 41 days after sand was added to the Plexiglass airlift reactor. Many of the particles were covered with a very thin biofilm (see Figure 5.40). The initial steady-state conditions are shown in Table 5.21.

Table 5.21. Operating and Reactor Conditions During Run 5

Operating Conditions and System Characteristics	Initial Conditions	Conditions after Step Change
Dilution Rate (h^{-1})	0.0420	0.0945
Phenol Concentration in Feed (mg/L)	158	183
Loading (g/L·d)	0.159	0.415
Suspended Biomass Concentration (mg DW/L)	160	washout
Phenol Concentration in the Reactor (mg/L)	5	washout
EPS (g glucose equiv. / g sand)	0.0016	0.0017
Dry Weight (g DW/g sand)	0.047	0.055
Biofilm thickness (μm)	9.2	10.6
% Bare Carrier Particles	30	10
Sand Concentration (g/L)	20.6	settled out

Figure 5.40. Appearance of the bioparticles prior to Run 5.

A steady state was achieved at a dilution rate of 0.0420 h^{-1} and a feed concentration of 158 mg/L phenol. The dilution rate was increased to 0.0945 h^{-1} which was above the critical dilution rate of 0.071 h^{-1} for an equivalent suspended-cell reactor. The average feed concentration after the step change was 183 mg/L phenol. The response of the suspended cell and phenol concentrations is shown in Figure 5.41. The suspended cell concentration dropped from 160 to 35 mg DW/L in 145 hours. The phenol concentration in the reactor rose from 5 to 182 mg/L (the feed concentration). The scatter in the suspended cell and phenol concentrations in Figure 5.41 is possibly a result of fluctuating oxygen concentrations, which was a result of the sparger plugging on several occasions during the run. The run was terminated because the suspended cells had washed out and there was very little sand in the samples for biofilm measurement.

Several weeks later, a plug consisting of biomass and sand was discovered in the tube connecting the riser to the downcomer. The reactor was encased in foam insulation to minimize heat loss, so the problem was not noted until after the experiment. The plug prevented circulation between the riser and downcomer sections and was very difficult to dislodge. It was possible that during one of the episodes of sparger plugging, sand which had collected on the incline immediately prior to the entrance of the tube

could have caused a blockage. After air-flow was restored to the system, further settling could have occurred due to the lack of circulation of the fluid in the reactor.

The settling out of bioparticles is reflected in the decrease in the mass of sand in the samples, as shown in Figure 5.42. There was very little sand, if any, in the effluent tanks, therefore the loss of circulating sand must have been due to settling in the reactor. The result is that as the run progressed, the reactor became more characteristic of a suspended-cell system without biofilm-coated particles. That the suspended cells washed out of the system is not surprising considering the dilution rate was above the critical dilution rate of a suspended-cell system.

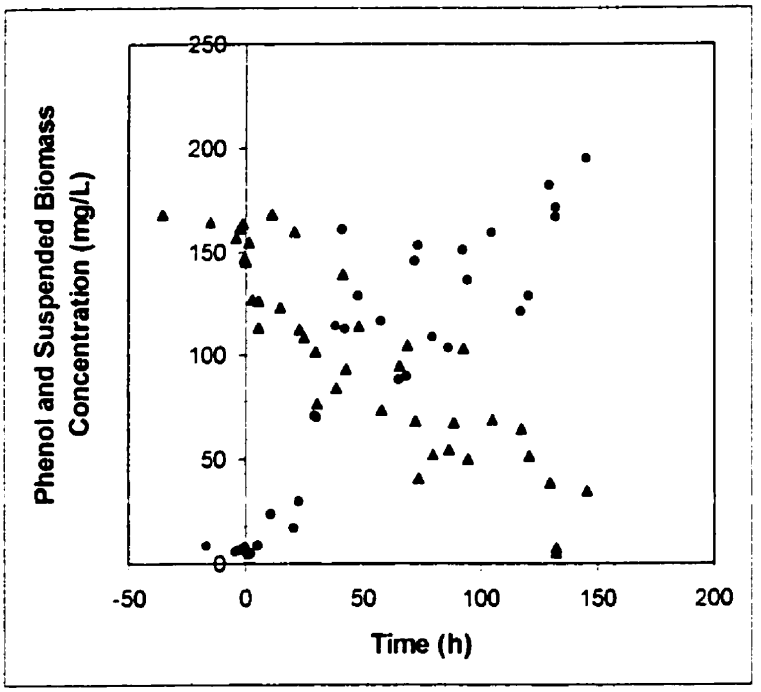

Figure 5.41. Response of the bulk phenol concentration (•) and the suspended biomass concentration (▲) to an increase in the dilution rate from 0.0420 to 0.0945 h^{-1} and a small increase in feed concentration from 158 to 183 mg/L phenol in the ICFBR during Run 5.

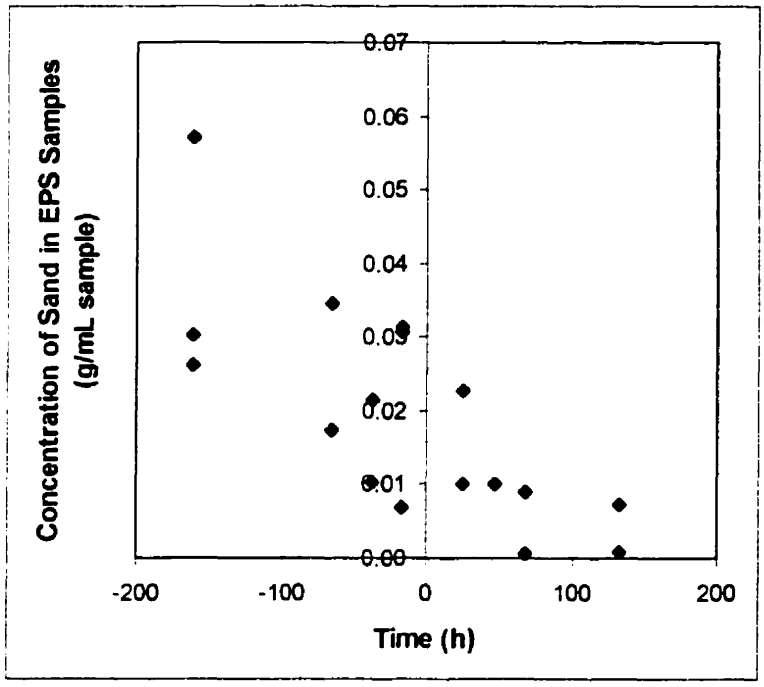

Figure 5.42. Decreasing concentration of sand in EPS samples during Run 5.

The biofilm thickness may have increased after the step change, but the data are not clear. There is little difference between the average biofilm dry weight before and after the step change (see Figure 5.43). There was considerable scatter in the EPS results in Figure 5.44; however it appears that the EPS content of the biofilm did not increase appreciably during the run. Although there is limited information from the biofilm thickness data in Figure 5.45, it appears that there was no increase in the biofilm thickness within 20 hours of the step change.

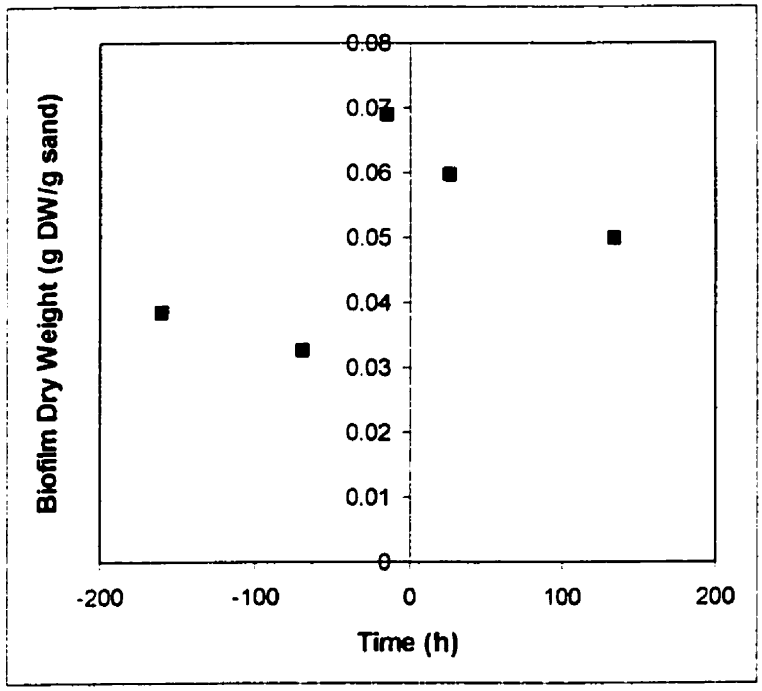

Figure 5.43. Dry weight analysis for Run 5.

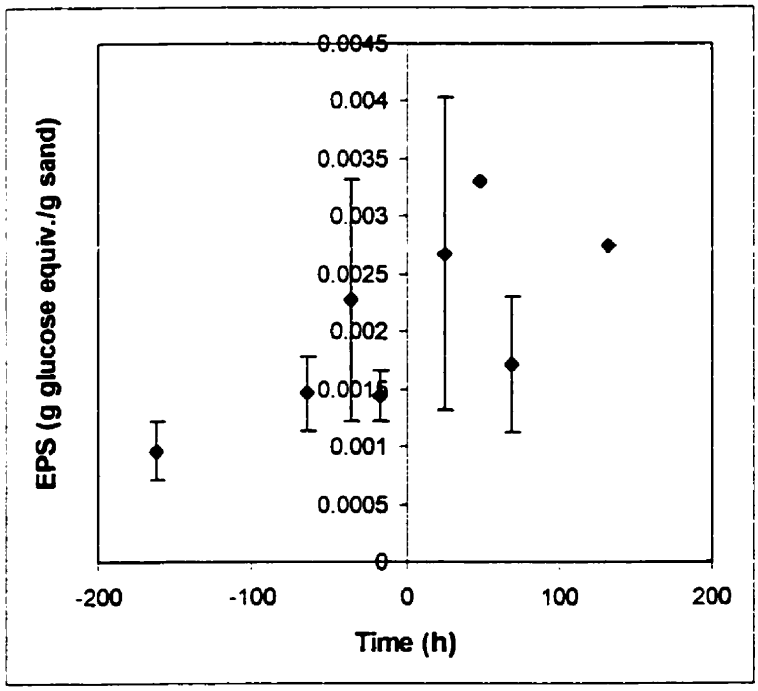

Figure 5.44. Average EPS content of the biofilm during Run 5. Error bars indicate the standard deviation.

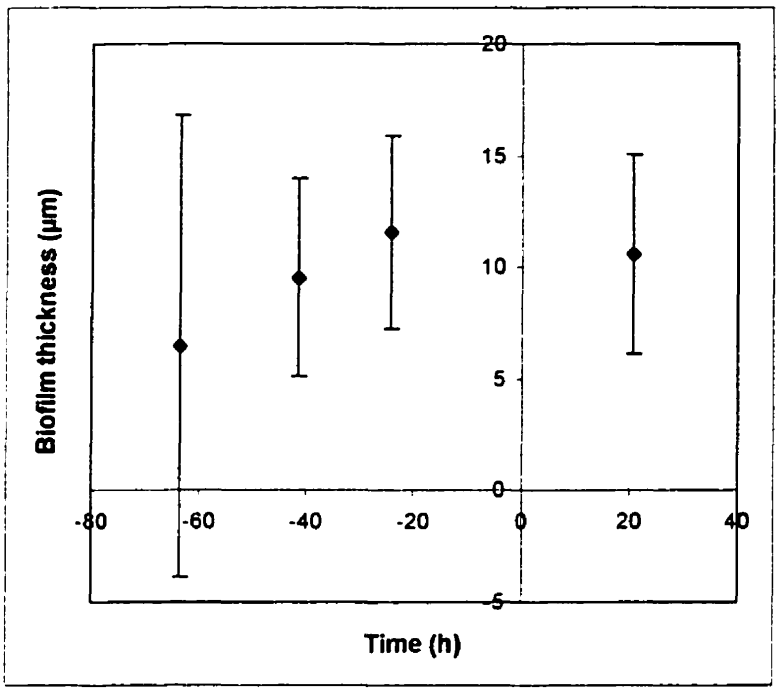

Figure 5.45. Average biofilm thickness during Run 5. Error bars indicate the 80% confidence interval.

Run 8

Run 8 immediately followed Run 7, during which a pseudo-steady state had been achieved after 500 hours after the step change. The broth was strongly coloured with a yellow pigment. The wall growth that had been present at the beginning of Run 7 was highly heterogeneous with long streamers several millimetres in length. The biofilm was fairly thin (approximately 4 µm) (see Figure 5.46). The initial conditions prior to the step change are listed in Table 5.22.

The dilution rate was increased from 0.0374 to 0.170 h^{-1}, which is far in excess of what would be required to wash out an equivalent suspended-cell system. After the step change, the suspended biomass rapidly washed out within 50 hours and the phenol concentration approached the feed concentration (shown in Figure 5.46). As the phenol concentration rose, the wall growth began to detach until only a patchy remnant remained.

Figure 5.46. Appearance of the biofilm immediately prior to Run 8.

Table 5.22. Operating Conditions and System Variables During Run 8

Operating Conditions and System Characteristics	Initial Conditions	Conditions after Step Change
Dilution Rate (h^{-1})	0.0374	0.170
Phenol Concentration in Feed (mg/L)	592	506
Loading (g/L·d)	0.530	2.06
Suspended Biomass Concentration (mg DW/L)	589	washout
Phenol Concentration in the Reactor (mg/L)	4.1	washout
Biofilm Dry Weight (g/g sand)	0.016	0.031
EPS (g glucose equiv. /g sand)	0.00087	0.0011
Average Biofilm Thickness (μm)	4	4
% Bare Particles	20	10
Sand Concentration (g/L)	16.7	

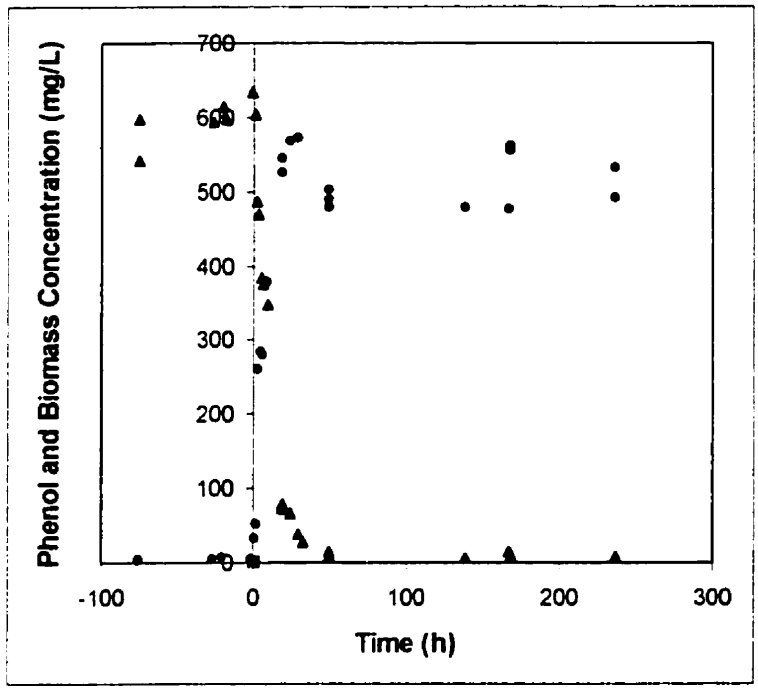

Figure 5.47. . Response of the bulk phenol concentration (•) and the suspended biomass concentration (▲) to an increase in the dilution rate from 0.0374 to 0.170 h^{-1} and a decrease in the feed concentration from 592 to 506 mg/L phenol in the ICFBR during Run 8.

In the next 250 hours, the biofilm did not appear to grow very much (see Figure 5.48). The EPS content, shown in Figure 5.49, did not appear to change after the step change. This is also reflected in the biofilm thickness data in Figure 5.50. It is not clear if the biofilm thickness actually decreased at the end of the run as suggested by Figure 5.50, because of the scatter in the data. For unknown reasons, the biofilm dry weight shown in Figure 5.51, appeared to increase during the run.

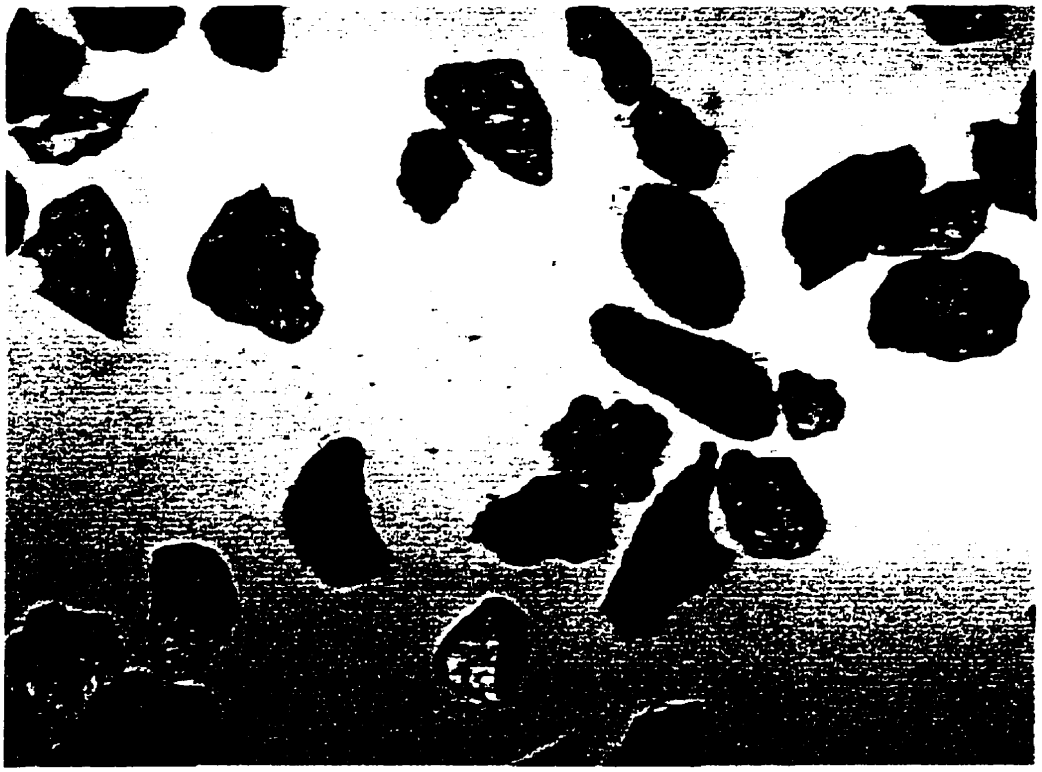

Figure 5.48. Appearance of the biofilm 250 hours after the step change in Run 8.

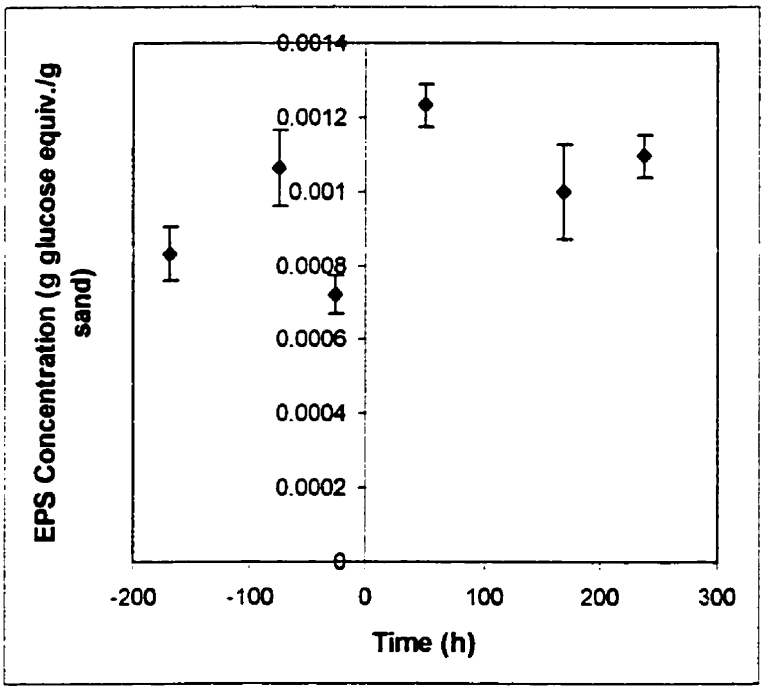

Figure 5.49. Average EPS content of the biofilm during Run 8. Error bars indicate the standard deviation.

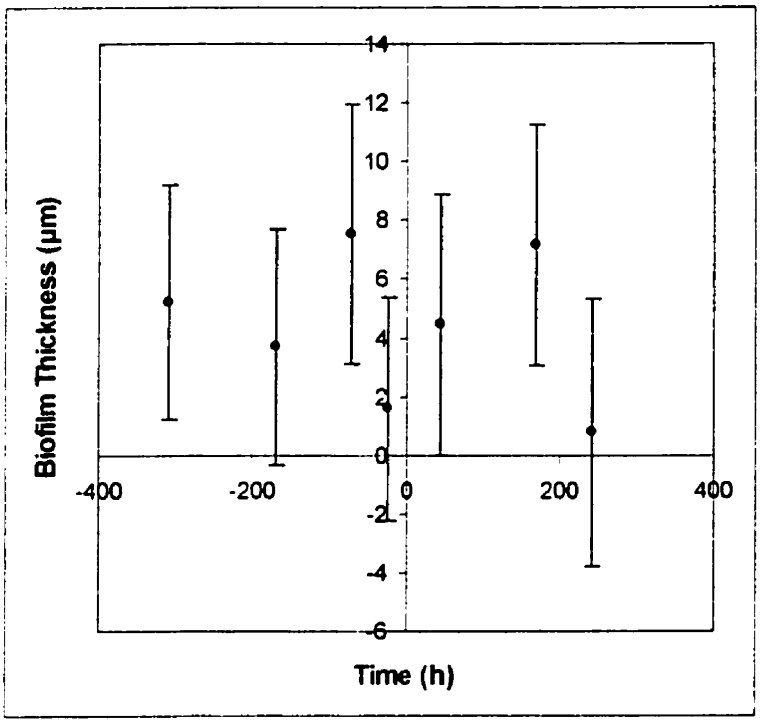

Figure 5.50. Average biofilm thickness during Run 8. Error bars indicate an 80% confidence interval.

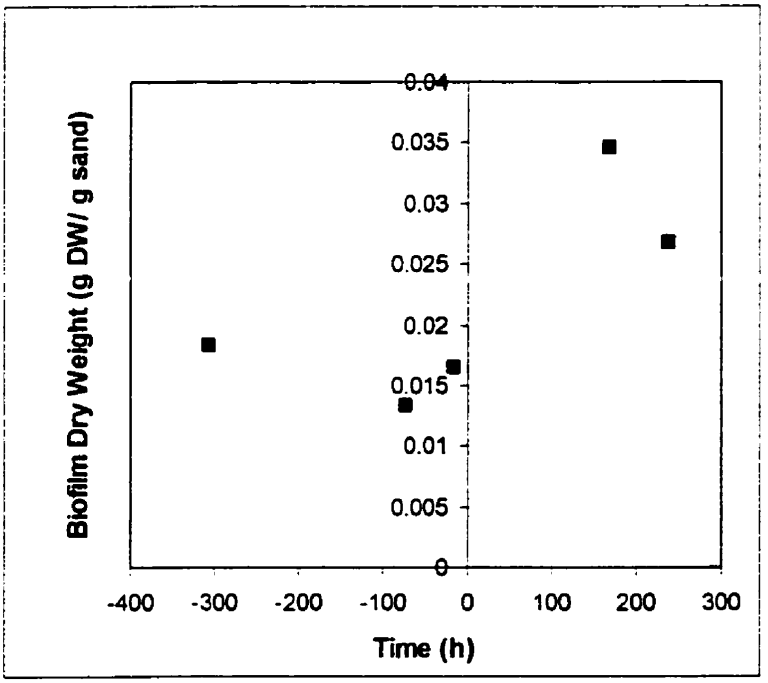

Figure 5.51. Biofilm dry weight during Run 8.

5.2.3 Phenol Growth Dynamics

5.2.3.1 Phenol Removal Mechanisms

Although biodegradation can be considered the primary mechanism by which phenol was removed in the ICFBRs, several other processes must also be considered. These include stripping, sorption, bioconversion and chemical modification.

Stripping

Despite the volatility of phenol, air stripping is not usually considered to be a major removal mechanism in biological wastewater treatment systems due to the low concentrations present under normal operating conditions (Stover and Kincannon, 1981; Kincannon et al., 1983; Petrasek et al., 1983). Under shock-loading conditions, air stripping may be a more significant removal mechanism, particularly if there is a system failure in which the phenol concentrations rise to high levels.

The amount of phenol removed through air stripping, r_{St} [mol/L·d], can be estimated by assuming a gas-liquid equilibrium and applying Henry's Law. The appropriate expression is as follows:

$$r_{St} = \frac{H}{P_T} Q_A \rho_g \frac{S_{b,m}}{V} \qquad (5.10)$$

where H is the Henry's law coefficient [atm·L/mol], Q_A is the air sparging rate [L/d], ρ_g is the molar density of the air [mol/L], $S_{b,m}$ is the bulk phenol concentration expressed on a molar basis [mol/L], V is the volume of the liquid which is sparged [L] and P_T is the total pressure [atm]. Kincannon et al. (1983) reported a value of $1.3 \cdot 10^{-3}$ atm·L/mol for the Henry's Law constant for phenol in an activated sludge system.

The steady-state phenol removal rates ranged from 0.15 to 0.53 g/L·d. The removal of phenol due to air stripping was approximately 0.00001 to 0.0003 g/L·d using Equation 5.10, which is a negligible fraction of the total removal. The phenol concentration in the reactor was highest at the end of Run 8, where it reached 506 mg/L (average over a 5-day period). At that point, the suspended biomass had washed out of the reactor, and the biofilm did not appear to be active. Equation 5.10 would predict a removal rate due to stripping of 0.019 g/L·d assuming an equilibrium between the gas and liquid phases. The average reactor concentration and feed concentration over a 5-day period were almost identical, resulting in a phenol removal rate of 0.0003 g/L·d, which is lower than the predicted stripping rate. Thus, it is likely that

the assumption of an equilibrium between the gas and liquid was not valid, and the other predicted stripping rates are high. Based on these calculations, it was concluded that stripping was not a significant phenol removal mechanism.

Sorption

Sorption of phenol by activated sludge is not generally considered to be a major removal mechanism (Kincannon et al., 1983; Petrasek et al., 1983). Reported concentrations of sorbed phenol in activated sludge have been very low (Petrasek et al., 1983). The significance of sorption of phenol to a biofilm has not been investigated. Indeed, it would be difficult to distinguish between phenol that is adsorbed to the biofilm and phenol that is included in the interstitial voids within the biofilm or phenol that is diffusing within the EPS matrix of the biofilm. Sorption to the sand is also unlikely to be a major attenuation mechanism.

Biodegradation, bioconversion and abiotic degradation

Biodegradation, bioconversion and abiotic degradation are difficult to differentiate. Under steady-state conditions, phenol was the only compound present (using GC-MS analysis), indicating that bioconversion was unlikely to be a significant removal mechanism. However, during unsteady-state conditions after step changes, there was some evidence of other compounds present. These are discussed further in Section 5.2.3.2. The relative proportion of these compounds (in terms of peak height using GC-MS analysis) appeared to be small compared to the amount of phenol present; thus, for modeling purposes, the process of bioconversion was not included. The process of abiotic degradation was not possible to differentiate in this study. If it occurred at all, it was included in the biological degradation component as the end result was the same – mineralization of the phenol.

5.2.3.2 Intermediate Metabolites

The presence of compounds other than phenol was investigated by measuring the absorbance of filtered samples of the broth between 200 – 450 nm using a spectrofluorometer (as described in Section 3.3.3). Spectral scans for Runs 5, 6, 7, and 8 are shown in Figures 5.52, 5.53, 5.54 and 5.55, respectively. Several absorbance peaks were observed and are listed in Table 5.23. The characteristic peak for phenol (at

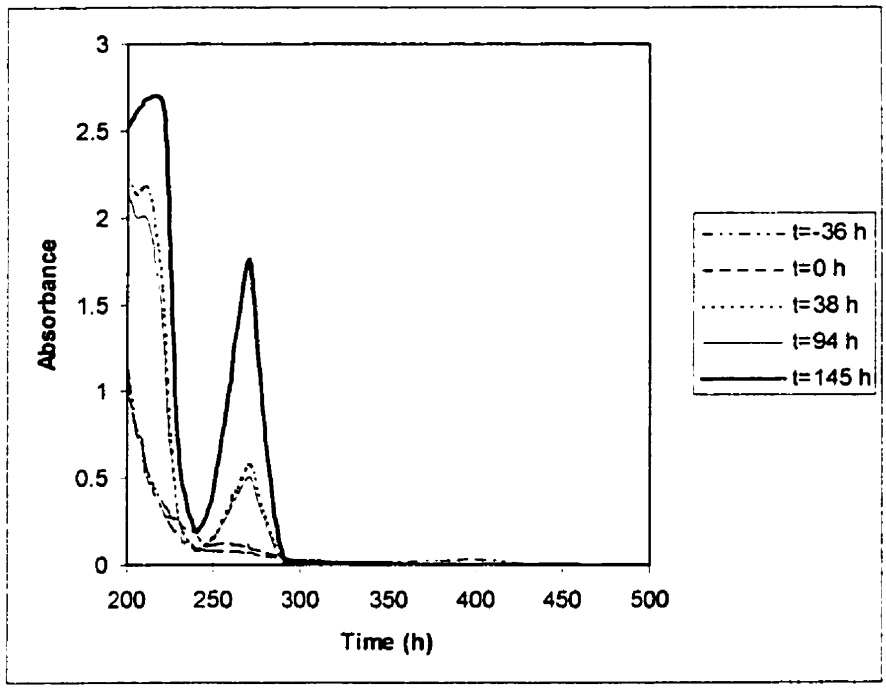

Figure 5.52. Absorbance spectra of a series of filtered samples taken from the ICFBR during Run 5.

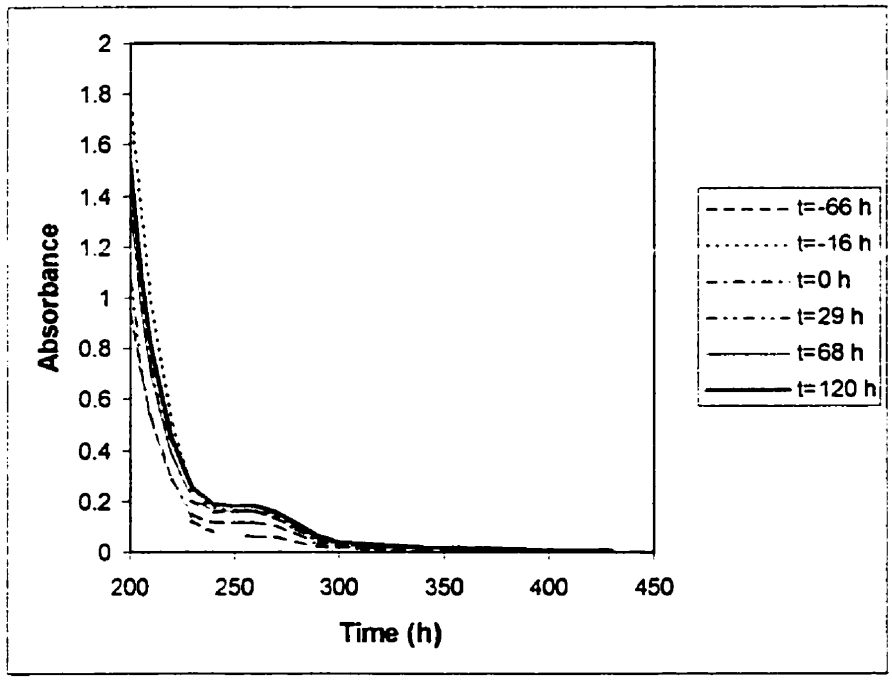

Figure 5.53. Absorbance spectra of a series of filtered samples taken from the ICFBR during Run 6.

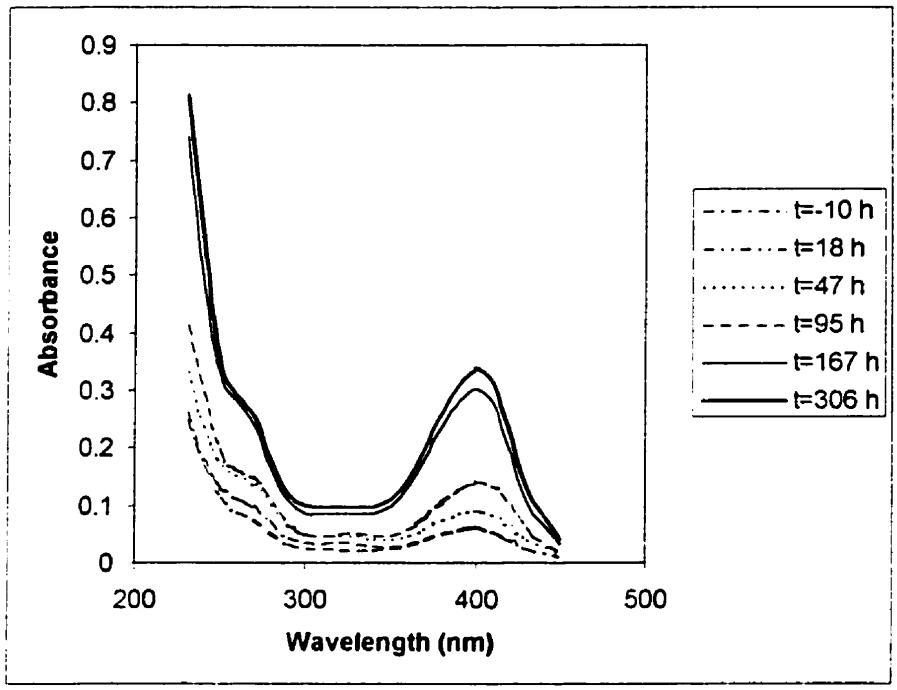

Figure 5.54. Absorbance spectra of a series of filtered samples taken from the ICFBR during Run 7.

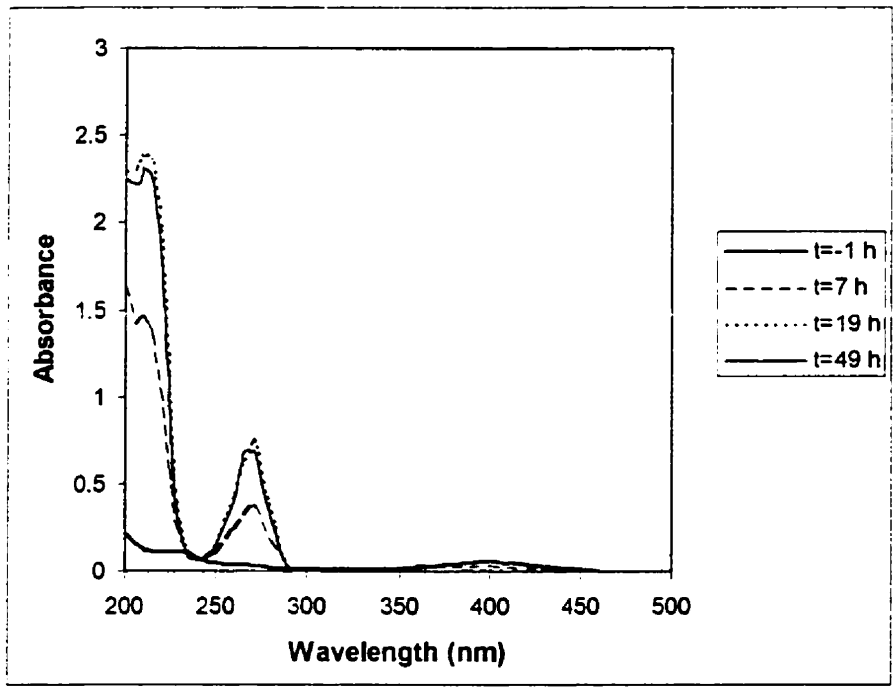

Figure 5.55. Absorbance spectra of a series of filtered samples taken from and ICFBR during Run 8. Samples were diluted by a factor of 10.

270 nm) was observed in Runs 5, and 8, in which the phenol concentration rose to levels above the critical substrate concentration and the suspended cells washed out.

The two low-response runs (Runs 6 and 7 in Figures 5.53 and 5.54, respectively) were quite different from each other. The absorbance spectrum in Run 6 appeared to have an increase in absorbance at a wavelength of 255-258 nm, which increased in height as the run progressed. The absorbance spectrum in Run 7 had an absorbance maximum at 400 nm, which increased markedly over the course of the run. This was observed as the samples became progressively more yellow.

Others have detected the presence of other compounds in the broth during the degradation of phenol by various mesophilic strains of *P. putida*. Xu and Majidi (1994) identified catechol, 2-oxopent-4-enotic acid, 4-hydroxy-2-oxovalerate, 2-hydroxymuconic semialdehyde, 4-oxalocrotonic acid (enol form) and 4-oxalocrotonic acid (keto form) from a culture of *P. putida* DMP-1 using laser desorption time-of-flight mass spectrometry. Several have identified an intermediate metabolite with an absorbance maximum at 375 nm and have attributed it to the presence of 2-hydroxymuconic semialdehyde (Molin and Nilsson, 1985; Li and Humphrey, 1989; Xu and Majidi, 1994). 2-hydroxymuconic semialdehyde is characterized by a yellow colour (Molin and Nilsson, 1985). It is one of the intermediates in the *meta* pathway (see Figure 2.2). The *P. putida* strain used in the current research does not possess the *meta* pathway (Kolenc et al., 1988), thus the yellow-pigmented compound observed in the current work is unlikely to be 2-hydroxymuconic semialdehyde.

Allsop (1989) reported the presence of an intermediate metabolite with a peak at the wavelength of 260 nm, which he attributed to the presence of acetyl-coenzyme A which has a peak at 260 nm. Acetyl-coenzyme A is an intermediate metabolite in the *ortho* pathway. The presence of the compound at 260 nm correlated well with the presence of dissolved organic carbon that could not be attributed to glucose or phenol (NPNG-DOC) during dynamic experiments.

Table 5.23. Ultraviolet Absorbance Peaks Observed During Step-change Experiments[1]

Run	Absorbance Peaks (nm)
5	209, 210, 215, 270, 400
6	255-258
7	400
8	209, 210, 211/212, 270, 400

[1] Scans performed for a limited number of samples in each run. Not all samples in each run contained each peak listed in the table.

Allsop (1989) noted the presence of a yellow-green colour in the broth during dynamic experiments, although its presence was not necessarily linked to surges in NPNG-DOC. He suggested that the colour may have been due to the production of a pigment, which is a common feature of fluorescent *Pseudomonads* (including *P. putida*) (Palleroni, 1975). Kotturi (1989) also reported the presence of a yellow-green colour during experiments with the same strain of *P. putida* which was used in this study.

The absorbance scans in this study (in Figures 5.52-5.55) bear little resemblance to those of Allsop (1989) who reported an absorbance maximum at 260 nm for intermediate-response types of experiments. The runs in which there were high-level responses all had peaks corresponding to the phenol peak at 270 nm; however, phenol has two peaks, including another at 214 nm (see Figure 5.55). The peak at 214 nm was often replaced by others at wavelengths in the range of 209-215 nm (see Table 5.23). Runs 6 and 7 were both classified as low-response; however, the spectral scans of the two experiments were very different with increasing amounts of compounds absorbing at 255-258 nm and 400 nm, respectively.

A possible explanation for some of the peaks is the excretion of intermediate metabolites which would result from uncoupled metabolism of the type noted during the batch kinetics experiment with unacclimated cultures (see Section 5.1.1.2). The absorbance peaks of intermediate compounds in the *ortho* pathway for phenol biodegradation are shown in Table 5.24.

Table 5.24. Ultraviolet Absorbance Peaks for Intermediate Metabolites in the *Ortho* Pathway of Phenol Biodegradation[1]

Compound	Ultraviolet Absorbance Peak (nm)
Catechol	219, 266
Cis-cis-muconate	257
Muconolactone	212
β-ketoadipate enol lactone	215
Succinate	208
Acetyl coA	260

[1] as cited by Allsop (1989)

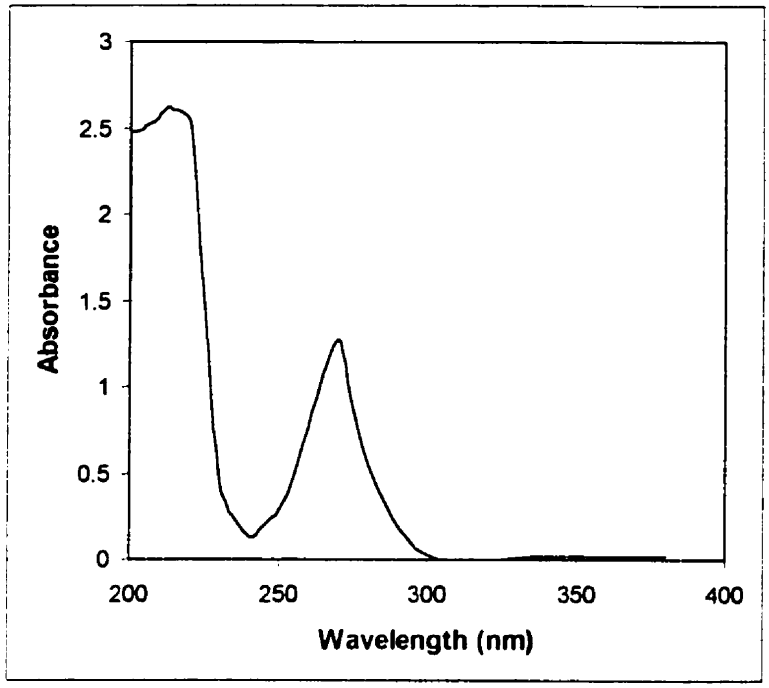

Figure 5.56. Absorbance spectrum of phenol between 200 and 400 nm.

A number of the intermediate metabolites have peaks (208-215 nm) that may be difficult to distinguish if there is any phenol present, because of the large first peak at 214 nm; however, a first peak value of 214 nm was quite rare in the samples in which phenol was evident. For the washout experiments (Runs 4,5 and 8), the peaks may correspond to the presence of β - ketoadipate enol lactone (Runs 4 and 5), succinate and muconolactone (Runs 5 and 8). Runs 5 and 8 also yielded samples which had peaks at 210 nm which cannot be explained by the intermediate metabolites listed in Table 5.24.

The two low-response experiments (Runs 6 and 7) had very different spectral profiles. Run 6 did not contain any peaks as such; however the 'hump' in Figure 5.53 had a consistent maximum at 255-258 nm (the absorbance was the same for each wavelength) which is similar to the peak for *cis-cis*-muconate at 257 nm. The strong peak at 400 nm in Run 7 does not correspond to any metabolites found in the *ortho* pathway. The yellow compound was also detected at the beginnings of Run 5 at a low level and Run 8 (which immediately followed Run 7). The compound may simply be a pigment that is secreted by *P. putida* Q5. A yellow-green compound reported by Kotturi (1989) may be another example.

The spectral evidence suggests that a number of intermediate metabolites from the *ortho* pathway may have been excreted into the broth during step changes in which there was a high response; however no

conclusions can be drawn without analysis that can specifically identify each compound (eg. GC-MS). The detected compounds could also be a result of cell leakage due to damage to the cell membrane (see Section 2.1.2), particularly because several were present when the phenol concentration rose to inhibitory levels. The compounds could also be extracellular anabolites. There is no data to indicate the relative importance of these compounds to the dissolved organic carbon.

5.2.4 Biofilm Characteristics and Development

5.2.4.2 Biofilm Formation and Development

The biofilms observed in this study tended to be very thin, even after fairly long periods of time for biofilm development (30-80 days). These startup times are similar to those used for nitrifying bacteria which have a relatively low maximum growth rate (0.033 h^{-1} at 20°C; Garrido et al., 1997) which is in the same order of magnitude as the maximum growth rate for *P. putida* Q5 at 10°C. A difference between this study and those in which nitrifying biofilms were developed, is that the dilution rates were much higher in the other studies (2 h^{-1} as opposed to 0.04 h^{-1}, for example) (Garrido et al., 1997). A difficulty when using toxic and inhibitory substrates is that the high dilution rates (which in other cases would enhance biofilm growth because of the high substrate levels and the lack of competition for substrate with suspended cells), inhibit growth and may prevent development of a mature biofilm. This was seen during Run 8 where there was little apparent growth of the biofilm even 250 hours after the step increase to a dilution rate of 0.17 h^{-1}. The feed concentration of 506 mg/L phenol was clearly inhibitory.

An important factor in the development of a mature biofilm is abrasion due to bare or partially covered particles. Gjaltema et al. (1995, 1997b) and Tijhuis et al. (1995) have reported that detachment is influenced strongly by the concentration of bare carriers in the reactor. The abrasion rate per particle increases with the size of the particle and the sharpness or roughness of the particle (Gjaltema et al., 1997b). Gjaltema et al.(1997b) suggest that during the startup of ICFBRs, the abrasion stress is initially high until a sufficient portion of the carriers become covered or partly covered with biofilm, at which point the abrasion stress is reduced and biofilm formation proceeds at a faster rate. Thus, the successful startup of an ICFBR reactor may depend upon achieving a growth rate in the primary biofilm layer which is high enough to overcome the detachment forces which result from the high level of abrasion. The thin biofilm

thickness reported in this work may have been due to a high level of abrasion. Thicker biofilms were achieved in runs in which the concentrations of particles were lower (eg. Run 6 with biofilm thicknesses of 13-40 μm). In other reactors described in the literature, development of fairly thick biofilms has been achieved with fairly high particle concentrations (eg. 150 g/L) by operating at high organic loadings and above the critical dilution rate for an equivalent suspended-cell culture. For reasons already discussed this is less desirable for reactors treating toxic or inhibitory substrates if the feed concentrations are subtantially above S^*.

Once biofilm development was well underway, approximately 5-10% of the particles remained bare, even during Run 6 where the biofilm thicknesses were quite thick. Examples are shown in Figures 5.57 and 5.58.

Figure 5.57. Example of a bare carrier during Run 4.

Figure 5.58 . An example of a bare particle (in the background) during Run 6.

The bare particles generally appeared to have smooth flat surfaces and sharp edges, unlike the other sand particles that were highly irregular and rounded. These observations are supported by the findings of Gjaltema et al. (1997a), who reported that the adhesion of *P. putida* to particles in ICFBRs depended to a great degree on the surface roughness. The initial biofilm development occurred in pits and hollows on the particle surface, and was much more affected by shear stress than physico-chemical properties of the particle surface (Gjaltema et al., 1997a).

5.2.4.3 Biofilm Morphology

The biofilms observed during Runs 1, 5, 7 and 8 were thin and smooth. A portion of the bioparticles (at least 50%) were covered with thin patchy growth. An example of both types of bioparticles is shown in Figure 5.59. Gjaltema et al. (1997a, b) reported that smaller particles are more likely to develop a biofilm because their impact upon colliding with other particles is less. This was not found to be the case. Biofilm

growth appeared on particles of all sizes, and patchy growth seemed to be as common on small particles as on larger ones; however this was not confirmed statistically.

The biofilms observed at steady-state conditions for Runs 2 and 3 were also smooth and thin; however, after the step changes in each experiment, protuberances developed (See Figures 5.19, 5.20, 5.23 and 5.24 in Section 5.2.2.1). The formation of protuberances became more pronounced after a reactor upset following Run 3, during which a high-concentration feed was delivered to the system and particles were lost to the effluent tank (possibly as a result of pH problems and the 'lift-out' phenomenon). An example is shown in Figure 5.60. Heterogeneous biofilms also formed during Run 6, possibly as a result of the low shear stress arising from the low particle concentration and thick biofilms that developed. An example of this type of biofilm is shown in Figure 5.61. The development of 'fluffy' biofilms after an increase in substrate loading has been reported in other studies as well (Tang et al., 1987; Kwok et al., 1998). 'Hairy' biofilms have been reported at low particle concentrations (Tijhuis et al., 1996). These observations are consistent with the hypothesis postulated by van Loosedrecht et al. (1995a). They suggested that biofilm structure is a function of the balance between detachment forces and surface loading. When the substrate surface loading increases, the biofilm preferentially grows in a heterogeneous morphology, which increases the surface area of the biofilm. Over time, this reduces the substrate surface loading and the protuberances erode to a new steady-state biofilm thickness. Kwok et al. (1998) observed that their 'fluffy' biofilms eroded over time, which agrees with the hypothesis. In cases where the abrasive force is low, the heterogeneous structure may persist.

Prior to the step change in Run 6, the protuberances began to break off from the bioparticles and form settleable suspended biomass in the reactor. This led to problems with solids separation and a build-up of suspended solids in the ICFBR. As the run progressed, the suspended solids became less heterogeneous and more rounded and solid in appearance. They also became larger, until they were comparable in size to some of the smaller bioparticles. An example is shown in Figure 5.62. This phenomenon is similar to the formation of granules reported by Tijhuis et al. (1995) and Gjaltema et al. (1997b). Tijhuis et al. (1995) reported that they removed a portion of the flocs and granules from their ICFBR reactor, presumably because of problems with solids separation.

Figure 5.59. Example of a thin, smooth biofilm-coated particle (centre) and partially-covered bioparticles (upper right) during Run 7.

Figure 5.60. Bioparticles with protuberances which developed after a reactor upset following Run 3.

Figure 5.61. Example of a heterogeneous biofilm structure with a thicker base biofilm prior to Run 6.

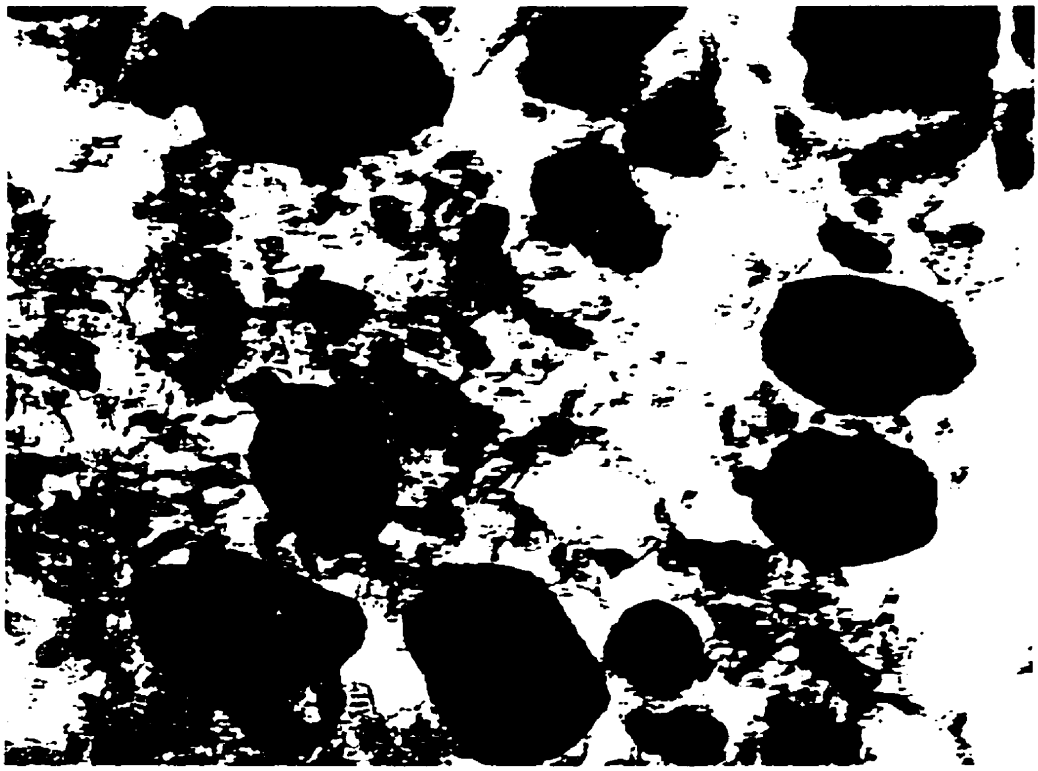

Figure 5.62 . Example of bioparticles, granules and settleable suspended solids which occurred during Run 6.

Another difficulty arising from the buildup of granules and flocs within the ICFBR was that suspended biomass consumed much of the phenol in the reactor. Given that the biofilm thicknesses were reasonably thick (with an average of up to 40 μm), substrate or oxygen depletion within the inner layers of the biofilm were likely. Several examples of sloughing were observed, probably as a result of decay in the inner regions of the biofilm. An example is shown in Figure 5.63, in which a portion of the bare particle surface had been exposed as a result of a large piece of the biofilm being removed.

Figure 5.63. Example of sloughing during Run 6.

5.3 Model Verification

5.3.1 Model Solution

The model described in Section 3.0 could not be solved analytically, so numerical methods were used. A steady-state form of the model was solved to provide initial conditions, which were needed to solve the unsteady state model.

5.3.1.1 Steady-state Model

The steady-state model was solved using the von Neuman integral method used in fluid dynamics. The significant advantage of the integral method is that the original formulation, which consists of a system of partial and ordinary diffential equations, is transformed to a set of diffential equations only, which can be readily integrated with standard Runge-Kutta methods. The MATLAB program that was used to solve the steady-state model is listed in Appendix B.

The phenol profile within the biofilm is approximately parabolic, and is related to boundary layer problems solved using a similar approximation by von Kármán (1921) (as cited in Holman, 1990). When the phenol concentration in the bulk fluid is inhibitory, the growth rate in the biofilm may be higher in the interior of the biofilm than at the surface (Gantzer, 1989); however, it is expected that the shape of the phenol profile in the biofilm would also have an approximately parabolic form as shown in Figure 2.5. This assumption simplifies the mathematics, and can satisfy the boundary conditions pertaining to the biofilm/bulk fluid and the biofilm/substratum interfaces. In principle other higher order profiles could be assumed in order to improve the accuracy of the simulations. In this particular case, the resulting curvature was small because the biofilm thicknesses were very thin (see the discussion in Section 5.3.3) and the growth rate can be assumed constant over the bioiflm profile. For this case the parabolic solution is the exact solution for a steady-state solution. This approach avoids numerical solution using finite elements which would require a grid which changes with time, leading to a much more complex solution.

The type of substrate profile depends upon the substrate concentration in the bulk fluid, the substrate uptake rate of the cells and the biofilm thickness. There are three categories of substrate profiles in the biofilm, which are shown in Figure 2.5. At one extreme is a flat profile in which there is no resistance to mass transfer, often found in very thin biofilms (case 'a' in Figure 2.5). At the other extreme is a deeply penetrated biofilm in which the substrate concentration within the biofilm reaches zero, either at the biofilm/particle interface or within the biofilm (case 'c' in Figure 2.5). This type of substrate profile is undesirable because the biofilm becomes susceptible to sloughing as the EPS structure weakens in substrate-depleted regions (Wagner and Hempel, 1988; Applegate and Bryers, 1991). Between the two extremes is a substrate profile which is approximately parabolic in shape and does not reach a zero concentration (case 'b' in Figure 2.5). In heterogeneous biofilms, the substrate profile may look quite different, particularly if there is convective transport within the void spaces; however, such a case is not considered here. For *P. putida* Q5 growing at 10°C, biofilm thicknesses below 45 μm are expected to resemble those in case 'b' (Patoine, 1989).

Because relatively thin biofilms were observed during this study, a parabolic phenol profile in which the substrate concentration did not reach zero was assumed. The profile was given the general form

$$S_f = a'(r - r_p)^2 + b'(r - r_p) + c' \qquad \textbf{(5.11)}$$

where a', b' and c' are constants. The expression was solved using the expressions for the boundary conditions and replaced the variable S_f in the model with the coefficient of the second degree term in the profile function in Equation 5.11. The development of the model solution is described in detail in Appendix A. This substitution transformed the set of equations into a set of four ODEs with the coefficient of the second power in the profile function in Equation 5.11. The values of S_b, X_S, a' and r_f that were determined from the steady state model, were used as initial condition inputs to the unsteady-state model.

5.3.1.2 Unsteady-state Model

The unsteady-state model was solved numerically using the stiff ODE solver, ODE23s, in MATLAB. The code is listed in Appendix B. The model was transformed into a form that was amenable to the solver by using the parabolic approximation discussed in the previous section and two other key transformations.

The first transformation employed was the Leibniz rule to deal with the moving boundary problem posed by the growth of the biofilm and the change in the variable r_f which was the limit of an integral term. The second was the consolidation of an untidy group in the balance on the substrate concentration within the biofilm. This resulted in a new lumped-term variable, θ, which replaced a' as one of the four unknowns (see Equation A-35 in Appendix A-2). The result was a set of four equations of the form:

$$\frac{dS_b}{dt} = f_1(S_b, X_S, r_f, \theta) \tag{5.12}$$

$$\frac{dX_S}{dt} = f_2(S_b, X_S, r_f) \tag{5.13}$$

$$\frac{d\theta}{dt} = f_3(r_f, \theta) + \frac{dr_f}{dt} \times f_4(S_b, r_f, \theta) \tag{5.14}$$

$$\frac{dr_f}{dt} = f_5(r_f, \theta) \tag{5.15}$$

where f_1, f_2, f_3, f_4 and f_5 are functions of the indicated variables.

5.3.2 Experimental Verification of the Model

5.3.2.1 Experimental Verification of the Steady-state Model

Steady-state values for each of the four variables were obtained using the steady-state model. Initially, the steady state model was difficult to fit to the data using experimentally determined values for each parameter. There were two problems encountered during the fitting procedure.

The first problem was that the experimental values for the specific detachment rate, r_D, were unreliable. The difficulties in evaluating r_D were discussed in Section 5.1.4.4. The values listed in Table 5.25 were chosen to reflect the particle concentrations that were used in each run, and also were slightly adjusted to better fit the model to the data.

The second problem was that the values for the maintenance coefficient, m, did not appear to work well with the steady-state data from the ICFBR. A value of 0.044 g/g·h was determined from CSTR experiments with suspended cell cultures at 10°C. It was clear from the yield data listed in Table 5.25, that there was a difference between the first three experiments and the last group of experiments. The lamps for the spectrofluorometer and the spectrophotometer used to evaluate the phenol concentration and the optical density of the broth were changed between the analysis of the two sample sets. Both instruments were recalibrated, and the calibration for the spectrofluorometer was checked five times during the data analysis for Runs 5-8, during which no shift in the calibration was detected. No explanation can be offered for the high yield values in Runs 5-8. Consequently, to reflect the changes in the yield, two different values of m were used. A value for m of 0.03 g/g·h was used for Runs 1-3 and a value of 0.01 g/g·h was used for subsequent experiments. These values of m roughly approximate the observed values of Y_{XS} using Equation 2.7. For example, for Runs 1 and 7, the calculated values of Y_{XS} are 0.8 and 1, respectively.

Table 5.25 Experimental Values of Observed Yield (Y_{XS}) and Sand Concentration (C_p) and Values of the Maintenance Coefficient (m) and the Specific Detachment Rate (r_D) used in the Model Simulations.

Run	Experimental Values		Parameter Values	
	Y_{XS} [g/g]	C_P [g/L]	m [g/g·h]	r_D [h^{-1}]
1	0.6	20.8	0.03	0.024
2	0.6	22.6	0.03	0.025
3	0.5	11.4	0.03	0.018
5	1.0	18.3	0.01	0.022
7	0.8	18.5	0.01	0.022
8	1.0	16.7	0.01	0.022

The results of the model fitting are shown in Table 5.26. The model predicted the bulk phenol concentrations fairly well for the first three experiments. The fitted values for Runs 5 to 8 were lower than measured. The measured values were higher than expected and it was possible that there was some interference by other compounds. This was likely the case during the steady-state period prior to the step change in Run 8 during which what was likely a yellow pigment was secreted into the broth. The yellow compound was washed out quickly as the run progressed. The fitted values of the suspended biomass concentration were typically lower than observed experimentally, but were usually within 10% of the experimental value. The model predicted thin biofilms for the selected values of r_D. This was consistent with experimental observation. The biofilms for which there was no thickness data during Runs 1,2 and 3, were very thin prior to the step changes; thus, the fitted values were reasonable. The simulation values listed in Table 5.26 for steady-state conditions were used as initial values for the unsteady-state model. The parameter values for the steady-state and unsteady-state models were consistent for each run.

Table 5.26 Comparison of Experimental and Simulated Values of the Measured Variables in the ICFBR at Steady State.

Run	S_L [mg/L]		X_V [mg/L]		δ [μm]	
	Experimental	Model	Experimental	Model	Experimental	Model
1	1.1	1.7	135	132	-	1.0
2	1.8	1.7	115	98	-	1.3
3	0.6	1.0	112	107	-	1.7
5	4.9	1.5	160	144	9	2.3
7	2.2	1.5	158	173	3	2.2
8	4.1	1.7	581	542	4	5.4

5.3.2.2 Experimental Verification the Unsteady-state Model with High-response Experiments

The calibration procedure for the unsteady-state model is summarized in Section 3.5.3. The fit of the model to the experimental results was first explored with the high-response experiments because those experiments gave the most information about the sensitivity of the system to shock loads. The discussion will focus on Runs 1 and 8 because problems were experienced with clogging of the downcomer with particles during Run 5 as a result of sparger plugging. Run 1 was a moderate shock load during which the dilution rate was increased from 0.034 to 0.059 h^{-1} and the average feed concentration was increased from 251 to 296 mg/L phenol. Run 8 was a more severe shock load during which the dilution rate was increased

from 0.037 to 0.17 h^{-1} and the average feed concentration changed from 592 to 506 mg/L phenol. Both step changes resulted in the washout of suspended biomass and increases in the bulk phenol concentrations, approaching feed concentrations. The response of the bulk variables, phenol concentration and suspended biomass concentration will be discussed first.

Bulk Parameters, S_b and X_S

The first attempt at fitting the model to the experiments was made with the Haldane model for the kinetics, using parameters determined from acclimated cultures. The resulting simulations are shown in Figures 5.64 and 5.65. In both cases, the unsteady-state model predicted that the systems would recover from the shock. In the case of Run 8 (Figure 5.65), the unsteady-state model predicted that the system would exhibit large transients in the bulk phenol and suspended biomass concentrations, and that the phenol concentration would exceed 300 mg/L phenol, which is well into the inhibitory range. Neither simulation fit the data.

The changes in bulk phenol concentration during the high-response experiments were quite rapid, with concentrations rising to inhibitory levels within ten hours. The shortest generation time of *P. putida* Q5 at 10°C is, at best, seven hours. The generation times during the experiments were much longer, because the steady-state specific growth rates were low. Thus, acclimation could not have occurred quickly enough for the cells to adjust to the changing conditions.

When comparing the kinetics of acclimated and unacclimated *P. putida* Q5 in Section 5.1.1.2, two striking differences were noted. For unacclimated cultures, the critical specific growth rate, μ^*, was lower and the specific growth rate under inhibitory conditions decreased more rapidly as the phenol concentration increased. Both characteristics have a significant effect on how the system responds to changes in phenol concentration and how a model predicts the response.

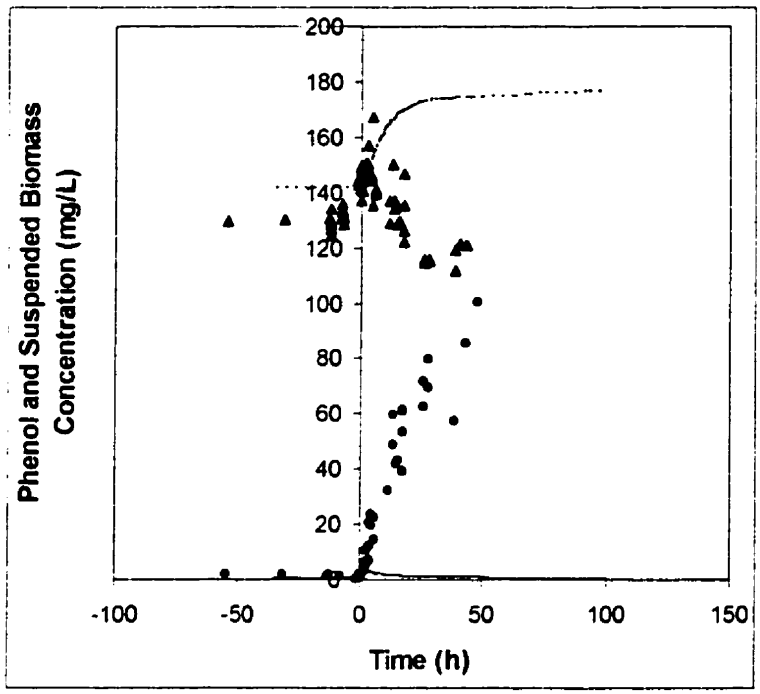

Figure 5.64. Simulation of the bulk phenol concentration (———) and the suspended biomass concentration (- - - - -) for Run 1 using Haldane kinetics determined for acclimated cultures. The simulation is plotted with the experimental response of the bulk phenol concentration (•) and the suspended biomass concentration (▲) to an increase in the feed concentration from 251 to 296 mg/L and an increase in dilution rate from 0.034 to 0.059 h^{-1} .

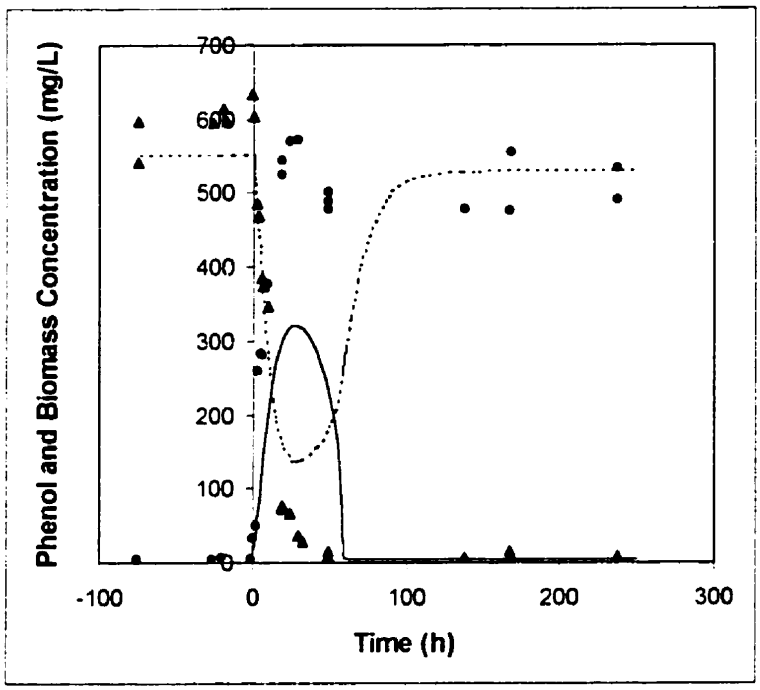

Figure 5.65. Simulation of the bulk phenol concentration (———) and the suspended biomass concentration (- - - - -) for Run 8 using Haldane kinetics determined for acclimated cultures. The simulation is plotted with the experimental response of the bulk phenol concentration (•) and the suspended biomass concentration (▲) an increase in the dilution rate from 0.037 to 0.17 h^{-1}. The feed concentration changed from 592 mg/L to an average of 506 mg/L after the step change.

A second attempt at fitting the model to the experiments was made with the kinetics determined using unacclimated kinetics. The Luong model was used because it was better at predicting the specific growth rates of unacclimated batch cultures than the Haldane model (see Section 5.1.1.2), in part because it predicts stronger inhibition at higher phenol concentrations.

The results from the simulations using unacclimated kinetics are shown in Figures 5.66 and 5.67. The simulation of Run 8 predicted a rapid washout of suspended cells and an increase of the phenol concentration to a level approaching the feed concentration with no recovery. The fit of the model to the dynamic response was very good. Worden and Donaldson (1987) also found it necessary to increase the level of inhibition to fit a dynamic ICFBR model to two pulse experiments; they accomplished this by decreasing the value of K_I.

The simulation of the moderate shock in Run 1, did not predict the response of the system (in Figure 5.66). The model predicted a small transient in the bulk phenol concentration, followed by a return to low levels. The simulated suspended biomass concentration increased quickly to a maximum and then

leveled off to a new steady state. The experimental data showed an increase in the phenol to 100 mg/L as the suspended biomass began to wash out, at which point the run was terminated.

In shock-loading experiments with suspended-cell cultures, properly calibrated Haldane kinetics can usually predict the complete washout of a culture which has been subjected to a large shock load (Garcia Sanchez et al., 1998); however, the Haldane model cannot predict washout accurately at lower shock loads (Garcia Sanchez et al., 1998). The predictive capability of other balanced-growth models such as the model of Luong (1987) appears to be similar in a biofilm reactor. Run 8 represented a severe shock load to the ICFBR; system failure was successfully simulated using balanced growth kinetics that had been determined using unacclimated cultures. The system failure in Run 1, however, was not predicted accurately using balanced growth kinetics.

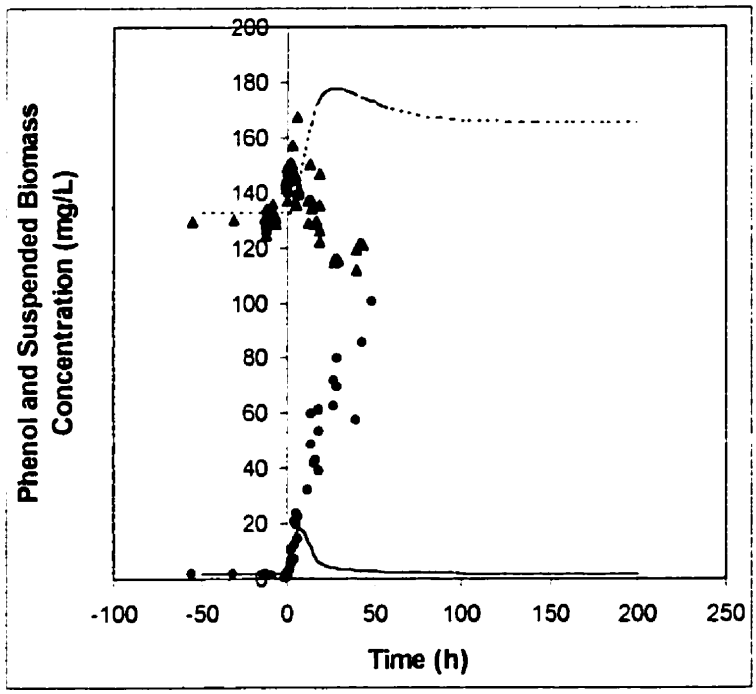

Figure 5.66. Simulation of the bulk phenol concentration (———) and the suspended biomass concentration (- - - - -) for Run 1 using Luong kinetics determined for unacclimated cultures. The simulation is plotted with the experimental response of the bulk phenol concentration (•) and the suspended biomass concentration (▲) to an increase in the feed concentration from 251 to 296 mg/L and an increase in dilution rate from 0.034 to 0.059 h^{-1}.

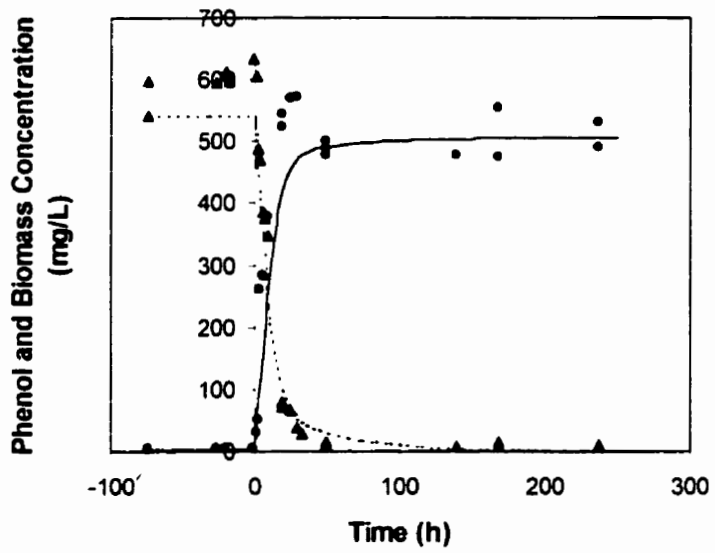

Figure 5.67. Simulation of the bulk phenol concentration (———) and the suspended biomass concentration (- - - - -) for Run 8 using Luong kinetics determined for unacclimated cultures. The simulation is plotted with the experimental response of the bulk phenol concentration (•) and the suspended biomass concentration (▲) an increase in the dilution rate from 0.037 to 0.17 h^{-1}. The feed concentration changed from 592 mg/L to an average of 506 mg/L after the step change.

The acclimated and unacclimated kinetics used in both sets of simulations utilized the concept of balanced growth; however, results from shock-loading experiments using continuous suspended cultures suggest that unbalanced growth is likely (Storer and Gaudy, 1969; Yang and Humphrey, 1975; Yongaçoglu et al., 1981; Sokol, 1988a; Allsop et al., 1993; Garcia Sanchez et al., 1998). The various hypotheses concerning unbalanced growth include changes in the cell structure and RNA content, storage or excretion of intermediate metabolites, metabolic overflow, double inhibition by intermediate metabolites and phenol, and growth rate hysteresis. These were described in Section 2.3.1.2.

The presence of intermediate compounds was not investigated for Run 1. The presence of intermediates in Run 8 after the step change was not confirmed, possibly because the phenol concentration was high in the samples that were investigated. However, it is very likely that in both experiments, growth either stopped or was affected by the phenol or intermediate concentrations reached during the experiments in a way that affected the outcome of the experiment.

Growth rate hysteresis has been approached in a number of ways by other researchers. Most have produced time lag models that are of limited use. Several utilize variables that are difficult to measure *a*

priori, including the value of μ immediately after a step change (Yang and Humphrey, 1975) or the ratio of enzyme activity to the maximum enzyme activity of the cells (Yongaçoglu et al., 1981), which limit the utility of the models for predictive purposes. Others represent the step change in some way, as the ratio of dilution rates before and after a step change (Li and Humphrey, 1989). Time constants to model the delay in the ability of the cell to react to the shift in feed conditions have also been applied; however, they have been limited to small perturbations (Young et al., 1970), or have required the use of separate time constants for uptake and growth with little experimental verification (Chiam and Harris, 1983).

In this work, a very simple adjusting factor (Equation 5.16) was added to the model to allow for growth-rate hysteresis. Unlike other models, the adjusting factor changed according to the phenol concentration that the bacteria were being subjected to at any given time. The steady-state phenol concentrations in the system were very low; thus, if during a simulation the phenol concentration in the bulk fluid (or the biofilm) departed significantly from the steady-state value, it was assumed that the cells were undergoing some sort of hysteresis. This is supported by the observations of strongly unbalanced growth in some of the unacclimated-culture batch kinetics experiments at concentration increases as low as 50 mg/L phenol (see Figure 5.9 in Section 5.1.1.2). Another assumption underlying the adjusting function was that as conditions proceeded farther away from the steady-state phenol concentration, $S_b(0)$, the suppression of growth became more severe, although it was assumed that growth was possible to some extent.

The adjusting factor was expressed as a suppression of cell-growth that was proportional to the difference between the bulk phenol concentration and the steady-state phenol concentration to which the cells had been acclimated. Thus, the growth rate of the suspended cells was expressed as follows:

$$\mu_b(t) = k(S_b(t) - S_b(0))\mu_{b,b}(t) \qquad \textbf{(5.16)}$$

where the bulk concentration of phenol at time t, $S_b(t)$, and at the initial steady state value, $S_b(0)$, were expressed in mg/cm^3 and the specific growth rate corresponding to $S_b(t)$ assuming balanced growth, $\mu_{b,b}$, was expressed in h^{-1}. The specific growth rate within the biofilm was expressed similarly.

$$\mu_f(r,t) = k(S_f(r,t) - S_f(r,0))\mu_{f,b}(r,t) \qquad \textbf{(5.17)}$$

A disadvantage of the function is that is does not predict metabolic overflow – that is, the conversion of phenol to other products that are not used for growth. Very low concentrations of non-

phenol compounds compared to the concentrations of phenol present were detected in the bulk fluid in the samples that were analyzed using GC-MS. Thus, the diversion of substrate to the production of other compounds rather than to growth was not considered significant enough to induce one to complicate the model further. The introduction of intermediate compounds introduces significant complexity to the model formulation as shown by Garcia Sanchez et al. (1998) for suspended-cell cultures, with the addition of a number of parameters which have to be identified.

Simulations of Runs 1 and 8 using a value of 10 cm^3/mg for k, are shown in Figures 5.68 and 5.69. k was determined through trial and error using the data from Run 1 only. The unsteady-state model with the growth-rate adjusting function fit the data for Run 1 (Figure 5.68) much better than before. The model predicted a steeper increase in phenol concentration and a steeper decline than the data indicated, 40 hours after the step change and beyond, however, without additional data, it is difficult to ascertain whether the reactor would have recovered or if the change in slope in each case is due to measurement error. The

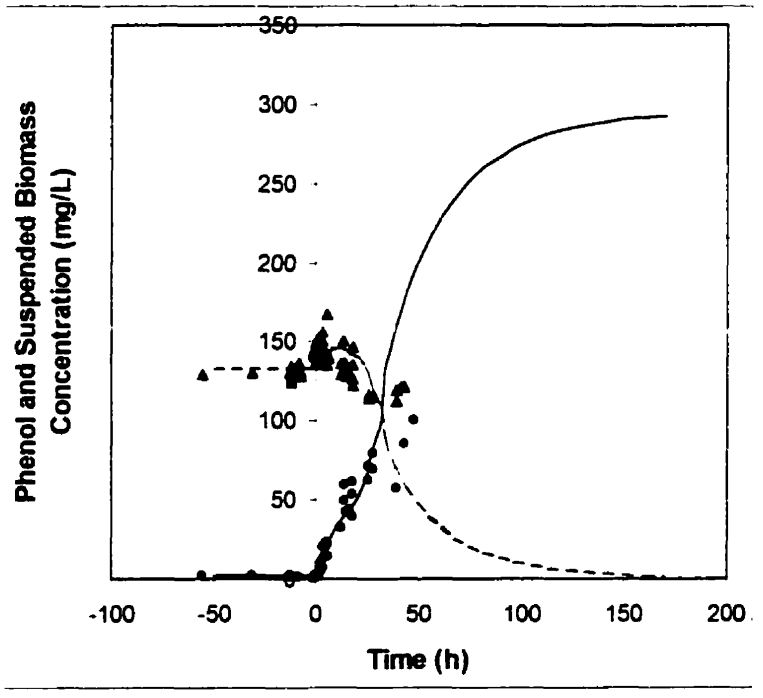

Figure 5.68. Simulation of the bulk phenol concentration (———) and the suspended biomass concentratoin (- - - - -) for Run 1 using Luong kinetics determined for unacclimated cultures, adjusted to account for suppression of growth during shock-loading. The simulation is plotted with the experimental response of the bulk phenol concentration (•) and the suspended biomass concentration (▲) to an increase in the feed concentration from 251 to 296 mg/L and an increase in dilution rate from 0.034 to 0.059 h^{-1}.

simulation in Figure for Run 8 was slightly steeper than in the previous case (Figure 5.69), which better reflected the data.

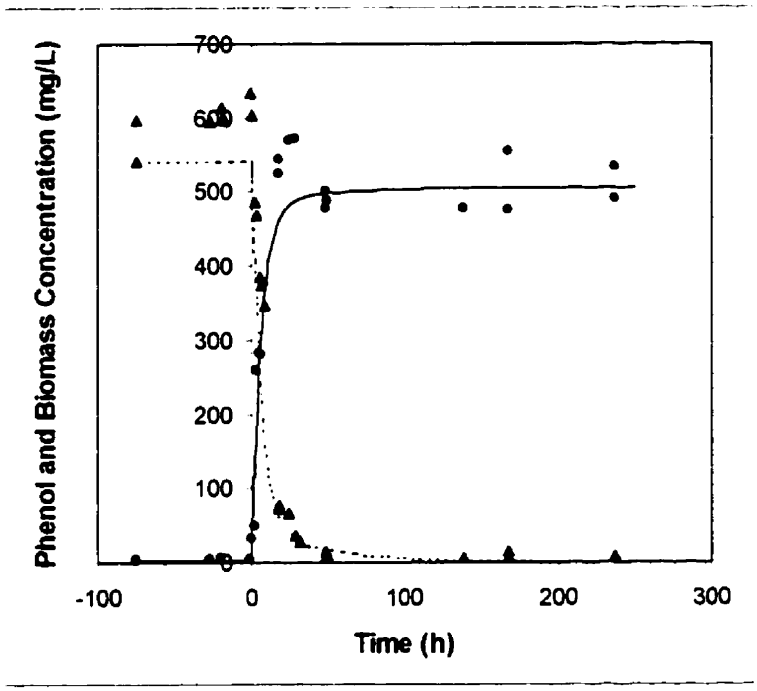

Figure 5.69. Simulation of the bulk phenol concentration (———) and the suspended biomass concentration (- - - - -) for Run 8 using Luong kinetics determined for unacclimated cultures, adjusted to include suppression of growth during the shock-load. The simulation is plotted with the experimental response of the bulk phenol concentration (•) and the suspended biomass concentration (▲) to an increase in the dilution rate from 0.037 to 0.17 h^{-1}. The feed concentration changed from 592 mg/L to an average of 506 mg/L after the step change.

A simulation of Run 5, shown in Figure 5.70, was attempted even though there were problems with solids suspension during the run due to sparger plugging. In Run 5, the dilution rate was increased from 0.042 to 0.095 h^{-1} and the average feed concentration changed from 158 to183 mg/L phenol. During the experiment the suspended biomass washed out of the reactor and the phenol concentration approached the feed concentration. The simulation predicted that the system would react only slightly to the step change with full recovery after a small transient in the phenol concentration. A check of the sand concentration in the EPS samples taken over the course of the run, confirmed that the solids had settled out in the reactor, likely in the arm of the downcomer where plugging was observed later. A plot of a simulation of the same run, except with inactive biofilm to simulate the absence of bioparticles, resulted in

washout of the suspended biomass (in Figure 5.71). The rate of washout in the simulation was steeper than the rate of washout that was observed in the system; however, bioparticles were present (in decreasing amounts) at the beginning of the run, and likely absorbed some of the shock. The difference between the two simulations illustrates the importance of the biofilm to the stability of the reactor, even though the average initial biofilm thickness was fairly thin (9 μm - measured and 2.3 μm – used in the simulation).

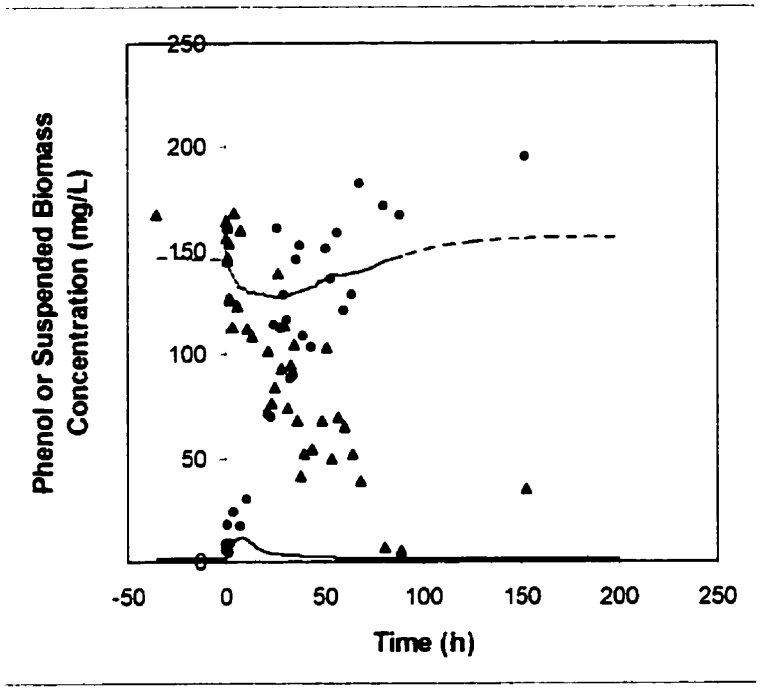

Figure 5.70. Simulation of the bulk phenol concentration (———) and the suspended biomass concentration (- - - - -) for Run 5 using Luong kinetics determined for unacclimated cultures, adjusted to include suppression of growth during the shock-load. The simulation is plotted with the experimental response of the bulk phenol concentration (•) and the suspended biomass concentration (▲) to an increase in the dilution rate from 0.042 to 0.095 h^{-1} at a feed concentration of 160 mg/L.

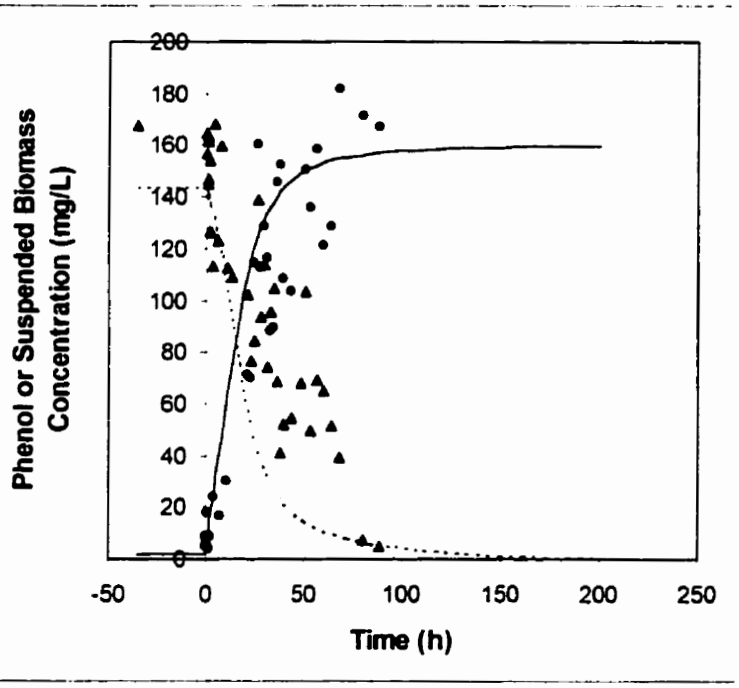

Figure 5.71. Simulation of the bulk phenol concentration (———) and the suspended biomass concentration (- - - - -) for Run 5 assuming that the biofilm was inactive. Luong kinetics determined for unacclimated cultures, adjusted to include suppression of growth during the shock-load, were used. The simulation is plotted with the experimental response of the bulk phenol concentration (•) and the suspended biomass concentration (▲) to an increase in the dilution rate from 0.042 to 0.095 h^{-1} at a feed concentration of 160 mg/L.

Biofilm Parameters, δ and S_f

The simulation of biofilm thickness during Run 1 is shown in Figure 5.72. The model predicted that the biofilm thickness would increase marginally from an extremely thin layer (≈1 μm) and then would be eroded as detachment forces exceeded the growth rate of the biofilm during the rise in the bulk phenol concentration beyond the critical substrate concentration. Practically speaking, such dynamics would be difficult to observe in the ICFBR because the resolution of the biofilm thickness measurement was not narrow enough to distinguish biofilm thickness at this level. Although biofilm thickness was not measured during this run, the biofilm appeared extremely thin and difficult to distinguish under the microscope. No change was observed over the course of the run.

The simulation of the biofilm thickness during Run 8 is shown in Figure 5.73. The model predicted that within 200 hours of the step change the biofilm would be eroded by abrasive forces, from an initial biofilm thickness of approximately 5μm. During Run 8, the concentration in the reactor rapidly

reached 570 mg/L phenol (a feed tank with a concentration of 730 mg/L was used after the step change in dilution rate, but subsequent tanks averaged 506 mg/L) At this concentration, assuming unacclimated Luong kinetics, one would expect that the biomass would be completely inhibited. It is not clear from the biofilm thickness data if this was the case, considering the resolution of the biofilm thickness measurement and the scatter in the data. The dip in the biofilm thickness at the end of the experiment (in Figure 5.73) was not reflected in the EPS measurements or visual observations. A thin biofilm appeared to be forming gradually on a portion of the particles after the step change, suggesting that the biofilm cells had adapted to the high bulk phenol concentration and were growing enough to compensate for detachment forces. The smooth appearance of the biofilm that was forming (see Figures 5.46 and 5 48) also suggested that the rate of growth was very slow; otherwise, protuberances would be expected.

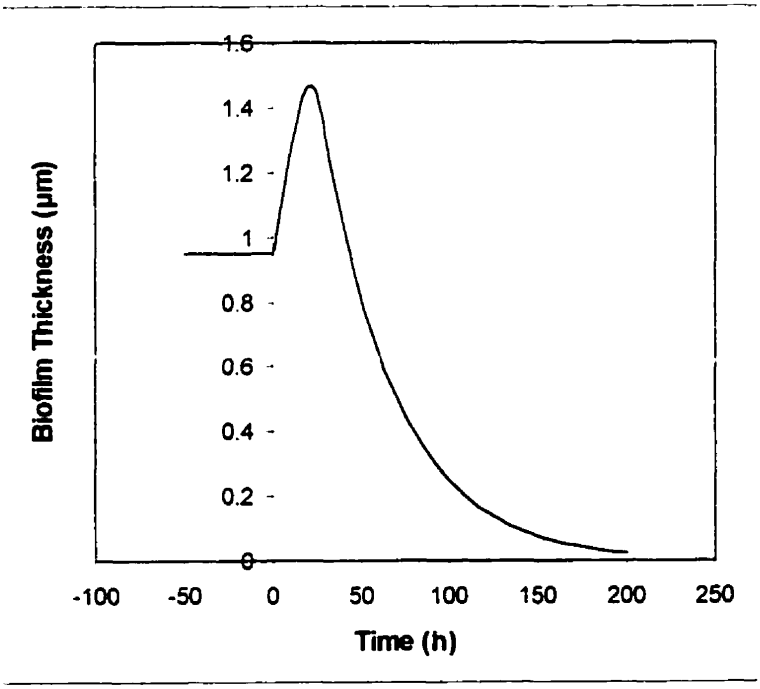

Figure 5.72. Simulation of the biofilm thickness during Run 1 assuming Luong kinetics developed for unacclimated cultures and an adjustment of the growth rate to account for growth-rate suppression during a shock load. The feed concentration was increased from 251 to 296 mg/L and the dilution rate increased from 0.034 to 0.059 h^{-1}.

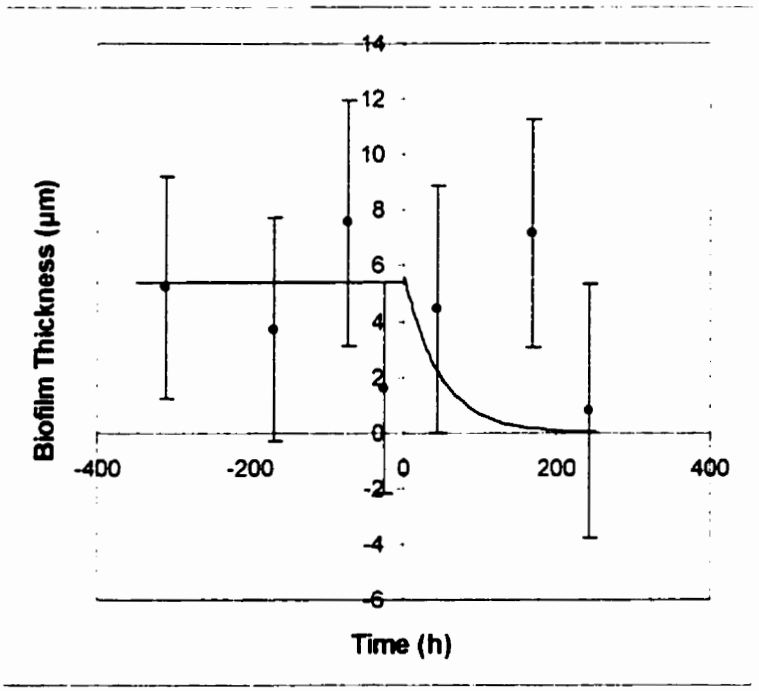

Figure 5.73. Simulation of the biofilm thickness (——) during Run 8 assuming Luong kinetics determined for unacclimated cultures, adjusted to include suppression of growth during the shock load. The simulation is plotted with the experimental response of the biofilm thickness (•) to an increase in the dilution rate from 0.037 to 0.17 h^{-1}. The feed concentration changed from 592 mg/L to an average of 506 mg/L after the step change.

The phenol concentration profile in the biofilm could not be measured; however, values for S_f could be extracted from the model. A plot of the phenol concentration profile during Run 1 is shown in Figure 5.74. The length of each line in the plot is the predicted biofilm thickness at each time listed during the run. The flat profiles indicate that the rate of consumption of phenol was reaction-rate-limited rather than diffusion-limited. This was expected because the biofilm was very thin. The profile corresponds to the fully penetrated biofilm (line 'a') in Figure 2.5.

5.3.2.3 Experimental Verification the Unsteady-state Model with Low-response Experiments

The unsteady-state model with kinetics developed for unacclimated cultures using the model of Luong (1987) adjusted for growth-rate hysteresis was applied to experiments in which there was a low level of response to the step change. The low-response experiments included Runs 2, 3 and 7. In Run 2, the feed

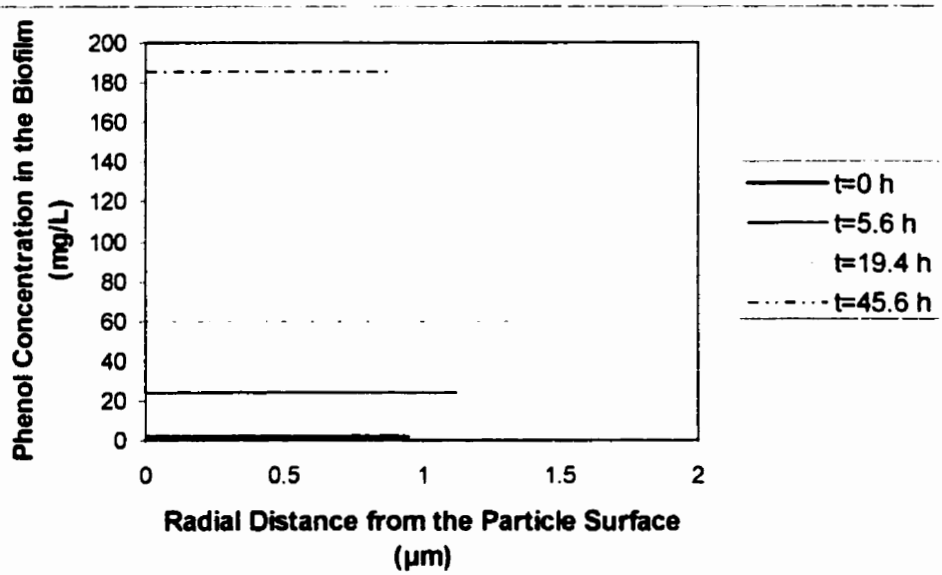

Figure 5.74. Simulated phenol concentration profiles in the biofilm during Run 1 assuming Luong kinetics developed for unacclimated cultures and an adjustment of the growth rate to account for growth-rate suppression during a shock load. The feed concentration was increased from 251 to 296 mg/L and the dilution rate increased from 0.034 to 0.059 h^{-1}

concentration was increased from 180 to 303 mg/L phenol; the dilution rate changed from 0.045 to 0.037 h^{-1}. In Run 3, the dilution rate was shifted from 0.025 up to 0.059 h^{-1} and the feed concentration was 248 mg/L phenol. In Run 7, the feed concentration was increased from 192 to 712 mg/L phenol; the dilution rate shifted slightly from 0.037 to 0.031 h^{-1}. During each of these runs, there was little response in the bulk phenol concentration and the suspended biomass concentration increased.

Bulk Parameters, S_b and X_S

The simulation of Run 2 is shown in Figure 5.75. The model predicted the lack of response in the bulk phenol concentration. Although the steady-state suspended biomass concentration in the experiment was higher than predicted, the model correctly predicted the rate of increase observed in the experiment and the general form, as the suspended biomass concentration reached a new steady state in approximately 50 hours.

The simulation of Run 3, in Figure 5.76 is less accurate. It correctly predicts that the step change would not cause washout, and that the system would recover; however, the transient response in the phenol concentration predicted by the model did not occur. The model also did not accurately predict the new steady-state suspended biomass concentration after the step change.

The simulation of Run 7, in Figure 5.77, predicted a rapid washout of the biomass and rapid increase in the phenol concentration. Experimentally, however, there was no response in the bulk phenol concentration and the suspended biomass concentration rapidly increased to the new-steady state. The only explanation for the difference between the experimental observations and the model predictions is the profusion of wall growth observed in the upper section of the riser. The wall growth consisted of long streamers several millimetres in length. Wall growth has been attributed to enhancing the stability in continuous suspended-cell cultures biodegrading phenol in laboratory-scale reactors in another study, to the extent that the researchers were not able to wash out the culture even at fairly high dilution rates (D>0.5 h^{-1}; μ^*=0.21 h^{-1}; S_o=200 mg/L) (Howell et al., 1972). Thus it is not surprising that wall growth was able to absorb the shock load delivered to the system, even though it covered only a small portion of the inner reactor surface (approximately 10%).

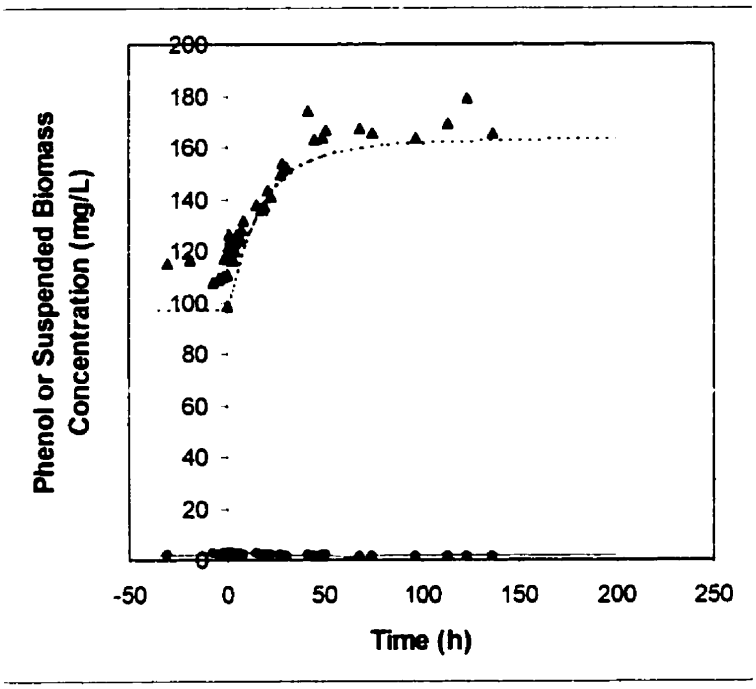

Figure 5.75. Simulation of the bulk phenol concentration (———) and the suspended biomass concentration (- - - - -) for Run 2 using Luong kinetics determined for unacclimated cultures, adjusted to include suppression of growth during the shock-load. The simulation is plotted with the experimental response of the bulk phenol concentration (•) and the suspended biomass concentration (▲) to an increase in the feed concentration from 180 to 270 mg/L phenol and a change in the dilution rate from 0.0451 to 0.0368 h^{-1}.

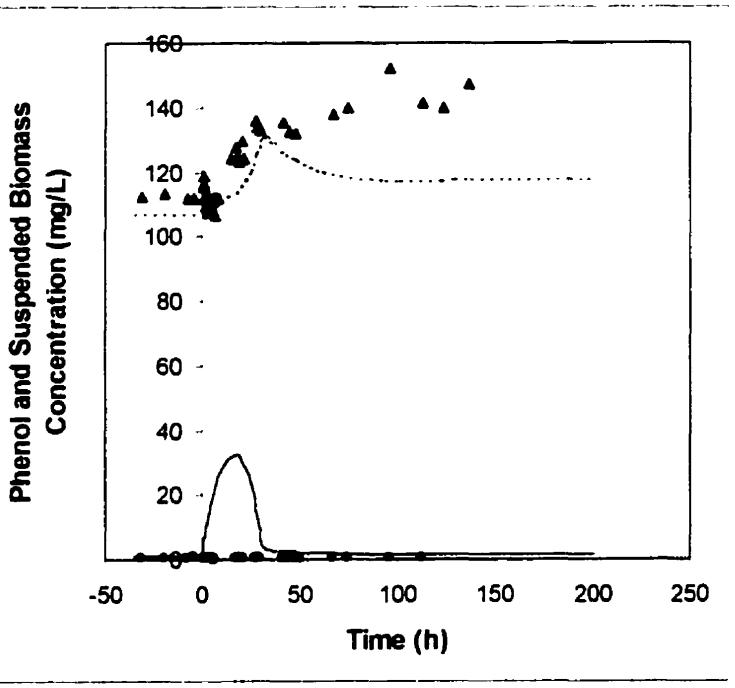

Figure 5.76. Simulation of the bulk phenol concentration (———) and the suspended biomass concentration (- - - - -) for Run 3 using Luong kinetics determined for unacclimated cultures, adjusted to include suppression of growth during the shock-load. The simulation is plotted with the experimental response of the bulk phenol concentration (•) and the suspended biomass concentration (▲) to an increase in the dilution rate from 0.025 to 0.059 h^{-1}.

Biofilm Parameters, δ and S_f

The simulation of biofilm thickness during Run 2 is shown in Figure 5.78. Although the phenol loading after the step change was 40% higher than before, there was little response in the biofilm thickness, likely because there was little change in the phenol concentration in the reactor during the step change. The final steady-state biofilm thickness predicted by the model was slightly lower than the initial steady-state biofilm thickness, as a result of the lower dilution rate.

The simulation of biofilm thickness during Run 3 is shown in Figure 5.79. The model predicted that the biofilm thickness would gradually increase within 150 h by 6 μm to a new steady state value. The predicted response was greater than that of Run 2, because the step change was larger (130% increase in loading). Although there was no biofilm thickness data for this run, the EPS content of the biofilm doubled within 120 h of the step change (in Figure 5.25). The simulation suggests that the biofilm approachs a new steady-state thickness at approximately 150 hours. It is possible that the EPS content of the biofilm had not

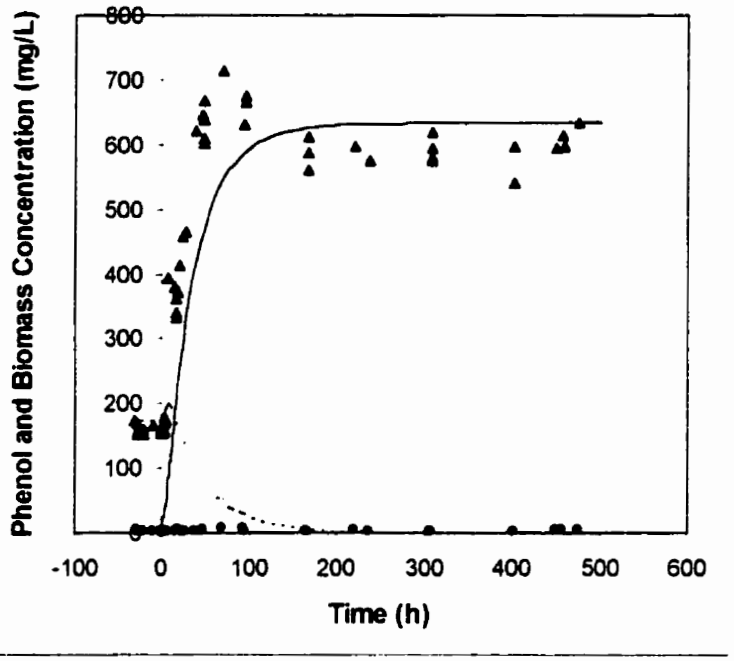

Figure 5.77. Simulation of the bulk phenol concentration (———) and the suspended biomass concentration (- - - - -) for Run 7 using Luong kinetics determined for unacclimated cultures, adjusted to include suppression of growth during the shock-load. The simulation is plotted with the experimental response of the bulk phenol concentration (•) and the suspended biomass concentration (▲) to an increase in the feed concentration from 192 to 633 mg/L in the ICFBR during Run 7. The dilution rate shifted slightly from 0.038 to 0.037 h^{-1}.

reached steady state when the run was terminated.

The formation of protuberances was observed after the step changes in Runs 2 and 3. The model was developed only for smooth, diffusion-only types of biofilms and cannot predict the formation of heterogeneous structures. This limitation is not likely to cause difficulties in the model predictions for the biofilms in Runs 2 and 3, because the biofilms were very thin and the issues of transport phenomena were not as important. This would not have been the case if the biofilms had been thicker.

A plot of the phenol concentration profile in the biofilm during Run 3 is shown in Figure 5.80. The length of each line in the plot is the predicted biofilm thickness at each time listed during the run. The higher phenol concentrations at t=4 h and t=28 h are a result of the transient in the bulk phenol concentration that was predicted by the model (but did not occur during the experiment). As before, the flat profiles indicate that the rate of consumption of phenol was reaction-rate-limited rather than diffusion-limited. The biofilm in this case was also initially very thin. Even after the biofilm grew, as a result of the

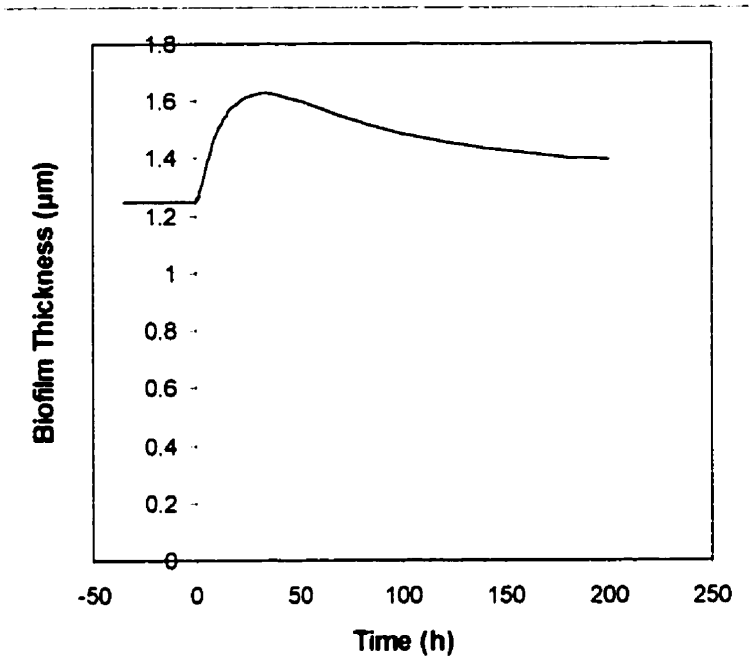

Figure 5.78. Simulation of the biofilm thickness (———) during Run 2 using Luong kinetics determined for unacclimated cultures, adjusted to include suppression of growth during the shock load. The feed concentration was increased 180 to 270 mg/L phenol and the dilution rate changed from 0.0451 to 0.0368 h^{-1}.

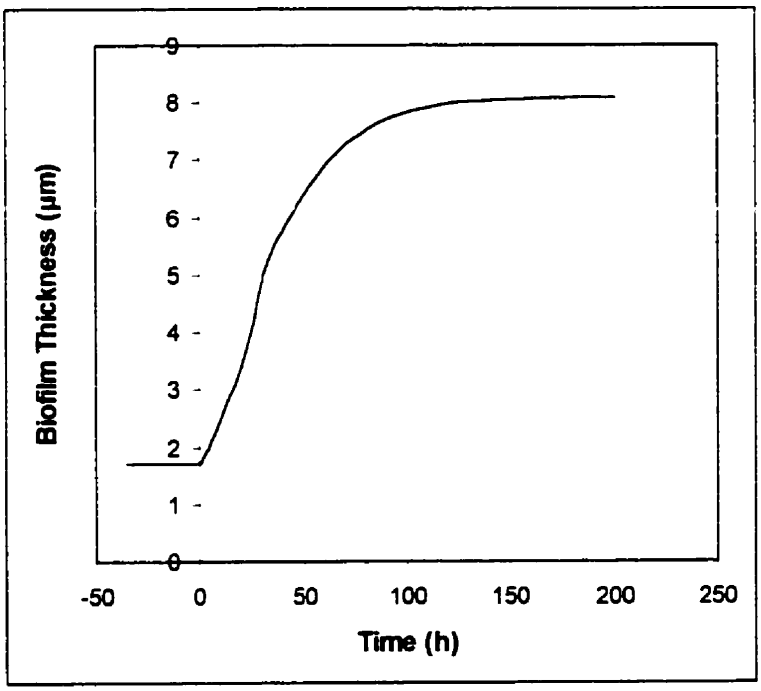

Figure 5.79. Simulation of the biofilm thickness (———) during Run 3 using Luong kinetics determined for unacclimated cultures, adjusted to include suppression of growth during the shock load. The system was subjected to an increase in the dilution rate from 0.025 to 0.059 h^{-1}. The feed concentration was 248 mg/L.

step change, the phenol concentration profile remained fairly flat.

The predicted concentration of phenol at the biofilm surface and in the bulk fluid were similar At t=4 h, when the predicted phenol concentration in the bulk fluid was 16.67 mg/L, the phenol concentration at the biofilm surface was 16.64 mg/L. At t=41.5 h, when the biofilm was thicker, the predicted phenol concentrations in the bulk fluid and at the biofilm surface were 2.40 and 2.27 mg/L. The concentration boundary layer between the bulk fluid and the biofilm surface did not appear to exert a significant influence on the predicted results. This is consistent with Figure 2.5 for the case of a thin biofilm that is fully penetrated. This finding puts into the question the need to include the concentration boundary layer in the model. This question is examined in the next section.

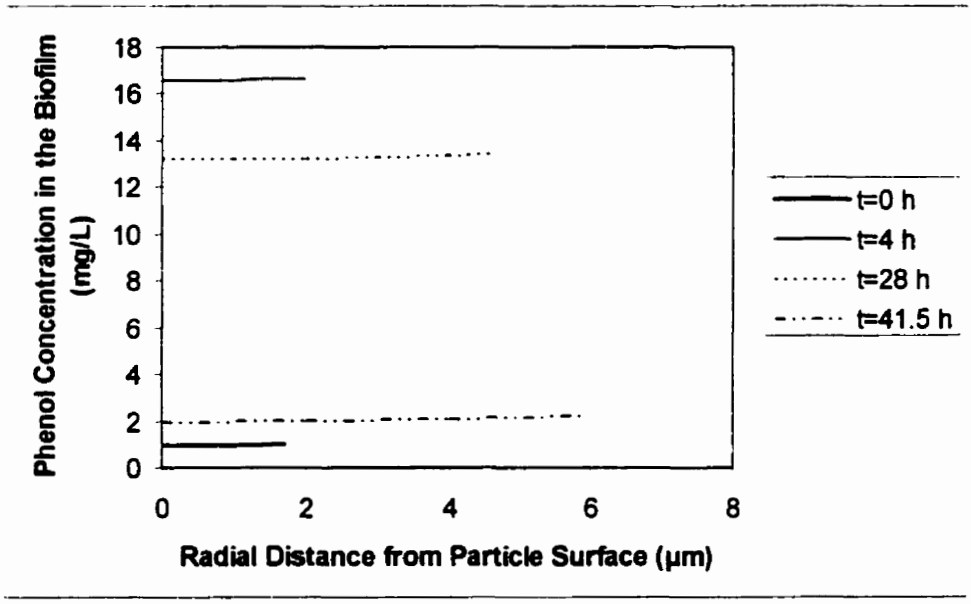

Figure 5.80. Simulated phenol concentration profiles in the biofilm during Run 3 using Luong kinetics determined for unacclimated cultures, adjusted to include suppression of growth during the shock load. The system was subjected to an increase in the dilution rate from 0.025 to 0.059 h^{-1}.

5.3.3 A Re-examination of the Significance of Internal and External Mass Transfer

The predicted phenol concentration profiles within the biofilms were relatively flat, which indicated that internal diffusion was unimportant for the conditions tested. The small predicted differences between the phenol concentration in the bulk fluid and in the biofilm, also indicate that the concentration boundary layer

was unimportant for the conditions tested. The assumptions of internal and external mass transfer complicate the model considerably. Thus, the significance of the roles of internal and external mass transfer need to be re-examined.

External mass transfer through a concentration boundary layer, and internal diffusion are connected through the boundary condition at the interface of the biofilm and the bulk fluid. The importance of both processes depends upon the thickness of the biofilm (see Figure 2.5). External mass transfer has been neglected in some ICFBR models (Shieh, 1980; Stathis, 1980; Mulcahy et al., 1981; Andrews, G.F., 1982; Park et al., 1984a, b; Worden and Donaldson, 1987; Hermanowicz and Cheng, 1990; Coelhoso et al., 1992); however, its relevance depends upon the biofilm thickness and penetration of the substrate. In some modeling studies, the inclusion of external mass transfer resistance has been found to be important (Tang and Fan, 1987; Livingston and Chase, 1989; Tijhuis et al., 1995), with decreases in substrate concentration across the concentration boundary layer of up to 54% reported (Livingston and Chase, 1989).

The biofilms during the runs for which simulations were performed were very thin. The biofilms were much thicker in Run 6 (up to 40 μm), but problems with solids accumulation during the run made it impossible to fit the model to the steady-state data. The range of operating conditions for which experiments were performed did not include steady state conditions above the critical dilution rate (for suspended-cell cultures). It is at higher dilution rates or at low particle concentrations that higher biofilm thicknesses are more likely to occur. To test the importance of internal and external mass transfer for higher biofilm thicknesses, a simulation was performed.

The steady state of a system with a feed concentration of 200 mg/L phenol and a dilution rate of 0.17 h^{-1} was determined using the steady state model. The dilution rate was beyond the critical value of 0.07 h^{-1} at which a comparable suspended-cell culture would wash out. The predicted biofilm thickness was 14 μm. The predicted steady-state conditions in the bulk fluid were a phenol concentration of 2.45 mg/L and a suspended biomass concentration of 104 mg/L. It is interesting that the model predicted that suspended cells would be present, considering the dilution rate. The presence of suspended cells, however, would be expected at lower concentrations that those observed at $D>D^*$, because the suspended cells are produced through the detachment process. The presence of suspended cells under high-dilution rate

conditions has not been reported (or measured) in the literature (Tang et al., 1987; Worden and Donaldson, 1987) and should be investigated.

The effect of a step increase to a dilution rate of 0.25 h^{-1} was simulated. The predicted response of the system is shown in Figure 5.81. The unsteady-state model predicted a small transient in the phenol concentration, and a dip in the suspended biomass concentration, with a recovery to a new steady state within 100 hours. The predicted biofilm thickness increased from 14 to 19.4 μm, as shown in Figure 5.82. The appearance of the predicted phenol concentration profile within the biofilm is very different from before, as shown in Figure 5.83. The parabolic concentration profile for the initial and final steady states in the simulation suggest that under these conditions, diffusion cannot be neglected. The difference between the predicted phenol concentrations in the bulk fluid and the biofilm surface were 2.5 and 2.2 mg/L at the initial steady-state and 3.3 and 2.9 mg/L at the final steady state. While these differences are not large, they represent a 12% difference in concentration. At higher bulk phenol concentrations, possibly during a larger shock-load in which there is a larger phenol transient, the effect of a concentration boundary layer might be more important.

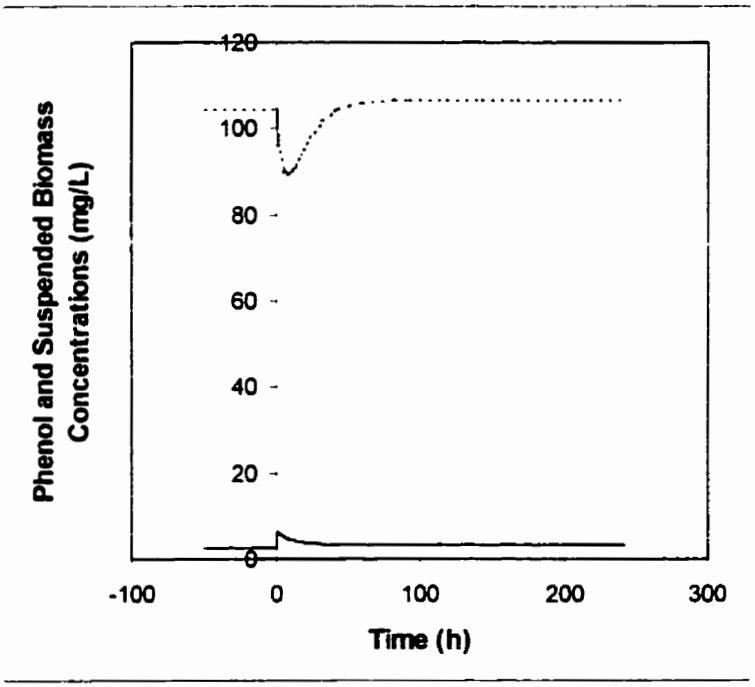

Figure 5.81 Simulation of the response in the phenol concentration (——) and the suspended biomass concentration (- - - -) in the ICFBR to a step change from a dilution rate of 0.17 to 0.25 h^{-1} at a constant feed concentration of 200 mg/L using the parameter set for Run 7 (r_D=0.02 h^{-1}).

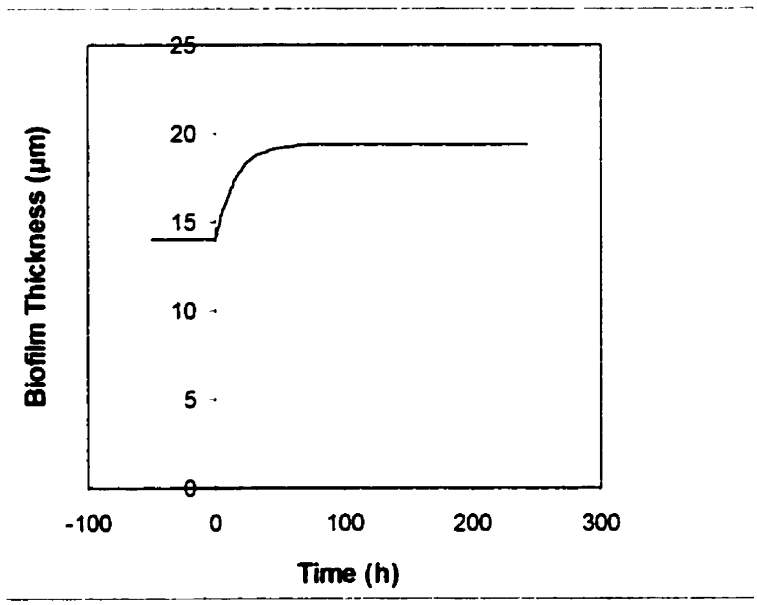

Figure 5.82 Simulation of the response in the biofilm thickness to a step change from a dilution rate of 0.17 to 0.25 h^{-1} at a constant feed concentration of 200 mg/L using the parameter set for Run 7 (r_D=0.02 h^{-1}).

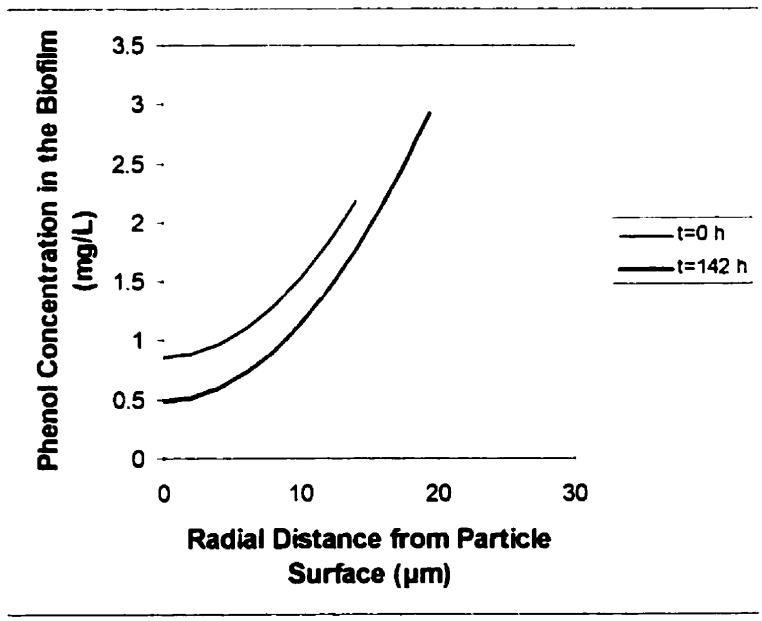

Figure 5.83 Simulation of the phenol concentration profile within the biofilm during a step change from a dilution rate of 0.17 to 0.25 h^{-1} at a constant feed concentration of 200 mg/L using the parameter set for Run 7 (r_D=0.02 h^{-1}).

Both internal and external mass transport processes appear to be a necessary part of the model in cases where the biofilm is moderately thick (≈ 15 μm). Although only thin biofilms were predicted using the unsteady-state model for the conditions tested in the laboratory, thick biofilms were observed during Run 6, which could not be modeled due to experimental difficulties. Internal mass tranport limitations were important in Run 6 because evidence of sloughing was observed for some of the bioparticles. The model predicted that at higher dilution rates, thicker biofilms would be produced. For such biofilms, the concentration profiles indicated that diffusion was important. Thus, the process of diffusion should remain in the model, despite the complexities that arise in solving the model.

The case for external mass transport (and the parameter k_f) is less clear. The difference between the bulk and surface phenol concentrations was only 12%; however at concentrations of approximately 3 mg/L phenol, this difference is probably not very important. Under conditions where there are large transients, this difference may be more significant and may affect the outcome of the success of the model prediction. Thus, the process of external mass transport should remain in the model until its importance can be examined experimentally under more demanding conditions than were tested in this work. The added complexity to the model is relatively minor.

5.3.4 Applications and Limitations of the Unsteady-state Model

Applications

The unsteady-state model was calibrated for a wide range in the types of response possible for such a system. The experiments included low-level response runs in which there was no change in the phenol concentration and washout experiments in which the suspended biomass (but not the bioparticles) was washed out of the system as the phenol concentration rose above inhibitory levels. Thus, the ability of the model to describe a wide variety of responses was tested. Steady-state conditions at dilution rates above the critical dilution rate for suspended-cell cultures were not tested, and should be included in future work along with shock loads in that region of the solution space.

The unsteady-state model was able to simulate the responses of the ICFBRs fairly well. Although it predicted a transient in Run 3 that did not occur, it correctly predicted that the system would reach a new steady state. The model also predicted that during washout experiments the biofilm would be eroded as

detachment exceeded the growth rate. Although this was not confirmed experimentally, the phenomenon under other conditions has been reported (van Benthum et al., 1997).

A key result is that the model could predict the washout of suspended biomass that occurred during two of the shock loads. This has not been demonstrated previously for ICFBRs in the literature. To successfully predict washout, the model required the inclusion of kinetics developed for unacclimated cultures and an adjustment factor that was used to represent growth rate hysteresis. Although others have acknowledged that the kinetic parameters for cultures undergoing a shock load might be different than those calculated from steady-state values (Rittmann et al., 1992), this is the first application of unacclimated kinetics applied to the unsteady-state modeling of shock loads. The adjustment factor that was used to model growth rate hysteresis was a function of the phenol concentration in the reactor as the response to a shock load progressed relative to the preshock steady-state concentration of phenol. The new adjustment factor approach using the same value of k was used for the simulation of every experiment.

The unsteady-state model can be used to predict the four state variables of the system: the bulk phenol and suspended biomass concentrations, the biofilm thickness and the phenol concentration profile within the biofilm. Others have shown results for substrate concentration only (Tang et al., 1987; Worden and Donaldson, 1987), although presumably other variables could have been extracted from the information produced by the models.

Limitations

Although the unsteady-state model was useful in simulating the responses of the ICFBRs to a variety of step changes, its use is limited in a number of ways. Dilution rates above the critical value (for suspended-cell cultures) were not tested and the responses of systems with thicker biofilms were not tested.

The model is currently limited to smooth-types of biofilms. Heterogeneous bioparticles with protuberances were observed as a result of some of the shock-loads, although most of the examples were of systems that contained very low particle concentrations. Before the model could be improved in this respect, more basic information is needed about predictively modeling the detachment rate and understanding the way that detachment and surface loading of substrate interact to determine biofilm structure. The formation of heterogeneous structures may be a way that biofilms behave during transient

conditions (depending of course on abrasive forces). This is an area that is not yet well understood for ICFBR systems.

Information concerning substrate-depleted regions in the biofilm can be extracted from the model output; however, another concern, which is not currently addressed by the model, is oxygen depletion. At 10°C the solubility of oxygen is relatively high and the substrate uptake rates are relatively low; thus, oxygen consumption for the thin biofilms observed during the experiments was not likely to result in oxygen-depleted layers within the biofilm. This is discussed further in Appendix F. At higher temperatures and higher substrate loadings, oxygen depletion within the biofilm could be a more significant concern. Oxygen consumption and diffusion into the biofilm could be added to the kinetics.

Similarly, the model does not include the diffusion of carbon dioxide out of the biofilm. The 'lift-out' phenomenon, in which bioparticles become buoyant and are carried out of the bioreactor, has been attributed to the build-up of carbon dioxide bubbles in the biofilm due to the production rate of carbon dioxide by bacterial metabolism having become greater than its diffusion rate out of the biofilm to the bulk solution (Krouwel and Kossen, 1981; Patoine, 1989). This phenomenon was experienced following a feed tank mix-up after Run 3. It is more likely to be a problem at higher substrate loadings and higher biofilm thicknesses. The production rate of carbon dioxide can be calculated stoichiometrically from the rate of phenol biodegradation (which is known); however, the form of the carbon dioxide is a function of pH. Thus, the formation of hydrogen ions also must be included. The kinetics of phenol degradation are also pH sensitive (Patoine, 1989).

Another problem that was experienced during the experiments was the formation of flocculent solids and the development of granules. Others have reported similar phenomena (Tijhuis et al., 1995; Gjaltema et al., 1997b). The steady-state and unsteady-state models are currently limited to conditions where the suspended solids leave the system at the same rate as the effluent. The model also assumes that the bioparticles do not leave the system. Particularly when flocculent solids develop, particles can become entrained in masses of suspended biomass and may be carried out of the system. Gradual attrition of bioparticles has also been reported in the literature, although the design of the solids separator was different than the ones used in this study (Gjaltema et al., 1997b).

Another limitation of the model is that it was developed using a pure culture. Practically speaking, it should be modified to apply to mixed cultures that would be used in full-scale applications. This would not simply be a matter of altering the kinetics to represent a different group of organisms. A difficulty with mixed-culture ecosystems is the presence of protozoa and other predators of bacteria. Flagellates, which were present as a contaminant of the sand, had a devastating impact on the bacterial population at the beginning of this research. The impact of predation on the functioning and dynamics of an ICFBR cannot be overlooked if mixed cultures are used. Modification of the model may require the inclusion of a separate balance on predators in order to allow the model to reflect the impact of predation and the changing dynamics of the system arising from an overgrowth of predators or death due to levels of phenol that are toxic to the predators but only growth inhibitory to the bacteria.

6 Conclusions and Recommendations

6.1 Conclusions

The research consisted of three main goals:

- to gain a better understanding of the growth and phenol biodegradation kinetics of *P. putida* Q5, particularly at temperatures between 10-25°C,
- to investigate the response of *P. putida* Q5 and that of an ICFBR under shock or variable loading conditions of phenol concentration and dilution rate, and
- to develop a practical process model.

6.1.1 Phenol Biodegradation Kinetics

Phenol Biodegradation with Acclimated Cultures

The phenol biodegradation kinetics of *P. putida* Q5 were evaluated using batch and continuous cultures at 10, 15, 20 and 25°C, and a concentration range of 1 to 640 mg/L phenol. In continuous cultures the dilution rate was varied from 0.031 to 0.23 h^{-1}, depending upon the temperature.

1 The Haldane model was found to describe the relationship between the phenol concentration and the specific growth rate of *P. putida* Q5 quite well; however, the model of Webb (1963) was slightly better at 10 and 25°C and the model of Edwards (1970) was slightly better at 15 and 20°C. Practically speaking, the models were indistinguishable at initial concentrations in batch culture below 200 mg/L phenol at the temperatures studied.

2. The temperature dependence of the specific growth rate, μ_{max}, was found to be described better by the square-root model (Equation 2.30) (Ratkowsky et al., 1982) than the Arrhenius model (Equation 2.24) (Arrhenius, 1908), which is more commonly used in the literature. The saturation constant, K_S, increased with increasing temperature and was best described by the Arrhenius model (Equation 5.1); the temperature characteristic, ΔH^*, was 47.6 kJ/mol, which is within the range reported in the literature (Marr et al., 1963; Knowles et al., 1965; Stevens et al., 1989). The inhibition constant, K_I, was found to increase with increasing temperature, which indicates that the inhibition effect is stronger at the lower temperatures. The square-root model (Equation 5.3) fit the data slightly better than the Arrhenius model. The overall temperature-dependent kinetic equation is expressed as:

$$\mu = \frac{[0.209(T+6.4)]^2 \times S}{S + 1.53\times 10^7 e^{\left(\frac{-5.72\times 10^3}{T+273}\right)} + \frac{S^2}{[0.128(T+91.7)]^2}} \qquad (5.7)$$

where μ is the specific growth rate [h^{-1}] and S is the phenol concentration [mg/L].

The temperature-dependence of the Haldane model for phenol biodegradation has not been reported previously in the literature.

3. The maintenance coefficient, m, was 3-5 times higher in batch cultures (where S is greater than the critical substrate concentration, S^*) than in continuous cultures at 10°C and 25°C. Values of observed yield were also higher in batch cultures than in continuous cultures for a given specific growth rate. The Pirt (1965) definition of the maintenance concept (Equation 2.7) would indicate that the same observed yield, Y_{XS}, would be expected for a given growth rate, assuming that the maintenance coefficient is constant. Thus, the maintenance coefficient cannot be assumed to be constant over a wide range of substrate conditions, and Equation 2.7 should be used with caution when applied to inhibitory substrates; it should probably be used only for cases where the substrate concentration is less than S^*.

4. The yield data varied considerably between experiments; thus, it was not possible to develop a quantitative relationship between temperature and the true growth yield, Y_g, or the maintenance coefficient, m. However, two general conclusions about the trends observed in the parameter estimates can be made. First, Y_g has been reported in the literature to be constant with respect to temperature, the results of this study do not disagree. Secondly, the maintenance coefficient determined in the present study was found to increase with temperature in both batch and continuous cultures; this trend is consistent with prior work (Fieschko and Humphrey, 1983; Heijnen and Roels, 1981; Mainzer and Hempfling, 1976).

Phenol Biodegradation with Unacclimated Cultures

Batch kinetic experiments were performed at 10°C using cells taken from the ICFBR and initial phenol concentrations of 25 to 315 mg/L.

5. The phenol biodegradation kinetics of acclimated cultures differed from the kinetics of cultures that have been exposed to the low levels of phenol found in ICFBRs at normal steady-state operating conditions (at 10°C in batch cultures). The critical specific growth rates (the maximum observable specific growth rates) of the two cultures were different (μ^*=0.09 h^{-1} for acclimated cultures and μ^*=0.07 h^{-1} for unacclimated cultures) and the specific growth rate decreased much more quickly at higher phenol concentrations (S>200 mg/L) for the unacclimated cultures. The Haldane model did not describe the data at the higher phenol concentrations very well. A simplified version of the model of Luong (1987) described the data better (r^2=0.78 compared to r^2=0.69 for the Haldane (1930) model). The resulting expression for unacclimated phenol biodegradation kinetics at 10°C was:

$$\mu = \frac{0.0876 \times S(1 - \frac{S}{401})}{4.38 + S} \qquad \textbf{(5.8)}$$

where S is the phenol concentration [mg/L] and μ is the specific growth rate [h^{-1}]

6.1.2 ICFBR Performance

Two ICFBRs were operated at a variety of steady-state conditions with feed concentrations ranging from 180 to 590 mg/L phenol and dilution rates ranging from 0.025 to 0.069 h^{-1}, resulting in organic loadings of 0.15 to 0.50 g phenol/L·d. The phenol concentrations in the feed better represented industrial levels than those used previously for shock-loading experiments in ICFBRs (Tang et al., 1987; Worden and Donaldson, 1987). Periods from 31 to 80 days were allowed for the biofilm development under steady-state conditions. Steady-state biofilm thicknesses ranged from 3 to 35 μm, depending upon the organic loading and particle concentration (11-23 g/L). After steady state was reached, the systems were perturbed with step changes in either the feed concentration or the feed rate. The resulting increases in organic loading ranged from 40 to 500% of the initial steady-state values. Unsteady-state response of ICFBR systems with psychrotrophic organisms at low temperatures has not been investigated previously.

Bioparticle Characteristics and Development

6. High levels of abrasion can hinder biofilm growth, even at moderate gas flow rates (u_{Gr}=0.9 cm/s) and relatively low particle concentrations (18-22 g/L). This is particularly true if the temperature is low (eg. 10°C), resulting in low growth rates, and if the dilution rate is below μ^* because there is increased competition for substrate by suspended cells. Particle size did not appear to be a factor in biofilm development; this contrasts with the findings of Gjaltema et al. (1997b) who concluded that biofilms formed preferentially on smaller particles due to the lower impact upon colliding with other particles.
7. Approximately 5-10% of the sand particles did not develop a biofilm, even when most particles in the ICFBR were covered with a fairly thick biofilm (≈35 μm). The uncovered particles were markedly different in appearance from those that developed biofilms: they were typically smooth, whereas the biofilm-coated particles were irregular and rounded. Thus, it can be tentatively concluded that a fraction of the sand remained uncovered because of lack of surface roughness, although surface chemistry effects cannot be ruled out. This finding is consistent with other reports (Gjaltema et al., 1997a).
8. The extracellular polymeric substances (EPS) in the biofilm accounted for only 3-5% of the biofilm dry weight. This contrasts with other studies in which the EPS was reported to be a significant portion of the biofilm (up to 90% as TOC (Bakke et al., 1984)).

Response of the ICFBRs to Shock Loading

9. During the various shock-load experiments conducted, two types of responses were noted: low- and high-level responses. During low-level responses, there was no response in the bulk phenol concentration and the suspended biomass concentration increased to a new steady state value. During high-level responses, the phenol concentration rapidly increased to levels approaching the feed concentration and the suspended biomass washed out; however, the bioparticles were retained in the system. The experimental work shows clearly that washout of suspended biomass and leakage of phenol leading to system failure is possible in an ICFBR system. This has not been previously demonstrated in the literature. Factors leading to system failure include:

- thin biofilms which may arise from an imbalance in detachment forces and substrate surface loading,
- competition with suspended cells for substrate,
- high feed concentrations which may lead to high concentration transients, and
- relatively large changes in organic loading rate (200-500%).

Even though bioparticles are retained during a system failure, the system will not necessarily recover, particularly if the biofilms are thin and the reactor phenol concentration enters into a strongly inhibitory regime (>200 mg/L).

10. In laboratory-scale reactors, where the reactor surface-area-to-volume ratio is low, wall growth can significantly alter the response of the system to shock loads, and must therefore be avoided if the results are to be meaningful.
11. Spectrophotometric analysis of the fermentation broth during the shock loading experiments indicated that compounds other than phenol were present. The observed peaks were suggestive of intermediate metabolites from the *ortho* pathway for phenol biodegradation, which is possessed by *P. putida* Q5. Another compound, possibly a yellow-coloured pigment, was also noted. GC-MS analysis confirmed that at steady-state conditions, phenol is the only compound present.
12. Air stripping was calculated to be a minor removal mechanism of phenol, even when phenol concentrations were above 100 mg/L during process failure.

6.1.3 Unsteady-state ICFBR Model

A unique unsteady-state process model was developed and implemented. The model included the contribution of suspended cells to the removal of phenol in the reactor, and included terms for diffusions both within the biofilm and in the diffusion boundary layer surrounding each bioparticle as well as the process of detachment. The model could represent a wide variety of conditions (described above) and a wide range of responses – from no response in the reactor phenol concentration to system failure. Unlike other models, the model could also simulate the response of all four process variables: the bulk phenol concentration, the suspended biomass concentration, the concentration profile of the substrate in the biofilm

and the biofilm thickness. The solution of the model was simple enough that the model could be used for estimation and nonlinear control in the future.

Conclusions Arising from the Unsteady-state Model

13. The use of kinetics determined using unacclimated cultures was needed to model the response of the system. The use of kinetics determined using acclimated cultures resulted in simulations that incorrectly predicted the recovery of the system to a severe shock load (dilution rate shift from 0.037 to 0.17 h^{-1}).

14. Growth rate hysteresis was another key concept that was required in the model to represent the sensitivity of the system to transient conditions during a shock load. An adjusting factor was expressed as a suppression of cell-growth that was proportional to the difference between the bulk phenol concentration and the steady-state phenol concentration to which the cells had been acclimated. Thus, the growth rate of the suspended cells was expressed as follows:

$$\mu_b(t) = k(S_b(t) - S_b(0))\mu_{b,b}(t) \qquad \textbf{(5.16)}$$

where the bulk concentration of phenol at time t, $S_b(t)$, and at the initial steady state value, $S_b(0)$, are expressed in mg/cm^3 and the specific growth rate corresponding to $S_b(t)$ assuming balanced growth, $\mu_{b,b}$, is expressed in h^{-1}. The specific growth rate within the biofilm may be expressed similarly.

$$\mu_f(r,t) = k(S_f(r,t) - S_f(r,0))\mu_{f,b}(r,t) \qquad \textbf{(5.17)}$$

The addition of the adjustment factor to account for growth rate hysteresis enabled the model to correctly simulate system failure (ie. washout of the suspended biomass and breakthrough in the phenol concentration) for a moderate shock load (dilution rate shift from 0.034 to 0.059 h^{-1} and a feed concentration increase from 251 to 296 mg/L phenol). Such system failures have not been previously demonstrated for ICFBRs.

15. Simulated phenol concentrations within the biofilm confirmed that for thin biofilms (such as the ones that were observed during a number of the experiments performed), internal and external mass transfer resistances were not significant. However, simulations of concentration profiles for thicker biofilms confirmed that under operating conditions that were outside the ones verified experimentally, internal and external mass transfer processes are significant and should be included in the model.

6.2 Recommendations

Biofilm Development

The process of developing biofilm-coated particles in an ICFBR reactor that is fed toxic or inhibitory compounds is an area that needs further work. With the techniques used in this research and others, it is possible to operate for long periods of time (eg. 50 days) without developing full coverage of the carrier particles, particularly if the initial carrier concentration is high. The high dilution rate approach suggested by Tijhuis et al. (1992a) may not be appropriate if the concentration of phenol in the feed stream is significantly above the critical substrate concentration. In practice, a reactor cannot operate for any period of time at the conditions that were noted in Runs 5 and 8 (ie. at dilution rates above μ^* during which the phenol concentration in the reactor approached the feed concentration).

Parameters of importance would include: the suspended cell concentration (needed for primary biofilm formation but provides competition with biofilm cells for substrate), the carrier concentration, the substrate concentration in the reactor, and the reactor hydrodynamics. Startup regimes might include batch, fed batch or sequencing batch steps to allow for high suspended-cell concentrations and high phenol concentrations, although to do so in an ICFBR reactor might require adjustments to the reactor. Another approach might involve the gradual addition of bare carrier particles in order to minimize abrasion so that biofilm development might occur at a faster rate. Once the bioparticles are partially covered, the detachment rate decreases (Gjaltema et al., 1997c). The steady-state model could be used to predict steady-state operating conditions that would be conducive to the development of thicker biofilms than were observed during this study.

Kinetics

Preliminary results indicated that suspended cells that are acclimated to very low concentrations of phenol are more inhibited by shock loads of phenol than are suspended cells that are acclimated to high concentrations. These results have important ramifications for our understanding of the dynamic response of systems to shock loads of toxic or inhibitory feed streams. Much of the kinetics research reported in the literature has been done with acclimated cells. It is an area that should be investigated further.

Biofilm Structure

The structure of biofilms grown in flow cells and annular reactors has been the subject of a number of studies using novel experimental techniques, including the use of microelectrodes, micro-optrodes for oxygen, confocal microscopy and microsectioning (de Beer and Muyzer, 1995). The results will likely change the way we model and work with biofilms of these types. To date, there is very little understanding of the microstructure of biofilms that are subject to the level of abrasion found in ICFBRs. For example, the smooth biofilms that were observed during this research may have had a complex network of pores in which convective transport was occuring, or the biofilms may have been of the diffusion-only type. Investigations of this type would provide a fundamental understanding of mass transfer effects and perhaps the 'lift out' phenomenon.

Intermediate Metabolites

Despite the large volume of work that has been done in the last 20 years to understand phenol biodegradation kinetics, there is very little information about the excretion of substances into the medium during the dynamic response of systems to shock loads. It would be useful to identify these compounds (some are likely intermediate metabolites), and to determine the extent to which these compounds have an effect on the dynamic response of systems. For example, these compounds may repress certain metabolic pathways.

Lift-out Phenomenon

Lift-out of bioparticles has been reported previously for both lab-scale (Patoine, 1989) and full-scale (Tijhuis et al., 1996) ICFBRs. The model could be modified to include the formation of carbon dioxide gas bubbles so that potential problems with lift-out could be predicted.

Predators / Microbial Ecosystems

During the initial part of this research, problems were experienced with a flagellate which was a contaminant in the sand used as the carrier. The ability of the flagellate to decimate the population of bacteria in the reactor highlighted the importance of investigating mixed culture/complex ecosystem types of biofilm reactors (rather than simply pure cultures) and perhaps eventually incorporating the findings into models. Nevertheless, pure culture studies are still valuable because they enable important features of the response of systems to be interpreted.

NOMENCLATURE

a	interfacial area per unit liquid volume, [m^{-1}]
a'	curvature factor in Equation 5.11, [mg/cm^5]
a_S	interfacial area per liquid volume of the biofilm, [m^{-1}]
A	Arrhenius frequency factor, [h^{-1}]
A_{bp}	surface area of the bioparticle, [cm^2]
A_E	enzyme activity, units not listed in original paper
A_{EM}	maximum enzyme activity, units not listed in original paper
A_I	Arrhenius frequency factor related to K_I, [mg/L]
A_S	Arrhenius frequency factor related to K_S, [mg/L]
b	regression coefficient in square-root temperature relationships, [$K^{-1}h^{-1/2}$]
b'	constant in Equation 5.11, [mg/cm^4]
b_I	regression coefficient in square-root relationship for K_I, [$K^{-1}(mg/L)^{-1/2}$]
b_S	regression coefficient in square-root relationship for K_S, [$K^{-1}(mg/L)^{-1/2}$]
Bo	Bond number, $Bo=gd_c^2\rho_L\,\sigma$
B_1, B_2, B_3	dimensionless constants in Equation 2.64
c	regression coefficient in square-root temperature relationships, [K^{-1}]
c_p	heat capacity, [J/gK]
c'	constant in Equation 5.11, [mg/cm^3]
C	concentration of component C in a biofilm, [g/L]
C_{aq}	concentration of component C in the aqueous phase, [mg/L]
C_O	dissolved oxygen concentration, [g/L]
C_O^*	equilibrium concentration of dissolved oxygen in water, [g/L]
C_{Ob}	bulk dissolved oxygen concentration, [g/L]
C_{OS}	concentration of dissolved oxygen at biofilm surface, [g/L]
C_p	particle concentration in the reactor, [g/L]
C_{po}	particle concentration over the sparger, [g/L]

d_{bp}	bioparticle ferret diameter, [cm]
d_c	diameter of column, [m]
d_d	internal diameter of the downcomer section in the ICFBR, [cm]
d_p	bare particle diameter, [cm]
d_{ps}	specific surface diameter, [m^2]
d_p	screen diameter, [cm]
d_p^*	equivolume sphere diameter, [m^2]
d_r	internal diameter of the riser section in the ICFBR, [cm]
d_{top}	internal diameter of the top of the riser section in the ICFBR, [cm]
D	dilution rate, $D = Q / V_L$, [h^{-1}]
D_e	effective diffusivity in the biofilm, [cm^2/s]
D_e/D_w	relative effective diffusivity in the biofilm (as compared to that of the component in water)
$D_{i,f}$	diffusivity in biofilm of component i, [cm^2/s]
$D_{i,w}$	diffusivity in water of component i, [cm^2/s]
D_L	diffusivity in the liquid, [cm^2/s]
$D_{O,w}$	diffusivity of oxygen in water, [cm^2/s]
$D_{S,f}$	diffusivity of substrate in the biofilm, [cm^2/s]
$D_{S,w}$	diffusivity of the substrate in water, [cm^2/s]
DBSM	dilute basal salts medium
$[E_T]$	total enzyme concentration, [mol/L]
f	fraction of active bacteria in the biofilm
f_{DW}	ratio of dry weight to wet cell weight, [g DW/g wet weight]
f_I	inactive fraction in the biofilm
f_{IB}	fraction of inactive bacteria in the biofilm
f_1, f_2, f_3, f_4, f_5	function expressions for the unsteady-state model (Equations 5.12-5.15)
F_o	lumped term in Appendix G, $F_o = (k \rho c_p)(t / r_f^2)$
Fr	Froude number, $Fr = u_G / (g d_c)^{1/2}$

g	gravitational acceleration [m/s^2]
Ga	Galileo number, $Ga = g d_c^3 \rho_L^2 \mu_L^{-2}$
h	Plank's constant, [J/s]
h_c	height of column, [m]
H	Henry's Law constant, [atm·L/mol]
ΔH^*	Arrhenius temperature characteristic, [J/mol]
ΔH_I^*	Arrhenius temperature characteristic relating to K_I, [J/mol]
ΔH_S^*	Arrhenius temperature characteristic relating to K_S, [J/mol]
ΔH^o	enthalpy of activation, [J/mol]
J	flux of phenol, [g/cm^2.h]
k	heat transfer coefficient, [W/mK]
k_1, k_2, k_3, k_4	empirical constants with dimensions consistent with equations in which they are found
k_d	endogenous decay coefficient, [h^{-1}]
k_l	liquid-biofilm mass transfer coefficient for oxygen, [m/h]
k_P	growth associated product formation coefficient, [g product/g biomass]
k_P'	non-growth associated product formation coefficient, [g product/g biomass.h]
k_S	liquid-biofilm mass transfer coefficient for substrate, [cm/s]
K_1, K_2, K_3, K_4	empirical constants with dimensions consistent with equations in which they are found
K_b	Boltzmann's constant, [J/molecule.K]
K_I	Haldane inhibition constant, [g/L]
K_La	overall gas-liquid mass transfer coefficient, [h^{-1}]
K_S	Monod constant, [g/L]
L	thickness of liquid-to-biofilm diffusion boundary layer, [cm]
L_f	biofilm thickness, [cm]
m	substrate maintenance coefficient, [g/g·h]
m_{bf}	mass of biofilm on a single particle, [g]

m_p	mass of one particle, [g]
M_p	mass of particles in system, [g]
M_W	molar mass, [g/mol]
M_1, M_2, M_3	masses in biofilm dry weight procedure, [g]
n_{bp}	number of bioparticles in a sample for image analysis
n_p	number of bare particles in a reference sample
N_{AB}	number of active bacteria
N_B	number of bacteria
N_p	total number of particles in the reactor at any given time
N_{pi}	total number of particles added to the reactor initially
N_{ps}	number of particles in a sample
P	mass of sand added to an ICFBR reactor, [g]
P_T	total pressure in ICFBR, [atm]
q_P	specific rate of product formation, [g/h]
q_S	specific rate of substrate uptake, [g/h]
Q	feed rate, [L/h]
Q_A	air sparging rate, [L/d]
r	radial position within biofilm, [cm]
r_d	rate of endogenous decay, [g/L·h]
r_D	specific rate of detachment, [h^{-1}]
r_f	radial position at biofilm surface, [cm]
r_m	rate of cell maintenance, [g/L·h]
r_p	radial position at particle surface, [cm]
r_P	rate of product formation, [g/L·h]
r_S	rate of substrate uptake, [g/L·h]
r_{St}	rate of stripping, [mol/L·d]
r_X	rate of cell growth, [g/L·h]
R	gas constant, [J/mol·K]

R_{ad}	rate of adhesion of cells to biofilm, [g DW/L·h]
R_{det}	rate of biofilm detachment, [g DW/L·h]
Re	Reynolds number, $Re = du\rho_L / \mu_L$
Re_p	particle Reynolds number, $Re_p = \rho d_p u / \mu_L$
Re_w	Reynolds number at the wall, $Re_w = d_c u \rho_L / \mu_L$
R_S	reaction term for consumption of substrate, [g/L·h]
S	substrate concentration, [g/L]
S^*	substrate concentration when $\mu = \mu^*$, [g/L]
S_b	substrate concentration in the bulk liquid, [g/L]
$S_{b,m}$	substrate concentration in the bulk liquid, [mol/L]
$\dot{S}$	deviation variable, effluent substrate concentration, $\dot{S} = S - S_o$, [g/L]
Sc	Schmidt number, $Sc = \nu / D_L$
S_f	substrate concentration within biofilm, [g/L]
Sh	Sherwood number, $Sh = k_L d_p / D_L$
S_I	bacteriostatic substrate concentration, [g/L]
S_o	substrate concentration in the feed, [g/L]
S_s	substrate concentration at biofilm surface, [g/L]
S_{ss}	steady-state phenol concentration, [g/L]
S_w	specific surface area, [cm^2/g]
ΔS°	entropy of activation, [J/mol]
ΔS_H°	entropy of activation corresponding to high-temperature enzyme inactivation, [J/mol]
ΔS_L°	entropy of activation corresponding to low-temperature enzyme inactivation, [J/mol]
t	time, [h]
$\dot{t}$	characteristic time, $\dot{t} = t / \tau$
$t_{0.1}$	Student's t statistic with a tail area probability of 10%
T	temperature, [K]

$T_{0.5H}$	temperature at which controlling enzyme is half active due to high temperature inactivation, [K]
$T_{0.5L}$	temperature at which controlling enzyme is half active due to low temperature inactivation, [K]
T_i	initial temperature, [°C]
T_{max}	maximum temperature for growth, [K]
T_{min}	minimum temperature for growth, [K]
T_o	characteristic temperature, [°C]
T_{oI}	characteristic temperature relating to K_I, in the square-root model [°C]
T_{oS}	characteristic temperature relating to K_S, in the square-root model [°C]
T_{opt}	optimum temperature for growth, [K]
T_S	surface temperature, [K]
T'	effective temperature, [K]
ΔT	change in temperature, [K]
u	superficial velocity of the fluid, [m/s]
u_G	gas superficial velocity, [m/s]
$u_{G,r}$	gas superficial velocity in the riser section, [m/s]
u_p	hindered settling velocity, [m/s]
u_t	terminal settling velocity for a particle in stagnant fluid, [m/s]
u'	average turbulence intensity, [m/s]
u^*	root mean squared velocity, [m/s]
V	volume of sparged fluid, [L]
V_{bp}	volume of a bioparticle, [cm^3]
V_{cell}	volume of one cell, [cm^3]
V_L	volume of liquid in the reactor, [L]
V_M	molar volume of a substance at normal boiling point, [cm^3/mol]
V_R	reactor liquid volume, [L]
V_s	sample volume, [L]

X	concentration of viable cells, [g/L]
X_{DW}	biofilm concentration on a sand basis, [g DW/g sand]
X_f	biofilm biomass concentration in reactor, [g DW/L]
X_s	suspended biomass concentration in the reactor, [g DW/L]
X_{s0}	suspended biomass concentration in the feed stream, [g DW/L]
Y_g	true growth yield coefficient, [g DW/ g substrate]
Y_{PS}	product yield coefficient based on substrate consumed, [g product/ g substrate]
Y_{XS}	observed growth yield coefficient, [g DW/ g substrate]
Y_{XO}	growth yield coefficient on oxygen, [g DW/ g oxygen]

Greek symbols

α	time constant, [h^{-2}]
δ	biofilm thickness, [cm]
ε	porosity of expanded bed
ε	specific energy dissipation, [m^2/s^3]
ε_G	gas phase holdup
$\varepsilon_{G,d}$	gas phase holdup in the downcomer
$\varepsilon_{G,r}$	gas phase holdup in the riser
ε_L	liquid phase holdup
ε_S	solid phase holdup
$\varepsilon(t)$	perturbation variable
η_e	effectiveness factor
κ	transmission coefficient
Φ	sphericity factor
Φ_c	Carman's surface factor ($\Phi_c = 6\,\rho_p S_w d_p$)
Φ_S	solids fraction in the suspension
θ_h	hydraulic retention time, [h]

θ	lumped term variable in the unsteady-state model defined in Equation A-35
μ	specific growth rate, [h^{-1}]
$\bar{\mu}$	specific growth rate – deviation variable, [h^{-1}]
μ^*	maximum observable specific growth rate, [h^{-1}]
μ_b	specific growth rate in bulk liquid, [h^{-1}]
μ_f	specific growth rate in the biofilm (at a given radial distance), [h^{-1}]
μ_L	viscosity of a liquid, [cP]
μ_m	Monod maximum specific growth rate, [h^{-1}]
μ_{max}	Haldane maximum specific growth rate, [h^{-1}]
μ_S	predicted specific growth rate at steady state, [h^{-1}]
μ_W	viscosity of water, [mPa]
ν	kinematic viscosity, $\nu = \mu_L \rho$, [$g/cm^2 \cdot s$]
ρ_{bf}	wet density of biofilm, [g/cm^3 wet biofilm]
ρ_{cell}	density of a cell, [g/cm^3]
ρ_f	biofilm dry density, [g DW/cm^3 wet volume]
ρ_L	density of a liquid, [g/cm^3]
ρ_p	particle density, [g/cm^3]
σ	surface tension (in K_La correlations), [g/s^2]
τ, τ_l	time constant (depending on context), [h]
τ	shear stress, [Pa]
τ_W	shear stress at the wall, [Pa]

REFERENCES

Adair, C., D C. Kilsby and P. T. Whittal (1989) Comparison of the Schoolfield (non-linear Arrhenius) model and the square root model for predicting bacterial growth in foods. Food Microbiol. 6, 7-18.

Aiba, S., S. Nagai, Y. Nishizawa and M. Onodera (1967) Energetic and nucleic analyses of a chemostatic culture of *Azotobacter vinelandii*. J. Gen. Appl. Microbiol. 13, 73-83.

Aiba, S., M. Shoda and M. Nagalani (1968) Kinetics of product inhibition in alcohol fermentation. Biotechnol. Bioeng. 10, 845-864.

Allsop, P. J. (1989) The Dynamics of Aerobic Phenol Degradation. Ph.D. Thesis, University of Waterloo, Waterloo, ON.

Allsop, P. J., Y. Chisti, M. Moo-Young and G. R. Sullivan (1993) Dynamics of phenol degradation by *Pseudomonas putida*. Biotechnol. Bioeng. 41, 572-580.

Andrews, G. F. (1982) Fluidized-bed fermenters: A steady-state analysis. Biotechnol. Bioeng. 24, 2013-2030.

Andrews, J. F. (1968) A mathematical model for the continuous culture of microorganisms utilizing inhibitory substrates. Biotechnol. Bioeng. 10, 707-723.

Applegate, D. H. and J. D. Bryers (1991) Effects of carbon and oxygen limitations and calcium concentrations on biofilm removal processes. Biotechnol. Bioeng. 37, 17-25.

Arrhenius, S. (1908) Immunochemie. Ergebn. Physiol. 7, 480-551.

Arters, D. C. and L.-S. Fan (1986) Solid-liquid mass transfer in a gas-liquid-solid fluidized bed. Chem. Eng. Sci. 41, 107-115.

Arvin, E. and P. Harremoës (1990) Concepts and models for biofilm reactor performance. Wat. Sci. Technol. 22, 171-192.

Arvin, E., B. K. Jensen and A. T. Gundersen (1991) Biodegradation kinetics of phenols in an aerobic biofilm at low concentration. Wat. Sci. Technol. 23, 1375.

Baier, R. E. (1975) Applied chemistry at protein interfaces. In Applied Chemistry at Protein Interfaces, R. E. Baier, ed., pp. 59-104, American Chemical Society, Washington, DC.

Baier, R. E. (1980) Substrata influences on adhesion of microorganisms and their resultant new surface properties. In Adsorption of Microorganisms to Surfaces, G. Bitton and K. C. Marshall, ed., pp. 1-25, John Wiley & Sons, New York.

Baier, R. E. and L. Weiss (1975) Demonstrations of the involvement of adsorbed proteins in cell adhesion and cell growth on solid surfaces. In Applied Chemistry at Protein Interfaces, Vol 145, R. E. Baier, ed., pp. 300-307, American Chemical Society, Washington, DC.

Bajpai, P. and A. Margaritis (1987) The effect of temperature and pH on ethanol production by free and immobilized cells of *Kluyveromyces marxianus* grown on Jerusalem artichoke extract. Biotechnol. Bioeng. 30, 306-313.

Bakke, R. (1983) Dynamics of Biofilm Processes: Substrate Load Variations. Masters Thesis, Montana State University, Bozeman, MT.

Bakke, R., M. G. Trulear, J. A. Robinson and W. G. Characklis (1984) Activity of *Pseudomonas aeruginosa* in biofilms: Steady state. Biotechnol. Bioeng. 26, 1418-1424.

Begovich, J. M. and J. S. Watson (1978) Hydrodynamic characteristics of three-phase fluidized beds. In Fluidization, J. F. Davidson and D. L. Keairns, ed., p. 190, Cambridge University Press, Cambridge.

Bello, R. A., C. W. Robinson and M. Moo-Young (1985) Gas holdup and overall volumetric oxygen transfer coefficient in airlift contactors. Biotechnol. Bioeng. 27, 369-381

Beltrame, P., P. L. Beltrame and P. Carniti (1984) Influence of feed concentration on the kinetics of biodegradation of phenol in a continuous stirred reactor. Wat. Res. 18, 403-407.

Benefield, L. and F. Molz (1983) A kinetic model for the activated sludge process which considers diffusion and reaction in the microbial floc. Biotechnol. Bioeng. 25, 2591-2615.

Benefield, L. and F. Molz (1985) Mathematical simulation of a biofilm process. Biotechnol. Bioeng. 27, 921-931.

Beyenal, H., S. Seker, A. Tanyola‡ and B. Salih (1997) Diffusion coefficients of phenol and oxygen in a biofilm of *Pseudomonas putida*. AIChE J. 43, 243-250.

Bird, R. B., W. E. Stewart and E. N. Lightfoot (1960) Transport Phenomena, p. 593, John Wiley & Sons, New York.

Bishop, P. L., J. T. Gibbs and B. E. Cunningham (1997) Relationship between concentration and hydrodynamic boundary layers over biofilms. Environ. Technol. 18, 375-386.

Bishop, P. L., T. C. Zhang and Y.-C. Fu (1995) Effects of biofilm structure, microbial distributions and mass transport on biodegradation processes. Wat. Sci. Technol. 31, 143-152.

Blackwell, L. G. (1971) A Theoretical and Experimental Evaluation of the Transient Response of the Activated Sludge process. PhD Thesis, Clemson University, Clemson, SC.

Box, G. E. P., W. G. Hunter and J. S. Hunter (1978) Statistics for Experimenters: An Introduction to Design, Data Analysis, and Model Building, John Wiley & Sons, Toronto.

Brocklehurst, T. F. and B. M. Lund (1981) Properties of Pseudomonads causing spoilage of vegetables stored at low temperature. J. Appl. Bacteriol. 50, 259-266.

Brown, C. M. and A. H. Rose (1969) Effects of temperature on composition and cell volume of *Candida utilis*. J. Bacteriol. 97, 261-272.

Bryers, J. D. and W. G. Characklis (1982) Processes governing primary biofilm formation. Biotechnol. Bioeng. 24, 2451-2476.

Buchanan, R. L. and L. A. Klawitter (1992) The effect of incubation temperature, initial pH and sodium chloride on the growth kinetics of *Escherichia coli* 0157:H7. Food Microbiol. 9, 185-196.

Burton, D. and K. Ravishankar (1989) Treatment of Hazardous Petrochemical and Petroleum Wastes - Current, New and Emerging Technologies, Noyes Publications, Park Ridge, NJ.

Campbell, A. (1957) Synchronization of cell division. Bact. Rev. 21, 263-269.

Canillac, N., M. T. Pommier and A. M. Gounot (1982) Effet de la température d'incubation sur la composition lipidique de Corynébactériacées du genre Arthrobacter. Can. J. Microbiol. 28, 284-290.

Carter, J. L. and W. F. Barry (1975) Effects of shock temperature on biological systems. J. Environ. Div. ASCE 101, 229-243.

Chang, H. T., B. E. Rittmann, D. Amar, R. Heim, O. Ehlinger and Y. Lesty (1991) Biofilm detachment mechanisms in a liquid-fluidized bed. Biotechnol. Bioeng. 38, 499-506.

Characklis, W. G. (1990) Biofilm processes. In Ecological and Applied Microbiology: Biofilms, W. G. Characklis and K. C. Marshall, ed., pp. 195-231, Wiley, New York.

Characklis, W. G. and B. E. Christensen (1990) Physical and chemical properties of biofilms. In Ecological and Applied Microbiology: Biofilms, W. G. Characklis and K. C. Marshall, ed., pp. 93-130, John Wiley & Sons, New York.

Chase, L. M. (1977) A dynamic kinetic model of the activated sludge process. Biotechnol. Bioeng. 19, 1431-1447.

Cheng, Y.-W. and S. W. Hermanowicz (1990) Hydrodynamic characteristics of particles in biological fluidized beds. In Environmental Engineering - Proceedings of the 1990 Specialty Conference, Arlington, Virginia, July 8-11, C. R. O'Melia, ed., pp. 4-9, ASCE, New York.

Chi, C. T. and J. A. Howell (1976) Transient behavior of a continuous stirred tank biological reactor utilizing phenol as an inhibitory substrate. Biotechnol. Bioeng. 18, 63-80.

Chiam, H. F. and I. J. Harris (1983) Application of a noninhibitory growth model to predict the transient response in a chemostat. Biotechnol. Bioeng. 25, 1613-1623.

Chisti, M. Y. and M. Moo-Young (1987) Airlift reactors: Characteristics, applications and design considerations. Chem. Eng. Commun. 60, 195-242.

Chohji, T., T. Sawada and S. Kuno (1976) Macromolecule synthesis in *Escherichia coli* BB under various growth conditions. Appl. Environ. Microbiol. 31, 864-869.

Chohji, T., T. Sawada and S. Kuno (1983) Effects of temperature shift on growth rate of *Escherichia coli* BB at lower glucose concentration. Biotechnol. Bioeng. 25, 2991-3003.

Christiansen, J. A. and P. W. Spraker (1982) Improving effluent quality of petrochemical wastewaters with mutant bacterial cultures. In Proceedings of the 37th Industrial Waste Conference, Purdue University - 1982, J. M. Bell, ed., pp. 567-576, Ann Arbor Science, Ann Arbor, MI.

Clarkson, W. W., C.-P. Yang and A. R. Harker (1993) 2,4-D degradation in monoculture biofilm reactors. Wat. Res. 27, 1275-1284.

Coelhoso, I., K. Boaventura and A. Rodrigues (1992) Biofilm reactors: An experimental and modeling study of wastewater denitrification in fluidized-bed reactors of activated carbon particles. Biotechnol. Bioeng. 40, 625-633.

Cooney, C. L. and D. I. C. Wang (1976) Transient response of *Enterobacter aerogenes* under a dual nutrient limitation in a chemostat. Biotechnol. Bioeng. 18, 189-198.

D'Adamo, P. D., A. F. Rozich and A. F. J. Gaudy (1984) Analysis of growth data with inhibitory carbon sources. Biotechnol. Bioeng. 26, 397-402.

Daigger, G. T. and C. P. L. J. Grady (1982a) An assessment of the role of physiological adaptation in the transient response of bacterial cultures. Biotechnol. Bioeng. 24, 1427-1444.

Daigger, G. T. and C. P. L. J. Grady (1982b) The dynamics of microbial growth on soluble substrates: A unifying theory. Wat. Res. 16, 365-382.

de Beer, D. and G. Muyzer (1995) Multispecies biofilms: Report from the discussion session. Wat. Sci. Technol. 32, 269-270.

de Beer, D. and P. Stoodley (1995) Relation between the structure of an aerobic biofilm and transport phenomena. Wat. Sci. Technol. 32, 11-18.

de Beer, D., P. Stoodley and Z. Lewandowski (1994a) Liquid flow in heterogeneous biofilms. Biotechnol. Bioeng. 44, 636-641.

de Beer, D., P. Stoodley, F. Roe and Z. Lewandowski (1994b) Effects of biofilm structures on oxygen distribution and mass transport. Biotechnol. Bioeng. 43, 1131-1138.

de Mendonca, M. M., J. Silverstein and N. E. J. Cook (1992) Short and long-term responses to changes in hydraulic loading in a fixed denitrifying biofilm. Wat. Sci. Technol. 26, 535-544.

Denac, M., S. Uzman, H. Tanaka and I. J. Dunn (1983) Modeling of experiments on biofilm penetration effects in a fluidized bed nitrification reactor. Biotechnol. Bioeng. 25, 1841-1861

Donaldson, T. L., G. W. Strandberg, J. Hewitt, G. S. Shields and R. M. Worden (1987) Biooxidation of coal gasification wastewaters using fluidized-bed bioreactors. Environ. Prog. 6, 205-211

Donovan, R. S., C. W. Robinson and B. R. Glick (1995) An inexpensive system to provide sparged aeration to shake flask cultures. Biotechnol. Tech. 9, 665-670.

Duddridge, J. E., C. A. Kent and J. F. Laws (1982) Effect of surface shear stress on the attachment of *Pseudomonas fluorescens* to stainless steel under defined flow conditions. Biotechnol. Bioeng. 24, 153-164.

Eckenfelder, W. W. and A. J. Englande (1970) Temperature effects on biological waste treatment processes. In International Symposium on Water Pollution Control in Cold Climates held at the University of Alaska, July 22-24, R. S. Murphy, D. Nuquist and P. W. Neff, ed., pp. 180-190, U.S. Environmental Protection Agency, Washington, DC.

Edwards, V. H. (1970) The influence of high substrate concentrations on microbial kinetics. Biotechnol. Bioeng. 12, 679-712

Eismann, F., P. Kuschk and U. Stottmeister (1994) Temperature dependence of phenol degradation at various substrate concentrations by a sediment population from a lignite processing deposit under methanogenic conditions. Poster presented at the International Symposium/Workshop on Environmental Biotechnology, July 4-8, Waterloo, Canada.

Elmaleh, S. (1990) Rule of thumb modelling of biofilm reactors. Wat. Sci. Technol. 22, 405-418.

Esener, A. A., J. A. Roels and N. W. F. Kossen (1981) The influence of temperature on the maximum specific growth rate of *Klebsiella pneumoniae*. Biotechnol. Bioeng. 23, 1401-1405.

Esener, A. A., J. A. Roels and N. W. F. Kossen (1983) The influence of temperature on the energetics of *Klebsiella pneumoniae*. Biotechnol. Bioeng. 25, 2093-2098.

Etzensperger, M., S. Thoma, S. Petrozzi and I. J. Dunn (1989) Phenol degradation in a three-phase biofilm fluidized sand bed reactor. Bioprocess Eng. 4, 175-181.

Eyring, H. and D. W. Urry (1965) Thermodynamics and chemical kinetics. In Theoretical and Mathematical Biology, T. H. Waterman and H. J. Morowitz, ed., pp. 57-95, Baisdell Publishing Co., New York.

Fan, L.-S., S.-J. Hwang and A. Matsuura (1984) Hydrodynamic behaviour of a draft tube gas-liquid-solid spouted bed. Chem. Eng. Sci. 39, 1677-1688.

Fan, L.-S., R. Leyva-Ramos, K. D. Wisecarver and B. J. Zehner (1990) Diffusion of phenol through a biofilm grown on activated carbon particles in a draft-tube three-phase fluidized-bed bioreactor. Biotechnol. Bioeng. 35, 279-286.

Farmer, I. S. and C. W. Jones (1976) The effect of temperature on molar growth yield and maintenance requirement of *Escherichia coli* during aerobic growth in continuous culture. FEBS Lett. 67, 359-363.

Feist, C. F. and G. D. Hegeman (1969) Phenol and benzoate metabolism by *Pseudomonas putida*: Regulation of tangential pathways. J. Bacteriol. 100, 869-877.

Fieschko, J. and A. E. Humphrey (1983) Effects of temperature and ethanol concentration on the maintenance and yield coefficient of *Zymomonas mobilis*. Biotechnol. Bioeng. 25, 1655-1660.

Fletcher, M. (1976) The effects of proteins on bacterial attachment to polystyrene. J. Gen. Microbiol. 94, 400-404.

Fletcher, M. (1977) The effects of culture concentration and age, time, and temperature on bacterial attachment to polystyrene. Can. J. Microbiol. 23,

Fletcher, M. and G. I. Loeb (1979) Influence of substratum characteristics on the attachment of a marine pseudomonad to solid surfaces. Appl. Environ. Microbiol. 37, 67-72.

Fletcher, M. and K. C. Marshall (1982) Bubble contact angle method for evaluating substratum interfacial characteristics and its relevance to bacterial attachment. Appl. Environ. Microbiol. 44, 184-192.

Folsom, B. R., P. J. Chapman and P. H. Pritchard (1990) Phenol and trichloroethylene degradation by *Pseudomonas cepacia* G4: Kinetics and interactions between substrates. Appl. Environ. Microbiol. 56, 1279-1285.

Fowler, H. W. and A. J. McKay (1980) The measurement of microbial adhesion. In Microbial Adhesion to Surfaces, J. M. Lynch, S. Melling, P. R. Ratter and B. Vincent, ed., pp. 143, Ellis Horwood, Chichester.

Friedman, M. M. and H. van Doesburg (1980) Evaluation of temperature effects in aerated biotreaters. In AIChE Symposium Series - 209, Vol. 77, G. F. Bennett, ed., pp. 112-121, American Institute of Chemical Engineers, New York.

Fujie, K., W. -T. Tang, T. -R. Long, L. -S. Fan (1979) unpublished results, Ohio State University.

Gadani, V., P. Villon, J. Manem and B. Rittmann (1993) A new method to solve a non-steady-state multispecies biofilm model. Bull. Math. Biol. 55, 1039-1061.

Galil, N., M. Rebhun and Y. Brayer (1988) Disturbances and inhibition in biological treatment of wastewater from an integrated refinery. Wat. Sci. Technol. 20, 21-29.

Gantzer, C. J. (1989) Inhibitory substrate utilization by steady-state biofilms. J. Environ. Eng. 115, 302-319.

Garcia Sanchez, J. L., B. Kamp, K. A. Onysko, H. M. Budman and C. W. Robinson (1998) Double inhibition model for degradation of phenol by *Pseudomonas putida* Q5. Biotechnol. Bioeng. 60, 560-567.

Garrido, J. M., W. A. J. van Benthum, M. C. M. van Loosdrecht and J. J. Heijnen (1997) Influence of dissolved oxygen concnetration on nitrite accumulation in a biofilm airlift suspension reactor. Biotechnol. Bioeng. 53, 168-178.

Gaspillo, P.-A. D. and S. Goto (1991) Mass transfer in bubble slurry column with static mixer in draft tube. J. Chem. Eng. Japan 24, 680-682.

Gaudy, A. F. J. (1975) The transient respose to pH and temperature shock loading of fermentation systems. Biotechnol. Bioeng. 17, 1051-1064.

George, T. K. and A. F. J. Gaudy (1973) Transient response of continuously cultured heterogeneous populations to changes in temperature. Appl. Microbiol. 26, 796-803.

Gilley, J. W. and H. R. Bungay (1968) Frequency response analysis of dilution rate effects on yeast growth. Biotechnol. Bioeng. 10, 99-103.

Gjaltema, A., P. A. M. Arts, M. C. M. van Loosdrecht, J. G. Kuenen and J. J. Heijnen (1994) Heterogeneity of biofilms in rotating annular reactors: Occurence, structure and consequences. Biotechnol. Bioeng. 44, 194-204.

Gjaltema, A., L. Tijhuis, M. C. M. van Loosdrecht and J. J. Heijnen (1995) Detachment of biomass from suspended nongrowing spherical biofilms in airlift reactors. Biotechnol. Bioeng. 46, 258-269.

Gjaltema, A., N van der Marel, M. C. M. van Loosdrecht and J. J. Heijnen (1997a) Adhesion and biofilm development on suspended carriers in airlift reactors: Hydrodynamic conditions versus surface characteristics. Biotechnol. Bioeng. 55, 880-889.

Gjaltema, A., M. C. M. van Loosdrecht and J. J. Heijnen (1997b) Abrasion of suspended biofilm pellets in airlift reactors. Effect of particle size. Biotechnol. Bioeng. 55, 206-215.

Gjaltema, A., J. L. Vinke, M. C. M. van Loosedrecht and J. J. Heijnen (1997c) Abrasion of suspended biofilm pellets in airlift reactors: Importance of shape, structure and particle concentrations. Biotechnol. Bioeng. 53, 88-89.

Godbole, S. P., A. Schumpe and Y. T. Shah (1983) Hydrodynamics and mass transfer in bubble columns: Effect of solids. Chem. Eng. Commun. 24, 255-258.

Goto, S., Y. Matsumoto and P. Gaspillo (1989) Mass transfer and reaction in bubble column slurry reactor with draft tube. Chem. Eng. Commun. 85, 181-191.

Gounot, A.-M. (1991) Bacterial life at low temperature: physiological aspects and biotechnological implications. J. Appl. Bacteriol. 71, 386-397.

Grady, C. P. L. J. and H. C. Lim (1980) Biological Wastewater Treatment - Theory and Applications, Marcel Dekker, New York.

Haldane, J. B. S. (1930) Enzymes, Longmans, Green and Co., Ltd., London.

Han, K. and O. Levenspiel (1988) Extended monod kinetics for substrate, product and cell inhibition. Biotechnol. Bioeng. 32, 430-437.

Harremoës, P., J. Jansen and G. H. Kristensen (1980) Practical problems related to nitrogen bubble formation in fixed film reactors. Prog. Wat. Technol. 12, 253-270.

Harvey, R. J. (1970) Metabolic regulation in glucose limited chemostat cultures of *Escherichia coli*. J. Bacteriol. 104, 698-706.

Hayduk, W. and H. Laudie (1974) Prediction of diffusion coefficients for nonelectrolytes in dilute aqueous solutions. AIChE J. 20, 611-615.

Heijnen, J. J., A. Mulder, R. Weltevrede, P. H. Hols and H. L. J. M. Leeuwen (1990) Large-scale anaerobic/aerobic treatment of complex industrial wastewater using immobilized biomass in fluidized bed and air-lift suspension reactors. Chem. Eng. Technol. 13, 202-208.

Heijnen, J. J. and J. A. Roels (1981) A macroscopic model describing yield and maintenance relationships in aerobic fermentation processes. Biotechnol. Bioeng. 23, 739-763.

Heijnen, J. J., M. C. M. van Loosdrecht, A. Mulder and L. Tijhuis (1992) Formation of bioiflms in a biofilm air-lift suspension reactor. Wat. Sci. Technol. 26, 647-654.

Heipieper, H.-J., H. Keweloh and H.-J. Rehm (1991) Influence of phenols on growth and membrane permeability of free and immobilized *Escherichia coli*. Appl. Environ. Microbiol. 57, 1213-1217.

Heipieper, H.-J., H. Keweloh and J. H. Rehm (1990) Influence of phenols on the membrane permeability of free and immobilized bacteria. In Lectures held at the 8th DECHEMA Annual Meeting of Biotechnologists, May 28-30, D. Behrens and P. Krämer, ed., pp. 641-644, DECHEMA Deutsche Gesellschaft für Chemisches Apparatewesen, New York.

Heitzer, A., H.-P. E. Kohler, P. Reichert and G. Hamer (1991) Utility of phenomenological models for describing temperature dependence of bacterial growth. Appl. Environ. Microbiol. 57, 2656-2665.

Herbert, R. A. (1986) The ecology and physiology of psychrophilic microorganisms. In Microbes in Extreme Environments, R. A. Herbert and G. A. Cod, ed., pp. 1-23, Academic Press, London.

Herendeen, S. L., R. A. VanBogelen and F. C. Neidhardt (1979) Levels of major proteins of *Escherichia coli* during growth at different temperatures. J Bacteriol. 139, 185-194

Hermanowicz, S. W. and Y.-W. Cheng (1990) Biological fluidized bed reactor: Hydrodynamics, biomass distribution and performance. Wat. Sci. Technol. 22, 193-202.

Herskowitz, M. and J. C. Merchuck (1986) A loop three-phase fluidized-bed reactor. Can. J. Chem. Eng. 64, 57-61.

Hilge-Rotmann, B. and H. J. Rehm (1990) Studies of the physiology of free and immobilized *Saccharomyces cerevisiae*. In Lectures held at the 8th DECHEMA Annual Meeting of Biotechnologists, May 28-30, Vol. 4, D. Behrens and P. Krämer, ed., pp. 163-166, DECHEMA Deutsche Gesellschaft für Chemisches Apparatewesen, New York.

Hill, G. A. (1974) Kinetics of Phenol Degradation by *Pseudomonas putida*. Masters Thesis, University of Waterloo, Waterloo, ON.

Hill, G. A. and C. W. Robinson (1975) Substrate inhibition kinetics: Phenol degradation by *Pseudomonas putida*. Biotechnol. Bioeng. 7, 1599-1615.

Hoehn, R. C. and A. D. Ray (1973) Effects of thickness on bacterial film. J. Wat. Pollut. Control Fed. 45, 2302-2320.

Holladay, D. W., C. W. Hancher, D. D. Chilcote and C. D. Scott (1978) Biodegradation of phenolic waste liquors in stirred-tank, columnar and fluidized-bed bioreactors. AIChE Symposium Series, Food, Pharmaceutical and Bioengineering 74, 241-252.

Holman, J. P. (1990) Heat Transfer, 7th ed., McGraw-Hill, Inc., Toronto.

Horn, H. and D. C. Hempel (1997) Substrate utilization and mass transfer in an autotrophic biofilm system: Experimental results and numerical simulation. Biotechnol. Bioeng. 53, 363-371.

Howell, J. A. and B. Atkinson (1976) Influence of oxygen and substrate concentrations on the ideal film thickness and maximum overall substrate uptake rate in microbial film fermentors. Biotechnol. Bioeng. 28, 15-35.

Howell, J. A., C. T. Chi and U. Pawlowsky (1972) Effect of wall growth on scale-up problems and dynamic operating characteristics of the biological reactor. Biotechnol. Bioeng. 14, 253-265.

Howell, J. A. and M. G. Jones (1980) The development of a two-component operon-type theory model for phenol degradation. In AIChE Symposium Series 209, Vol. 77, G. F. Bennett, ed., pp. 122-128, American Institute of Chemical Engineers, New York.

Howell, J. A. and M. G. Jones (1981) The development of a two component operon-type theory model for phenol degradation. AIChE Symp. Ser. 77, 122-128.

Huang, J. and K. L. Pinder (1995) Effects of calcium on development of anaerobic acidogenic biofilms: Biotechnol. Bioeng. 45, 212-218.

Huang, S.-Y. and J.-C. Chen (1988) Analysis of the kinetics of ethanol fermentation with *Zymomonas mobilis* considering temperature effect. Enzyme Microb. Technol. 10, 431-439.

Hutchinson, D. H. and C. W. Robinson (1988) Kinetics of the simultaneous batch degradation of *p*-cresol and phenol by *Pseudomonas putida*. Appl. Microbiol. Biotechnol. 29, 599-604.

Ingraham, J. L., O. Maaloe and F. C. Neidhardt (1983) Growth of the Bacterial Cell, Sinauer Associates, Inc., Sunderland, MA.

Inniss, W. E. and C. I. Mayfield (1978) Psychrotrophic bacteria in sediments from the Great Lakes. Wat. Res. 12, 237-241.

Iwami, N., A. Imai, Y. Inamori and R. Sudo (1992) Treatment of a landfill leachate containing refractory organics and ammonium nitrogen by the microorganism-attached activated carbon fluidized bed process. Wat. Sci. Technol. 26, 1999-2002.

Jadhav, S. V. and V. G. Pangarkar (1988) Particle-liquid mass transfer in three phase sparged reactor. Can. J. Chem. Eng. 66, 572-578.

Jadhav, S. V. and V. G. Pangarkar (1991) Particle-liquid mass transfer in three-phase sparged reactors: Scale-up effects. Chem. Eng. Sci. 46, 919-927.

Jensen, R. H. and C. A. Woolfolk (1985) Formation of filaments by *Pseudomonas putida*. Appl. Environ. Microbiol. 50, 364-372.

Jian-an, C. and T. J. Nieuwstad (1992) Modelling the three-phase flow in a pilot-scale airlift internal-loop reactor for wastewater treatment. Environ. Technol. 13, 101-113.

Jones, P. G., R. A. Van Bogelen and F. C. Neidhardt (1987) Induction of proteins in response to low temperature in *Escherichia coli*. J. Bacteriol. 169, 2092-2095.

Joshi, J. B., V. V. Ranade, S. D. Gharat and S. S. Lele (1990) Sparged loop reactors. Can. J. Chem. Eng. 68, 705-741.

Julseth, C. R. and W. E. Inniss (1990) Heat shock protein induction and the acquisition of thermotolerance in the psychrotrophic yeast *Trichosporon pullulans*. Current Microbiol. 20, 391-396.

Kaballo, H.-P., Y. Zhao and P. A. Wilderer (1995) Elimination of *p*-chlorophenol in biofilm reactors - a comparative study of continuous flow and sequenced batch operation. Wat. Sci. Technol. 31, 51-60.

Karel, S. F., S. B. Libicki and C. R. Robertson (1985) The immobilization of whole cells: Engineering principles. Chem. Eng. Sci. 40, 1321-1354.

Keweloh, H., R. Backhaus, G. Weyrauch, H.-J. Heipieper and H. J. Rehm (1990a) Influence of phenols on the membrane of free and immobilized bacteria. In Lectures held at the 8th DECHEMA Annual Meeting of Biotechnologists, May 28-30, Vol. 4, D. Behrens and P. Kr„mer, ed., pp. 477-480, DECHEMA Deutsche Gesellschaft für Chemisches Apparatewesen, New York.

Keweloh, H., G. Weyrauch and H.-J. Rehm (1990b) Phenol-induced membrane changes in free and immobilized *Escherichia coli*. Appl. Microbiol. Biotechnol. 33, 66-71.

Kim, B. R. and M. T. Suidan (1989) Approximate algebraic solution for a biofilm model with the Monod kinetic expression. Wat. Res. 23, 1491-1498.

Kim, J. W., M. J. Humenick and N. E. Armstrong (1981) A comprehensive study on the biological treatabilities of phenol and methanol - I. Analysis of bacterial growth and substrate removal kinetics by a statistical method. Wat. Res. 15, 1221-1231.

Kincannon, D. F., E. L. Stover, V. Nichols and D. Medley (1983) Removal mechanisms for toxic priority pollutants. J. Wat. Pollut. Control Fed. 55, 157-163.

Kissel, J. C., P. L. McCarty and R. L. Street (1984) Numerical simulation of mixed-culture biofilm. J. Environ. Div. ASCE 110, 393-411.

Kjeldgaard, N. O., O. Maaloe and M. Schaechter (1958) The transition between different physiological states during balanced growth of *Salmonella typhimurium*. J. Gen. Microbiol. 19, 607-616.

Klein, J. and H. Eng (1979) The measurement of abrasion. In Characterization of Immobilized Biocatalysts, Dechema Monographs, Vol. 84, K. Buchholz, ed., pp. 292-299, DECHEMA Deutsche Gesellschaft für Chemisches Apparatewesen, New York.

Knowles, G., A. L. Downing and M. J. Barrett (1965) Determination of kinetic constants for nitrifying bacteria in mixed culture with the aid of an electric computer. J. Gen. Microbiol. 38, 263-278.

Koch, B., M. Ostermann, H. H"ke and D.-C. Hempel (1991) Sand and activated carbon as biofilm carriers for microbial degradation of phenols and nitrogen-containing aromatic compounds. Wat. Res. 25, .

Kochbeck, B., M. Lindert and D. C. Hempel (1992) Hydrodynamics and local parameters in three-phase-flow in airlift-loop reactors of different scale. Chem. Eng. Sci. 47, 3443-3450.

Koide, K., A. Takazawa, M. Kounura and H. Matsunaga (1984) Gas holdup and volumetric liquid-phase mass transfer coefficient in solid-suspended bubble columns. J. Chem. Eng. Japan 17, 459-466.

Kolenc, R. J., W. E. Inniss, B. R. Glick, C. W. Robinson and C. I. Mayfield (1988) Transfer and expression of mesophilic plasmid-mediated degradative capacity in a psychrotrophic bacterium. Appl. Environ. Microbiol. 54, 638-641.

Kotturi, G. (1989) Low-temperature Bioregeneration of Spent Activated Carbon by a Phenol-degrading Pseudomonad. M.A. Sc. Thesis, University of Waterloo, Waterloo, ON.

Kotturi, G., C. W. Robinson and W. E. Inniss (1991) Phenol degradation by a psychrotrophic strain of *Pseudomonas putida*. Appl. Microbiol. Biotechnol. 34, 539-543.

Krishnan, P. and A. F. J. Gaudy (1976) Response of activated sludge to quantitative shock loading. J. Wat. Pollut. Control Fed. 48, 906-919.

Krouwel, P. G. and N. W. F. Kossen (1981) Gas production by immobilized microorganisms: Calculation of theoretical maximum productivity. Biotechnol. Bioeng. 23, 651-655.

Kumaran, P. and Y. L. Parachuri (1997) Kinetics of phenol biotransformation. Wat. Res. 31, 11-22.

Kushalkar, K. B. and V. G. Pangarkar (1994) Particle-liquid mass transfer in a bubble column with a draft tube. Chem. Eng. Sci. 49, 139-144.

Kwok, W. K., C. Picioreanu, S. L. Ong, M. C. M. van Loosdrecht, W. J. Ng and J. J. Heijnen (1998) Influence of biomass production and detachment forces on biofilm structures in a biofilm airlift suspension reactor. Biotechnol. Bioeng. 58, 400-407.

Langeveld, L. P. M. and F. Cuperus (1980) The relation between temperature and growth in pasteurized milk of different types of bacteria which are important to the deterioration of that milk. Neth. Milk Dairy J. 34, 106-125.

Lazarova, V. Z., B. Capdeville and L. Nikolov (1992) Biofilm performance of a fluidized bed biofilm reactor for drinking water denitrification. Wat. Sci. Technol. 26, 555-566.

Leudeking, R. and E. L. Piret (1959) A kinetic study of the lactic acid fermentation batch process at controlled pH. J. Biochem. Microbiol. Technol. Eng. 1, 393-412.

Lewandowski, G., B. Baltzis and C. P. Varuntanya (1986) The use of pure cultures as a means of understanding the performance of mixed cultures in biodegradation of phenolics. In Biotechnology for Degradation of Toxic Chemicals in Hazardous Wastes, R. J. Schultze, E. D. Smith, J. Bandy, Y. C. Wu and J. V. Basililo, ed., Noyes Data Corp., Park Ridge, NJ.

Li, J.-K. and A. E. Humphrey (1989) Kinetic and fluorometric behaviour of a phenol fermentation. Biotechnol. Lett. 11, 177-182.

Liu, Y. (1998) Energy uncoupling in microbial growth under substrate-sufficient conditions. Appl. Microbiol. Biotechnol. 49, 500-505.

Livingston, A. G. (1991) Biodegradation of 3,4-dichloroaniline in a fluidized-bed bioreactor and a steady-state biofilm. Biotechnol. Bioeng. 38, 260-272.

Livingston, A. G. (1993) A novel membrane bioreactor for detoxifying industrial wastewater: I. Biodegradation of phenol in a synthetically concocted wastewater. Biotechnol. Bioeng. 41, 915-926.

Livingston, A. G. and H. A. Chase (1989) Modeling phenol degradation in a fluidized-bed bioreactor. AIChE J. 35, 1980-1992.

Livingston, A. G. and H. A. Chase (1990) Liquid-solid mass transfer in a three phase draft tube fluidized bed reactor. Chem. Eng. Commun. 92, 225-244.

Loeb, G. I. and R. A. Neihof (1975) Marine conditioning films. In Applied Chemistry at Protein Interfaces, R. E. Baier, ed., pp. 319-335, American Chemical Society, Washington, DC.

Lu, Y. and J. J. Ganczarcyk (1984) Application of carrier/activated sludge process for treatment of phenolic wastewater. In Proceedings of the 38th Industrial Waste Conference, Purdue University - 1983, J. M. Bell, ed., pp. 643-657, Butterworth, Toronto.

Luong, H. G. T. (1987) Generalization of Monod kinetics for analysis of growth data with substrate inhibition. Biotechnol. Bioeng. 29, 242-248.

Mainzer, S. E. and W. P. Hempfling (1976) Effects of growth temperature on yield and maintenance during glucose-limited continuous culture of *Escherichia coli*. J. Bacteriol. 126, 251-256.

Manickan, T. S. and A. F. J. Gaudy (1983) Comparison of activated sludge response to quantitative, hydraulic and combined shock for the same increases in mass loading. In Proceedings of the 37th Industrial Waste Conference, Purdue University - 1982, J. Bell, ed., pp. 601-618, Ann Arbor Science, Ann Arbor, MI.

Mao, H. H., Y. Chisti and M. Moo-Young (1992) Multiphase hydrodynamics and solid-liquid mass transport in an external loop airlift reactor - a comparative study. Chem. Eng. Commun. 113, 1-13.

Marr, A. G., E. H. Nilson and D. J. Clark (1963) The maintenance requirement of *Escherichia coli*. Ann. N.Y. Acad. Sci. 102, 536-548.

Marshall, K. C., R. Stout and R. Mitchell (1971) Mechanism of the initial events in the sorption of marine bacteria to surfaces. J. Gen. Microbiol. 69, 337-348.

Massol-Deya, A. A., J. Whallon, R. F. Hickey and J. M. Tiedje (1995) Channel structures in aerobic biofilms of fixed-film reactors treating contaminated groundwater. Appl. Environ. Microbiol. 61, 769-777.

McCallum, K. L., J. J. Heikkila and W. E. Inniss (1986) Temperature-dependent pattern of heat-shock protein synthesis in psychrophilic and psychrotrophic microorganisms. Can. J. Microbiol. 32, 516-521.

McLellan, J. C. and A. W. Busch (1969) Hydraulic and process aspects of reactor design II - Response to variations. In Proceedings of the 24th Industrial Waste Conference, D. E. Bloodgood, ed., pp. 493-506, Purdue University Press, Lafayette, IN.

McMeekin, T. A., J. Olley and D. A. Ratkowsky (1987) Temperature effects on bacterial growth rates. In Physiological Models in Microbiology, Vol. 1, M. J. Bazin and J. I. Prosser, ed., pp. 75-89, CRC Press,Inc., Boca Raton, FL.

Meadows, P. S. (1971) The attachment of bacteria to solid surfaces. Arch. Microbiol. 75, 374-381.

Melin, E. S., K. T. J„rvinen and J. A. Puhakka (1998) Effects of temperature on chlorophenol biodegradation kinetics in fluidized-bed reactors with different biomass carriers. Wat. Res. 32, 81-90.

Mennett, R. H. and T. O. M. Nakayama (1971) Influence of temperature on substrate and energy conversion in *Pseudomonas fluorescens*. Appl. Microbiol. 22, 772-776.

Merchuk, J. C., G. Osemberg, M. Siegel and M. Shacham (1992) A method for evaluation of mass transfer coefficients in the different regions of airlift reactors. Chem. Eng. Sci. 47, 2221-2226.

Mirpuri, R., W. Jones and J. D. Bryers (1997) Toluene degradation kinetics for planktonic and biofilm-grown cells of *Pseudomonas putida* 54G. Biotechnol. Bioeng. 53, 535-546.

Moletta, K., G. Goma and G. Durand (1978) Influence de la temp,rature sur la cin,tique de croissance et le coefficient de maintenance de *Candida lipolytica*. Arch. Microbiol. 118, 293-299.

Molin, G. and I. Nilsson (1985) Degradation of phenol by *Pseudomonas putida* ATCC 11172 in continuous culture at different rates of biofilm surface to culture volume. Appl. Environ. Microbiol. 50, 946-950.

Monod, J. (1949) The growth of bacteria cultures. Ann. Rev. Microbiol. 3, 371.

Morgan, M. S. and V. H. Edwards (1971) Simulation of the effects of temperature on microbial cell propagators. Chem. Eng. Prog. Symp. Ser. 67, 51-58.

Muck, R. E. and C. P. L. J. Grady (1974) Temperature effects on microbial growth in CSTRs. J. Environ. Div. ASCE 100, 1147-1163.

Mulcahy, L. T. and W. K. Shieh (1987) Fluidization and reactor biomass characteristics of the denitrification fluidized bed biofilm reactor. Wat. Res. 21, 451-458.

Mulcahy, L. T., W. K. Shieh and E. J. La Motta (1980) Kinetic model of biological denitrification in a fluidized bed biofilm reactor (FBBR). Prog. Wat. Technol. 12, 143-158.

Mulcahy, L. T., W. K. Shieh and E. J. Lamotta (1981) Simplified mathematical models for a fluidized-bed biofilm reactor. AIChE Symp. Ser. 77, 273-285.

Nagai, S., Y. Nishizawa and S. Aiba (1969) Kinetics of nucleic acid synthesis in the growth of *Azotobacter vinelandii*. J. Gen. Appl. Microbiol. 15, 427-438.

Nagaoka, H. and K. Sugio (1994) Effect of turbulent structure on filament-type biofilm reaction. Wat. Sci. Technol. 30, 111-120.

Ng, H., J. L. Ingraham and A. G. Marr (1962) Damage and derepression in *Escherichia coli* resulting from growth at low temperature. J. Bacteriol. 84, 331.

Nguyen-Tien, K., A. N. Patwari, A. Schumpe and W.-D. Deckwer (1985) Gas-liquid mass transfer in fluidized particle beds. AIChE J. 31, 194-201.

Nicolella, C., R. Di Felice and M. Rovatti (1996) An experimental model of biofilm detachment in liquid fluidized bed biological reactors. Biotechnol. Bioeng. 51, 713-719.

Nielsen, P. H. and P. Harremoës (1995) Solids: Report of the discussion session. Wat. Sci. Technol. 32, 273-275.

O'Dowd, W., D. N. Smith, J. A. Ruether and S. C. Saxena (1987) Gas and solids behavior in a baffled and unbaffled slurry bubble column. AIChE J. 33, 1959-1970.

Ohashi, A. and H. Harada (1994) Characterization of detachment mode of biofilm developed in an attached-growth reactor. Wat. Sci. Technol. 30, 35-45.

Ohashi, A. and H. Harada (1996) A novel concept for evaluation of biofilm adhesion strength by applying tensile force and shear force. Wat. Sci. Technol. 34, 201-211.

Okabe, S., T. Yasuda and Y. Watanabe (1997) Uptake and release of inert fluorescence particles by mixed population biofilms. Biotechnol. Bioeng. 53, 459-469.

Ong, S. K. and A. R. Bowers (1990) Steady-state analysis for biological treatment of inhibitory substrate. J. Environ. Div. ASCE 116, 1013-1028.

Onysko, K. A. (1993) Health and Safety Assessment Report for Dynamic Response of an Immobilized-cell Fluidized-bed Airlift Bioreactor Degrading Phenol, Department of Chemical Engineering, University of Waterloo, Waterloo, ON.

Pacepavicius, G., Y. L. Lau, D. Liu, H. Okamura and I. Aoyama (1997) A rapid biochemical method for estimating biofilm mass. Environmental Toxicology and Water Quality: An International Journal 12, 97-100.

Palleroni, N. J. (1975) General properties and taxonomy of the genus *Pseudomonas*. In Genetics and Biochemistry of *Pseudomonas*, P. H. Clarke and M. H. Richmond, ed., John Wiley & Sons, Toronto.

Palumbo, S. A. and L. D. Witter (1969) Influence of temperature on glucose utilization by *Pseudomonas fluorescens*. Appl. Microbiol. 18, 137-141.

Park, Y., M. E. Davis and D. A. Wallis (1984a) Analysis of a continuous aerobic fixed-film bioreactor. I. Steady-state behaviour. Biotechnol. Bioeng. 26, 457-467.

Park, Y., M. E. Davis and D. A. Wallis (1984b) Analysis of a continuous, aerobic, fixed-film bioreactor. II. Dynamic behavior. Biotechnol. Bioeng. 26, 468-476.

Patoine, M.-C. (1989) Low-temperature Biodegradation of Phenol in an Immobilized-cell Fluidized-bed Reactor. M.A.Sc. Thesis, University of Waterloo, Waterloo, ON.

Pawlowsky, U. and J. A. Howell (1973a) Mixed culture biooxidation of phenol. I. Determination of kinetic parameters. Biotechnol. Bioeng. 15, 889-896.

Pawlowsky, U. and J. A. Howell (1973b) Mixed culture biooxidation of phenol. II. Steady state experiments in continuous culture. Biotechnol. Bioeng. 25, 897-903.

Pawlowsky, U., J. A. Howell and C. T. Chi (1973) Mixed culture biooxidation of phenol. III. Existence of multiple steady states in continuous culture with wall growth. Biotechnol. Bioeng. 15, 905-916.

Perez, J. and T. W. Jeffries (1992) Roles of manganese and organic acid chelators in regulating lignin degradation and biosynthesis of peroxidases by *Phanerochaete chrysosporium*. Appl. Environ. Microbiol. 58, 2402-2409.

Perret, C. J. (1960) A new kinetic model of a growing bacterial population. J. Gen. Microbiol. 22, 589-617.

Perry's Chemical Engineers' Handbook, Sixth edition (1984), R. H. Perry, D. W. Green, J. O. Maloney, ed., McGraw-Hill, Inc., Toronto, p. 3-103.

Petrasek, A. C., I. J. Kugelman, B. M. Austern, T. A. Pressley, L. A. Winslow and R. H. Wise (1983) Fate of toxic organic compounds in wastewater treatment plants. J. Wat. Pollut. Control Fed. 55, 1286-1296.

Pirt, S. J. (1965) The maintenance energy of bacteria in growing cultures. Proc. Roy. Soc. Ser. B. 163, 224-231.

Pisano, S. L., J. C. O'Shaughnessy, D. LaMarre, C. Gray, S. Pederson and M. Sykes (1990) Toxic organic shock loading of rotating biological contactors and sequencing batch reactors. In Proceedings of the 44th Industrial Waste Conference, Purdue University - 1989, J. Bell, ed., pp. 125-140, Lewis Publishers, Inc., Chelsea, MI.

Potier, P., P. Drevet, A. M. Gounot and A. Hipkiss (1990) Temperature-dependent changes in proteolytic activities and protein composition in the psychrotrophic bacterium *Arthrobacter blobiforms* $S_1$55. J. Gen. Microbiol. 136, 283-291.

Potthoff, M. and M. Bohnet (1993) Influence of solids concentration and static mixers on fluid dynamics in three-phase fluidized bed bioreactors. Chem. Eng. Technol. 16, 147-152.

Powell, M. S. and N. K. H. Slater (1982) Removal rates of bacterial cells from glass surfaces by fluid shear. Biotechnol Bioeng. 24, 2527-2537.

Powell, M. S. and N. K. H. Slater (1983) The deposition of bacterial cells from laminar flows onto solid surfaces. Biotechnol. Bioeng. 25, 891-900.

Ratkowsky, D. A., R. K. Lowry, T. A. McMeekin, A. N. Stokes and R. E. Chandler (1983) Model for bacterial culture growth rate throughout the entire biokinetic temperature range. J. Bacteriol. 154, 1222-1226.

Ratkowsky, D. A., J. Olley, T. A. McMeekin and A. Ball (1982) Relationship between temperature and growth rate of bacterial cultures. J. Bacteriol. 149, 1-5.

Ratkowsky, D. A., T. Ross, T. A. McMeekin and J. Olley (1991) Comparison of Arrhenius-type and Belehr dek-type models for prediction of bacterial growth in foods. J. Appl. Bacteriol. 71, 452-459.

Reynolds, J. H., E. J. Middlebrooks and D. B. Procella (1974) Temperature-toxicity model for oil refinery waste. J. Environ. Div. ASCE 100, 557-576.

Rittmann, B. E. and P. McCarty (1978) Variable-order model of bacterial-film kinetics. J. Environ. Div. ASCE 104, 889-900.

Rittmann, B. E. and P. L. McCarty (1980a) Evaluation of steady-state biofilm kinetics. Biotechnol. Bioeng. 22, 2359-2373.

Rittmann, B. E. and P. L. McCarty (1980b) Model of steady-state-biofilm kinetics. Biotechnol. Bioeng. 22, 2343-2357.

Rittmann, B. E. and P. L. McCarty (1981) Substrate flux into biofilms of any thickness. J. Environ. Div. ASCE 107, 831-849.

Rittmann, B. E., F. Trinet, D. Amar and H. T. Chang (1992) Measurement of the activity of a biofilm. Effects of surface loading and detachment on a three-phase, liquid-fluidized-bed reactor. Wat. Sci. Technol. 26, 585-594.

Robinson, C. W. (1992) Laboratory Research Health and Safety Manual: Regulations and Guidelines, Departmental of Chemical Engineering, University of Waterloo, Waterloo, ON.

Robinson, J. A., M. G. Trulear and W. G. Characklis (1984) Cellular reproduction and extracellular polymer formation by *Pseudomonas aeruginosa* in continuous culture. Biotechnol. Bioeng. 26, 1409-1417.

Rozich, A. F. and A. F. J. Gaudy (1983) Response of phenol-acclimated activated sludge process to quantitative shock loading. J. Wat. Pollut. Control Fed. 57, 795-804.

Rutter, P. R. and B. Vincent (1988) Attachment mechanisms in the surface growth of microorganisms. In Physiological models in Microbiology, Vol. 2, M. J. Bazin and J. I. Prosser, ed., pp. 87-107, CRC Press, Inc., Boca Raton, FL.

Ryhiner, G., S. Petrozzi and I. J. Dunn (1988) Operation of a three-phase biofilm fluidized sand bed reactor for aerobic wastewater treatment. Biotechnol. Bioeng. 32, 667-688.

Ryu, D. Y. and R. I. Mateles (1968) Transient response of continuous cultures to changes in temperature. Biotechnol. Bioeng. 10, 385-397.

Sáez, P. B. and B. E. Rittmann (1988) Improved pseudoanalytical solution for steady-state biofilm kinetics. Biotechnol. Bioeng. 32, 379-385.

Sänger, P. and W.-D. Deckwer (1981) Liquid-solid mass transfer in aerated suspensions. Chem. Eng. J. 22, 179-186.

Sakoda, A., J Wang and M Suzuki (1996) Mirobial activity in biological activated carbon bed by pulse responses. Wat. Sci. Technol 34, 213-222.

Saleh, M. M. and A. F J. Gaudy (1978) Shock load response of activated sludge with constant recycle sludge concentration. J. Wat. Pollut. Control Fed. 50, 764-774.

Sanders, J. D (1973) Temperature-nutrient Relationships in Microbial Growth. Masters Thesis, University of Missouri-Columbia, Columbia, MO.

Sano, Y., N. Yamaguchi and T Adachi (1974) Mass transfer coefficients for suspended particles in agitated vessels and bubble columns. J Chem. Eng. Japan 7, 255-261.

Sauer, T. and D.-C. Hempel (1987) Fluid dynamics and mass transfer in a bubble column with suspended particles. Chem. Eng. Technol. 10, 180-189.

Saxena, S. C., N. S. Rao and P. R. Thimmapuram (1992) Gas phase holdup in slurry bubble columns for two- and three-phase systems. Chem. Eng. J 49, 151-159.

Schaechter, M., O. Maaloe and N. O. Kjeldgaard (1958) Dependency on medium and temperature of cell size and chemical composition during balanced growth of *Salmonella typhimurium*. J. Gen. Microbiol. 19, 592-606.

Schaezler, D. J., W. H. McHarg and A. W. Busch (1971) Effect of the growth rate on the transient responses of batch and continous microbial cultures. In Biological Waste Treatment, R. P. Canale, ed., pp. 107-129, Wiley Interscience, New York.

Schoolfield, R. M., P. J. H. Sharpe and C. E. Magnuson (1981) Non-linear regression of biological temperature-dependent rate models based on absolute reaction-rate theory J Theor Biol. 88, 719-731.

Schröder, M., C. Müller, C. Posten, W.-D. Deckwer and V. Hecht (1997) Inhibition kinetics of phenol degradation from unstable steady-state data. Biotechnol. Bioeng. 54, 567-576.

Schumpe, A., A. K. Saxena and K. D. P. Nigam (1987) Gas/liquid mass transfer in a bubble column with suspended nonwettable solids. AIChE J. 33, 1916-1920.

Sharpe, P. J. H. and D. W. DeMichele (1977) Reaction kinetics of poikilotherm development. J. Theor. Biol. 64, 649-670.

Shieh, W. K. (1980) Suggested kinetic model for the fluidized-bed biofilm reactor. Biotechnol. Bioeng. 22, 667-676.

Shieh, W. K. (1981) Comments on biologically active fluidized beds. Biotechnol. Bioeng. 23, 2145-2147.

Shreve, G. S., R. H. Olsen and T. M. Vogel (1991) Development of pure culture biofilms of *Pseudomonas putida* on solid supports. Biotechnol. Bioeng. 37, 512-518.

Shreve, G. S. and T. M. Vogel (1993) Comparison of substrate utilization and growth kinetics between immobilized and suspended *Pseudomonas* cells. Biotechnol. Bioeng. 41, 370-379.

Shuler, M. L. and F. Kargi (1992) Bioprocess Engineering: Basic Concepts, Prentice Hall, Englewood Cliffs, NJ.

Siegel, M. H. and C. W. Robinson (1992) Applications of airlift gas-liquid-solid reactors in biotechnology. Chem. Eng. Sci. 47, 3215-3229.

Sittig, M. (1975) Environmental Sources and Emissions Handbook, Noyes Data Corporation, Park Ridge, NJ.

Sokol, W. (1987) Oxidation of an inhibitory substrate by washed cells (oxidation of phenol by *Pseudomonas putida*). Biotechnol. Bioeng. 30, 921-927.

Sokol, W (1988a) Dynamics of continuous stirred-tank biochemical reactor utilizing inhibitory substrate. Biotechnol. Bioeng. 31, 198-202.

Sokol, W (1988b) Uptake rate of phenol by *Pseudomonas putida* grown in unsteady state. Biotechnol. Bioeng. 32, 1097-1103

Sokol, W. and J. A. Howell (1981) Kinetics of phenol oxidation by washed cells. Biotechnol. Bioeng. 23, 2039-2049.

Stainer, R. Y., N. J. Palleroni and M. Doudoroff (1966) The aerobic pseudomonads: A taxonomic study. J. Gen. Microbiol 43, 159-271.

Stathis, T. C. (1980) Fluidized bed for biological wastewater treatment. J Environ. Div. ASCE 106, 227-241

Stephenson, J. P. and K. L. Murphy (1980) Kinetics of biological fluidized bed wastewater denitrification. Prog. Wat. Technol. 12, 159-172.

Stevens, D. K. (1988) Interaction of mass transfer and inhibition in biofilms. J. Environ. Eng. 114, 1352-1358.

Stevens, D. K., P. M. Berthouex and T. W. Chapman (1989) Dynamic model of nitrification in fluidized bed. J. Environ. Div. ASCE 115, 910-929

Stewart, P. S. (1998) A review of experimental measurements of effective diffusive permeabilites and effective diffusion coefficients in biofilms. Biotechnol. Bioeng. 59, 261-272.

Storer, F. F. and A. F. J. Gaudy (1969) Computational analysis of transient response to quantitative shock loadings of heterogenous populations in continuous culture. Environ. Sci. Technol. 3, 143-149.

Stover, E. L. and D. F. Kincannon (1981) Biological treatability of specific organic compounds found in chemical industry wastewaters. In Proc. 36th Indust. Waste Conf., Purdue Univ., J Bell, ed., pp. 1-16, Lewis publishers, Inc., Chelsea, MI.

Suidan, M. T. (1986) Performance of deep biofilm reactors. J. Environ. Eng. 112, 78-93.

Suidan, M. T., B. E. Rittmann and U. K. Traegner (1987) Criteria establishing biofilm kinetic types. Wat. Res. 21, 491-498.

Suidan, M. T., A. M. Wuellner and T. K. Boyer (1991) Anaerobic treatment of a high-strength industrial waste bearing inhibitory concentrations of 1,1,1-trichloroethane. Wat. Sci. Technol. 23, 1385-1394.

Sun, Y. and S. Furusaki (1988) Mean bubble diameter and oxygen transfer coefficient in a three-phase fluidized bed bioreactor. J. Chem. Eng. Japan 21, 20-24.

Sun, Y., T. Nozawa and S. Furusaki (1988) Gas holdup and volumetric oxygen transfer coefficient in a three-phase fluidized bed bioreactor. J. Chem. Eng. Japan 21, 15-19.

Sundstrom, D. W., H. E. Klei and G. T. Brookman (1976) Response of biological reactors to sinusoidal variations of substrate concentration. Biotechnol. Bioeng. 18, 1-14.

Sutton, P. M. and P. N. Mishra (1990) Fluidized bed biological wastewater treatment: Effects of scale-up on system performance. Wat. Sci. Technol. 22, 419-430.

Tan, Y., Z.-X. Wang and K. C. Marxhall (1996) Modeling substrate inhibition of microbial growth. Biotechnol. Bioeng. 52, 602-608.

Tang, W.-T. and L.-S. Fan (1987) Steady-state phenol degradation in a draft tube, gas-liquid-solid fluidized-bed bioreactor. AIChE J. 33, 239-249.

Tang, W.-T. and L.-S. Fan (1989) Hydrodynamics of a three-phase fluidized bed containing low-density particles. AIChE J. 35, 355-364

Tang, W.-T. and L.-S. Fan (1990) Gas-liquid mass transfer in a three-phase fluidized bed containing low-density particles. Ind. Eng. Chem. Res. 29, 128-133.

Tang, W.-T., K. Wisecarver and L.-S. Fan (1987) Dynamics of a draft tube gas-liquid-solid fluidized-bed bioreactor for phenol degradation. Chem. Eng. Sci. 42, 2123-2134.

Tempest, D. W. (1967) Studies on the growth of *Aerobacter aerogenes* at low dilution rates in a chemostat. In Microbial Physiology and Continuous Culture, E. O. Powell, ed., pp. 240-254, HMSO, London.

Tempest, D. W. and J. R. Hunter (1965) The influence of temperature and pH value on the macromolecular composition of magnesium-limited and glycerol-limited *Aerobacter aerogenes* growing in a chemostat. J. Gen. Microbiol. 41, 267-273.

Tempest, D. W., J. R. Hunter and J. Sykes (1965) Magnesium-limited growth of *Aerobacter aerogenes* in a chemostat. J. Gen. Microbiol. 39, 355-366.

Tijhuis, L., B. Hijman and M. C. M. van Loosdrecht (1996) Influence of detachment, substrate loading and reactor scale on the formation of biofilms in airlift reactors. Appl. Microbiol. Biotechnol. 45, 7-17.

Tijhuis, L., J. L. Huisman, H. D. Hekkelman, M. C. M. van Loosdrecht and J. J. Heijnen (1995) Formation of nitrifying biofilims on small suspended particles in airlift reactors. Biotechnol. Bioeng. 47, 585-595.

Tijhuis, L., L. P. M. van der Pluym, M. C. M. van Loosdrecht and J. J. Heijnen (1992a) Formation of biofilms on small suspended particles in airlift reactors. Wat. Sci. Technol. 26, 2015-2019.

Tijhuis, L., M. C. M. van Loosdrcht and J. J. Heijnen (1992b) Nitrification with biofilms on small suspended particles in airlift reactors. Wat. Sci. Technol. 26, 2207-2211.

Tijhuis, L., H. Zwols, K.-H. van Meekeren, M. C. M. van Loosdrecht and S. J. Heijnen (1993) Dynamics of biofilm formation on small suspended particles in airlift reactors. Poster presented at the ECB-6 Conference, Florence, June 13-17.

Topiwala, H. and C. G. Sinclair (1971) Temperature relationship in continuous culture. Biotechnol. Bioeng. 13, 795-813.

Tosteson, T. R. and W. A. Corpe (1975) Enhancement of adhesion of the marine *Chlorella vulgaris* to glass. Can. J. Microbiol. 21, 1025-1031.

Touloukian, Y. S., S. C. Saxena and P. Hestemans (1975) A Comprehensive Compilation of Data by the Thermophysical Properties Research Center (TPRC, Purdue University), Vol. II, Viscosity, IFI/Plenum, New York.

Turakhia, M. H. and W. G. Characklis (1989) Activity of *Pseudomonas aeruginosa* in biofilms: Effect of calcium. Biotechnol. Bioeng. 33, 406-444.

Turakhia, M. H., K. E. Cooksey and W. G. Characklis (1983) Influence of a calcium-specific chelant on biofilm removal. Appl. Environ. Microbiol. 46, 1236-1238.

van Benthum, W. A. J., M. D. M. van Loosedrecht and J. J. Heijnen (1997) Control of heterotrophic layer formation on nitrifying biofilms in a biofilm airlift suspension reactor. Biotechnol. Bioeng. 53, 399-405.

van Loosdrecht, M. C. M., D. Eikelboom, A. Gjaltema, A. Mulder, L. Tijhuis and J. J. Heijnen (1995a) Biofilm structures. Wat. Sci. Technol. 32, 35-43.

van Loosdrecht, M. C. M., J. Lyklema, W. Norde and A. J. B. Zehnder (1989) Bacterial adhesion: A physicochemical approach. Microb. Ecol. 17, 1-15.

van Loosdrecht, M. C. M., J. Lyklema, W. Norde and A. J. B. Zehnder (1990) Influence of interfaces on microbial activity. Microbiol. Rev. 54, 75-87.

van Loosdrecht, M. C. M., L. Tijhuis, A. M. S. Wijdieks and J. J. Heijnen (1995b) Population distribution in aerobic biofilms on small suspended particles. Wat. Sci. Technol. 31, 163-171.

Visser, A., Y. Gao and G. Lettinga (1993) Effects of short-term temperature increases on the mesophilic anaerobic breakdown of sulfate containing synthetic wastewater. Wat. Res. 27, 541-550.

Voice, T. C., D. Pak, X. Zhao, J. Shi and R. F. Hickey (1992) Biological activated carbon in fluidized bed reactors for the treatment of groundwater contaminated with volatile aromatic hydrocarbons. Wat. Res. 26, 1389-1401.

von Kármán, T. (1921) Ober laminaire und turbulente Reibung. Angew. Math. Mech. 1, 233-252.

Wagner, K. and D. C. Hempel (1988) Biodegradation by immobilized bacteria in an airlift-loop reactor - Influence of biofilm diffusion limitation. Biotechnol. Bioeng. 31, 559-566.

Wanner, O. (1995) New experimental findings and biofilm modelling concepts. Wat. Sci. Technol. 32, 133-140.

Webb, J. L. (1963) Enzyme and Metabolic Inhibitors, Academic Press, Boston, MA.

Weber, A. S., M.-S. Lai, W. Lin, J. G. Goeddertz, W.-C. Ying and J. Duffy (1992) Anaerobic/aerobic biological activated carbon (BAC) treatment of a high strength phenolic wastewater. Environ. Prog. 11, 310-317.

Whyte, L. G. and W. E. Inniss (1992) Cold shock proteins and cold acclimation proteins in a psychtrotrophic bacterium. Can. J. Microbiol. 38, 1281-1285.

Wilderer, P. A., A. Cunningham and U. Schindler (1995) Hydrodynamics and shear stress: Report from the discussion session. Wat. Sci. Technol. 32, 271-272.

Wilke, C. R. and P. Chang (1955) Correlation of diffusion coefficients in dilute solutions. AIChE J. 1, 264-270.

Williamson, K. and P. L. McCarty (1976) A model of substrate utilization by bacterial films. J. Wat. Pollut. Control Fed. 48, 9-24.

Willocx, F., M. Mercier, M. Hendrikx and P. Tobback (1993) Modelling the influence of temperature and carbon dioxide upon the growth of *Pseudomonas fluorescens*. Food Microbiol. 10, 159-173.

Wisecarver, K. D. and L.-S. Fan (1989) Biological phenol degradation in a gas-liquid-solid fluidized-bed reactor. Biotechnol. Bioeng. 33, 1029-1038.

Worden, R. M. and T. L. Donaldson (1987) Dynamics of a biological fixed film for phenol degradation in a fluidized-bed bioreactor. Biotechnol. Bioeng. 30, 398-412.

Xiu, Z.-L., A.-P. Zeng and W.-D. Deckwer (1998) Multiplicity and stability analysis of microorganisms in continuous culture. Effects of metabolic overflow and growth inhibition. Biotechnol. Bioeng. 57, 251-261.

Xu, N. and V. Majidi (1994) Identification of metabolic intermediates in microbial degradation of phenol using laser desorption time-of-flight mass spectometry. The Science of the Total Environment 156, 139-143.

Yang, R. D. and A. E. Humphrey (1975) Dynamic and steady-state studies of phenol biodegradation in pure and mixed cultures. Biotechnol. Bioeng. 17, 1211-1235.

Yano, T. and S. Koga (1969) Dynamic behaviour of the chemostat subject to substrate inhibition. Biotechnol. Bioeng. 11, 139-153.

Yano, Y., T. Nakahara, S. Kamiyama and K. Yamada (1966) Kinetic studies on microbial activities in concentrated solutions: Part 1. Effect of excess sugars on oxygen uptake rate of a cell free respiratory system. Agr. Biol. Chem. 30, 42-48.

Yongaçoglu, S., K. Toda, J. E. Prenosil and I. J. Dunn (1981) Dynamics and control of a biological phenol wastewater treatment reactor. In Advances in Biotechnology: Proc. 6th Internat. Ferment. Symp, Vol. 1, M. Moo-Young, C. W. Robinson and C. Vezina, ed., pp. 365-370, Pergamon Press, Toronto.

Young, T. B., D. F. Bruley and H. R. Bungay (1970) A dynamic mathematical model of the chemostat. Biotechnol. Bioeng. 12, 747-769.

Young, T. B. and H. R. Bungay (1973) Dynamic analysis of a microbial process: A systems engineering approach. Biotechnol. Bioeng. 15, 377-393.

Yun, H. S., J. Hong and H. C. Lim (1996) Regulation of ribosome synthesis in *Escherichia coli*: Effects of temperature and dilution rate changes. Biotechnol. Bioeng. 52, 615-624.

Zhang, T. C. and P. L. Bishop (1994a) Experimental determination of the dissolved oxygen boundary layer and mass transfer resistance near the fluid-biofilm interface. Wat. Sci. Technol. 30, 47-58.

Zhang, T. C. and P. L. Bishop (1994b) Structure, activity and composition of biofilms. Wat. Sci. Technol. 29, 335-344.

Zhang, W., E. Bouwer, L. Wilson and N. Durant (1995) Biotransformation of aromatic hydrocarbons in subsurface biofilms. Wat. Sci. Technol. 31, 1-14.

Zwietering, M. H., J. T. de Koos, B. E. Hasenack, J. C. de Witt and K. van't Riet (1991) Modelling of bacterial growth as a function of temperature. Appl. Environ. Microbiol. 57, 1094-1101.

Appendix A: Mathematical Development for the Solution of the Steady-state and Unsteady-state Models

A-1 Mathematical Development for the Solution of the Steady-state Model.

At steady state, the rate of change of each variable in the system is zero. The expressions developed for each variable in Section 4.2 at steady state are listed below.

The balance on the substrate in the bulk fluid, S_b, (Equation 4.1 with 4.2 and 4.3 substituted) becomes:

$$\frac{dS_b}{dt} = D[S_o - S_b(t)] - (\frac{\mu_b}{Y_g} - m) X_S - \frac{4\pi r_f^2 N_p k_s (S_b - S_f\big|_{r_f})}{\varepsilon_L V_R} = 0 \qquad \textbf{(A-1)}$$

The balance on the suspended biomass in the bulk fluid, X_S, (Equation 4.10 with 4.11 substituted) becomes:

$$\frac{dX_S}{dt} = \mu_b X_S - DX_S - \frac{4\pi N_p \rho_f r_D (r_f^3 - r_p^3)}{3\varepsilon_L V_R} = 0 \qquad \textbf{(A-2)}$$

The balance on the substrate in the biofilm, S_f, in spherical coordinates (Equation 4.5) becomes:

$$\frac{\partial S_f}{\partial t} = D_{S,f} \frac{1}{r^2} (\frac{\partial}{\partial r} (r^2 \frac{\partial S_f}{\partial r})) - (\frac{\mu_f}{Y_g} - m) f \rho_f = 0 \qquad \textbf{(A-3)}$$

which is subject to the following boundary conditions:

$$D_{S,f} \frac{\partial S_f}{\partial r} = 0 \quad at \quad r = r_p \qquad \textbf{(A-3a)}$$

$$D_{S,f} \frac{\partial S_f}{\partial r} = k_s (S_b - S_{f\,r_f}) \quad at \quad r = r_f \qquad \textbf{(A-3b)}$$

The balance on the biomass in the biofilm, expressed in terms of the radial distance to the surface of the biofilm from the centre of the bioparticle, r_f (Equation 4.16) becomes:

$$\frac{dr_f}{dt} = \frac{1}{r_f^2} (\int_{r_p}^{r_f} \mu_f r^2 dr - \frac{1}{3}(r_f^3 - r_p^3) r_D) = 0 \qquad \textbf{(A-4)}$$

Assuming a parabolic profile for the substrate concentration in the biofilm, the expression for the substrate concentration in the biofilm, S_f, is

$$S_f = a'(r - r_p)^2 + b'(r - r_p) + c' \qquad \textbf{(A-5)}$$

$$\frac{\partial S_f}{\partial r} = 2a'(r - r_p) + b' \qquad \textbf{(A-6)}$$

but from Equation A-3a,

$$\frac{\partial S_f}{\partial r} = 0 \text{ at } r = r_p \qquad \textbf{(A-7)}$$

thus

$$b' = 0 \qquad \textbf{(A-8)}$$

At $r=r_f$,

$$D_{Sf}\frac{\partial S_f}{\partial r} = k_s(S_b - S_{f\,r_f}) \qquad \textbf{(A-3b)}$$

Substituting Equations A-5 and A-6 gives

$$2a'D_{S.f}(r_f - r_p) = k_s(S_b - a'(r_f - r_p)^2 + c') \qquad \textbf{(A-9)}$$

Rearranging to isolate c' gives,

$$c' = S_b - a'(r_f - r_p)^2 - \frac{2D_{S.f}}{k_s}(r_f - r_p) \qquad \textbf{(A-10)}$$

Substituting Equation A-10 into Equation A-5 gives,

$$S_f = a'((r - r_p)^2 - (r_f - r_p)^2 - \frac{2D_{S.f}}{k_s}(r_f - r_p) + S_b) \qquad \textbf{(A-11)}$$

Thus,

$$\frac{\partial S_f}{\partial r} = 2a'(r - r_p) \qquad \textbf{(A-12)}$$

$$\frac{\partial S_f^2}{\partial r^2} = 2a' \qquad \textbf{(A-13)}$$

From Equation A-3b,

$$S_f\Big|_{r_f} = S_b - \frac{2a'D_{S.f}}{k_s}(r_f - r_p) \tag{A-14}$$

Substituting Equation A-12 into Equation A-3 and multiplying by

$$r^2\ D_{S.f}\left(\frac{\partial}{\partial r}(2a'r^2(r-r_p)) - r^2\left(\frac{\mu_f}{Y_g} - m\right)f\ \rho_f = 0\right. \tag{A-15}$$

Integrating with respect to r

$$D_{S.f}\int_{r_p}^{r_f}\left(\frac{\partial}{\partial r}(2a'r^2(r-r_p))dr - f\rho_f\int_{r_p}^{r_f}(r^2\left(\frac{\mu_f}{Y_g} - m\right))dr = 0\right. \tag{A-16}$$

Solving

$$2a'D_{S.f}\,r_f^{\,2}(r_f - r_p) - \frac{f\rho_f}{Y_g}\int_{r_p}^{r_f}(r^2\mu_f)dr - \frac{f\rho_f m}{3}(r_f^3 - r_p^3) = 0 \tag{A-17}$$

From Equation A-4

$$\int_{r_p}^{r_f} r^2\mu_f dr = \frac{r_D}{3}(r_f^3 - r_p^3) \tag{A-18}$$

Substituting Equation A-18 into A-17

$$2a'D_{S.f}\,r_f^{\,2}(r_f - r_p) - \frac{f\rho_f r_D(r_f^3 - r_p^3)}{3Y_g} - \frac{f\rho_f m}{3}(r_f^3 - r_p^3) = 0 \tag{A-19}$$

Collecting terms

$$2a'D_{S.f}\,r_f^{\,2}(r_f - r_p) - \frac{1}{3}f\rho_f(r_f^3 - r_p^3)\left(\frac{r_D}{Y_g} + m\right) = 0 \tag{A-20}$$

Rearranging to isolate a'

$$a' = \frac{f\rho_f(r_f^3 - r_p^3)\left(\frac{r_D}{Y_g} + m\right)}{6D_{S.f}r_f^2(r_f - r_p)} \tag{A-21}$$

Substituting Equation A-14 into A-1,

$$D(S_o - S_b) - (\frac{\mu_b}{Y_g} + m) X_S - \frac{8\pi r_f^2 N_p a' D_{S,f}(r_f - r_p)}{\varepsilon_L V_R} = 0 \quad \textbf{(A-22)}$$

Substituting Equation A-21 into A-22, **(A-23)**

$$D(S_o - S_b) - (\frac{\mu_b}{Y_g} + m) X_S - \frac{4\pi r N_p f \rho_f (\frac{r_D}{Y_g} + m)(r_f^3 - r_p^3)}{3\varepsilon_L V_R} = 0 \quad \textbf{(A-22)}$$

Rearranging to isolate X_S

$$X_S = \frac{1}{(\frac{\mu_b}{Y_g} + m)} (D(S_o - S_b) - \frac{4\pi N_p f \rho_f (\frac{r_D}{Y_g} + m)(r_f^3 - r_p^3)}{3\varepsilon_L V_R} \quad \textbf{(A-24)}$$

Substituting Equation A-24 into A-2 and consolidating common terms,

$$\frac{4\pi N_p \rho_f (r_f^3 - r_p^3)}{3\varepsilon_L V_R} (r_D (\frac{\mu_b}{Y_g} + m) - f(\mu_b - D)(\frac{r_D}{Y_g} + m)) + D(\mu_b - D)(S_o - S_b) = 0 \quad \textbf{(A-25)}$$

Isolating r_f,

$$r_f = (\frac{3\varepsilon_L V_R D(D - \mu_b)(S_o - S_b)}{4\pi N_p \rho_f (r_D (\frac{\mu_b}{Y_g} + m) - f(\mu_b - D)(\frac{r_D}{Y_g} + m))} + r_p^3)^{\frac{1}{3}} \quad \textbf{(A-26)}$$

Substituting Equation A-26 into Equation A-18 gives,

$$\int_{r_f}^{r_p} r^2 \mu_f dr - \frac{r_D}{3} (\frac{3\varepsilon_L V_R D(D - \mu_b)(S_o - S_b)}{4\pi N_p \rho_f (r_D (\frac{\mu_b}{Y_g} + m) - f(\mu_b - D)(\frac{r_D}{Y_g} + m))}) = 0 \quad \textbf{(A-27)}$$

Equations A-26 and A-27 were solved numerically for different values of S_b until a value of S_b for which the function value was zero, was found. There were two solutions: a trivial solution for $r_f = r_p$ and a steady-state solution for which $r_f > r_p$. The trivial solution corresponds to the case of a bioreactor without immobilized biomass.

A-2 Mathematical Development for the Solution of the Unsteady-state Model.

Basic mass balances

The expressions developed for each variable in Section 4.2 at unsteady state are listed below

The balance on the substrate in the bulk fluid, S_b, (Equation 4.1 with 4.2 and 4.3 substituted) becomes:

$$\frac{dS_b}{dt} = D[S_o - S_b(t)] - (\frac{\mu_b}{Y_g} + m) X_S - \frac{4\pi r_f^2 N_p k_s (S_b - S_f|_{r_f})}{\varepsilon_L V_R} \qquad \textbf{(A-28)}$$

The balance on the suspended biomass in the bulk fluid, X_S, (Equation 4.10 with 4.11 substituted) becomes:

$$\frac{dX_S}{dt} = \mu_b X_S - DX_S - \frac{4\pi N_p \rho_f r_D (r_f^3 - r_p^3)}{3\varepsilon_L V_R} \qquad \textbf{(A-29)}$$

The balance on the substrate in the biofilm, S_f, (Equation 4.5) becomes:

$$\frac{\partial S_f}{\partial t} = D_{S,f} \frac{1}{r^2} (\frac{\partial}{\partial r} (r^2 \frac{\partial S_f}{\partial r})) - (\frac{\mu_f}{Y_g} + m) f \rho_f \qquad \textbf{(A-30)}$$

which is subject to the following boundary conditions:

$$D_{S,f} \frac{\partial S_f}{\partial r} = 0 \quad at \quad r = r_p \qquad \textbf{(A-3a)}$$

$$D_{S,f} \frac{\partial S_f}{\partial r} = k_s (S_b - S_{f\,r_f}) \quad at \quad r = r_f \qquad \textbf{(A-3b)}$$

The balance on the biomass in the biofilm, expressed in terms of the radial distance to the surface of the biofilm from the centre of the bioparticle, r_f (Equation 4.16) becomes:

$$\frac{dr_f}{dt} = \frac{1}{r_f^2} (\int_{r_p}^{r_f} \mu_f r^2 dr - \frac{1}{3}(r_f^3 - r_p^3) r_D) \qquad \textbf{(A-31)}$$

The parabolic approximation for substrate concentration in the biofilm, S_f, is shown in Appendix A-1, Equations A-5 to A-14.

Applying the parabolic approximation the balance on the bulk phenol concentration

Substituting Equation A-14 into A-28 gives,

$$\frac{dS_b}{dt} = D(S_o - S_b) - (\frac{\mu_b}{Y_g} - m) X_S - \frac{8\pi r_f^2 N_p a' D_{S.f}(r_f - r_p)}{\varepsilon_L V_R} \quad \textbf{(A-32)}$$

Applying the parabolic approximation to the balance on phenol concentration in the biofilm

Multiplying Equation A-30 by r^2 gives,

$$\frac{\partial r^2 S_f}{\partial t} - D_{S.f}(\frac{\partial}{\partial r}(r^2 \frac{\partial S_f}{\partial r})) - (\frac{\mu_f}{Y_g} - m) r^2 f \rho_f \quad \textbf{(A-33)}$$

Integrating with respect to r gives,

$$\int_{r_p}^{r_f} \frac{\partial r^2 S_f}{\partial t} dr = \int_{r_p}^{r_f} D_{S.f} (\frac{\partial}{\partial r}(r^2 \frac{\partial S_f}{\partial r}))dr - \int_{r_p}^{r_f} (\frac{\mu_f}{Y_g} - m) r^2 f \rho_f dr \quad \textbf{(A-34)}$$

Equation A-34 will be evaluated term by term.

Term 1: $$\int_{r_p}^{r_f} \frac{\partial r^2 S_f}{\partial t} dr \quad \textbf{(A-34a)}$$

Applying the Leibniz rule to term A-34a gives,

$$\int_{r_p}^{r_f} \frac{\partial r^2 S_f}{\partial t} dr = \frac{d}{dt}\int_{r_p}^{r_f} r^2 S_f dr - \frac{dr_f}{dt} r_f^2 S_f\Big|_{r_f} \quad \textbf{(A-34a-1)}$$

Substituting Equation A-11 for S_f and Equation A-14 for $S_{f,rf}$ gives,

$$\int_{r_p}^{r_f} \frac{\partial r^2 S_f}{\partial t} dr = \frac{d}{dt}\int_{r_p}^{r_f} r^2 (a'((r - r_p)^2 - (r_f - r_p)^2 - \frac{2D_{S.f}}{k_s}(r_f - r_p)) + S_b)dr \quad \textbf{(A-34a-2)}$$
$$- \frac{dr_f}{dt} r_f^2 (S_b - \frac{2a' D_{S.f}}{k_s}(r_f - r_p))$$

Expanding and integrating yields,

$$\int_{r_p}^{r_f} \frac{\partial r^2 S_f}{\partial t} dr = \frac{d}{dt}(a'(\frac{r_f^5 - r_p^5}{5} - \frac{r_f^4 - r_p^4}{2} r_p + \frac{r_f^3 - r_p^3}{3} r_p^2)$$
$$- a'(\frac{2D_{S.f}}{k_s}(r_f - r_p) + (r_f - r_p)^2)(\frac{r_f^3 - r_p^3}{3}) + S_b(\frac{r_f^3 - r_p^3}{3})) \quad \textbf{(A-34a-3)}$$
$$- \frac{dr_f}{dt} r_f^2 (S_h - \frac{2a'D_{S.f}}{k_s}(r_f - r_p))$$

Let θ be defined as,

$$\theta = a'(\frac{r_f^5 - r_p^5}{5} - \frac{r_f^4 - r_p^4}{2} r_p + \frac{r_f^3 - r_p^3}{3} r_p^2) - a'(\frac{2D_{S.f}}{k_s}(r_f - r_p)$$
$$+ (r_f - r_p)^2)(\frac{r_f^3 - r_p^3}{3}) + S_b(\frac{r_f^3 - r_p^3}{3}) \quad \textbf{(A-35)}$$

Thus Equation A-34a-3 can be restated as,

$$\int_{r_p}^{r_f} \frac{\partial r^2 S_f}{\partial t} dr = \frac{d\theta}{dt} - \frac{dr_f}{dt} r_f^2 (S_b - \frac{2a'D_{S.f}}{k_s}(r_f - r_p)) \quad \textbf{(A-34a-4)}$$

Term 2: $\int_{r_p}^{r_f} D_{S.f} (\frac{\partial}{\partial r}(r^2 \frac{\partial S_f}{\partial r})) dr$ **(A-34b)**

Substituting Equation A-12 into A-34b gives

$$\int_{r_p}^{r_f} D_{S.f} (\frac{\partial}{\partial r}(r^2 \frac{\partial S_f}{\partial r})) dr = D_{S.f} \int_{r_p}^{r_f} \frac{\partial}{\partial r}(2a'r^2(r - r_p) dr \quad \textbf{(A-34b-1)}$$

$$\int_{r_p}^{r_f} D_{S.f} (\frac{\partial}{\partial r}(r^2 \frac{\partial S_f}{\partial r})) dr = 2a'D_{S.f} \int_{r_p}^{r_f} (3r^2 - 2rr_p) dr \quad \textbf{(A-34b-2)}$$

$$\int_{r_p}^{r_f} D_{S.f} (\frac{\partial}{\partial r}(r^2 \frac{\partial S_f}{\partial r})) dr = 2a'D_{S.f}(r_f^3 - r_f^2 r_p) \quad \textbf{(A-34b-3)}$$

Replacing terms 1 and 2 in Equation A-34 with A-34a-4 and A-34b-3 and rearranging gives,

$$\frac{d\theta}{dt} = 2a'D_{S,f}(r_f^3 - r_f^2 r_p) + \frac{dr_f}{dt} r_f^2 (S_b - \frac{2a'D_{S,f}}{k_s}(r_f - r_p)) \\ - f\rho_f \int_{r_p}^{r_f} (\frac{\mu_f}{Y_g} m) r^2 dr \qquad \textbf{(A-36)}$$

where a' is expressed as,

$$a' = \frac{\theta - S_b(r_f^3 - r_p^3)/3}{(\frac{r_f^5 - r_p^5}{5} - \frac{r_f^4 - r_p^4}{2} r_p + \frac{r_f^3 - r_p^3}{3} r_p^2) - (\frac{2D_{S,f}}{k_s}(r_f - r_p) + (r_f - r_p)^2)(\frac{r_f^3 - r_p^3}{3})} \qquad \textbf{(A-37)}$$

Then a system of four nonlinear ODEs given by Equations A-36, A-28, A-29 and A-31 is obtained.

Appendix B Parameter Values and Operating Conditions used in the Steady-state and Unsteady-state Simulations

Table B-1 Parameter Values used in the Steady-state and Unsteady-state Simulations

Parameter		Notation in MATLAB code	Run				
			1	2	3	5	8
Haldane kinetics	μ_{max} [h^{-1}]	mumax	0.112	0.112	0.112	0.112	0.112
	K_S [g/cm^3]	Ks	2.5×10^{-3}	2.5×10^{-3}	2.5×10^{-3}	2.5×10^{-3}	2.5×10^{-3}
	K_I [mg/cm^3]	ki	0.175	0.175	0.175	0.175	0.175
Luong kinetics	μ_{max} [h^{-1}]	mumax	0.08762	0.08762	0.08762	0.08762	0.08762
	K_S [mg/cm^3]	Ks	4.3×10^{-3}	4.3×10^{-3}	4.3×10^{-3}	4.3×10^{-3}	4.3×10^{-3}
	S_I [mg/cm^3]	ki	0.401	0.401	0.401	0.401	0.401
Y_g [mg DW/mg phenol]		yg	1.39	1.39	1.39	1.39	1.39
m [mg phenol/mg DW·h]		m	0.03	0.03	0.03	0.01	0.01
$D_{S,w}$ [cm^2/s]		dsw	0.056952	0.056952	0.056952	0.056952	0.056952
$D_e D_w$ [-]		dedw	0.1	0.1	0.1	0.1	0.1
ρ_f [mg/cm^3]		rof	230	230	230	240	290
f [-]		ff	0.85	0.85	0.85	0.85	0.85
r_D [h^{-1}]		rd	0.024	0.025	0.018	0.022	0.022
k_s [cm/h]		kss	39.6	39.6	39.6	39.6	39.6
ε_L [-]		epsl	0.97	0.97	0.97	0.97	0.97
r_p [cm]		rp	9.75×10^{-4}	9.75×10^{-4}	9.75×10^{-4}	9.75×10^{-4}	9.75×10^{-4}
V_R [cm^3]		vr	4.22×10^{3}	3.46×10^{3}	4.22×10^{3}	4.22×10^{3}	3.46×10^{3}
N_p [-]		np	8.74×10^{6}	7.61×10^{6}	4.79×10^{6}	8.09×10^{6}	5.63×10^{6}

Table B-2. Operating Conditions used in the Steady-state and Unsteady-state Simulations

Initial/Final Conditions	Operating Condition Parameters	Notation in MATLAB code	Run				
			1	2	3	5	8
Initial Conditions used in steady-state simulations	D [h^{-1}]	d	0.034	0.0451	0.025	0.042	0.037
	S_o [mg/cm^3]	so	0.251	0.180	0.248	0.160	0.592
Step increases used in unsteady-state simulations	D [h^{-1}]	d	0.0592	0.0368	0.0593	0.0945	0.170
	S_o [mg/cm^3]	so	0.296	0.270	0.238	0.160	0.506

Appendix C MATLAB Code for Steady-state and Unsteady-state Simulations

C-1 MATLAB Code for the Steady-state Model using Haldane Kinetics

```
clear
d=0.0374;
so=592/1000;
np=5.63e6;
vr=3.46*1000;
mumax=0.112;
Ks=2.5/1000;
ki=175/1000;
yg=1.39;
m=0.01;
dsw=1.582e-5*3600;
dedw=0.1;
rof=240;
ff=0.85;
rd=0.022;
kss=0.011*3600;
epsl=0.97;
rp=1.95e-2/2;
dsf=dsw*dedw;
i=0;
for sb=0.0005:0.000002:0.002,
   i=i+1
   sbb(i)=sb;
   mub=mumax*sb/(Ks+sb+sb*sb/ki);
   mu(i)=mub;
   num=(mub-d)*d*(so-sb)*3*epsl*vr;
   den=4*3.14*np*rof*((mub-d)*ff*(rd/yg+m)-rd*(mub/yg+m));
   rf=(rp^3+num/den)^(1/3)
   rff(i)=rf;
   a=(ff*rof*0.333*(rf^3-rp^3))*(m+rd/yg)/(2*rf^2*dsf*(rf-rp));
   aa(i)=a;
   xs(i)=(d*(so-sb)-4*3.14159*np*ff*rof/(3*epsl*vr)*(rd/yg+m)*(rf^3-
rp^3))/(mub/yg+m);
   sum=0;
   ii=0;
   for r=rp:(rf-rp)/1000:rf,
      ii=ii+1;
      sf=sb+a*((r-rp)^2-2*dsf*(rf-rp)/kss-(rf-rp)^2);
      sff(ii)=sf;
      muf=mumax*sf/(Ks+sf+sf*sf/ki);
      sum=sum+muf*r*r*(rf-rp)/(1000);
   end
   f(i)=10e7*(sum-(rf^3-rp^3)*rd/(3))
end
```

C-2 MATLAB Code for the Steady-state model using Luong kinetics

```
clear
d=0.0451;
so=180/1000;
np=7.61e6;
vr=3.46*1000;
mumax=0.08762;
Ks=4.38/1000;
ki=401/1000;
yg=1.39;
m=0.03;
dsw=1.582e-5*3600;
dedw=0.1;
rof=230;
ff=0.85;
rd=0.024;
kss=0.011*3600;
epsl=0.97;
rp=1.95e-2/2;
dsf=dsw*dedw;
i=0;
for sb=0.0008:0.00001:0.004,
   i=i+1
   sbb(i)=sb;
   mub=mumax*sb*(1-sb/ki)/(Ks+sb);
   mu(i)=mub;
   num=(mub-d)*d*(so-sb);
   den=4*3.14*0.332*np*rof*((mub-d)*ff*(rd/yg+m)-
rd*(mub/yg+m))/epsl/vr;
   rf=(rp^3+num/den)^(1/3)
   rff(i)=rf;
   a=(ff*rof*0.333*(rf^3-rp^3))*(m+rd/yg)/(2*rf^2*dsf*(rf-rp));
   aa(i)=a;
   xs(i)=(d*(so-sb)-4*3.14159*np*ff*rof/(3*epsl*vr)*(rd/yg+m)*(rf^3-
rp^3))/(mub/yg+m);
   sum=0;
   ii=0;
   for r=rp:(rf-rp)/1000:rf,
      ii=ii+1;
      sf=sb+a*((r-rp)^2-2*dsf*(rf-rp)/kss-(rf-rp)^2);
      sff(ii)=sf;
      muf=mumax*sf*(1-sf/ki)/(Ks+sf);
      sum=sum+muf*r*r*(rf-rp)/(1000);
   end
   f(i)=10e7*(sum-(rf^3-rp^3)*rd/(3))
end
```

C-3 MATLAB Code to calculate θ from the steady-state value of a

```
rf=0.01030133;
a=4.378e2;
sb=0.766/1000;
dsw=1.582e-5*3600; cm2/h
dedw=0.1;
kss=0.011*3600; cm/h
rp=0.0195/2; cm
dsf=dsw*dedw;
theta=a*((rf^5-rp^5)/5-(rf^4-rp^4)/2*rp+(rf^3-rp^3)/3*rp^2)-
a*(2*dsf/kss*(rf-rp)+(rf-rp)^2)*(rf^3-rp^3)/3+sb*(rf^3-rp^3)/3
```

C-4 MATLAB Code for the Unsteady-state Model using Haldane Kinetics

```
function dy=dynamic(t,y)
  DYNAMIC t,y) returns the state derivatives of the unsteady state
ICFBR model.
  Run by typing [t,y]=ode23s 'dynamic',[interval],[initial guesses for
Sb, Xs, theta, rf
d=0.170; h-1
so=506/1000; mg/cm3
np=5.63e6;
vr=3.46*1000; cm3
mumax=0.112; h-1
Ks=2.5/1000; mg/cm3
ki=175/1000; mg/cm3
yg=1.39; mg/mg
m=0.01; h-1
dsw=1.582e-5*3600; cm2/h
dedw=0.1;
rof=290; mg/cm3
ff=0.85;
rd=0.022;
kss=0.011*3600; cm/h
epsl=0.97;
rp=0.0195/2; cm
dsf=dsw*dedw;
mub=mumax*y(1)/(Ks+y(1)+y(1)^2/ki);
p1=y(1)*(y(4)^3-rp^3)/3;
p2=(((y(4)^5-rp^5)/5-rp*(y(4)^4-rp^4)/2+rp*rp*(y(4)^3-rp^3)/3)-
(2*dsf*(y(4)-rp)/kss+(y(4)-rp)^2)*(y(4)^3-rp^3)/3);
a=(y(3)-p1)/p2;
sfrf=y(1)-2*a*dsf/kss*(y(4)-rp);
sum1=0;
sum2=0;
i=0;
for r=rp:(y(4)-rp)/100:y(4),
      i=i+1;
      sf=y(1)+a*((r-rp)^2-2*dsf*(y(4)-rp)/kss-(y(4)-rp)^2);
      muf=mumax*sf/(Ks+sf+sf*sf/ki);
      sum1=sum1+muf*r*r*(y(4)-rp)/(100);
      sum2=sum2+(muf/yg+m)*r*r*(y(4)-rp)/100;
end
integ=1/y(4)^2*(sum1-1/3*(y(4)^3-rp^3)*rd);
group=2*dsf*a*y(4)*y(4)*(y(4)-rp)-ff*rof*sum2;
dy(1,1)=d*(so-y(1))-(mub/yg+m)*y(2)-4*pi*(y(4))^2*np*2*dsf*a*(y(4)-
rp)/(epsl*vr);
dy(2,1)=(mub*y(2)-d*y(2)+4*pi*(y(4)^3-rp^3)*np*rof*rd/(3*epsl*vr));
dy(3,1)=(group+integ*sfrf*y(4)*y(4));
dy(4,1)=integ
```

C-5 MATLAB code for the unsteady-state Model using Luong Kinetics

```
function dy=dynalu(t,y)
  DYNALU(t,y) returns the state derivatives of the unsteady state
IOFBR model.
  Run by typing [t,y]=ode23s('dynamic',[interval],[initial guesses for
Sb, Xs, theta, rf]
d=0.0368; h-1
so=270/1000; mg/cm3
np=7.61e6;
vr=3.46*1000; cm3
mumax=0.08762; h-1
Ks=4.38/1000; mg/cm3
ki=401/1000; mg/cm3
yg=1.39; mg/mg
m=0.03; h-1
dsw=1.582e-5*3600; cm2/h
dedw=0.1;
rof=230; mg/cm3
ff=0.85;
rd=0.024;
kss=0.011*3600; cm/h
eps1=0.97;
rp=0.0195/2; cm
dsf=dsw*dedw;
mub=mumax*y(1)*(1-y(1)/ki)/(Ks+y(1));
if mub<0
   mub=0;
end
p1=y(1)*(y(4)^3-rp^3)/3;
p2=(((y(4)^5-rp^5)/5-rp*(y(4)^4-rp^4)/2+rp*rp*(y(4)^3-rp^3)/3)-
(2*dsf*(y(4)-rp)/kss+(y(4)-rp)^2)*(y(4)^3-rp^3)/3);
a=(y(3)-p1)/p2;
sfrf=y(1)-2*a*dsf/kss*(y(4)-rp);
sum1=0;
sum2=0;
i=0;
for r=rp:(y(4)-rp)/100:y(4),
      i=i+1;
      sf=y(1)+a*((r-rp)^2-2*dsf*(y(4)-rp)/kss-(y(4)-rp)^2);
      muf=mumax*sf*(1-sf/ki)/(Ks+sf);
      if muf<0
         muf=0;
      end
      sum1=sum1+muf*r*r*(y(4)-rp)/(100);
      sum2=sum2+(muf/yg+m)*r*r*(y(4)-rp)/100;
end
integ=1/y(4)^2*(sum1-1/3*(y(4)^3-rp^3)*rd);
group=2*dsf*a*y(4)*y(4)*(y(4)-rp)-ff*rof*sum2;
dy(1,1)=d*(so-y(1))-(mub/yg+m)*y(2)-4*pi*(y(4))^2*np*2*dsf*a*(y(4)-
rp)/(eps1*vr);
dy(2,1)=(mub*y(2)-d*y(2)+4*pi*(y(4)^3-rp^3)*np*rof*rd/(3*eps1*vr));
dy(3,1)=(group+integ*sfrf*y(4)*y(4));
dy(4,1)=integ;
```

C-6 MATLAB Code for the Unsteady-state Model using Luong kinetics Adjusted for Suppressed Growth During Shock-loading

```
function dy=dynammm(t,y)
  DYNAMMM t,y  returns the state derivatives of the unsteady state
IOFBR model.
  Run by typing:
 [t,y]=ode23s('dynammm',[time interval],[initial guesses for Sb, Xs,
theta, rf])
d=0.0593; h-1
so=248/1000; mg/cm3
np=4.79e6;
vr=4.22*1000; cm3
sbo=1.035e-3;
mumax=0.08762;
Ks=4.38/1000;
ki=401/1000;
yg=1.39; mg/mg
m=0.028; h-1
dsw=1.582e-5*3600; cm2/h
dedw=0.1;
rof=230; mg/cm3
ff=0.85;
rd=0.016;
kss=0.011*3600; cm/h
eps1=0.97;
rp=0.0195/2; cm
dsf=dsw*dedw;
adjf=y(1)-sbo;
if adjf<0
   mub=mumax*y(1)*(1-y(1)/ki)/(Ks+y(1));
else
   mub=(1-adjf*10)*mumax*y(1)*(1-y(1)/ki)/(Ks+y(1));
   if mub<0
      mub=0;
   elseif (1-adjf*10)<0
      mub=0;
   end
end
p1=y(1)*(y(4)^3-rp^3)/3;
p2=(((y(4)^5-rp^5)/5-rp*(y(4)^4-rp^4)/2+rp*rp*(y(4)^3-rp^3)/3)-
(2*dsf*(y(4)-rp)/kss+(y(4)-rp)^2)*(y(4)^3-rp^3)/3);
a=(y(3)-p1)/p2;
sfrf=y(1)-2*a*dsf/kss*(y(4)-rp);
sum1=0;
sum2=0;
i=0;
for r=rp:(y(4)-rp)/100:y(4),
      i=i+1;
      sf=y(1)+a*((r-rp)^2-2*dsf*(y(4)-rp)/kss-(y(4)-rp)^2);
      adjfsf=sf-sbo;
      if adjfsf<0
         muf=mumax*sf*(1-sf/ki)/(Ks+sf);
      else
         muf=(1-adjfsf*10)*mumax*sf*(1-sf/ki)/(Ks+sf);
         if muf<0
            muf=0;
```

```
        elseif (1-adjf*10)<0
           muf=0;
        end
      end
      sum1=sum1+muf*r*r*(y(4)-rp)/(100);
      sum2=sum2+(muf/yg+m)*r*r*(y(4)-rp)/100;
end
integ=1/y(4)^2*(sum1-1/3*(y(4)^3-rp^3)*rd);
group=2*dsf*a*y(4)*y(4)*(y(4)-rp)-ff*rof*sum2;
dy(1,1)=d*(so-y(1))-(mub/yg+m)*y(2)-4*pi*(y(4))^2*np*2*dsf*a*(y(4)-
rp)/(epsl*vr);
dy(2,1)=(mub*y(2)-d*y(2)+4*pi*(y(4)^3-rp^3)*np*rof*rd/(3*epsl*vr));
dy(3,1)=(group+integ*sfrf*y(4)*y(4));
dy(4,1)=integ;
```

Appendix D Data from Kinetic Studies

D-1 Data from Batch Experiments at 10°C used for the Temperature-dependent Growth Model (Haldane Equation)

Table D-1 Data from Batch Run 10B-1

Time [h]	X_S [mg/L]	S_b [mg/L]
0.37	53.4	12.50
0.73	55.7	11.27
1.23	60.7	7.72
1.57	62.1	5.09
1.92	63.0	5.80
2.48	66.3	2.11
2.82	70.9	1.97
3.48	70.9	1.67

Table D-2. Data from Batch Run 10B-2

Time [h]	X_S [mg/L]	S_b [mg/L]
0.30	50.2	12.81
0.70	54.3	9.25
1.18	55.2	7.50
1.52	58.0	4.67
1.85	59.8	2.53
2.43	62.6	1.15
4.80	64.0	1.15
3.42	64.9	0.91

Table D-3. Data from Batch Run 10B-3

Time [h]	X_S [mg/L]	S_b [mg/L]
0.17	50.3	16.25
0.57	50.3	11.26
1.15	53.9	7.58
1.48	55.3	6.00
1.80	56.6	2.90
2.28	60.2	3.28
2.73	61.6	1.07
3.35	61.2	1.51

Table D-4. Data from Batch Run 10B-4

Time [h]	X_S [mg/L]	S_b [mg/L]
0.23	49.4	16.31
0.68	52.1	11.48
1.18	56.6	8.26
1.50	58.9	6.77
1.83	60.7	4.15
2.40	64.3	2.32
2.77	69.8	0.95
3.40	69.8	1.13

Table D-5 Data from Batch Run 10B-5

Time [h]	X_S [mg/L]	S_b [mg/L]
0.17	34.9	31.83
0.68	38.1	34.67
1.22	36.2	33.10
1.67	37.1	32.34
2.70	38.5	30.01
3.72	41.7	25.81
4.70	45.3	16.99
5.57	49.8	11.46
6.53	54.8	4.85
7.52	61.6	1.87
8.77	60.7	1.40

Table D-6 Data from Batch Run 10B-6

Time [h]	X_S [mg/L]	S_b [mg/L]
0.18	36.7	44.56
0.73	37.1	46.51
1.60	39.0	37.40
2.58	42.6	20.65
3.07	44.8	11.65
3.55	48.5	6.99
4.20	52.1	3.74
4.67	53.9	3.89
5.37	56.6	4.20
6.02	54.4	4.84

Table D-7 Data from Batch Run 10B-7

Time [h]	X_S [mg/L]	S_b [mg/L]
0.17	61.6	51.37
0.65	61.6	48.00
1.58	64.3	41.19
2.05	65.7	38.42
2.70	67.5	28.92
3.32	71.1	17.90
3.78	73.8	12.81
4.33	77.9	5.43

Table D-8 Data from Batch Run 10B-8

Time [h]	X_S [mg/L]	S_b [mg/L]
0.20	43.9	55.95
0.75	43.5	53.59
1.32	44.8	52.67
2.05	46.7	51.82
2.73	47 6	50.73
3.65	49.4	37.45
4.57	53.9	32.09
5.43	57.5	25.20
6.10	60.7	21.44
6.73	62.5	13.48
7.55	67.0	2.63
10.13	79.3	3.88
10.45	78.8	2.28

Table D-9 Data from Batch Run 10B-9

Time [h]	X_S [mg/L]	S_b [mg/L]
0.15	71.1	57.30
0.67	77.9	50.73
1.17	82.0	47.86
1.77	87 4	40.18
2.20	88.8	33.84
2.70	95.1	29.05
3.27	98.8	17.49
3.75	103.7	6.79
4.25	108.3	6.42
4.83	113.7	6.27
5.37	113.3	1.84

Table D-10 Data from Batch Run 10B-10

Time [h]	X_S [mg/L]	S_b [mg/L]
0.08	38.5	59.73
0.58	44.4	58.58
1.12	45.3	57.43
1.63	46.2	53.19
2.27	49.8	51.84
3.05	52.5	48.60
4.03	54.4	47.46
5.02	60.7	27.03
6.05	65.2	21.03
7.07	71.6	14.36
8.00	77.0	7.62
9.98	85.2	1.77
11.85	85.6	2.41
22.73	86.1	-

Table D-11 Data from Batch Run 10B-11

Time [h]	X_S [mg/L]	S_b [mg/L]
0.22	37.6	72.47
0.80	35.8	73.23
1.62	35.8	73.56
2.60	38.1	66.23
3.10	39.4	50.98
3.58	40.8	44.02
4.23	44.4	28.85
4.70	46.7	20.83
5.37	47.6	7.26
6.00	52.5	3.74
6.48	53.0	3.22
6.83	52.1	

Table D-12 Data from Batch Run 10B-12

Time [h]	X_S [mg/L]	S_b [mg/L]
0.22	38.1	80.22
0.97	39.0	78.60
1.73	41.2	78.20
2.65	42.1	76.44
3.62	44.4	65.39
4.25	46.7	58.51
4.92	48.9	56.54
5.68	49.8	46.35
6.17	51.6	44.83
6.65	54.4	36.99
8.10	69.3	18.78
10.77	74.3	2.27
23.50	88.8	2.85

Table D-13 Data from Batch Run 10B-13

Time [h]	X_S [mg/L]	S_b [mg/L]
0.20	64.3	87.57
0.70	64.8	83.83
1.22	67.5	80.79
1.82	69.3	76.65
2.25	72.9	73.82
2.73	76.6	70.48
3.30	79.7	67.85
3.83	81.5	66.13
4.27	85.2	58.45
5.28	92.0	48.54
5.73	96.0	57.22
6.27	103.3	45.92
6.70	105.5	40.31
7.27	112.3	33.30
7.65	118.2	23.83
8.28	130.5	12.30
8.68	135.0	5.29
9.08	140.9	1.95
9.47	142.2	1.33

Table D-14. Data from Batch Run 10B-14

Time [h]	X_S [mg/L]	S_b [mg/L]
0.27	77.9	98.29
0.70	78.4	87.77
1.65	82.9	80.76
2.10	86.1	75.50
2.77	93.3	64.98
3.35	95.1	51.74
3.77	100.1	47.61
4.35	105.1	39.01
4.80	111.9	33.20
5.30	116.4	23.02
5.78	122.3	16.01
6.25	129.6	6.76
6.82	134.5	1.72

Table D-15 Data from Batch Run 10B-15

Time [h]	X_S [mg/L]	S_b [mg/L]
0.15	31.7	109.54
0.78	33.1	99.77
1.68	32.6	92.86
2.28	35.3	92.19
3.23	36.2	88.98
4.12	38.5	87.30
5.30	41.2	82.07
5.98	43.5	91.54
6.63	45.8	57.38
8.13	54.4	53.00
9.58	63.9	41.46
9.92	62.1	36.07

Table D-16 Data from Batch Run 10B-16

Time [h]	X_S [mg/L]	S_b [mg/L]
0.12	86.5	152.69
0.88	89.7	151.93
1.62	93.3	151.17
2.52	96.5	146.87
3.52	104.2	136.26
4.12	110.1	130.69
4.78	112.3	111.73
5 53	121.9	109.88
6.02	127.3	69.30
6.52	133.6	55.68
7.95	149.0	34.92
10.62	173.0	2.05

Table D-17 Data from Batch Run 10B-17

Time [h]	X_S [mg/L]	S_b [mg/L]
0.08	87.0	161.79
0.85	89.2	152.94
1.58	92.0	151.17
2.52	92.9	141.82
3.47	97.4	122.10
4.10	101.9	114.01
4.75	105.5	113.00
5.53	114.2	83.32
6.00	117.3	69.57
6.48	125.0	68.09
7.95	139.1	10.77
10.62	164.0	1.35

Table D-18 Data from Batch Run 10B-18

Time [h]	X_S [mg/L]	S_b [mg/L]
0.17	45.1	162.80
0.82	46.9	157.24
1.70	46.0	152.94
2.53	47.4	151.42
3.33	48.8	143.59
4.30	50.2	138.78
5.10	52.9	126.14
5.82	55.2	127.81
6.82	58.0	108.70
8.33	63.0	80.64
10.07	71.8	43.65

Table D-19 Data from Batch Run 10B-19

Time [h]	X_S [mg/L]	S_b [mg/L]
0.13	82.0	195.83
1.10	86.1	180.33
1.95	89.2	168.87
2.87	91.5	165.16
3.78	96.9	152.01
4.73	104.2	148.14
5.48	111.0	136.19
6.45	118.7	85.78
7.52	127.7	76.01
9.70	154.0	5.48
12.10	152.2	4.60
22.65	148.6	3.17

Table D-20 Data from Batch Run 10B-20

Time [h]	X_S [mg/L]	S_b [mg/L]
0.15	78.8	211.67
1.08	83.4	201.56
1.93	89.2	194.48
2.87	91.1	183.36
3.83	99.2	175.94
4.77	106.9	186.55
5.50	111.9	131.64
6.45	122.3	115.07
7.50	135.4	109.88
9.70	162.2	39.01
12.08	187.5	2.39
22.63	185.3	3.46

Table D-21 Data from Batch Run 10B-21

Time [h]	X_S [mg/L]	S_b [mg/L]
0.07	62.1	273.02
1.07	67.0	271.33
2.07	71.1	266.28
3.00	74.7	253.47
3.97	79.7	249.42
4.97	85.6	246.05
5.97	93.3	241.00
7.97	106.5	227.51
9.97	125.0	198.86
12.13	141.3	148.64
21.75	197.5	3.05
23.60	190.3	2.90

Table D-22 Data from Batch Run 10B-22

Time [h]	X_S [mg/L]	S_b [mg/L]
0.08	56.6	366.55
1.08	62.1	361.49
2.08	64.0	358.46
3.03	64.9	346.33
4.00	67.6	344.30
5.17	69.0	334.70
6.00	76.4	343.80
8.00	80.5	340.43
10.00	86.0	339.16
12.00	99.4	296.19
21.80	183.1	18.61
23.60	196.5	4.04
25.60	190.9	3.62

D-2 Data from Continuous Experiments at 10°C

Table D-23 Data from Continuous Experiments at 10°C

Run	D (1/h)	S_o [mg/L]	S [mg/L]	X_s [mg/L]
10C-1	0.0308	316.9	3.7	130
10C-2	0.037	200	2.4	96.6
10C-3	0.037	379	2.7	198
10C-4	0.039	203	2.4	105
10C-5	0.042	217	2.5	109
10C-6	0.042	226	1.7	96
10C-7	0.06	191	1.7	111
10C-8	0.06	186	1.2	121

D-3 Data from Batch Experiments at 15°C

Table D-24 Data from Batch Run 15B-1

Time [h]	X_S [mg/L]	S_b [mg/L]
0.08	33.5	23.66
0.43	35.5	14.93
0.78	37.5	16.18
1.03	39.1	13.28
2.42	48.4	1.65
2.88	55.2	1.57
3.40	54.8	1.10

Table D-25 Data from Batch Run 15B-2

Time [h]	X_S [mg/L]	S_b [mg/L]
0.08	46.6	24.80
0.63	51.8	21.66
1.20	55.4	15.13
1.65	59.0	2.16
2.20	61.8	1.10
2.73	66.6	1.07
21.17	53.8	4.85

Table D-26. Data from Batch Run 15B-3

Time [h]	X_S [mg/L]	S_b [mg/L]
0.18	47.0	41.12
0.68	51.0	42.47
1.35	55.8	30.67
1.92	57.4	18.47
2.72	67.4	10.63
3.57	75.0	3.22
4.47	81.5	4.06
5.55	81.1	5.33
7.60	80.7	1.55

Table D-27 Data from Batch Run 15B-4

Time [h]	X_S [mg/L]	S_b [mg/L]
0.08	42.1	55.78
0.32	42.5	51.57
1.07	44.9	47.78
1.72	47.0	41.88
2.42	52.2	32.78
2.67	55.4	28.65
3.08	57.0	19.89
3.50	59.8	10.87
4.03	65.8	5.06
4.53	70.2	1.67

Table D-28 Data from Batch Run 15B-5

Time [h]	X_S [mg/L]	S_b [mg/L]
0.08	44.5	71.84
0.77	46.1	
1.45	51.0	65.83
2.00	53.8	55.45
2.77	60.2	46.35
3.65	67.0	36.23
4.57	77.0	6.21
5.65	91.1	6.42
7.70	91.9	2.56

Table D-29 Data from Batch Run 15B-6

Time [h]	X_S [mg/L]	S_b [mg/L]
0.03	97.1	98.15
0.37	95.2	95.59
1.12	95.7	86.56
1.78	105.4	76.85
2.47	112.3	64.98
2.73	114.6	58.11
3.15	121.5	38.83
3.57	130.2	32.36
4.12	138.0	14.22
4.57	145.9	2.36

Table D-30 Data from Batch Run 15B-7

Time [h]	X_S [mg/L]	S_b [mg/L]
0.07	51.8	110.89
0.47	53.8	107.86
0.75	53.4	102.30
1.05	54.6	98.59
1.40	57.0	99.43
1.83	59.4	92.86
2.32	63.4	86.29
2.92	69.8	92.35
3.88	78.7	64.04
4.57	85.9	33.54
6.08	107.1	17.78
6.63	122.0	20.22
6.98	125.6	7.72
12.90	131.2	7.35

Table D-31 Data from Batch Run 15B-8

Time [h]	X_S [mg/L]	S_b [mg/L]
0.05	90.7	126.40
0.47	95.9	127.41
0.65	96.7	123.19
1.08	100.3	119.99
1.38	102.7	125.05
1.92	111.2	109.54
2.52	120.4	95.56
2.97	131.6	84.43
3.50	137.2	73.48
3.92	145.3	57.89
4.38	155.3	49.80
5.12	168.5	21.15
5.80	183.8	8.59
6.28	198.6	8.09
8.52	201.9	7.77
12.48	197.0	5.39

Table D-32 Data from Batch Run 15B-9

Time [h]	X_S [mg/L]	S_b [mg/L]
0.07	67.6	155.32
0.73	66.3	147.23
1.85	78.2	165.83
2.52	82.8	127.00
2.95	90.6	122.76
3.52	96.2	113.66
4.00	102.1	106.78
4.90	116.9	102.52
5.55	126.1	105.84
6.47	140.3	76.18
7.85	169.3	3.64
10.08	183.6	-
13.82	182.7	3.26

Table D-33 Data from Batch Run 15B-10

Time [h]	X_S [mg/L]	S_b [mg/L]
0.05	77.9	223.47
0.77	79.1	219.09
1.87	86.7	207.96
2.55	92.7	201.90
3.00	96.3	180.33
3.55	101.5	171.23
4.03	106.7	163 55
4.93	115.6	139.03
5.58	122.4	128.92
6.53	133.6	103.64
8.65	156.9	53.93
10.12	177.8	-
13.88	179.8	3.57

Table D-34 Data from Batch Run 15B-11

Time [h]	X_S [mg/L]	S_b [mg/L]
0.05	87.5	283.13
0.85	86.7	277.06
1.95	93.9	251.98
2.63	98.7	254.82
3.07	100.7	241.87
3.63	103.9	238.64
4.12	109.2	224.08
5.00	113.2	194.82
5.65	123.6	194.94
6.55	127.2	162.46
7.95	131.6	121.34
10.18	160.9	-
13.97	189.4	28.73
21.13	177.4	0.91

Table D-35 Data from Batch Run 15B-12

Time [h]	X_S [mg/L]	S_b [mg/L]
0.10	94.3	541.82
0.95	95.9	537.61
2.02	93.9	515.70
2.73	94.3	513.17
3.73	97.1	505.59
4.22	99.5	503.90
5.12	100.7	487.05
4.75	101.5	438.18
6.67	103.5	445.76
8.05	107.5	434.80
10.27	112.4	372.45
14.08	124.8	-
21.25	168.5	46.94
24.07	195.8	3.66
27.45	175.4	4.57

D-4 Data from Continuous Experiments at 15°C

Table D-36 Data from Continuous Experiments at 15°C

Run	D (1/h)	S_o [mg/L]	S [mg/L]	X_s [mg/L]
15C-1	0.0547	133.6	1.24	105
15C-2	0.0986	200.1	3.5	112
15C-3	0.0911	200.8	4	105

D-5 Data from Batch Experiments at 20°C

Table D-37 Data from Batch Run 20B-1

Time [h]	X_S [mg/L]	S_b [mg/L]
0.07	39.0	18.69
0.32	43.0	17.87
0.47	44.4	15.91
0.70	47.9	8.62
0.98	51.0	4.84
1.22	54.6	3.36
1.72	58.6	2.16
2.33	59.9	3.33
2.78	59.4	2.31

Table D-38 Data from Batch Run 20B-2

Time [h]	X_S [mg/L]	S_b [mg/L]
0.03	35.9	20.60
0.18	37.7	21.08
0 40	38.6	17.97
0.77	41.3	14.28
1.33	47.5	6.06
1.95	55.5	6.13
2.42	54.6	4.79

Table D-39 Data from Batch Run 20B-3

Time [h]	X_S [mg/L]	S_b [mg/L]
0.07	30.2	23.36
0.30	33.3	29.43
0.73	35.9	15.95
1.27	40.8	8.15
1.78	44.4	5.15
2.80	44.8	3.58
3.28	45.2	3.59
3.72	46.1	3.59
4.32	45.7	3.49

Table D-40 Data from Batch Run 20B-4

Time [h]	X_S [mg/L]	S_b [mg/L]
0.07	38.6	29.11
0.23	41.3	28.42
0.37	42.6	22.52
0.67	45.2	24.60
0.88	47.9	12.82
1.12	50.1	8.07
1.62	57.7	2.86
2.22	60.8	2.79
2.72	61.7	3.59

Table D-41 Data from Batch Run 20B-5

Time [h]	X_S [mg/L]	S_b [mg/L]
0.05	49.1	33.74
0.30	53.1	24.25
0.52	54.7	28.84
0.90	58.2	15.19
1.42	65.8	10.57
2.00	76.1	11.26
2.55	77.3	3.07
3.00	77.3	-
3.45	77.3	4.74

Table D-42 Data from Batch Run 20B-6

Time [h]	X_S [mg/L]	S_b [mg/L]
0.07	36.4	46.55
0.28	38.6	44.97
0.55	46.1	42.23
0.83	42.1	40.36
1.05	43.0	36.69
1.57	48.8	31.08
1.98	53.7	25.01
2.42	57.7	13.70
3.20	68.3	2.40
4.32	68.3	2.53

Table D-43 Data from Batch Run 20B-7

Time [h]	X_S [mg/L]	S_b [mg/L]
0.03	44.4	55.54
0.25	46.1	53.38
0.47	47.9	50.72
0.68	50.1	47.63
0.95	51.9	42.59
1.27	54.6	37.05
1.63	59.0	30.22
2.03	68.3	23.00
2.52	76.7	4.36
2.98	77.2	7.21

Table D-44 Data from Batch Run 20B-8

Time [h]	X_S [mg/L]	S_b [mg/L]
0.07	47.9	82.65
0.30	49.5	80.62
0.52	52.3	81.46
0.92	55.9	76.66
1.53	57.8	71.63
1.98	62.2	51.27
2.65	71.3	7.71
3.85	92.7	13.46
4.83	94.3	5.39
5.22	95.5	3.54
5.73	94.3	3.63

Table D-45 Data from Batch Run 20B-9

Time [h]	X_S [mg/L]	S_b [mg/L]
0.08	79.4	111.88
0.32	81.6	109.49
0.68	86.9	95.35
1.00	89.2	83.85
1.40	100.3	56.66
1.78	107.8	40.73
2.25	127.8	8.98
2.73	133.1	5.27
3.13	129.5	5.99

Table D-46 Data from Batch Run 20B-10

Time [h]	X_S [mg/L]	S_b [mg/L]
0.03	38.6	118.59
0.18	39.9	122.90
0.55	41.7	122.66
1.07	43.9	113.80
1.50	48.4	100.14
1.82	51.9	83.01
2.20	55.5	78.70
2.70	63.9	65.88
3.27	78.1	43.51
3.82	93.6	16.77
4.25	98.9	8.62
4.75	98.5	3.67
5.22	102.0	3.83

Table D-47 Data from Batch Run 20B-11

Time [h]	X_S [mg/L]	S_b [mg/L]
0.03	44.8	134.64
0.55	46.6	124.58
0.90	48.8	120.27
1.55	55.5	107.33
2.10	61.7	88.04
2.52	68.3	78.10
3.13	79.0	65.52
4.18	106.0	15.33
4.68	122.0	2.68
5.48	124.7	2.91

Table D-48 Data from Batch Run 20B-12

Time [h]	X_S [mg/L]	S_b [mg/L]
0.08	82.5	169.26
0.27	84.7	156.24
0.63	86.9	158.76
0.87	88.7	150.86
1.22	95.8	134.64
1.73	109.6	115.23
2.30	121.5	82.41
2.83	138.0	26.59
3.85	144.6	10.37
4.32	144.6	7.09
4.75	143.7	6.59

Table D-49 Data from Batch Run 20B-13

Time [h]	X_S [mg/L]	S_b [mg/L]
0.05	120.7	202.20
0.28	118.4	213.22
0.85	120.2	190.22
1.72	136.6	149.01
2.30	153.0	109.49
2.82	170.8	76.90
3.33	189.0	30.19
3.72	207.6	7.93
4.18	223.6	14.13
4.88	219.6	10.35
5.58	221.8	-

Table D-50 Data from Batch Run 20B-14

Time [h]	X_S [mg/L]	S_b [mg/L]
0.10	90.1	392.13
1.25	91.8	362.24
1.82	97.1	363.39
2.40	102.9	331.76
2.93	113.1	327.16
3.42	130.4	287.49
3.80	133.5	269.76
4.27	138.8	263.53
4.98	153.5	238.62
5.68	172.6	224.72
6.18	189.4	304.38
8.37	288.3	183.27
12.37	255.1	-

Table D-51 Data from Batch Run 20B-15

Time [h]	X_S [mg/L]	S_b [mg/L]
0.07	84.7	446.33
0.42	80.3	423.75
1.03	79.4	411.52
1.88	84.7	395.69
2.47	87.4	389.94
2.97	92.3	389.22
3.45	97.6	378.43
3.87	102.0	364.76
4.33	105.1	324.38
5.05	112.7	311.45
5.75	119.8	297.07
6.25	125.5	192.62
8.43	249.7	20.12

Table D-52 Data from Batch Run 20B-16

Time [h]	X_S [mg/L]	S_b [mg/L]
0.10	99.4	680.39
0.60	100.7	664.82
1.30	106.5	644.45
1.87	109.1	646.85
2.45	117.6	610.91
2.95	125.5	610.91
3.38	130.4	580.97
3.75	138.4	589.35
4.38	155.3	546.23
4.80	165.9	509.09
5.42	184.1	443.21
6.13	211.6	428.84
12.18	273.3	54.68
12.42	263.5	6.11

D-6 Data from Continuous Experiments at 20°C

Table D-53 Data from Continuous Experiments at 20°C

Run	D (1/h)	S_o [mg/L]	S [mg/L]	X_s [mg/L]
20C-1	0.0434	118.7	1.17	81.1
20C-2	0.0547	131.87	1.68	82.8
20C-3	0.157	260.7	4.6	94
20C-4	0.213	236.1	38.5	76

D-7 Data from Batch Experiments at 25°C

Table D-54 Data from Batch Run 25B-1

Time [h]	X_S [mg/L]	S_b [mg/L]
0.03	47.9	17.30
0.17	48.3	18.52
0.40	50.2	16.29
0.68	53.8	10.30
1.00	58.0	4.58
1.80	59.8	4.43

Table D-55 Data from Batch Run 25B-2

Time [h]	X_S [mg/L]	S_b [mg/L]
0.03	55.2	23.05
0.13	57.1	20.32
0.45	66.3	7.76
0.78	72.2	3.27
0.97	72.7	3.38
1.62	70.9	5.20
1.97	72.2	6.18

Table D-56 Data from Batch Run 25B-3

Time [h]	X_S [mg/L]	S_b [mg/L]
0.05	38.6	31.24
0.22	40.0	29.32
0.37	43.2	27.55
0.62	46.5	20.51
0.78	49.7	15.76
0.97	53.8	9.54
1.17	56.6	6.32
1 37	59.4	6.23
1.65	60.3	5.99

Table D-57 Data from Batch Run 25B-4

Time [h]	X_S [mg/L]	S_b [mg/L]
0.03	55.7	34.50
0.13	58.4	33.16
0.30	61.2	28.75
0.37	63.0	6.41
0.52	65.8	4.74
0.62	67.6	3.74
0.78	69.9	1.93
1.12	70.9	0.86

Table D-58 Data from Batch Run 25B-5

Time [h]	X_S [mg/L]	S_b [mg/L]
0.05	55.2	31.66
0.28	59.4	25.54
0.62	64.0	15.25
0.80	70.9	7.43
1.10	81.9	7.50
1.47	78.2	6.04
1.83	78.7	4.34

Table D-59 Data from Batch Run 25B-6

Time [h]	X_S [mg/L]	S_b [mg/L]
0.08	31.7	47.48
0.22	33.6	46.76
0.37	36.3	44.82
0.53	37.3	42.38
0.67	48.3	38.99
0.83	51.1	35.97
1.02	52.5	33.17
1.27	59.8	24.92
1.48	62.6	18.35
1.70	68.6	11.02
1.93	75.0	4.70
2.28	76.8	2.76
2.70	77.8	8.50

Table D-60 Data from Batch Run 25B-7

Time [h]	X_S [mg/L]	S_b [mg/L]
0.05	72.7	97.03
0.17	72.2	95.88
0.27	73.6	93.15
0.40	74.5	93.43
0.57	77.8	85.67
0.72	81.4	81.07
0.85	83.3	77.62
1.02	86.0	76.78
1.18	87.9	71.87
1.40	95.7	53.47
1.55	98.9	44.75
1.85	106.3	33.09
2.12	118.7	13.80
2.47	124.2	4.98

Table D-61 Data from Batch Run 25B-8

Time [h]	X_S [mg/L]	S_b [mg/L]
0.03	31.7	81.22
0.13	31.7	81.34
0.28	32.7	81.22
0.48	33.6	78.82
0.72	35.4	76.66
0.92	37.7	74.51
1.15	40.9	68.88
1.37	41.4	68.88
1.63	46.0	63.37
1.97	53.4	58.58
2.38	61.2	38.14
4.15	76.8	2.76

Table D-62 Data from Batch Run 25B-9

Time [h]	X_S [mg/L]	S_b [mg/L]
0.08	8.5	103.11
1.50	15.0	82.41
2.67	11.5	93.91
4.08	10.5	92.95
5.92	12.5	92.10
7.67	20.0	86.85
8.58	23.5	74.56
9.83	34.0	52.71
11.00	45.5	32.68
12.58	59.0	2.67
13.22	59.0	2.30
14.75	66.0	2.95
15.75	64.5	2.78
25.13	70.0	-

Table D-63 Data from Batch Run 25B-10

Time [h]	X_S [mg/L]	S_b [mg/L]
0.33	10.6	183.99
1.42	15.6	180.88
3.33	21.6	174.41
4.83	30.4	150.45
6.83	44.6	123.38
7.83	51.5	101.10
8.83	59.8	74.99
9.67	60.3	58.94
10.25	59.4	18.57

Table D-64 Data from Batch Run 25B-11

Time [h]	X_S [mg/L]	S_b [mg/L]
0.13	46.0	189.26
1.78	47.4	177.28
2.55	53.4	173.93
3.65	65.8	144.94
4.40	79.1	129.37
5.32	88.3	109.49
5.70	95.2	77.86
6.67	125.6	16.10
7.30	176.2	10.06
8.52	199.7	15.09
9.58	229.1	15.14
12.32	244.8	13.90

Table D-65 Data from Batch Run 25B-12

Time [h]	X_S [mg/L]	S_b [mg/L]
0.20	24.8	307.61
1.60	29.0	319.59
2.30	36.8	252.99
3.88	52.0	252.99
5.12	53.4	162.91
6.08	104.9	136.56
7.03	141.7	88.40
7.75	173.5	5.63
9.27	179.0	4.60
15.78	182.2	5.46
18.27	181.7	5.56
19.57	179.0	3.59
20.50	185.4	5.10
21.67	176.7	5.99
24.55	173.0	6.13

Table D-66 Data from Batch Run 25B-13

Time [h]	X_S [mg/L]	S_b [mg/L]
0.03	46.9	426.06
1.22	46.0	424.91
1.93	48.8	408.23
2.82	58.0	391.56
3.33	63.5	385.23
3.78	67.6	367.99
4.33	79.6	336.36
4.72	92.0	330.61
5.80	124.7	274.55
6.43	140.3	216.57
8.23	231.9	17.97
9.45	242.5	15.57
24.33	209.8	7.62

Table D-67 Data from Batch Run 25B-14

Time [h]	X_S [mg/L]	S_b [mg/L]
0.27	42.3	423.76
1.53	45.1	403.63
2.40	49.7	373.74
3.40	60.3	351.89
4.10	75.0	321.99
4.60	85.1	309.05
5.18	89.7	254.91
5.87	121.5	215.62
7.03	176.2	102.54
7.40	188.2	49.14
8.38	234.7	49.64
9.00	240.6	15.28
10.37	243.9	16.36
11.55	243.9	14.18
13.73	231.4	13.18

Table D-68 Data from Batch Run 25B-15

Time [h]	X_S [mg/L]	S_b [mg/L]
0.33	65.8	420.45
2.68	64.0	411.83
3.82	67.6	373.02
4.77	75.5	342.83
5.68	93.9	334.21
6.20	100.8	280.30
6.63	121.0	234.78
7.23	141.3	195.97
7.73	165.2	159.08
8.67	208.9	40.92
9.30	241.1	3.74
11.10	254.9	3.18
12.33	246.6	3.25
27.23	201.1	2.80

D-8 Data from Continuous Experiments at 25°C

Table D-69 Data from Continuous Experiments at 25°C

Run	D (1/h)	S_o [mg/L]	S [mg/L]	X_s [mg/L]
25C-1	0.054	225	1.2	90
25C-2	0.11	186	5.9	111
25C-3	0.11	190	2.4	115
25C-4	0.11	283	3.8	183
25C-5	0.11	190	1.2	121
25C-6	0.12	202	3	119
25C-7	0.123	214	4.1	117
25C-8	0.234	216	4.2	122

Appendix E Data from Shock-loading Experiments in the ICFBR

Table E-1 Data from Run 1

Time [h]	X_S [mg/L]	S_b [mg/L]	S_o [mg/L]	EPS [g glucose/g sand]
-105.7	149	0.92		0.000148
-78.4	148	1.08	251.9	0.000113
-54.6	130	1.67		
-30.8	130	1.65		
-12.3	130	1.06		
-12.2	130	1.55		
-12.1	134	1.38		
-12.0	129			
-11.5	125			0.000233
-11.4	127	1.30		0.000297
-11.4		1.18	250.6	
-7.7	133			
-7.7	131	1.25		
-7.6	134			0.000312
-7.4	136	1.29		
-7.3	130			
-7.2	129			
-7.1	130			
-1.1	145	0.21		
-1.0	143			
-0.9	144		250.3	
-0.8	144	0.19		
-0.2	141	0.91		
0.0	137	0.76		
0.1	149	0.76		
0.2	144	0.72		
0.3	141	0.72		
0.3	145	0.69		
0.4	149	0.82		
0.5	148	0.89		
0.6	146	1.72		
0.6	146	1.01		
0.9	140	1.76		
1.0	145			
1.1	145	0.63		
1.5	149	1.06		
1.9	148	2.64		
2.0	145	2.63		
2.3	147	2.65		
2.6	151	3.51		
3.0	157	5.40		
3.3	150	6.43		
3.6	146	10.49		

Table E-1 continued

4.0	146	7.06		
4.3	145	12.31		
4.6	145	20.42		
5.0	168	19.71		
5.4	135	23.43		
6.6	139			
6.7	141	14.29		
5.9	140	22.26		
12.6	129			
12.7	137	32.38		
13.4	150			
13.9	134	48.94		
14.6	137	59.51		
15.6	128	41.67		
16.6	130	42.92		
18.2	147	38.96		
18.3	126	53.06		0.000268
18.7	135	60.69		
18.7	122	61.53		0.000501
25.8	116	62.36		
25.9	115	71.39		
28.3	115	79.72	295.1	
28.5	116	69.44		
39.3	112			
39.5	119	57.15		
39.6			285.5	
41.1	121			
43.1	121	85.42		
48.2		100.42		
48.3			308.8	0.000357
48.4			293.0	0.000410

Table E-2 Data from Run 2

Time [h]	X_S [mg/L]	S_b [mg/L]	S_o /mg/L]	EPS [g glucose/g sand]
-123.4	121	1.1		
-98.6	126	1.0	191.4	
-30.1	115	1.8	168.8	
-18.2	116			0.000577
-7.8				0.000711
-7.5				0.000699
-7.4				0.000607
-6.9	108	2.3		
-3.5	109	2.0		
-3.4	109			
-1.2	117	2.5		
-1.1	110	2.5		
0.1	111	2.1		
0.4	98	2.2		
0.6	119	2.2		
0.9	118	2.2		
1.1	122	2.3		
1.4	119	2.1	288.2	
1.6	126	1.5		
1.9	120	1.3		
2.1	124	1.9		
2.4	120	1.7		
2.6	124	2.2		
2.9	120	2.0		
3.1	116	1.7	292.8	
3.4	116	1.8		
4.4	120	1.8		
4.9	123	1.8		
5.4	126	1.6		
5.9	125	1.7		
6.4	126	1.9		
6.9	125	1.5		
7.4	124	1.7		
7.9	128	2.0		
8.4	132	1.9	303.5	
15.3	138	2.3		
17.6	136	1.9		
18.4	136	2.0		
19.2	137	1.8		
21.1	143	2.1		0.000723
21.2				0.000722
21.2				0.000669
22.4	141	1.7		
27.5	150	1.6		
28.9	154	1.3		

Table E-2 continued

31.0	152	1.4		
41.9	174	1.7		
45.1	163	1.3		
48.9	164	1.6		
51.2	167	1.6	319.4	0.000669
51.4			304.2	0.000609
67.8	168	1.4		
67.9			324.4	
75.1	166	1.4	285.5	
96.8	164	1.3		
113.4	169	1.3		
116.4				0.000803
116.4				0.000821
123.5	179	1.4		
136.9	166	1.4		

Table E-3 Data from Run 3

Time [h]	X_S [mg/L]	S_b [mg/L]	S_o /mg/L]	EPS [g glucose/g sand]
-99.4	107	1.1		
-72.9			248	
-30.9	113	0.3	254	
-19.0	113	0.3	251	
-9.0				0.000578
-8.8				0.000455
-8.7				0.000415
-7.7	112	0.3		
-4.5	112	0.9		
-4.4			239	
0.2	112	0.4		
0.4	116	0.3		
0.7	119	0.3		
0.9	115	0.5		
1.2	112	0.4		
1.4	112	0.6		
1.7	110	0.4		
1.9	113	0.5		
2.2	109	0.4		
2.4	111	0.4		
2.7	108			
3.7	108	0.4		
4.2	110	0.3		
4.7	109	0.3		
5.2	112	0.2		
5.7	111	0.2		
6.2	107	0.2		
6 7	112	0.3		
7.2	112			
7.7	112			
14.6	124			
16.8	128	0.5		
17.6	125	0.5		
18.5	123	0.4		
20.4	129	0.4		0.000612
20.4				0.000663
20.5				0.000642
21.7	124	0.4		
26.8	136	0.3		
28.2	134	0.7		
28.2			228	
29.9	133	0.5		
41.2	136	0.5		
44.3	132	0.3		
48.2	132	0.7		

Table E-3 continued

50.5		0.6	237	0.000715
50.7				0.000432
52.1				0.000519
67.2	138	0.4		
67.2			234	
74.3	140	0.4		
96.0	152	0.3		
112.7	141	0.3		
115.6				0.000762
115.6				0.000841
115.7				0.000855
122.8	140			
136.1	147		251	

Table E-4 Data from Run 5

Time [h]	X_S [mg/L]	S_b [mg/L]	S_o [mg/L]	EPS [g glucose/g sand]	Biofilm Dry Weight [g /g sand]
-35.9	168			0.00153	
-35.9				0.00301	
-16.9				0.00129	
-16.7				0.00153	
-16.6		8.6			
-15.4	164				0.069
-4.4	156	5.0	158.2		
-2.6	161	5.8			
-1.5	163	5.7	165.1		
-0.4	147				
0.3	145	7.9			
1.5	154	3.6			
2.5	127	4.4			
5.3	126	8.4			
5.6	113				
10.7	168	23.7			
14.2	123		121.1		
20.5	160	16.8			
22.3	112	29.7		0.00160	
24.4	109			0.00364	
25.0					0.060
29.5	102	70 9	169.1		
30.5	77	69.7			
38.2	84	114.1			
41.0	139	160.3	130.5		
42.3	93	112.6			
48.0	114	128.7		0.00171	
57.2	74	116.2			
65.4	95	88.2		0.00331	
68.6	105	89.5		0.00130	
72.3	68	145.4			
73.3	41	152.4			
79.2	52	108.3			
86.1	54	103.5			
88.6	68				
92.3	103	150.3	189.9		
94.4	50	135.9			
105.1	69	158.5			
116.8	65	121.1			
120.5	52	128.7			
129.6	39	181.7	188.9		
132.1	7	171.0		0.00274	
132.2	5	166.7		0.00213	
132.1					0.05
144.9	35	194.7			

Table E-5 Bioparticle Measurements from Image Analysis in Run 5

Time [h]	Average Ferret Diameter [mm]	Standard Deviation of the Ferret Diameter [mm]	Number of Particles Measured	Number of Bare Particles
Bare	0.195058	0.040366	325	-
-166.75	0.183816	0.043329	236	116
-63.70	0.207981	0.041517	22	3
-41.45	0.214161	0.044953	194	221
-24.20	0.218202	0.051356	281	57
20.52	0.216225	0.052392	267	18
81.13	0.250305	0.059233	167	12

Table E-6 Data from Run 6

Time [h]	X_S [mg/L]	S_b [mg/L]	S_o [mg/L]	EPS [g glucose/g sand]	Biofilm Dry Weight [g /g sand]
-191.1	285	5.6			
-166.7	387	6.6			
-163.0	322	3.7		0.00190	
-162.9				0.00516	
-162.8				0.00259	
-161.8			183		0.10
-94.0			198		
-65.8				0.00602	
-65.7				0.00497	
-65.6	198			0.00488	
-64.7					0.16
-37.8				0.00486	
-37.8				0.00376	
-37.8				0.00296	
-37.1	182	10.2			
-18.2				0.00390	
-18.2				0.00202	
-18.1				0.00342	
-17.8	255	13.5			
-16.3					0.13
-15.8		3.9	161		
-3.5	290	8.0			
-2.4	276	8.7	196		
-0.4	344				
-0.3	295	10.2			
-0.1	317				
0.7	318	7.0			
1.6	185	3.8			
4.5		6.2			
9.8	250	6.9			
13.5	319	7.6			
13.7			352		
19.7	240	9.7			
19.9			327		
21.4	252	9.0			
23.5	271	5.7		0..00809	
24.5					0.18
28.7	279	7.9	329		
29.5	326	7.4			
37.5	236		281		
37.7	329	9.7			
40.2		8.5			
41.5	286	6.1			
56.3	390	12.6			
64.5	493	8.4			

Table E-6 continued

67.8	249	6.0		0.00808	
71.4	350	3.1		0.00853	
72.4	348				
78.3	381	8.9			
85.3		8.0			
87.8	361				
91.3	363	7.7			
93.5	444	4.6			
104.2	194	3.4			
115.9	348	12.6			
119.6	349	6.7			
128.6	739	7.6			
131.3				0.00836	
131.4				0.00590	
131.5				0.01078	
132.0					0.18
144.0	1268	3.7			

Table E-7 Bioparticle Measurements from Image Analysis in Run 6

Time [h]	Average Ferret Diameter [mm]	Standard Deviation of the Ferret Diameter [mm]	Number of Particles Measured	Number of Bare Particles
Bare	0.195811	0.040666	323	-
-166.7	0.20464	0.043586	300	45
-64.7	0.265113	0.084431	142	1
-60.4	0.255051	0.066382	209	6
-25.1	0.276263	0.076827	115	4
22.7	0.263501	0.070947	117	3
80.2	0.239402	0.075111	199	19
129.0	0.22246	0.108001	159	12

Table E-8 Data from Run 7

Time [h]	X_S [mg/L]	S_b [mg/L]	S_o [mg/L]	EPS [g glucose/g sand]	Biofilm Dry Weight [g /g sand]
-31.9	173				
-29.3	169	1.5		0.00030	
-29.2	156	1.4		0.00029	
-29.1	154	1.4		0.00033	
-28.8	152	1.8	204.4		0.0067
-21.9	155	1.9		0.00038	
-21.8	159	2.1		0.00036	
-21.8	151	2.1		0.00032	
-21.7	152	2.2			0.0068
-10.4	167	2.5			
-10.2					0.0072
-1.8			209.9	0.00036	
-1.3		2.6		0.00041	
-1.3	162	2.4		0.00045	
-1.2	155	2.3			
-0.1	155	1.5	245.5		
0.5	154	1.5			
1.2	159	1.3			
1.3	154	1.4			
2.4	159	1.7			
2.5	155	1.7			
3.7	179	2.0			
3.7	169	2.0	685.1		
4.9	175	2.0			
6.6	395	3.4	739.1		
14.2	380				
16.5	362	3.4		0.00059	
16.6	341	2.6		0.00060	
16.6	333	3.1		0.00051	
18.2	371	4.2			0.0093
20.3	413	5.3	715.8		
22.8	457	2.9			
27.2	466	1.8			
37.4	622	2.0			
44.3	647	3.5			
46.2	667	4.7		0.00053	
46.3	639	4.3		0.00057	
46.3	602	4.5		0.00065	
47.3	609				0.0100
68.5	714	8.0			
93.0	632	7.6			
94.3	674	2.3		0.00060	
94.3	674	2.4		0.00061	
94.3	664	2.1		0.00065	
94.7					0.0108

Table E-8 continued

138.4			577.3		
165.2		3.8			
166.8	612			0.00083	
166.9	559			0.00072	
167.1	587	2.6			
167.4					0.0184
219.8	597	5.1			
236.1	574	3.5			
305.7		3.3	672.0		
307.1	619	1.9		0.00076	
307.2	574	1.6		0.00090	
307.3	594	2.9		0.00084	
307.5	579				
353.2		2.8			
385.5			552.5		
400.7	597	2.8		0.00107	
400.8	542	4.0		0.00096	
400.8	542	4.0		0.00116	
401.2			553.9		0.0134
449.0	594	4.2			
455.8	614	5.6			
457.9	597	11.7			
458.6					.0165
474.3	634	3.7			

Table E-9 Bioparticle Measurements from Image Analysis in Run 7

Time [h]	Average Ferret Diameter [mm]	Standard Deviation of the Ferret Diameter [mm]	Number of Particles Measured	Number of Bare Particles
Bare	0.190096	0.039641	254	-
-74.1	0.191908	0.038699	299	110
-32.9	0.192964	0.033654	244	132
-22.9	0.198877	0.038803	209	123
-10.2	0.200184	0.03519	244	100
14.2	0.185442	0.039048	269	68
44.3	0.193075	0.03686	275	95
93.0	0.200565	0.04	260	51
165.2	0.200534	0.038504	261	72
305.7	0.197485	0.035546	225	78
403.0	0.205163	0.038201	181	30
451.8	0.193278	0.040812	383	99

Table E-10 Data from Run 8

Time [h]	X_S [mg/L]	S_b [mg/L]	S_o [mg/L]	EPS [g glucose/g sand]	Biofilm Dry Weight [g /g sand]
-74.7	597	2.8		0.00107	
-74.6	542	4.0		0.00096	
-74.5	542	4.0		0.00116	
-74.2			553.9		0.013
-26.3	594	4.2		0.00074	
-19.5	614	5.6			
-17.5	597			0.0066	
-16.8				0.0077	0.017
-1.0	634	4.2			
0.7	604	31.9			
2.3	487	50.2			
3.5	469	260.0			
5.4	385	283.5			
6.7	375	279.9			
9.3	347	377.6			
18.7	78	524.8			
18.8	72	543.7			
24.2	66	568.5			
29.2	37	571.4	728.9		
32.3	27				
49.1	16	478.1		0.00125	
49.2	9	500.9		0.00117	
49.3	9	488.7		0.00128	
117.0			514.6		
138.6	7	478.1			
167.8	16	475.2		0.00109	
167.9	7	553.9		0.00091	
168.0					0.035
237.0	9	491.3		0.00106	
237.2	7	532.1	498.6	0.0114	
237.3					0.0269

Table E-11 Bioparticle Measurements from Image Analysis in Run 8

Time [h]	Average Ferret Diameter [mm]	Standard Deviation of the Ferret Diameter [mm]	Number of Particles Measured	Number of Bare Particles
bare	0.190096	0.039641	254	
-310.2	0.200534	0.038504	261	72
-169.7	0.197485	0.035546	225	78
-72.3	0.205163	0.038201	181	30
-23.5	0.193278	0.040812	383	99
45.4	0.198983	0.042596	209	27
168.0	0.204405	0.037263	228	26
242.6	0.191677	0.038479	165	29

Appendix F Dissolved Oxygen Calculations

The dissolved oxygen content of the fermentation broth was monitored during each of the dynamic runs, however, the calibration shifted during the runs and it was not possible to recalibrate without introducing contamination. The following calculations were performed to confirm that oxygen was not limiting.

Oxygen supply:

The oxygen transfer rate (OTR) is given as follows (Shuler and Kargi, 1992):

$$OTR = K_L a(C^* - C_L) \qquad \textbf{(F-1)}$$

The overall gas-liquid mass transfer coefficient, $K_L a$, was calculated using two correlations. The correlation of Bello et al. (1985) was developed for airlift reactors. The correlation of Nguyen-Tien et al. (1985) was developed for bubble columns containing glass beads and has been found to fit data for a fluidized bed reactor containing biofilm-covered sand particles quite well (Ryhiner et al., 1988). Note that both correlations are based upon the dispersion volume (hence the nomenclature $K_L a_D$) which in this case is approximately equal to the liquid volume. The results are presented in Table F-1.

Table F-1. Calculated Values for $K_L a$ Based upon Selected Correlations

Reference	Correlation	$K_L a$ for oxygen [h^{-1}]	Values of variables
Bello et al. (1985)	$K_L a_D = 0.76(1+\frac{A_d}{A_r})^{-2} u_{G,r}^{0.8}$ **(F-2)**	31.3	$A_d/A_r = 0.44$ $u_{G,r} = u_G = 0.0093$ m/s
Nguyen-Tien et al. (1985)	$K_L a_D = 0.39(1-\frac{\phi_S}{0.58})^{-1} u_G^{0.67}$ **(2.62)** $\phi_S = \frac{\varepsilon_S}{1-\varepsilon_G}$ **(2.63)**	≈0.1	$\varepsilon_S = 0.010$ $\varepsilon_G = 0.017$

The maximum rate of oxygen transfer would occur when C_L=0. Given that at 10°C, C^* is 11 mg/L O_2 (Perry's Chemical Engineers' Handbook, 1984), the predicted maximum OTR is in the range of 340-660 mg/L·h using both correlations.

Oxygen demand:

The biofilm thicknesses in this work were very thin. Model simulations in Sections 5.3.2.2 and 5.3.2.3 showed that the phenol concentration profiles in the biofilms are quite flat. It would be expected that the

oxygen concentration profiles within the biofilm are also flat, hence, in this analysis diffusion effects within the biofilm will be neglected

The oxygen uptake rate (OUR) is given as follows (Shuler and Kargi, 1992)

$$OUR = q_{O_2} X_{tot} = \frac{\mu X_{tot}}{Y_{X/O_2}} \qquad \textbf{(F-3)}$$

where q_{O_2} is the specific rate of oxygen consumption [mg O_2/g DW cells·h], X_{tot} is the total concentration of biomass (given as $X_{tot} = X_s + X_f$) [mg DW cells/L], μ is the specific growth rate [h^{-1}], and Y_{X/O_2} is the oxygen yield coefficient [g DW cells/g O_2]. The values of the specific oxygen rate of oxygen consumption and the oxygen yield coefficient are not available in the literature for *P. putida* Q5 at 10°C

Two approaches were taken. The first portion of Equation F-3 was used in the first approach (corresponding to OUR - 1 in Table F-2). The value of 0.8 mg O_2/mg DW·h, determined by Hill (1974) for a mesophilic culture of *P. putida* (ATCC 17484) at 30°C, was used for the specific rate of oxygen consumption. Because the specific growth rates at 10°C are much lower than at 30°C, it is quite possible that the specific rate of oxygen consumption is also much lower. The second approach (corresponding to OUR - 2 in Table F-2) involved the use of the second portion of Equation F-3. The steady-state value for μ was approximated as the dilution rate for each experiment; this assumption was reasonable because the contribution of the biofilm biomass to the total biomass concentration was relatively small. The value of 0.77 mg DW cells/mg O_2 determined by Worden and Donaldson (1987) for a mixed culture of mesophilic phenol degraders, was used for the oxygen yield coefficient.

Table F-2. Calculated Oxygen Uptake Rates During the Runs Used in the Simulations.

Run	Initial/final steady state	X_s (mg/L)	X_f (mg/L)	X_{tot} (mg/L)	OUR -1 [mg O_2/L·h]	OUR -2 [mg O_2/L·h]
1	initial	135	17	152	121	7.8
	washout	-	-	-	-	-
2	initial	115	18	133	107	7.8
	final	168	19	187	149	8.9
3	intial	112	9	121	97	3.9
	final	143	9	152	122	11.7
7	initial	154	20	174	139	8.5
	final	589	38	627	502	25.6
8	initial	581	35	616	493	29.9
	washout	-	-	-	-	-

The results obtained from the two approaches in Table F-2 are different by more than an order of magnitude The results from the first approach based upon a parameter determined at 30°C indicate that there may have been an oxygen limitation during the shock load in Run 7 and during the initial steady-state operating period in Run 8 However, the results from the second approach which incorporate the specific growth rates estimated for each experiment suggest that even during the high cell concentrations observed during Runs 7 and 8 (and relatively high organic loadings), that oxygen was not limiting. The results from the second approach are likely to better reflect what was happening during the experiments This can only be confirmed by determining the oxygen yield coefficient of *P. putida* Q5 at 10°C

Appendix G. Calculation of Temperature Effects

An assumption of the dynamic model was that the temperature of the biofilm and the bulk fluid were the same. The following calculations were performed to check if the assumption was reasonable.

The problem was solved by using the general solution for a step change in surface temperature for a hollow sphere and solving for the inner boundary of the biofilm. It was assumed that the biofilm had similar properties to water (Characklis, 1981) and that flow conditions were stagnant (worst case scenario). The parameter values used were:

r_p = 105 μm

r_f = 150 μm (assuming a biofilm thickness of 45 μm)

$R = r_p / r_f = 0.7$

k = 0.61 W/mK (Characklis, 1981)

ρ_{bf} = 1000 kg/m^3

c_p = 4.19 J/gK

$F_o = (k / \rho_{bf} c_p)(t / r_f^2) = 6.47 \times t$ s

T_i = 10°C

The solution is given as:

$$\frac{(T - T_i)}{(T_S - T_i)} = 1 + \frac{2}{\pi R} \sum_{n=1}^{\infty} \left[\frac{(-1)^n}{n} \sin(n\pi R) e^{(-n^2 \pi^2 F_o)} \right] \qquad \text{(G-1)}$$

The times (t) for the inner boundary of the biofilm to adjust from an initial temperature (T_i) of 10°C to step increases in the biofilm surface temperature (T_S) to 15, 20 and 30°C are 0.1, 0.2 and 0.2 s respectively. Since the order of magnitude of the response is a fraction of a second, the biofilm and the bulk fluid can be assumed to be the same temperature for the purposes of the model.